IMPROVING THE EFFICIENCY OF THE DESICCANT WHEEL POWERED BY RENEWABLE ENERGY UNDER DIFFERENT ENVIRONMENTAL CONDITIONS

A Thesis Submitted by

Yousef Ahmad Hasan Altork

B.Sc. Eng., M.Sc. Eng.

For the award of

Doctor of Philosophy

2021

DEDICATION

To my beloved parents,
Ahmad Altork and Ensaf Sakhrieh
My wife: Dua’a Salem
my daughter and son: Leen and Elias

ABSTRACT

The main advantage of using thermally driven cooling systems as a standalone system or combined with conventional systems is to reduce the amount of consumed electrical energy. Therefore, energy performance analysis is a key factor when designing, operating, and optimising thermally based air conditioning systems. A Solid Desiccant Cooling (SDC) system, powered by low or medium temperature heat from renewable energy sources, has the following benefits compared with other systems that can be used for cooling: the separation of dehumidification and cooling enables demand-oriented air conditioning which can help to reduce peak power requirements by using desiccant-assisted air conditioning systems, it is environmentally-friendly being Chlorofluorocarbon (CFC) free, controls humidity and temperature independently, and has a low lifetime operating cost. The SDC system has demonstrated its feasibility in different climatic conditions. The main part of the SDC system, which is responsible for the dehumidification process, is the Desiccant Wheel (DW) which has a major influence on overall system performance. Therefore, it is essential to identify the optimal operation of the DW. The operational parameters which most affect DW performance are DW rotational speed, regeneration temperature, and airflow rates. The optimal ranges of these parameters are described by previous studies under certain environmental and operational conditions.

At the time of writing, there has been no study that combined the parameters into non-dimensional form. Also, there are very few studies that have considered channel geometry and design parameters, and no studies that determined the optimal non-dimensional group's that most influence DW performance. The main goal of this study is to extend previous findings to situations not restricted to a specific design or climate. In addition, key gaps in the optimisation process for a specific design or environment will be identified and examined experimentally and computationally.

The study commenced with modelling the DW. The 1-D Gas Solid Side Resistance (GSSR) model was used to model the DW. Afterwards, the model was validated with three different sets of previously published experimental data. It was found that the maximum discrepancy between the two results was 12.3%, while the maximum reported discrepancy in the open literature was 15%. An experimental apparatus was designed and built to study the DW. The DW's parameters were divided into three categories: the process air and climate parameters, regeneration air parameters, and the DW design and operational parameters. The desiccant

material parameters were assumed to be constant. The non-dimensional groups were created and tested experimentally and computationally (due to the difficulty of changing some parameters experimentally). Varying different parameters' values in the same non-dimensional parameters' combinations and comparing the output results was the method implemented to test the non-dimensional groups. The non-dimensional groups were valid and the number of independent parameters was reduced from 16 to 9 non-dimensional groups.

The analysis of the non-dimensional groups was carried out with reference to a base value. The non-dimensional groups operating range and the effect on the performance indices were identified. Then, two of the non-dimensional groups were varied at the same time to investigate how each non-dimensional group affects others in regards to the system performance. The system performances were evaluated in terms of dehumidification effectiveness (η_{deh}), Dehumidification Coefficient of Performance (DCOP), and Sensible Energy Ratio (SER). A maximum value for η_{deh} and DCOP is desirable, which represents superior dehumidification performances. On the other hand, a higher value for SER means a higher temperature value of the treated air and hence a higher cooling load which must be avoided. It was found that some of the non-dimensional groups have a higher impact on the system performance than others. In addition, it was found that the best value of the η_{deh}, DCOP, or SER can vary depending on the values of other non-dimensional groups.

The last part of this study was optimising the non-dimensional groups. The optimisation was based on comparing the combined SDC system and VCC system with a standalone VCC system. Another performance index (η_{comp}) was introduced based on comparing the energy needed to operate both systems under the same conditions. By assuming the added heat to regenerate the DW comes from a solar thermal source, the performance index becomes $\eta_{comp,solar}$, which was used for the optimisation. The maximum achieved $\eta_{comp,solar}$ in all cases was around 2.0, which means that the standalone VCC system needs one hundred percent more power than the combined SDC system with the VCC system for the same cooling load and operating conditions. It was found that some of the non-dimensional groups had optimal values, while others could have a range of values. The percentage of the thermal energy added by solar thermal source to ensure just equality between both systems in respect of energy consumption was presented. It was found that the percentage values varied between 78.7 - 101%, while the average percentage at the optimal non-dimensional groups' values was around 88%.

CERTIFICATION OF THESIS

This thesis is entirely the work of Yousef Ahmad Hasan Altork except where otherwise acknowledged. The work is original and has not previously been submitted for any other award, except where acknowledged.

Dr Ahmad Sharifian-Barforoush

Principal Supervisor

Assoc Prof Andrew Wandel

Associate Supervisor

Student and supervisors signatures of endorsement are held at the University.

ACKNOWLEDGEMENTS

First of all, I thank Allah for helping me continue this project. There are a number of people without whom this thesis might not have been written, and to whom I am greatly indebted.

First and foremost, a special thank you to my principal supervisor, Dr Ahmad Sharifian-Barforoush, for his strategic advice, guidance, constructive criticism and technical assistance with the experimental and numerical part of the study. To my associate supervisor, Associate Professor Andrew Wandel, for his generosity, grounding advice and help with writing emendation. I am truly appreciative of their help and support throughout the duration of my studies, which has helped me broaden my knowledge and develop new skills.

I would also like to thank mechanical workshop technicians, Mr Oliver Kinder and Mr Brian Aston for their help in fabricating the experimental apparatus. I have not forgotten Ms Veronica Blair and Mrs Jodie Parke from financial services who helped contact the suppliers and purchase the equipment. Enormous thanks to Ms Libby Collett for proofreading this thesis.

A big thanks to my parents and siblings for their endless support throughout my studies. My wife, daughter, and son, who helped brighten life in Australia. Also to my extended family members and my friends for their direct or indirect support. Their support in this manner is much appreciated.

Last but not least, I would like to express my greatest appreciation to Al-Zaytoonah University of Jordan (ZUJ) which sponsored my studies. Without them, I would not have been able to achieve my goal.

To those whom I failed to mention but have been a great part of this endeavour, thank you.

Yousef Altork

University of Southern Queensland
May 2021

TABLE OF CONTENTS

LIST OF FIGURES

LIST OF TABLES

APPENDIX A

APPENDIX B

NOMENCLATURE

Symbol	Description	Units
Notation		
A_f	Cross sectional area of flow passage of one channel	m^2
A_t	Total cross-sectional area of one channel	m^2
a	Half height of flow passage of one channel	m
b	Half width of flow passage of one channel	m
C	Perimeter of air flow passage of one channel	m
$\dot{C}$	Capacity flow	W/K
c_p	Specific heat at constant pressure	kJ/kg K
De	Dehumidification capability	kg-water-vapor/kg-dry-air
D_h	Hydraulic diameter of flow passage of one channel	m
D_G	Gas phase diffusivity including ordinary and Knudsen diffusivity	m^2/s
D_k	Knudsen diffusivity	m^2/s
D_m	Mass diffusion coefficient of vapour in the air	m^2/s
D_o	Ordinary diffusivity/molecular diffusivity	m^2/s
D_s	Surface diffusivity	m^2/s

Symbol	Description	Units
f	Area ratio of air flow passage to the whole channel	--
Gz	Graetz number	--
h_{fg}	latent heat of condensation (water vapour)	kJ/kg
h_{vap}	latent heat of vaporization	kJ/kg
K_y	Coefficient of mass convection	kg/m^2 s
k	Thermal conductivity	W/m K
L	Desiccant wheel thickness	m
Le	Lewis number	--
m	Molecular weight of water	kg/mol
$\dot{m}$	Mass flow rate	kg/s
N	Desiccant wheel rotational speed	RPH
Nu	Nusselt number	--
Nu_{FD}	Nusselt number for fully developed region	--
P	Pressure	Pa
Pr	Prandtl number	--
P_{vs}	Saturation pressure of water vapour	Pa
$\dot{Q}_c$	Cooling load	W
q_{st}	Heat of sorption	kJ/kg adsorbate
r	Pore radius of the adsorbent	m
Re	Reynolds number	--
RH	Relative humidity	%
Sh	Sherwood number	--

Symbol	Description	Units
T	Temperature	°C, K
t	time	s
u	Velocity	m/s
W	The equilibrium isotherm of desiccant material	kg-adsorbate/kg-adsorbent
$\dot{W}$	power	W
Y	Specific humidity	kg-water-vapor/kg-dry-air
z	Axial direction	--

Greek symbols

α	Convective heat transfer coefficient	kW/m^2 K
δ	Channel wall thickness	m
ε	Desiccant porosity	--
η	Effectiveness	--
θ	Sector angle	degree
μ	Dynamic viscosity	Pa.s
μ_0	Initial dynamic viscosity	Pa.s
Φ	Volume ratio of desiccant material in layer (without desiccant $\Phi = 0$)	--
ρ	Density	kg/m^3

Subscripts

a	Air

Symbol	Description	Units
ad	additional	
atm	Atmospheric	
comp	comparison	
d	Desiccant material	
db	Dry bulb	
deh	Dehumidification	
evap	Evaporative cooler	
exch	Heat exchanger	
lat	Latent	
l	Liquid water	
m	Matrix	
p	Process	
r	Regeneration	
sen	sensible	
sg	Silica gel	
v	Water vapour	
wb	Wet bulb	

Abbreviations

CFC	Chlorofluorocarbon
COP	Coefficient of performance

Symbol	Description	Units
DCOP	Dehumidification coefficient of performance	
DW	Desiccant wheel	
EER	Energy efficiency ratio	
HCFC	Hydro-chlorofluorocarbon	
HFC	Hydro-fluorocarbon	
HVAC	Heating, ventilation, and air conditioning	
PDE	Partial differential equation	
RPH	Revolutions per hour	
rpm	Revolutions per minute	
SAE	Specific adsorption energy	
SDC	Solid desiccant cooling	
SER	Sensible energy ratio	
VCC	Vapour compression cycle	

CHAPTER 1: INTRODUCTION

1.1 Background

The energy consumption of Heating, Ventilation, and Air Conditioning (HVAC) and refrigeration systems are continuously increasing and at a rapid rate. The Department of Environment and Energy (2013) stated that Australia's energy consumption on HVAC in 2012 was approximately 40% of total building consumption and 70% of the base building consumption. The latter refers to that part of a multi-tenant building that directly serves and affects all tenants such as the building envelope and primary mechanical and supply systems. Moreover, based on data collected in Paris, it has been projected that 15% of the generated electricity worldwide is utilised for air conditioning and refrigeration systems (Choudhury et al. 2010). The majority of demands for HVAC come from the conventional Vapour Compression Cycle (VCC) systems, which consume a high amount of electricity.

In 2019, Australia's total electricity generation was 265 TWh (Department of the Environment and Energy 2020). Figure 1.1 shows that of all Australian electricity generation sources; only 21% of the total generated electricity was from renewable energy sources. Based on the findings of Choudhury et al. (2010), about 40 TWh of the electricity generated was used to operate air conditioning and refrigeration systems.

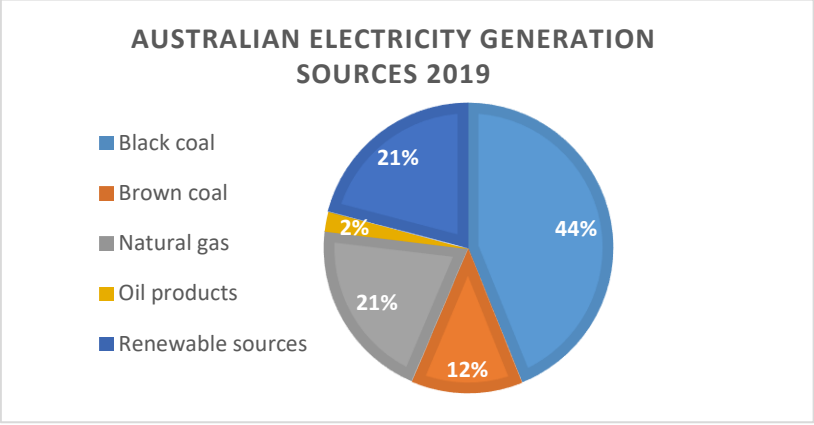

Figure 1.1: Australian electricity generation sources 2019 (Department of the Environment and Energy 2020).

The high reliance on HVAC and refrigeration systems on the use of electricity has led to the rise of greenhouse gases and has contributed to global warming (IEA 2005; Zouaoui et al. 2017). In addition, these traditional cooling devices use refrigerants like CFCs which are considered to be the main contributing factor for ozone layer depletion (Jani et al. 2016; Sahlot & Riffat 2016). Alternatives to CFC refrigerants such as HFCs and HCFCs are used nowadays. Although these refrigerants have less effect on the depletion of the ozone layer compared with CFCs, there are still a number of adverse consequences (Manzer 1990) caused by their use.

New technologies based on renewable energy sources are currently taking the place of the traditional methods of cooling. Some of these technologies are wholly operated by renewably generated electricity such as solar electric compression refrigeration (Fong et al. 2010). Other technologies depend on both thermal energy and electricity. The Solid Desiccant Cooling system (SDC) is one example of thermal-based cooling technique.

SDC systems have several significant advantages over other systems, especially VCC systems, including:

1. The regeneration temperature does not need to be too high (e.g. 50-80°C). Therefore, it can be obtained from renewable energy or waste sources. Accordingly, a substantial amount of energy saving can be achieved.
2. On a cost basis, the desiccant materials are inexpensive and widely available
3. The working refrigerants in the SDC system are air and water, and the most commonly used desiccant materials are silica gel, zeolite, and molecular sieve. Thus, both the refrigerant and the desiccant material are environmentally friendly
4. SDC systems, with the use of renewable energy and desiccant material, reduce air humidity that decreases the amount of energy required to cool (or warm) air

temperature. In contrast, because VCC systems treat the two latent and sensible heats simultaneously, they consume a large amount of electrical energy

5. The bond between the water vapour and the solid desiccant materials is not chemically based. Therefore, it is less subject to corrosion.

1.2 The principle of operation

The core principle of the operation of the SDC system is adsorbing water content from the process air. The main components of the system, represented by boxes in Figure 1.2 (a), are the Desiccant Wheel (DW), the sensible heat exchanger, the cooling unit (containing the cooling coil), and the heat source for the regeneration process.

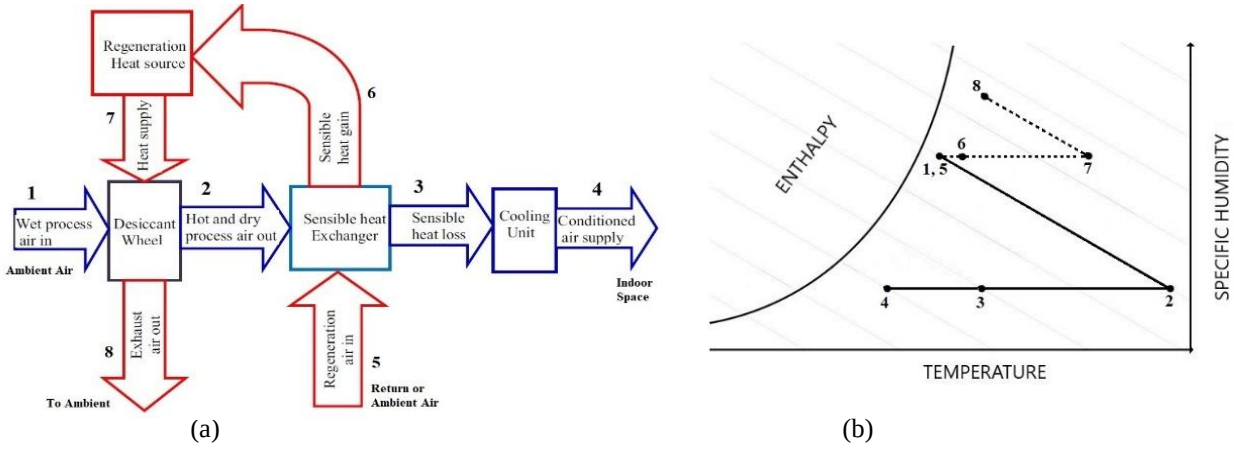

Figure 1.2: The principle of SDC (Jani et al. 2016). (a) Flow chart of cycle (b) SDC cycle on psychrometric chart (1-4 for process air, 5-8 for regeneration air). The blue arrows represent the process air and the red arrows represent the regeneration air.

Here comes the illustration of processes in Figure 1.2, the wet process air from the atmosphere at point ① enters the SDC system from the DW to remove the latent load. The DW adsorbs the air moisture and its absolute humidity decreases. As will be explained later, the temperature of the DW is higher than the ambient temperature that increases the process air temperature as shown in Figure 1.2 (b) (①→②). Air temperature at point ② is higher than the ambient temperature. Hence, ambient air can be used to reduce the air temperature. As shown in Figure 1.2 (b), process (② → ③) does not change the absolute humidity but will reduce the

temperature to a level slightly higher than the ambient temperature (see T_3 and T_1 in Figure 1.2 (b)). In some cases, return air from air-conditioned space might be used. In these case, T_3 could be less than the ambient temperature (T_1). Following this, another air cooling process (③→④) takes place by either VCC system or indirect evaporative cooler to reduce the air temperature and achieve a desired thermal comfort level. Therefore, the air temperature decreases and the air absolute humidity remains constant (③→④) if the temperature does not drop below dew point temperature.

DW temperature is higher than the ambient temperature due to the supplied thermal energy to the regeneration section. The thermal energy used to reactivate the coated desiccant material in the DW and to maintain the dehumidification of process air. The regeneration process starts at ⑤ where ambient air or return air from the indoor space or a combination of these enters the sensible heat exchanger in order to cool the process air. Accordingly, the temperature of the regeneration air increases with no change in absolute humidity. Further temperature increment occurs in the regeneration heat source from renewable energy, waste or electrical sources which provide the regeneration air with the required heat (⑥→⑦) to be able to reactivate the DW. The hot air passes through the regeneration section of the DW to adsorb moisture (⑦→⑧) and then the hot air with the high humidity discharges to the environment. Through the process (⑦→⑧), the regeneration air temperature decreases, while the absolute humidity increases.

The basic aspect of the SDC system is the DW which is responsible for dehumidification process. Figure 1.3 shows the detailed processes through the DW. The DW rotates continuously through two air streams that split it into two separate sections. The first section is where the process air passes and loses the water content because of the adsorbing material on the wheel (①→②). The hot regeneration air passes through the second section to reactivate the

desiccant (⑦→⑧) (Narayanan et al. 2011). The air streams through points ① and ⑧, as well as ② and ⑦, do not mix because each air stream passes through different channels.

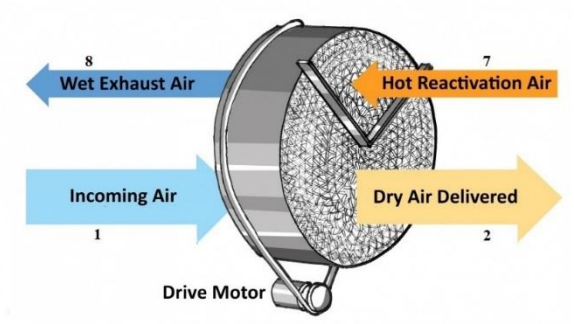

Figure 1.3: Desiccant Wheel with stream flow points (Misha et al. 2015)

During the adsorption process, an amount of heat called "the heat of sorption", is discharged from the desiccant material. This heat is transmitted through the supporting material to the flowing air which decreases the sorption capacity. Thus, both mass and heat transfer in the DW should be considered at the same time to simulate the system (Ge et al. 2008).

Considering the DW as an open system, both mass (moisture) and energy are conserved in the air streams and the desiccant material. The moisture conservation includes moisture content in the air and the desiccant material, the variation of moisture due to the axial flow of the air and the convective mass transfer, and mass diffusion within the solid desiccant in the axial direction. The energy conservation includes energy content in the humid air and desiccant material, the rate of energy variation in the air along the axial direction, the heat conduction in the air and desiccant material, the convective heat transfer between the air and solid desiccant, and the sensible heat transfer between the air and solid desiccant.

The review of the available international literature revealed that there is a lot of inconsistency between the results due to different operating conditions and designs, for example, the reported optimal rotational speed was varied between 4 to 100 RPH among different studies as will be discussed in details in chapter two. Here comes the importance of generalising the outcomes to

be applicable on more cases by applying the dimensional analysis technique. Also, there are very few studies that considered the channel geometry and design parameters.

1.3 Research objectives

The main aim of this study is to develop the operation of the DW to be more environmentally friendly by being able to operate at the highest possible efficiency under different climate conditions.

The main objectives of this study are:

1- To identify the parameters that affect the DW performance and combine these parameters into fundamental non-dimensional groups.
2- To validate the non-dimensional groups using experiments and simulations.
3- To determine the optimal values of the DW non-dimensional groups in order to reduce the overall required energy.
4- To study cases that have not previously been investigated.

1.4 Research limitations

The limitations of the research are outlined through the following:

1. The focus of this study will be on silica gel as a desiccant material for the DW. Therefore, the results cannot be generalized for different materials unless the same methodology is followed and the results match the outcomes of silica gel DW.
2. To emulate the high temperature and humidity conditions, an auxiliary heater and a humidifier is used in the inlet of process and regeneration air sections. LPG heater is used for heating the regeneration air, while the electric heater is used for the process air.

3. The DW used in this study has a sinusoidal channel, which is the most common, geometry. Some calculations in the simulation model are just applied for the sinusoidal channel. So in the case of different channel geometry, the channel geometry equations should be changed in the model.

1.5 Thesis organisation

This thesis has been presented in eight chapters.

Chapter one provides background and the advantages of the SDC systems, their principles of operation, the research aim and objectives, and the research limitations.

Chapter two rviews some of the previous studies related to SDC systems and divided them into historical backgrounds, economical comparison between SDC and VCC systems, parameters affecting desiccant wheel performance, and mathematical modelling of DWs.

Chapter three presents the mathematical model used to simulate the DW, the selected control volume, the model assumption to simplify the model, the governing equations that related to the desiccant material and the humid air which applies mass and energy conservation principle, the initial, boundary and auxiliary equations, the solution method followed to solve the governing equations, and finally the model validation by three different published experimental outcomes.

In chapter four, the experimental setup of the DW is presented. It also includes the main components of the DW system and the attachments, the DW specifications, the measuring and control devices, the system operation, the experimental and simulation data analysis, the performance indexes, and finally the experimental accuracy and uncertainty.

Chapter five starts with a brief introduction about the dimensional analysis method and its benefits for the experimental part of engineering study. Then, the extracted DW parameters to

form the non-dimensional groups from the presented mathematical model in chapter three are presented. Afterwards, the non-dimensional groups selecting criteria and methodology and the devised non-dimensional groups are also presented. Last and most importantly, testing the non-dimensional groups experimentally and through the simulation model in term of the non-dimensional performance indexes, which is presented in chapter four, is explained in detail in this chapter.

Chapter six presents the experimental and computational results of varying the non-dimensional groups in term of the performance indices in order to identify the non-dimensional groups operating range. Next, two of the non-dimensional groups are varied at the same time in order to investigate the effect of these non-dimensional groups on the system performance and to study the relationship between each of the non-dimensional groups.

In chapter seven, optimizing the non-dimensional groups is presented referring to the energy consumption, which is the main advantage of applying SDC systems. The optimisation is carried out by comparing the SDC system combined with VCC system and a standalone VCC system. Assuming the regeneration heat is supplied by a solar thermal source, a new performance index is presented for the purpose of comparison and optimisation.

Chapter eight provides a brief summary of the overall work of this study, the conclusions that have been arisen, and recommendations for future works.

CHAPTER 2: LITERATURE REVIEW

2.1 Introduction

Air conditioning systems are used to improve indoor air quality in order to reach the human comfort zone. In hot and humid countries, both cooling and dehumidification processes are essential for air treatment. The traditional methods of air conditioning deal with both latent and sensible loads by cooling the air below the dew point temperature which requires a high amount of electrical energy (Niemann et al. 2019). However, the desiccant material in SDC systems removes the latent load in the early stages before cooling the process air. Therefore, it will reduce the required energy especially if the SDC system powered by renewable energy sources.

It is essential to study the SDC system, its physical characteristics, and the parameters that affecting the system performance in order to operate the system in an optimum way and achieve the highest possible energy saving. Therefore, several mathematical models of the DW have been proposed for a better understanding of their operation and realising the effects of the operational parameters on their performance.

This chapter, as outlined in Figure 2.1, reviews previous studies on SDC systems and is divided into historical backgrounds, economical comparison between SDC and VCC systems, parameters affecting DW performance and mathematical modelling of DWs.

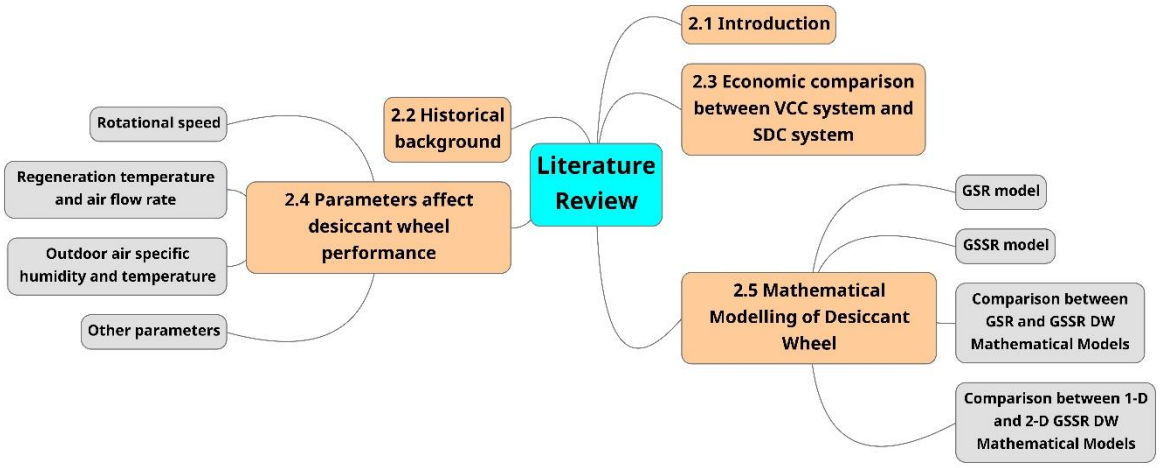

Figure 2.1: Literature review outline and roadmap.

2.2 The timeline of utilizing the SDC systems

Several studies have researched the SDC system from the middle of the last century until the early 1980s. Pennington (1955) suggested the first novel design for desiccant cooling by combining the rotary dehumidifier with a regenerative heat source and an evaporator cooler. Later, Dunkle (1965) suggested the same cycle with an additional heat exchanger and a molecular sieve as adsorption material. Subsequently, Lunde (1976) used the silica gel as a dehumidification medium and the regeneration heat was provided by a solar thermal system. Thereafter, Nelson et al. (1978) evaluated two different configurations of solid desiccant solar-powered open-cycle air conditioning system, ventilation and recirculation modes, and they found that a mid-sized area of flat plate solar collector can contribute sufficiently to overcome the sensible and latent loads. After this, a significant number of studies have been conducted to advance the performance of the SDC system by coupling the system to other systems or modifying the configuration.

2.3 Economic comparison between VCC system and SDC system

Ge et al. (2010) compared the thermodynamic and economic performance for a solar-driven desiccant cooling system containing two DWs with a VCC system. A cooling space of one

floor of a commercial building with 1550 m^2 in area and 6300 m^3 in volume in Berlin and Shanghai were used for this comparison. They found that the cooling load for the floor in Shanghai was 10% higher than in Berlin since Shanghai has higher ambient air temperature and solar radiation intensity. Both systems were able to meet the cooling load, but the desiccant cooling system was superior as it provided a higher level of fresh air with comparing with VCC system. The obtained economic results show that the initial cost for the desiccant cooling system was higher than the VCC system (€14790 in Berlin and €9980 in Shanghai), and however, the operating costs —including the energy and maintenance costs— for the desiccant cooling system was 3610 €/year and 1720 €/year lower than the VCC system in Berlin and Shanghai respectively. As a result, the payback period for the desiccant cooling system was 4.7 years in Berlin and 7.2 years in Shanghai.

Kousar et al. (2021) presented a detailed technical and economic evaluation and performance analysis of various configurations of the solar-assisted desiccant air cooling system. In general integration, a variety of solar-assisted desiccant cooling system configuration variants are considered, including (1) direct evaporative cooler on the process side and on the regeneration side; (2) direct evaporative cooler on the process side and counter flow type on the regeneration side with indirect evaporative cooler; (3) indirect counter-flow evaporative cooler on the process side and on the regeneration side. The technical evaluation is to evaluate the performance of all considered configurations of the solar-assisted desiccant cooling system. For economic feasibility assessment, all settings were tested under various operating conditions over 15 different selected dates in a typical summer. These operating conditions included different intake air temperatures, humidity, and solar radiation to obtain realistic estimates of system performance. The results of the seasonal tests show that the maximum values of the coefficient of performance of the first three configurations were 0.76, 0.99, and 1.85, and the maximum energy efficiency ratios were 7.19, 8.73, and 13.3, respectively. Using experimental

data, economic analysis shows that compared with the traditional system, the third configuration may save up to 62.9% of energy costs, with a payback period of 5.87 years.

In addition, many researchers such as Halliday et al. (2002), La et al. (2011), and Kabeel and Bassuoni (2013) studied the economic feasibility of the SDC system either coupled with a conventional VCC system or a standalone. They found that utilizing the SDC system can achieve a reduction in the power consumption up to 39%.

2.4 Parameters affect desiccant wheel performance

A large number of studies have been conducted to improve the performance of the SDC system. Some of these studies consider the operational parameters and other studies concentrate on the shape, geometry, configuration and the adsorbing material. This section will first present the effect of rotation speed on the DW performance. Then, it will focus on the other parameters' influence on the SDC system performance.

2.4.1 Rotational speed

The DW rotational speed is one of the major parameters that have a considerable effect on the system's overall performance and the system's energy consumption. Thus, many researchers have taken this topic into consideration when they analyse the SDC system and its components. The following studies demonstrate the optimal DW rotational speed in various working conditions.

2.4.1.1 The optimal DW rotational speed with respect to system performance

An experimental investigation was carried out on an open cycle desiccant cooling system operating in a ventilation mode at a laboratory site in Gaziantep University in Turkey (Çarpinlioglu & Yildirim 2005). Some different operational parameters like rotational speeds of the DW, air mass flow rate and regeneration temperature and their influence on the overall

performance were studied. The tested rotational speed of the DW was varied from 6 to 24 RPH. The air mass flow rate was found to be independent of the DW rotational speed and the regeneration temperature in the ranges tested. Furthermore, neglecting the influence of both the regeneration temperature and the mass flowrate by keeping them constant, the increase in the system COP (defined by the ratio of cooling capacity to regeneration thermal power) and cooling capacity were achieved by decreasing the value of the DW rotation speed to 4 RPH.

Chung and Lee (2011) analysed the effect of several operational parameters including air flow rate, air humidity, DW rotational speed and regeneration temperature regarding the system performance. They found that the regenerative temperature was the superior parameter that most affects the operational cost. In addition, the optimal rotation speed was 24 RPH.

Subramanyam et al. (2004) presented an experimental integration of a DW and a VCC system for low humidity air conditioning. In addition, the impact on the overall performance of some parameters such as compressor capacity, airflow rate and DW rotational speed were assessed. They found that the optimal DW rotational speed of 17.5 RPH achieved the highest COP and humidity removal.

A mathematical model is presented by Ge et al. (2010) to predict the performance of a new design utilising a compound silica gel haloid DW. They analysed the effect of some parameters such as the regeneration central angle, process air speed, the regeneration temperature, and the rotational speed on the overall performance. They found that a higher regeneration central angle maximises the moisture removal and the recommended value between 100° and 160°. Also, process air speed between 2.0 m/s and 3.5 m/s, and regeneration temperature in the range of 80-95°C are recommended. The optimal achieved speed was 12 RPH which maximised the moisture removal capability.

A DW numerical model was developed by Mandegari et al. (2014) to focus on the energy analysis for the DW. The model studied the energy effectiveness of the DW by varying the DW regeneration temperature and speed. They found that the optimal results of 21.2 RPH for the rotational speed and 61.9°C for the regeneration temperature to reach the minimum value for specific adsorption energy.

An investigation of the supply and regeneration areas' effect on performance was carried out experimentally (Zendehboudi & Esmaeili 2015) by examining some operational parameters like outlet air humidity, process removed moisture as a function of rotational speed and air specific humidity. A constant regeneration temperature of 80°C and a range of rotational speed of 4-12 RPH were used in the study. One of the obtained results was an increase in the rotational speed of the DW causing a reduction in the removal of moisture and an increase in the specific humidity of the process air, as well as an increase in air outlet temperature.

Heidarinejad and Pasdarshahri (2010) numerically studied the influence of the rotational speed of the DW and the regeneration temperature on system performance as well as output process air temperature by testing various operating models and validating the simulated with experimental results. They found that each model has specific optimal operational values, which reduce the energy consumption and minimise the output process air temperature.

Ruivo et al. (2015) experimentally investigated the effective parameters on the DW rotational speed from the measured and manufacturer's software data. The regeneration air was heated using either, a micro-cogeneration or a boiler, or both to a moderate temperature. One of the obtained results was that rotational speed affects enthalpy and dehumidification effectiveness parameters in various ways. For example, the enthalpy effectiveness parameter, which represents the ratio between the enthalpy increase on the process air to the maximum enthalpy

difference, increases with an increment in the rotational speed while a rotational speed of 10 RPH maximises dehumidification effectiveness.

2.4.1.2 The optimal DW rotational speed for different desiccant materials and operational parameters values

Ge et al. (2008) aimed to reduce the volume of the two-stage Desiccant Wheel's cooling system without affecting the system performance by coupling the two desiccant wheels with one rotor. Furthermore, different wheel thicknesses were tested under hot and humid conditions with various rotational speeds. The diameter of all used DWs was 400 mm. They found that a 100 mm wheel thickness was better than either 70 mm or 40 mm. For a 100 mm wheel thickness, the optimal speed was in the range of 4-8 RPH.

A study by De Antonellis et al. (2010) was carried out using a 2.5.1 GSR mathematical model and related computational results to investigate the desiccant wheel performance and optimisation. This model was used to show the effect of the working conditions on the DW rotational speed as well as DW performance. It was found that there were several optimal rotational speeds according to each specification. For example, if the rotational speed is high at low process air velocity, the desiccant material will take longer to cool down to start the dehumidification process and that affect negatively the dehumidification capacity.

Eicker et al. (2012) experimentally investigated the performance of several commercial DWs and determined the parameters that affect the DW performance. They found that the optimal rotational speed was lower if the absorption material was lithium chloride with rotational speed lying between 20-30 RPH, while, in the case of a silica gel material, the optimal rotational speed was between 85-100 RPH. The variation in the optimum rotational speed for the different desiccant material DWs is due to different sorption and matrix materials with higher dynamics for the adsorption processes.

Ahmed et al. (2005) presented a numerical model to evaluate the effect of the design parameters, including wheel thickness, wheel porosity and rotational speed and some other operational parameters, on DW performance. Additionally, they constructed an SDC system to validate the simulation model and to obtain an accurate performance under Cairo's climatic conditions. They found a good agreement between the experimental and simulation results. In addition, from the performance curves for various parameters, they found that each wheel thickness matched an optimal rotational speed to achieve the best performance under specific operational conditions.

Using MATLAB Simulink, a heat and mass transfer model of a DW for ventilation purposes in the air conditioning system was introduced by Nia et al. (2006). They studied the performance of the adiabatic DW as well as the optimal rotational speed for the outlet humidity profile. Furthermore, the simulated model was validated by comparing the actual experimental result from the previously published work with the model results. They found that both the actual and simulated results converged with a small error. They developed correlations between the processed air conditions as a function of the input parameters to simulate the SDC system and obtain the efficiency year-round. They found that the optimal rotational speed was at 15 RPH.

2.4.2 Regeneration temperature and air flow rate

Joudi and Madhi (1987) experimentally investigated a solar-powered desiccant cooling system under Basrah's (Iraq) climatic conditions with a constant regeneration temperature equals to 70°C by an auxiliary electric heater. The performance of the solar air heater was analysed and compared experimentally and theoretically. They found that the maximum average seasonal COP value was 2.8, which was obtained at 0.075 kg/s process air mass flow rate, and an

improvement in the performance could be achieved by higher values of the regeneration temperature of the range 55 - 75°C.

Camargo et al. (2005) presented a desiccant cooling system coupled with evaporative coolers, a counter-flow heat exchanger following the evaporative cooler, and the thermodynamic equations of the system. In addition, the paper analysed the influence of some operational parameters such as regeneration temperature, regeneration airflow/ process airflow (R/P) relationship and the thermodynamic conditions of the entering airflow on the system performance in muggy weather conditions. They found that it is better for the evaporative cooling technique and for the system as a whole to operate at a minimal value of both the regeneration temperature for the range of 115 - 160°C and R/P for the range 0.375 - 0.675. Moreover, it was found that the system was able to achieve human thermal comfort even in humid climates.

Yong et al. (2006) performed a number of experimental tests on a hybrid desiccant cooling system with LiCl adsorption material under high humidity climatic conditions. It was shown that both the regeneration temperature and airflow rate have a significant impact on system performance. Additionally, they found that the hybrid system can achieve higher performance and can meet the cooling demand around the year in high humidity locations.

Panaras et al. (2010) presented theoretically a desiccant air-conditioning system. The system was validated through a number of real experimental tests results. Different operational parameters such as weather conditions, airflow rate, and regeneration temperature and their influence on the system performance were studied. The authors found that the cooling load can be met by the proposed system and the influence of the operational parameters are as follows: both the air flow and regeneration temperature have a noteworthy impact on the system performance, and the regeneration temperature must lie between a specific range 60 – 80°C to

meet the required cooling capacity. In addition, an inverse relationship between the process air flow and the overall system COP was observed. Thus, a minimal possible value for the regeneration temperature with a convenient value for the air flow rate leads to an optimal value of the system COP.

Angrisani et al. (2012) experimentally investigated the performance of an SDC system powered by a low-grade temperature of 65°C supplied by a micro-cogenerator. The investigation took place as a function of regeneration temperature, the inlet process air specific humidity and temperature and the ratio between process and regeneration airflow rates. They found that the regeneration temperature has a higher effect on the dehumidification process than the regeneration airflow rate. Furthermore, regarding the DW performance, the process air specific humidity and regeneration temperature affect more than the process air temperature at fixed regeneration temperature (65°C).

Comino and Ruiz de Adana (2016) studied the effect of varying the airflow rate and the regeneration temperature on the system moisture removal capacity, sensible heat ratio of the DW at low temperature and the outlet process air condition using three simulated case studies. They found that a decoupling of the outlet air temperature and specific humidity is possible when the mentioned parameters are varied. Several values for the system moisture removal capacity were obtained when the sensible heat ratio value was constant, and vice versa. Furthermore, a control strategy was suggested for the DW to control the values of the system moisture removal capacity and the sensible heat ratio by adjusting the airflow rate and the regeneration temperature values.

2.4.3 Outdoor air specific humidity and temperature

A paper written by Kanoğlu et al. (2007) presented both the ventilation and recirculation cycle of SDC systems. The effect of ambient temperature and relative humidity were studied for both

cycles in terms of the COP and cooling load. They found that the ventilation and recirculation COPs for the system are 1.17 and 1.28, respectively. Additionally, it was found that both the COP and the cooling load decreases with increasing the ambient temperature and relative humidity and their values draw near zero at a high ambient temperature and relative humidity values.

Angrisani et al. (2011) experimentally analysed a Silica-gel DW included in an AHU coupled with a small chiller, gas boiler, and small cogenerator which were used to regenerate the DW. They also experimentally studied the influence of outdoor air humidity and temperature and regeneration temperature on DW performance. Finally, at a fixed regeneration temperature equals to 65°C, both the ventilation and internal latent loads were estimated, and a comparison was conducted with the required values in a number of cities around the world. The results reveal useful performance information for a DW powered from microgenerator low-level temperature. For a specific humidity higher than 15.5 g-water/kg-dry-air, the DW can handle the ventilation load only for low outdoor temperature, proving that the process air inlet temperature significantly affects the DW dehumidification process.

El-Agouz and Kabeel (2015) analysed a novel SDC system consisting of solar collectors, heat exchanger, DW, evaporative cooler, and ground heat exchanger. Some operational parameters were studied such as inlet air temperature, inlet air humidity, regeneration temperature, and heat exchanger effectiveness. They found that the efficiency of the solar collector increased with the increase in the inlet air temperature while it decreased with increasing inlet air specific humidity, regeneration temperature, and cooling coil unit effectiveness. The DW effectiveness increased with the increase in inlet air temperature and inlet air specific humidity, while it decreased with an increase in the regeneration temperature.

El-Agouz et al. (2018) theoretically investigated the performance of humidification–dehumidification desalination unit using DW or heat exchanger. They studied the influence of some parameters, such as inlet water and airflow rates ratio, inlet hot water temperature, inlet cooling water temperature, inlet air humidity and regeneration temperature, on fresh water production, gain output ratio, specific thermal energy, and recovery ratio to present the optimal values. They observed that the desalination unit using DW is better than that using a heat exchanger. Related to gain output ratio and specific thermal energy, some parameters, such as inlet cooling water temperature and inlet air humidity, had a minute effect, while inlet water and airflow rates ratio, inlet hot water temperature, and regeneration temperature had a notable effect.

2.4.4 Other parameters

Ge et al. (2012) theoretically presented and analysed a solar-powered desiccant cooling system under Shanghai conditions which are hot and humid in summer. They integrated each subsystem mathematical model to determine system performance and feasibility. Some operational parameters were also analysed. They showed that the cooling power in June and July were 2.9 kW and 3.5 kW and the solar COP, defined by cooling power divided by solar energy collected (Ge et al. 2012, p. 537), were 0.22 and 0.24 respectively, so the system could have met the cooling demand in these two months. But in August, the system needed about 2 minutes of switch time, which is the operation time in the dehumidification process, to provide the required cooling demand, and the cooling power could have reached up to 5 kW. In addition, it was found that by enlarging the area of the solar collectors, increasing the heated water flow rate by the solar system and reducing the volume of the water tank, the cooling power increases, but does not have a significant effect on the solar COP.

Rafique et al. (2016a) developed a mathematical model for a desiccant cooling system. The performance and the feasibility of the system were studied under Dhahran's (Saudi Arabia) climatic condition. A number of operating parameters were studied using performance curves to obtain the optimum values. They found that at 1.62 kg/s process airflow rate, a maximum amount of moisture removal at 17 g-water/kg-dry-air was achieved in July, while the cooling load value was 39 kW. By increasing the process flow rate to 2.15 kg/s the cooling load increased to 52 kW. Therefore, from the performance curves, the optimum value for process airflow rate at a required regeneration temperature can be obtained to ascertain the best COP value. An increment in the sensible energy ratio was noticed with increasing the inlet specific humidity, while it decreases with increasing inlet air temperature, regeneration temperature, and the ratio of regeneration to process airflow rate.

Similarly, in another paper, Rafique et al. (2016b) theoretically analysed the performance of the SDC system under five different cities in Saudi Arabia which are Jeddah, Jazan, Riyadh, Hail, and Dhahran. Jazan has the highest outdoor specific humidity among the mentioned cities which equals 20.06 g-water/kg-dry-air, while Hail is the lowest with 15.93 g-water/kg-dry-air. They found that the COP values ranged between 0.275 and 0.476. In addition, they found that the best value for moisture removal capacity occurred in Jazan while the minimum value was in Hail. A 15% increment in the evaporative cooler effectiveness caused a 15-25% improvement in the system COP depends on the city. Furthermore, the system COP decreased with increasing both the regeneration temperature and the airflow rate while the DW effectiveness increases with increasing ambient air specific humidity.

Ma et al. (2017) studied the effects of some operational parameters such as solar collector area, storage tank volume, backup heater capacity, and outdoor air specific humidity on the system performance under Brisbane's climatic condition. The last parameter, which is outdoor air specific humidity, was studied to control the on-off operation of the DW. The results show that

the solar collector area and the storage tank volume have a bigger influence on system performance. An increase in collector area or tank volume causes an increment in the solar fraction (defined by the ratio of solar energy contribution to the total energy input), the system COP, and a reduction in the backup heater energy consumption. Moreover, to reach the human comfort level and achieve low backup heater energy consumption a set point of 8.0 g-water/kg-dry-air was set for the outdoor air specific humidity.

2. 5 Mathematical modelling of DW

The standard and universal method to construct a DW mathematical model is by applying both mass and energy conservation principles. Other simplified or empirical models are also developed to simulate the DW, but their application is limited to a specific range of working condition. Two main models are used to simulate the process in the DW: Gas Side Resistance (GSR) models, and Gas Solid Side Resistance (GSSR) models. GSR models consider the convective heat and mass transfer between the air stream and the desiccant (Chung et al. 2009), while GSSR models consider also the heat conduction and mass diffusion within the solid desiccant layer (Ge et al. 2010). This section presents the related research that uses GSR model or GSSR model to simulate the DW, then a comparison between both models and between 1-D and 2-D GSSR models will be presented in order to prove the effectiveness of the 1-D GSSR model.

2.5.1 GSR mathematical model and related computational results

Charoensupaya and Worek (1988) presented a 1-D theoretical adiabatic, open-cycle DW model operating in ventilation mode. They studied the effect of channel length, mass fraction and desiccant isotherm. The results showed that the maximum achievable COP was 1.4 under certain parameters values.

Zheng and Worek (1993) developed 1-D mass and heat transfer DW model. The finite-difference method was used to solve and simulate the model. The effect of rotational speed on the adiabatic DW performance was studied by examining the output humidity profile of the process section. They found that there is an optimum rotation speed for every operating condition.

Simonson and Besant (1997), from the physical principles of heat and moisture transfer, developed a 1-D numerical model to predict the DW performance. Also, they used the model to identify the sensible, latent and total energy transfer effectiveness for different design and conditions. In this model, the energy released during water transfer from and to process air was included. It was found that energy diffusion has a significant impact on the system performance in the case of thin desiccant wall thickness.

Zhang et al. (2003) presented a 1-D mass and heat transfer model to analyse the temperature and humidity output profile from both sections: process and regeneration. The model was validated by real experimental DW. Some parameters such as regeneration temperature and air speed for regeneration and process air were studied. It was found that the temperature and humidity profile acts as a hump curve moving from the channel entrance to exit, thereby varying the maximum value within the channel. Therefore, to improve the DW performance, it was necessary to accelerate the hump motion which happened with high regeneration temperature and air speed values.

Golubovic and Worek (2004) studied the effect of inlet process and the regeneration of pressurised air on desiccant material separation factor and water condensation. A 1-D mathematical model solved by the implicit finite-difference method was developed. Unlike previous studies, they included water condensation in their model. It was found that in 40% of the regeneration section, condensation may occur due to high-pressure regeneration air. Also,

it leads to stopping the regeneration process and replacing it with the dehumidification of regeneration air instead.

Xuan and Radermacher (2005) developed a 1-D DW mathematical model. The model was used to study the DW performance in the transient condition when it acts as an enthalpy recovery wheel or for dehumidification purposes. The effect of regeneration temperature, DW rotational speed, and airflow rates was investigated. The parameters optimum values were compared with published experimental results and the manufacturer's data. A good agreement between them was achieved.

Golubovic et al. (2007) studied the influence of separation of the process air into two flows as shown in Figure 2.2: normal process air from ambient, and heated and humid air called purge air stream. A section of the DW where part of the process air passes through and produce a hot and relatively high humidity air called purge air; which mixes with the regeneration air before heating. By increasing the purge section angle (a section of the DW where the purge air passes through) the output humidity ratio decreased till reach a minimum possible value which called an effective purge angle. A 1-D mathematical model was adopted to investigate the wheel performance and compare it with a normal wheel. It was found that the wheel with an effective purge angle between 29.4º – 39.8º has better performance.

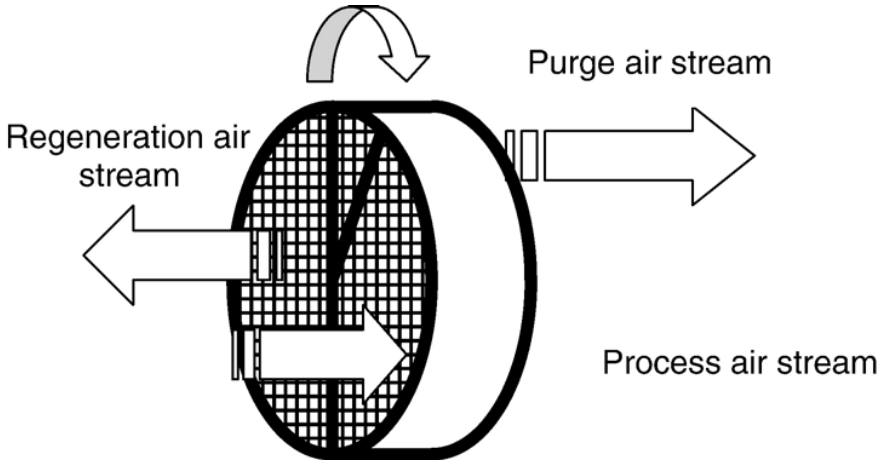

Figure 2.2: Schematic of rotary dehumidifier with purge angle.

Chung and Lee (2009) examined the optimal DW rotational speed and area ratio of process air section to regeneration air section for the regeneration temperature range from 50ºC to 150ºC. Moisture Removal Capacity (MRC) was used as a wheel performance term. A 1-D mathematical model was used to investigate the parameters influence on the MRC. They also studied the influence of the desiccant material isotherm, ambient air properties on the optimal parameters values. It was found that the desiccant material isotherm affects the optimum DW rotational speed value more than the area ratio value.

De Antonellis et al. (2015) studied numerically and experimentally the dehumidification process in the DW. A 1-D mathematical model was used to investigate the wheel performance and to optimize the configuration parameters values. It was found that the system can cover the building latent load. It was recommended that the ratio of process air flowrate to regeneration air flowrate be more than 1.3 to meet the required humidity output. Furthermore, the primary energy consumption was lower for DW system than for the electric steam dehumidifier by 3%.

Koronaki et al. (2016) predicted the performance of a DW through 1-D mathematical model. The model validated by two different desiccant material wheels; silica gel and lithium chloride. A good agreement was found. The model was used to compare the co-current and counter air flow streams. It was found that the counter-flow arrangement gives better performance.

Rafique (2016) investigated the performance of a DW through a 1-D mathematical model under different operating condition, studying the influence of process mass flowrates on heat and mass transfer coefficients. It was found that the process mass flowrate and the regeneration temperature had the most significant impact on the wheel performance. Additionally, an increase in the channel wall thickness leads to improve the dehumidification performance.

2.5.2 GSSR mathematical model and related computational results

Pesaran and Mills (1987) developed 1-D model of heat and mass transfer within the air stream and the desiccant material taking into consideration the moisture diffusion into silica gel particles. They found that surface diffusion has the most influence on moisture transfer for regular density silica gel. While, for intermediate density silica gel, both surface and Knudsen diffusion have a notable effect.

San and Hsiau (1993) proposed a 1-D mass and heat transfer DW model. They analysed the effect of axial heat conduction and mass diffusion on wheel performance. The model contains four partial differential equations solved by fully-implicit finite-difference scheme. It was found that the combination of convective heat transfer coefficient, wall thickness and desiccant material conductivity parameter had the most effect on the overall performance.

Zhang and Niu (2002) introduced a 2-D mass and heat transfer DW model including two diffusion terms; surface and a combined ordinary with Knudson. Using the model, they compared the performance of DW used as air dehumidifier and as enthalpy recovery. It was found that for dehumidification purposes the optimum rotational speed of the DW is much lower than for enthalpy recovery. On the other hand, the temperature and humidity profiles are more homogenous for enthalpy recovery DW. In both cases, the honeycomb channel shape provides better performance.

In another paper by Niu and Zhang (2002), the same mathematical model was used to study the influence of DW rotational speed, channel wall thickness and the relation between them. It was found that for every configuration there is an optimum rotation speed. Additionally, the optimum rotation speed was lower for higher channel wall thickness. And for fixed wheel mass, the thin channel wall thickness was more operational.

Sphaier and Worek (2004) developed a 2-D mass and heat transfer DW model which deals with mass diffusion and heat conduction in desiccant material. The model validated with published experimental results. It was found that the wheel performance increases with increasing mass fraction of desiccant in the wall and by decreasing the time needed for one revolution (higher rotational speed value).

Gao et al. (2005) introduced and defined 2-D DW mathematical model. The model able to present the detailed output temperature and humidity at any wheel depth and time from the process and regeneration section either in transient or steady-state condition. A good agreement between the model and experimental data was obtained. The model used to determine the effect of channel wall thickness and passage shape on the system performance. It was found that a higher value of channel wall thickness causes a time delay to reach the steady-state condition, but, a better Moisture Removal Capacity (MRC). Furthermore, regarding the passage shape's effect on MRC, it was found that the sinusoidal shape was the best, followed by a triangular shape and the worst was hexagon shape.

Ruivo et al. (2006) tested a number of hypotheses to simplify the heat and mass transfer in 1-D DW mathematical model. It was found that surface diffusion has much more effect than Knudsen diffusion which can be neglected. Additionally, the internal resistance of heat diffusion through the channel wall can be neglected due to the low impact. However, the variation in the desiccant material properties cannot be neglected for better phenomena description.

Later on, a two-part study done by researchers from Portugal considered 2-D DW mathematical model. In the first part, Ruivo et al. (2007a) compared between detailed and simplified heat and mass transfer DW models. In the simplified model, the airflow was treated as bulk flow and convective heat and mass coefficient was used to evaluate the heat and mass transfer

between the channel wall and airflow. In contrast, the detailed model did not assume the momentum transfer in desiccant material porous in the channel wall. Both models tested channel lengths ranging from 0.01 to 0.5 m. It was found that a good agreement achieved when the channel length more than 0.1 m. In the second part, Ruivo et al. (2007b) used the simplified model from part 1 to describe the phenomena in the desiccant wheel and enthalpy recovery wheel. The effect on the wheel performance of the channel dimensions, the wheel speed, and inlet air properties was studied. It was found that the model could be used for manufacturing and design purposes. In addition, the DW rotational speed and channel wall thickness are related, higher rotational speed is required when the channel wall is thinner.

Bareschino et al. (2015) evaluated a 1-D DW mathematical model called Variable Properties Model (VPM) based on changing the thermodynamic properties of humid air with temperature. The model validated by published experimental results from the literature. A good agreement was found by comparing the output temperature and humidity profiles, dehumidification performance, and dehumidification COP. It was found also that the VPM model data is closer to experimental results than the constant properties model.

Intini et al. (2015) investigated the performance of AQSOA zeolite DW numerically and experimentally. The 1-D mathematical model validated and calibrated through experiments with 0.66 g-water/kg-dry-air output humidity and 0.99ºC output temperature root mean square deviation. The model was used to study the effect of area ratio, inlet process air humidity and temperature, and air velocity on the system performance. It was found that a unity area ratio maximises the moisture removal capacity. While, at high regeneration temperature, a higher latent cooling results in a higher area ratio. Also, it was noticed that the inlet process air specific humidity highly affected the moisture removal performance, while the inlet temperature had a slight effect.

Muthu et al. (2016) developed a 2-D DW mathematical model considering both the solid-side and gas-side resistance to study the effect of the regeneration section angle on the wheel performance. The tested desiccant material was pure silica gel and composite materials. The model was validated by comparing the results with published data. It was found that the optimal regeneration section angle was between 120º and 180º. Outside this range, the moisture removal capacity dropped from 0.037g to 0.009g per angular degree.

Cheng et al. (2017) developed a 3-D DW mathematical model to describe the heat and mass transfer process in the wheel channels. Some parametric studies were conducted. It was found that the influence of specific heat capacity on moisture removal was insignificant, while a positive relationship was noticed between the thermal conductivity of the desiccant material and moisture removal. In contrast, larger desiccant porosity caused a negative impact on moisture removal capability. Also, it was noticed that a thinner channel wall thickness is more efficient and the circular channel shape was superior among other shapes.

2.5.3 Comparison between GSR and GSSR DW Mathematical Models

Narayanan et al. (2011) developed two 1-D DW mathematical models; GSR model and GSSR model. Both models showed a good agreement with published experimental results. The models were used to compare between parallel and counter air streams DW design as shown in Figure 2.3. It was found that the dehumidification process in counter flow design is better than parallel flow design. Moreover, they found that adding a cooling section to the wheel improves the dehumidification process.

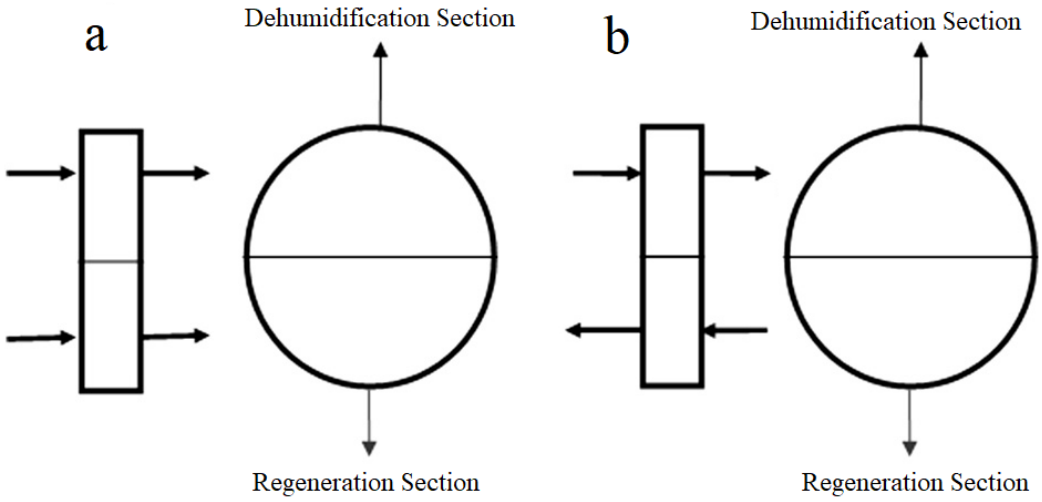

Figure 2.3: a. Parallel flow design. b. Counter flow design (Narayanan et al. 2011).

2.5.4 Comparison between 1-D and 2-D GSSR DW Mathematical Models

Sphaier and Worek (2006) presented both 1-D and 2-D mathematical model for DW and enthalpy recovery wheel and compared between them. The 1-D model is derived and it's a simple form of the 2-D model. Also, the 1-D model is easier than 2-D model and quicker in simulation. The 1-D model was ideal for DW for the low desiccant mass fraction. While for the enthalpy recovery wheel, the 2-D model is better.

Chung et al. (2009) used 1-D DW mathematical model to optimize the wheel rotational speed and area ratio of regeneration section to process section as a function of regeneration temperature. They validated the mathematical model by comparing the results with experimental results and by another paper used 2-D mathematical model done by Sphaier and Worek (2004) as shown in Figure 2.4. The results show that both 1-D and 2-D mathematical models are effective in modelling the DW for different system operational conditions.

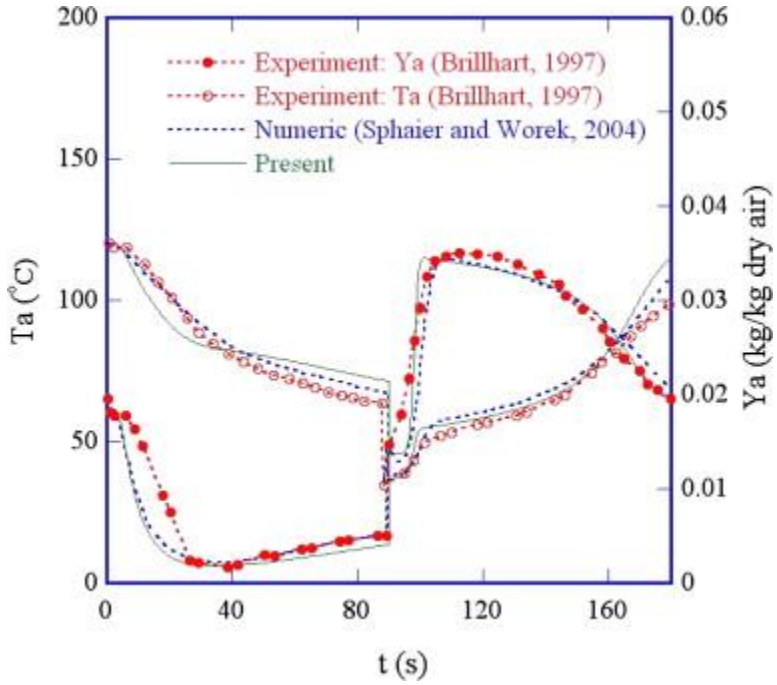

Figure 2.4: DW output temperature and humidity comparison between 1-D GSSR (in green), 2-D GSSR (in blue) mathematical model, and experimental (in red) (Chung et al. 2009).

2.6 Summary

This chapter presented a comprehensive review of the available literature of SDC system, the parameters that significantly affect the performance, and methods used to model the desiccant wheel. The main purposes of the literature review are to:

- understand the current situation of the research area,
- support the objectives of this study,
- specify the research gap,
- create the framework to conduct the research.

The key findings are summarised below.

Economically comparing the SDC system with the traditional VCC system, it was found that the initial cost of an SDC system is higher but the annual operation and maintenance costs are much less than for a VCC system. Also, it was found that the payback period for an SDC system is between 4 and 7 years.

The articles cited in section 2.4.1 are just a few numbers of the total articles that consider the rotational speed impact. It appears from the previous studies that the DW rotational speed has a significant impact on the system performance, the output condition of the process air, and the energy consumption. Correspondingly, there is a specific DW rotational speed for every configuration, adsorption material, and working parameters. It also found that regeneration temperature has the greatest influence on system performance, cooling capacity and system moisture removal capacity followed by process airflow rate. Furthermore, an optimization of the regeneration temperature and the airflow rates must be achieved to reduce the consumed energy. In addition, it noted from the previous studies that an increase in the values of regeneration temperature and inlet air temperature causes an increase of the system COP. While, an inverse relationship was observed between system COP and process air flowrate, ambient temperature and process air humidity.

Thus, it is concluded that the most influential operational parameters on DW performance are DW rotation speed, regeneration temperature, and airflow rates through the DW. According to previous studies, ranges of the best values or a specific value are given that maximises the system COP regardless of the effect of other parameters. For instance, in the case of a hot dry day, the required DW rotational speed and regeneration temperature will be less compared with humid days.

The review of the available international literature revealed that the focus was only on studying the effect of some operational and climate parameters on the overall system performance. In Addition, there is a lot of inconsistency between the results due to different operating conditions and designs, for example, the reported optimal rotational speed was varied between 4 to 100 RPH among different studies. Here comes the importance of generalising the outcomes to be applicable on more cases by applying the dimensional analysis technique. At the time of writing, there has been no study that combined the parameters into non-dimensional form. The

benefits of creating the non-dimensional groups are to reduce the required experiments, study the effect of some parameters that cannot be changed through experiments by changing other parameters values in the same group, and other benefits will be illustrated later. Also, there are very few studies that considered the channel geometry and design parameters. And there has been no study that optimises the most influential operational parameters on DW performance related to design parameters. In this research, non-dimensional groups will be formed and tested experimentally and through simulation. Then, how these non-dimensional groups are related in terms of performance indices will be presented.

Both GSR and GSSR models have been used effectively to simulate the DW. Because of the inclusion of the heat conduction and mass diffusion within the solid desiccant layer in the GSSR model, it is more accurate than the GSR model. And by comparing 1-D and 2-D GSSR models, it was found that the results of both models are very convergent. Previous studies show good results for the 1-D GSSR model which can be achieved with a maximum error of 15% from experimental results. Therefore, the 1-D GSSR model will be used in this study to simulate the DW.

To the best of the author's knowledge, no studies have been found in the open literature so far that optimise these most influential operational parameters on DW performance in a range of different climate conditions and related to design parameters.

CHAPTER 3: DESICCANT WHEEL MATHEMATICAL MODELLING

3.1 Introduction

The behaviour and performance of different systems can be determined through either experimental work or simulation models. For system optimization, the system variables' values could be changed to obtain the optimum in some cases. But in experimental studies, some variables related to geometry or material properties cannot be easily changed without incurring additional cost and time. Here comes the importance of simulation models by reducing the time and cost needed. Furthermore, a simulation model can estimate physical variables values at unreachable locations without impacting the system performance. Thus, constructing a reliable model for many systems becomes an essential target for several studies.

In this chapter, the 1-D DW mathematical model is introduced in depth, including the model itself, auxiliary equations, and initial and boundary conditions. Then, the solution technique is presented, followed by the model validation.

The mathematical model used takes account of heat and mass transfer between the air side and the desiccant side. Four partial differential equations (PDE) are used to investigate the DW performance and to optimize the parameters' values. The mathematical model validated by comparing the model results with three different published experimental results.

3.2 Mathematical model

The desiccant wheel is an air to air heat and mass exchanger. It rotates at relatively low speed. The DW matrix consists of two parts; the desiccant material and the substrate. The DW divided into two sections according to the air streams that pass through the wheel; the process section

where the air dehumidified, and the regeneration section where the air reactivated for the next cycle.

To establish the mathematical model, a control volume should be carefully selected to derive the appropriate equations. One sinusoidal channel with length dz is selected as a differential control volume as shown in Figure 3.1.

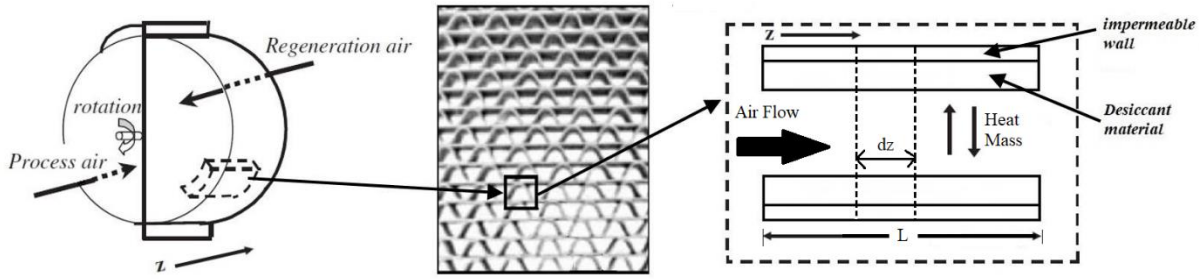

(a) (b) (c)

Figure 3.1: (a) Schematic representation of desiccant wheel, (b) cross-sectional area, and (c) single flow channel structure. (Heidarinejad and Pasdarshahri 2010)

3.2.1 Model assumptions

The following assumptions are undertaken to simplify the model and to reduce the computational time:

1. One dimensional air flow (Figure 3.1(c)),
2. Constant thermodynamic properties of air and desiccant,
3. All DW channels are assumed to be identical and the walls are impermeable (Figure 3.1 (b, c)),
4. The channel cross-section geometry is assumed to be triangular for some channel calculations,
5. The substrate is in the middle between two channels,
6. Heat and mass transfer coefficients are assumed constant.

3.2.2 Channel calculations

One sinusoidal matrix is shared between two channels as shown in Figure 3.1 (b). Figure 3.2 shows one channel and its dimensions, the following relation is adopted:

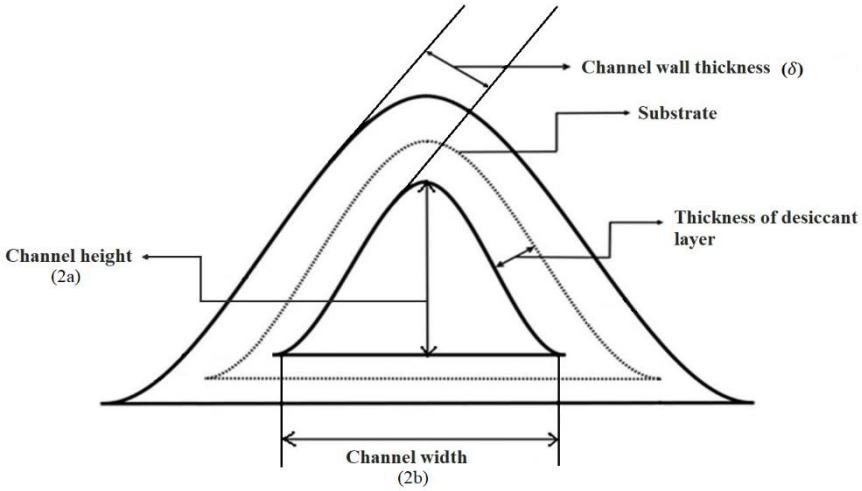

Figure 3.2: Cross-section of sinusoidal channel showing the dimensions.

The height of flow passage of one channel = 2a, the width of flow passage of one channel = 2b, and the thickness of the channel wall = δ.

The cross-sectional area of flow passage of one channel:

$$A_f \approx 2ab \tag{3.1}$$

Total cross sectional area of one channel:

$$A_t = \frac{1}{2} \times (2a + \delta)(2b + \delta) \tag{3.2}$$

The area ratio of air flow passage to the whole channel:

$$f = A_f / A_t \tag{3.3}$$

Volume ratio of desiccant material in layer:

$$\Phi = \frac{Desiccant\ material\ volume}{Desiccant\ material\ volume + volume\ of\ matrix\ material} \tag{3.4}$$

Perimeter of flow passage of one channel (Yadav & Bajpai 2013):

$$C \approx 2b + 2\sqrt{b^2 + (a\pi)^2}\,\frac{3 + \left(\frac{2b}{a\pi}\right)^2}{4 + \left(\frac{2b}{a\pi}\right)^2} \tag{3.5}$$

Hydraulic diameter of flow passage of one channel:

$$D_h = \frac{4A_f}{C} \tag{3.6}$$

3.2.3 Governing equations

The governing equations derivation is based on dividing the airflow passage control volume into two parts. The air part is first; this passes through the open area from the channel. Figure 3.3 shows the control volume of air for mass and energy conservation. The second part is the desiccant layer which consists of the desiccant material, the adsorbed humidity, and the substrate material. Figure 3.4 shows the control volume of the desiccant layer for mass and energy conservation. Both mass and energy conservation principles are illustrated by four governing equations (Ge et al. 2010).

The moisture (mass) conservation in the air can be expressed as (Ge et al. 2010):

$$\rho_a f A_t \left(\frac{\partial Y_a}{\partial t} + u\frac{\partial Y_a}{\partial z}\right) = K_y C (Y_d - Y_a) \tag{3.7}$$

The first part of the left-hand side of the above equation represents the change in moisture in the air within the control volume and the second part shows how the moisture changes due to flow through the control volume dz. While the right-hand side expresses the variation of air moisture caused by the convective mass transfer between the air side and the desiccant side.

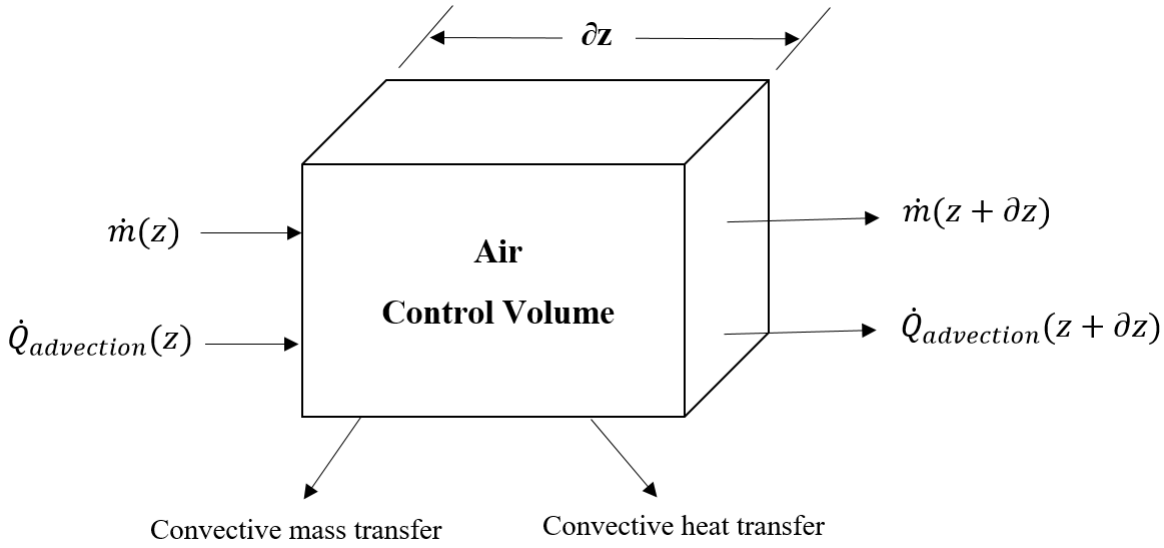

Figure 3.3: Control volume of air for mass and energy conservation.

Moisture (mass) conservation in desiccant is given by (Ge et al. 2010):

$$\rho_a \varepsilon (1-f) A_t \frac{\partial Y_d}{\partial t} + \rho_d (1-\varepsilon)(1-f) A_t \Phi \frac{\partial W}{\partial t} = \rho_a \varepsilon (1-f) A_t D_G \frac{\partial^2 Y_d}{\partial z^2} + \rho_d (1-\varepsilon)(1-f) A_t D_s \frac{\partial^2 W}{\partial z^2} + K_y C (Y_a - Y_d) \quad (3.8)$$

The left-hand side of the above equation includes the accumulation of moisture: trapped inside the pores of desiccant in the first term, and adsorbed by the surface of desiccant material in the second term. The first term on the right-hand side shows the gas phase diffusion in the desiccant pores containing air and water vapour within the desiccant side, while the second term shows the surface diffusion. The last term on the right-hand side of equation 3.8 represents the convective mass transfer between the air and desiccant, which is identical to the last term in the equation 3.7 but has the opposite sign.

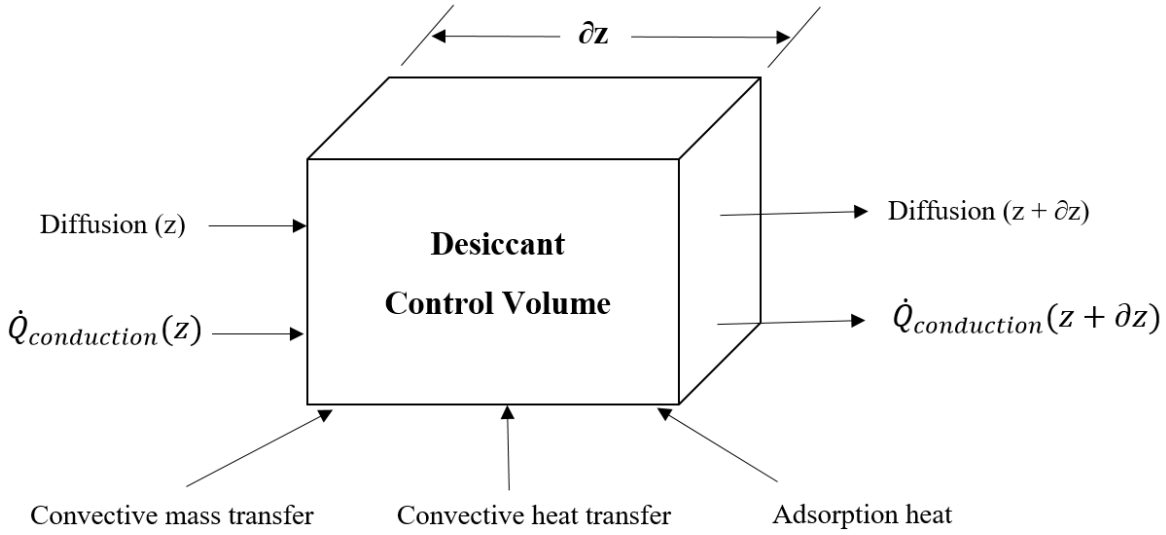

Figure 3.4: Control volume of desiccant for mass and energy conservation.

The thermal energy change for the humid air is described as (Ge et al. 2010):

$$\rho_a\left(c_{pa} + Y_a c_{pv}\right) f A_t \left(\frac{\partial T_a}{\partial t} + u\frac{\partial T_a}{\partial z}\right) = \alpha C(T_d - T_a) + K_y c_{pv} C(Y_d - Y_a)(T_d - T_a) \tag{3.9}$$

The first term of the left-hand side describes the heat storage term in the passing air and the second part shows how the heat changes in the control volume dz with respect to the cross-section (fA_t). The first term of the right-hand side points out the convective heat transfer between the two sides; air and desiccant sides. The second term represents the sensible heat transfer which related to connective heat transfer between the air side and desiccant side taking into consideration that the heat conduction in the air side is neglected.

The thermal energy conservation in the desiccant (Ge et al. 2010):

$$\rho_m c_{pm}(1-ƒ)A_t(1-\varepsilon)(1-\Phi)\frac{\partial T_d}{\partial t}$$

$$+\rho_d c_{pd}(1-ƒ)A_t(1-\varepsilon)\Phi\left(\frac{\partial T_d}{\partial t}-\frac{k_d}{c_{pd}\rho_d}\frac{\partial^2 T_d}{\partial z^2}\right) \tag{3.10}$$

$$=\alpha C(T_a-T_d)+K_y c_{pv}C(Y_a-Y_d)(T_a-T_d)+K_y C(Y_a-Y_d)q_{st}$$

The first term of the left-hand side represents the heat storage in the substrate material and the second term represents the heat storage in the desiccant material, while the third term represents the heat conduction in the desiccant material. The first two terms on the right hand side are almost the same as the first two terms on the right-hand side of equation 3.9, but in the desiccant side, i.e. they describe the convection and sensible heat transfer between the air side and desiccant side. The third term describes the heat transfer related to phase change of water by the released heat of adsorption from the moisture to the desiccant layer.

3.2.4 Initial and boundary conditions

The temperature and humidity ratio boundary conditions for the air are (Ge et al. 2010):

- For the process sector:

$$T_a(z=0,t)=T_{p,in}$$
$$Y_a(z=0,t)=Y_{p,in} \tag{3.11}$$

- For the regeneration sector:

$$T_a(z=L,t)=T_{r,in}$$
$$Y_a(z=L,t)=Y_{r,in} \tag{3.12}$$

The initial temperature of air and desiccant, humidity ratio of the air, and water content of the desiccant are assumed to be uniform:

$$T_a(z, t = 0) = T_{a0}$$

$$T_d(z, t = 0) = T_{d0}$$

$$W(z, t = 0) = W_0 \tag{3.13}$$

$$Y_a(z, t = 0) = Y_{a0}$$

$$Y_d(z, t = 0) = Y_{d0}$$

3.2.5 Auxiliary conditions

The relationship between specific humidity (Y) and relative humidity (RH) is described as (Zheng et al. 1995):

$$Y_d = \frac{0.62188 P_v}{P_{atm} - P_v} = \frac{0.62188 RH_d}{P_{atm}/P_{vs} - RH_d} \tag{3.14}$$

$$P_v = RH_d \, . P_{vs} \tag{3.15}$$

where P_v is water vapour pressure, P_{vs} is the saturation pressure of water vapour which determined by the following equation (Zhang, X. et al. 2003):

$$P_{vs} = \exp[23.196 - 3816.44/(T_d - 46.13)] \tag{3.16}$$

Porous materials are categorized into three types by their pore size (Zdravkov et al. 2007). The first is microporous, where the pore diameter is less than 2 nm. The second is macroporous, where the pore diameter is greater than 50 nm. The third is mesoporous, which lies in the middle. The silica gel pore size used is 11 nm. According to Ge, Ziegler and Wang (2010), if the material classified as mesoporous material, both ordinary and Knudsen diffusion should be taken into account. Gas phase diffusivity (D_G) represents the composite gas diffusivity of Knudsen and ordinary diffusion which can be calculated by (Pesaran & Mills 1987):

$$D_G = \left(\frac{1}{D_o} + \frac{1}{D_k}\right)^{-1} \tag{3.4}$$

where D_o is the ordinary diffusion which can be calculated by:

$$D_o = 1.735 \times 10^{-9} \frac{T_d^{1.685}}{P_v} \tag{3.5}$$

D_k is Knudsen diffusion which can be calculated by:

$$D_k = 97r \left(\frac{T_d}{m}\right)^{0.5} \tag{3.6}$$

The surface diffusivity D_s can be calculated by the following equation:

$$D_s = D_0 \exp\left(-0.974 \times 10^{-3} \frac{q_{st}}{T_d}\right) \tag{3.20}$$

where $D_0 = 1.6 \times 10^{-10}\ m^2/s$, q_{st} is the heat of adsorption which can be calculated by the obtained equilibrium adsorption equations (San & Hsiau 1993):

$$q_{st} = h_{fg}(1.0 + 0.2843e^{-10.28W}) \tag{3.7}$$

here h_{fg} is the latent heat of condensation and calculated by (Charoensupaya & Worek 1989):

$$h_{fg} = (2504.4 - 2.4425\, T_d) \times 1000 \tag{3.22}$$

The equilibrium isotherm for regular silica gel at 30ºC is calculated by the empirical curve-fit (Pesaran & Mills 1987):

$$RH_d = 0.0078 - 0.05759\, W + 24.16554\, W^2 - 124.78\, W^3 + 204.226\, W^4 \tag{3.23}$$

In order to determine the temperature and velocity profile along the channel, the Nusselt number (Nu) is evaluated by (De Antonellis et al. 2010):

$$Nu = Nu_{FD} + \frac{0.0841}{0.002907 + Gz^{-0.6504}} \tag{3.24}$$

where Nu_{FD} is the Nusselt number for the fully developed flow which depends on the channel geometry and is given by:

$$Nu_{FD} = 1.1791 \left[1 + 2.7701 \left(\frac{a}{b}\right) - 3.1901 \left(\frac{a}{b}\right)^2 + 1.9975 \left(\frac{a}{b}\right)^3 - 0.4966 \left(\frac{a}{b}\right)^4\right] \tag{3.25}$$

Graetz number (Gz) is a dimensionless number that characterises laminar flow in a channel. It is given by (Nellis & Klein 2009):

$$Gz = \frac{Re \Pr C}{4 L} \tag{3.26}$$

where Re is the Reynold number and given by:

$$Re = \frac{\rho_a u D_h}{\mu} \tag{3.27}$$

and μ is the dynamic viscosity and given by:

$$\mu = \mu_0 \left(\frac{T_{so} + C_0}{T + C_0}\right)\left(\frac{T}{T_{so}}\right)^{3/2} \tag{3.8}$$

where

μ_0 = Initial dynamic viscosity = $18.27 \times 10^{-6}\ Pa.s$

T_{so} = 291.15 K

C_0 = 120 K

Prandtl number (Pr) is defined as the ratio of momentum diffusivity to thermal diffusivity:

$$\Pr = \frac{\mu\, c_{pa}}{k_a} \tag{3.9}$$

The following heat transfer coefficient is adopted:

$$\alpha = \frac{Nu\, k_a}{D_h} \tag{3.30}$$

Sherwood number (Sh), which is the ratio of the convective mass transfer to the rate of diffusive mass transport, and Nusselt number are related using Lewis number (Le) (defined by the ratio of thermal diffusivity to mass diffusivity) from the Chilton–Colburn analogy (Geankoplis 2003):

$$Sh = Nu.\, Le^{1/3} \tag{3.31}$$

$$Le = \frac{k_a}{\rho_a c_{pa} D_m} \tag{3.32}$$

The following mass transfer coefficient is adopted (Sherony & Solbrig 1970):

$$K_y = \frac{\rho_a\, Sh\, D_m}{D_h} \tag{3.33}$$

The mass diffusion coefficient of vapour in the air is given by:

$$D_m = 2.302\ \times 10^{-5} \frac{P_0}{P_a} \left(\frac{T_a}{T_0}\right)^{1.81} \tag{3.34}$$

where

$P_0 = 0.98 \times 10^5\ Pa$

$T_0 = 256\ K$

3.3 Solution method

The Desiccant Wheel model described above consists of four non-linear PDE equations. The Finite Element Method (FEM) is used to solve the equation system through the PDE solver. Two separate programming transcripts have been written for the process and regeneration sections. Then, process and regeneration transcripts coupled in the program solver as shown in the flowchart in Figure 3.5. Real condition input data are used to simulate the system. The software called FlexPDE.

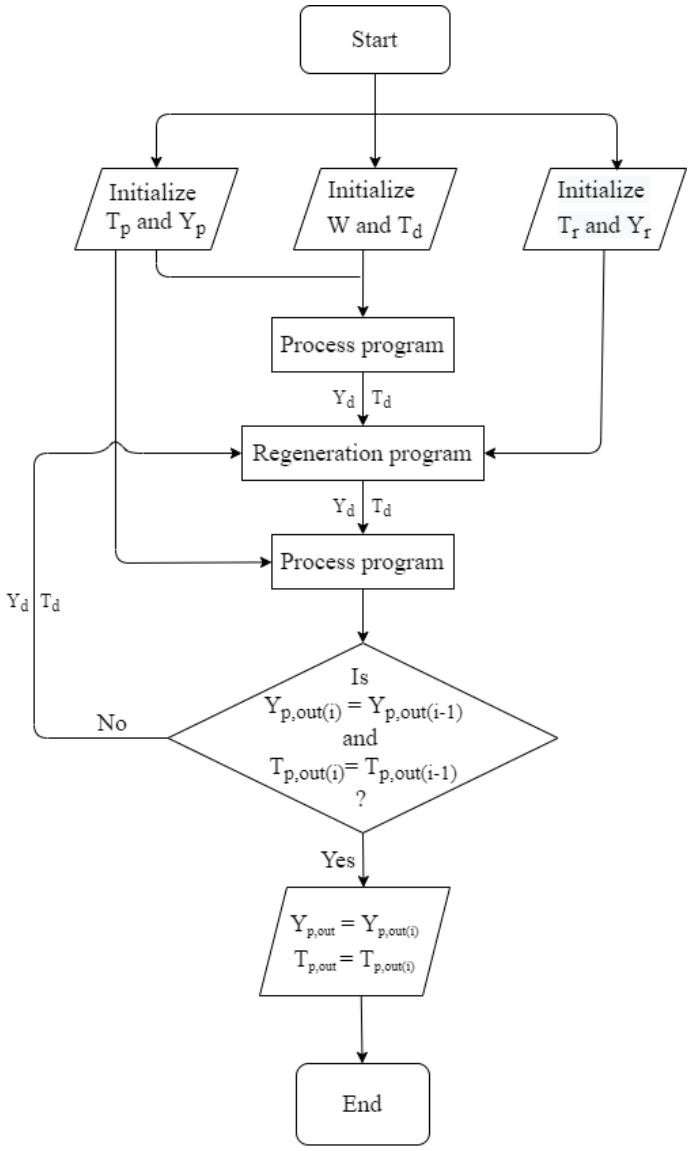

Figure 3.5: Program flow chart. The iteration counter is "i".

The simulation time is calculated based on the DW rotational speed and the area ratio of the process to regeneration air sections, i.e. in case if the rotational speed is 10 RPH and the area ratio equals 1, then the time needed for a full cycle is 360 s which divided equally into process section and regeneration section. But, for the same rotational speed and the area ratio equals 3, then the simulation time will be 270 s for the process section and 90 s for the regeneration section.

The time step (dt) is chosen carefully starting by high value then decreasing its value and compare the results, if the output result of the time step and the one before is equal, the time step is accredited. In this study, the starting value for dt is 1.0 s and decreased to 0.1 s by 0.1 s, the output results were inconsistent between 1.0 s and 0.2 s. Then, the desiccant wheel output conditions at dt equal 0.1 s were compared with 0.09 s and a lower value of 0.05 s, it was found that the results are very convergent. Therefore, a time step of 0.1 s is tested for different operation conditions and chosen for this study.

As regards reaching the steady-state operation of the system, it is clear from figure 3.5, that the output results of the process section are the entry condition to the regeneration section and vice versa. The iteration stops when the output condition of the process section is exactly the same as the previous one. In some cases, five iterations were enough to reach the steady-state, but in most cases, nine iterations were enough and it could reach thirteen iterations. It was found that the iteration number depends on the simulation time, the iteration number is lower in case of higher simulation time. The model is validated using three different published experimental results as will be presented in the next section.

3.4 Model validation

In order to validate the DW model, the computational results were compared with published experimental outcomes. Three different systems were used. A script has been developed based on the governing equation presented in previous sections and the model input data was as in the experimental studies. The results were in good agreement between the model and the experiment. The discrepancy between the two results was less than 12.3%, while the maximum reported discrepancy was 15% and the experimental uncertainties are within 14%, which is calculated using the following equation:

$$Error = \frac{Exp - Sim}{Exp} \times 100\% \tag{3.35}$$

The chosen experimental studies had the same desiccant material and the same material specifications. So, the same auxiliary conditions were adopted for all cases as in section 3.2.5. The parameters values which related to the substrate and dimensions were set separately for each validation.

3.4.1 First simulation validation

In the experimental study (Mandegari & Pahlavanzadeh 2013), the system tested under two climate conditions: hot-dry and hot-humid. The DW physical parameters are shown in Table 3.1.

Table 3.1: The physical properties of DW in Mandegari and Pahlavanzadeh's (2013) study.

Property	Value	Property	Value
Channel height (m)	1.75×10^{-3}	Ratio of process to regeneration section	3
Channel width (m)	3.5×10^{-3}	Process air velocity (m/s)	1.5
Porosity	0.7	Regeneration air velocity (m/s)	2.5
Pore radius (m)	11×10^{-10}	Desiccant material	Silica gel
Thickness of desiccant (m)	2×10^{-4}	Desiccant density (kg/m^3)	1129
Wheel thickness (m)	0.2	Desiccant specific heat (J/kg.K)	921
Wheel diameter (m)	0.4	Pressure (Pa)	101325
Heat transfer coefficient (kW/m^2 K)	39.237	Mass transfer coefficient (kg/m^2 s)	0.0546

The model and experimental outcomes are compared as shown in Table 3.2. A good agreement is observed between the two results: the maximum discrepancy in the outlet temperature and humidity was 4.0% and 6.3% respectively.

Table 3.2: Comparison between model and experimental result from Mandegari and Pahlavanzadeh (2013).

	DW inlet parameters				Exp outlet		Sim outlet		Error	
	N (RPH)	T_{reg} (ºC)	$T_{p,in}$ (ºC)	$Y_{p,in}$ (kg/kg)	$T_{p,out}$ (ºC)	$Y_{p,out}$ (kg/kg)	$T_{p,out}$ (ºC)	$Y_{p,out}$ (kg/kg)	T (%)	Y (%)
1	20	120.4	35.9	0.0067	43.9	0.0052	44.129	0.00508	-0.5	2.3
2	20	76.4	35.5	0.0119	43.4	0.0100	42.565	0.00937	1.9	6.3
3	20	144.8	36.1	0.0114	49.7	0.0084	47.7	0.0086	4.0	-2.4
4	24	124.3	33.7	0.0107	46.9	0.0077	46.375	0.00725	1.1	5.8
5	4	127.3	38.3	0.0123	40.0	0.0116	40.437	0.01175	-1.1	-1.3

3.4.2 Second simulation validation

A number of experimental data were presented by De Antonellis et al. (2010). One of these data sets was used to validate the presented DW model in section 3.2. The only varying

parameter was the DW rotational speed, while the input process and regeneration temperatures and humidity were constant.

The DW's substrate was made of ceramic fibre and the desiccant material was silica gel. The DW thickness was 0.2 m and the channel height, width and thickness are 1.8 mm, 3.2 mm and 0.2 mm respectively. Table 3.3 shows the input parameters for the model.

Table 3.3: Physical properties and input data used in the comparison between simulation results and experimental data from De Antonellis et al. (2010).

Parameter	**Value**	**Property**	**Value**
$T_{p,in}$ (ºC)	26.0	Porosity	0.48
T_{reg} (ºC)	60.0	Pressure (Pa)	95000
$Y_{p,in}$ (kg/kg)	0.0132	Pore radius (m)	9×10^{-10}
$Y_{r,in}$ (kg/kg)	0.0138	Desiccant density (kg/m^3)	1130
A_p/A_r	1.0	Desiccant specific heat (J/kg.K)	915
u_p (m/s)	1.0	Heat transfer coefficient (kW/m^2 K)	39.5
u_r (m/s)	1.0	Mass transfer coefficient (kg/m^2 s)	0.057

As shown in Figure 3.6, the results show good agreement between both the experimental results and the simulation data. As 71% of the data are within 10% discrepancy and the rest are in the range of 10-12.3%.

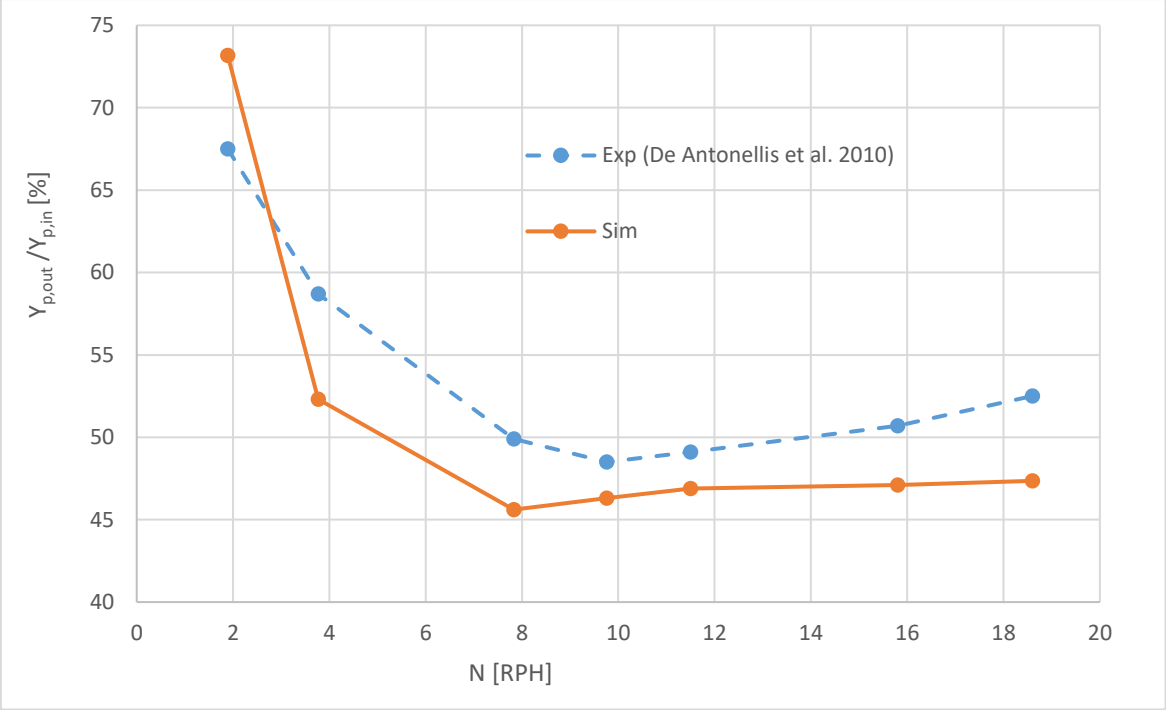

Figure 3.6: Comparison between simulation results and experimental data from De Antonellis et al. (2010).

3.4.3 Third simulation validation

An experimental work conducted at NIT Kurukshetra, India by Yadav and Bajpai (2013) used a DW with 0.1 m thickness, 0.37 m diameter and the desiccant material was silica gel. The channel height, width and thickness were 1.8 mm, 3.2 mm, and 0.34 mm, respectively. Both process and regeneration airspeed were 4 m/s. The area ratio of the process section to the regeneration section was 1.0. The rotational speed was 22 RPH. The input temperature and humidity were illustrated in Table 3.4. The data obtained on 1st October 2011.

Table 3.4: DW process and regeneration input temperature and humidity (Yadav & Bajpai 2013).

Time	$Y_{p,in}$ (kg/kg)	$T_{p,in}$ (ºC)	T_{reg} (ºC)
10:00	0.01426229	29.0	41.9
11:00	0.015024756	32.1	47.0
12:00	0.01554008	32.4	54.7
13:00	0.015523932	33.1	59.3
14:00	0.015239226	33.0	60.2
15:00	0.015876031	32.7	60.1
16:00	0.016325989	32.0	58.3
17:00	0.017090577	31.5	54.6
18:00	0.017538372	29.0	50.2

Figure 3.7 shows the comparison between the experimental and simulation results. The performance index used is moisture removal which indicates the difference between DW process inlet and outlet humidity. The discrepancy between the two results is within 5%.

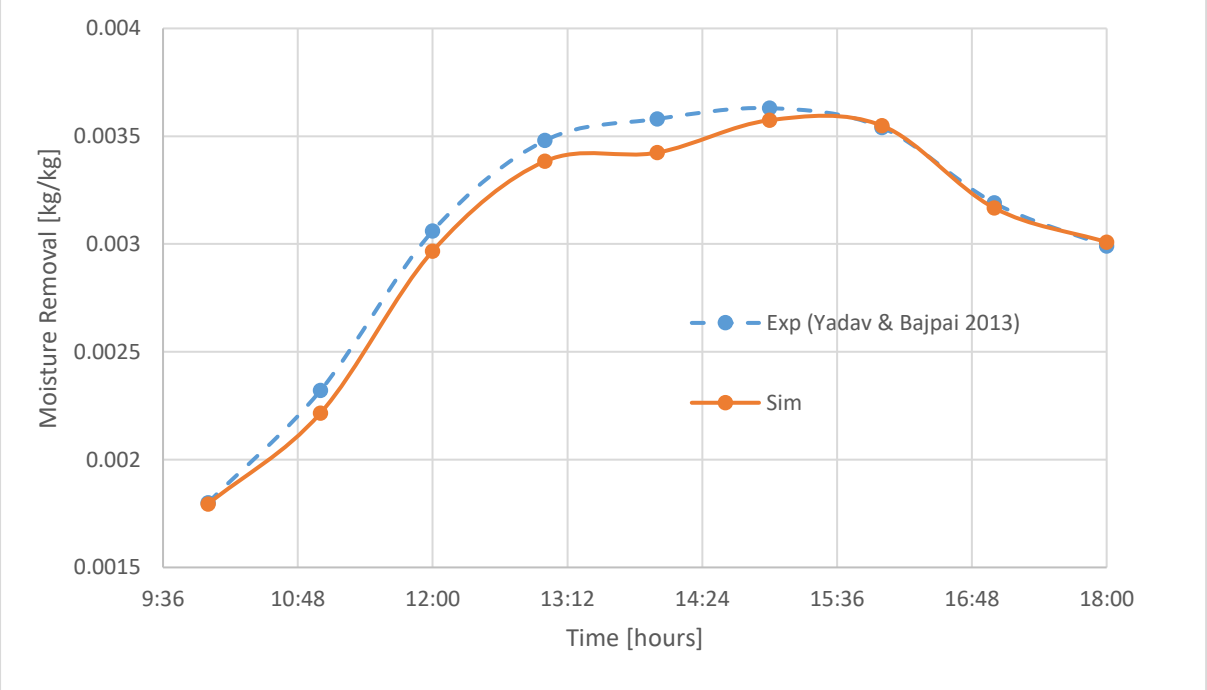

Figure 3.7: Comparison between simulation results and experimental data from Yadav and Bajpai (2013).

3.5 Summary and conclusions

The basic definition of GSSR mathematical model has been presented. The key summary and conclusions are as follows:

1. To simulate the DW, one sinusoidal channel is discretised with length dz and chosen as a differential control volume. Both mass and heat transfer occur simultaneously between the air stream and the channel. Mass and energy conservation principles are applied to derive the mathematical model.
2. The model has four PDEs with five unidentified variables ($T_a, T_d, Y_a, Y_d,$ and W). Therefore an auxiliary equation is adopted to solve the PDE equations set. Also, additional auxiliary equations are utilised to determine the variables' values.
3. FEM method is chosen to solve the governing equations through FlixPDE software. Two separate transcripts are written for process and regeneration sections, then they are coupled in the solver.

By validating the simulation outcomes with different published experimental results, the 1-D GSSR model has proven to be effective and agreed relatively well with the experimental results under different operation conditions.

CHAPTER 4: EXPERIMENTAL SETUP OF THE DESICCANT WHEEL SYSTEM

4.1 Introduction

An experimental apparatus is designed and built to conduct experimental investigations on the DW. The proposed system was used to validate the simulation model and compare the simulation results with experimental measurements for different operating conditions. The main component of the experimental setup is the DW and the attached devices, instruments, sensors, and controllers which are discussed in detail in this chapter. The followed methodology and test conditions to conduct the experiment are reported.

4.2 Experimental setup

The aims of the experimental setup are to study the performance of the desiccant wheel system under different operational conditions, to optimize the values of the operational parameters, to validate the simulation outcomes under Toowoomba's (Queensland, Australia) climatic conditions, and to examine the non-dimensional groups that will be introduced in the next chapter.

In this setup, as shown in the schematic diagram in Figure 4.1 and a photograph of the experimental setup in Figure 4.2, the desiccant wheel is attached to an LPG air heater, two inline duct suction blowers with speed controller, and some sensors and measuring devices which will be illustrated in the next section.

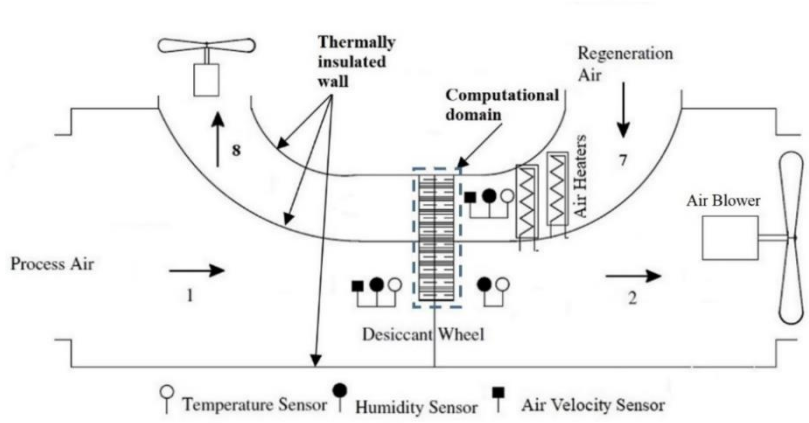

Figure 4.1: Schematic diagram of the experimental setup and instrumentations.

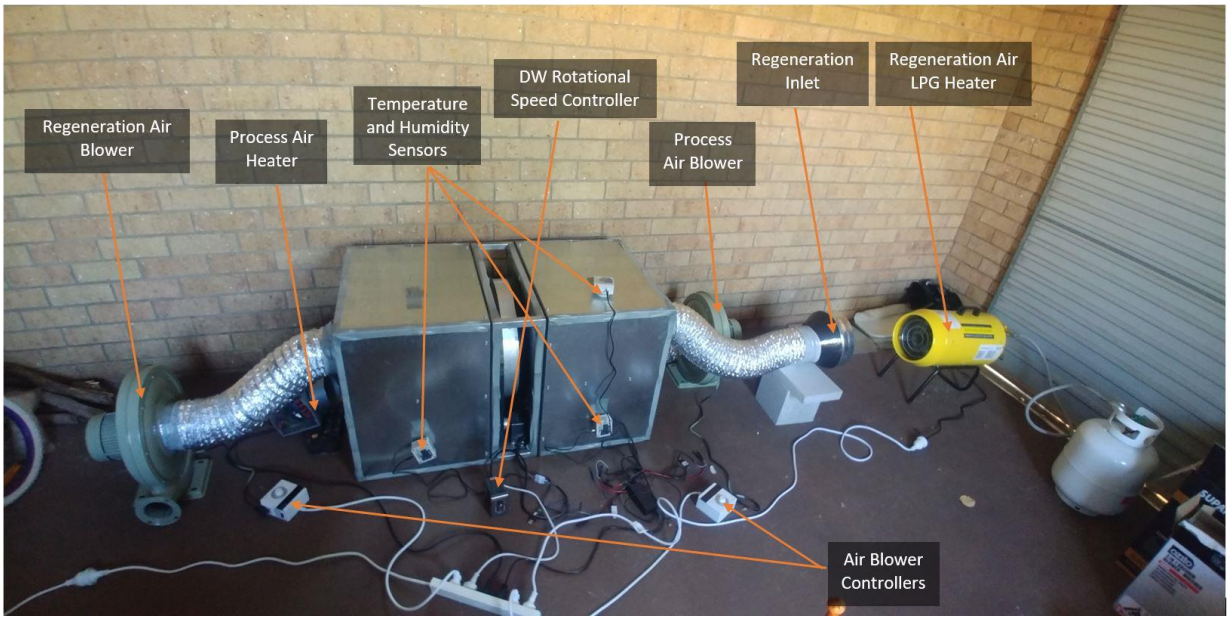

Figure 4.2: Experimental setup devices and sensors.

The system consists of two main sections:

- The desiccant wheel and the cassette
- The ducting system.

4.2.1 The desiccant wheel and the cassette

The DW is the main component in the SDC system. The DW is considered to be an open system air-to-air heat exchanger. The DW rotates continuously with relatively low speed to ensure both dehumidification and regeneration processes occur effectively. The DW structure consists of a matrix of sinusoidal, honeycomb, or triangular shape channels. Each channel contains a

desiccant material as well as a substrate. In general, the DW divided into two sections; process and regeneration, according to the air stream passes through. The angle of the process and regeneration sections is θ_p and θ_r, respectively. The DW rotational motion regenerates the saturated desiccant material due to the continuous changeover of the process and regeneration sections.

The DW used in this study is manufactured by "Puaide Environment Technology Limited (PureSci)". The DW's channels are made of a ceramic fibre substrate and the adsorption material is silica gel. Both materials are chemically bonded to form a sinusoidal, firm, solid, and corrosion-resistant structure as shown in Figure 4.3. The outer plate is made of a standard aluminium zinc plate, while the skeleton is made from a sheet of galvanised iron. NSK bearing is fitted in the DW's centre with a 20 mm inner diameter. The DW physical properties are shown in Table 4.1.

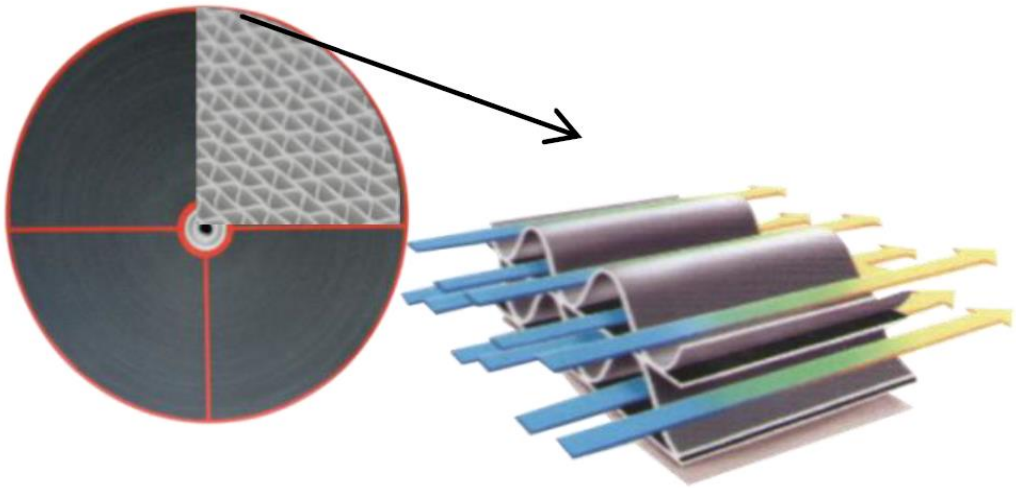

Figure 4.3: The design of the sinusoidal channels and the fitted bearing in PureSci DW (PureSci 2018).

Table 4.1: PureSci DW physical parameters values.

Item	**Value**	**Item**	**Value**
DW Diameter	450 mm	Pore size	11×10^{-10} mm
DW Depth	100 mm	Porosity	0.4
Channel height	2.40 mm	Volume ratio of desiccant material in a layer	0.48
Channel width	4.00 mm	Density of silica gel	1129 kg/m^3
Channel wall thickness	0.34 mm	Density of matrix material	625 kg/m^3

The cassette frame with a 600×600×170 mm dimension is made from a galvanised steel tube as shown in Figure 4.4. The cassette is divided into four sections to form process and regeneration parts. The process to regeneration angular ratio (θ_p/θ_r) of 1, 2, or 3 can be attained. Two Galvabond sheets were attached to the cassette with a hole cut to the same diameter as the DW using a waterjet cutting machine. In order to prevent air leakage in the gap between the DW and the sheets, one side adhesive sealing strips are used. For the gaps between the cassette and the DW, rectangular rubber strips are used.

Figure 4.4: Desiccant wheel's cassette divided into four parts to form the required θ_p/θ_r ratio, and a square hole in the bottom left corner for the driving motor.

The driving system consists of a geared 25W AC motor with a reduction ratio of 100:1, speed controller, pulley, and A-section industrial V belt as shown in Figure 4.5. The driving motor is fixed on a bottom plate.

Figure 4.5: The DW driving system including the motor attached with a gearbox and pulley connected with the DW by A-section industrial V belt, which located at the bottom left corner in figure 4.4.

Figure 4.6: Cross section of the desiccant wheel fitted in the cassette.

4.2.2 The ducting system

4.2.2.1 The duct and insulation

The left and right duct sides are identical. The frame is made from a galvanised steel tube with a 600×600×450 mm dimension. Similar to the DW cassette, the ducts are divided into 4 sections to correspond to the cassette as shown in Figure 4..

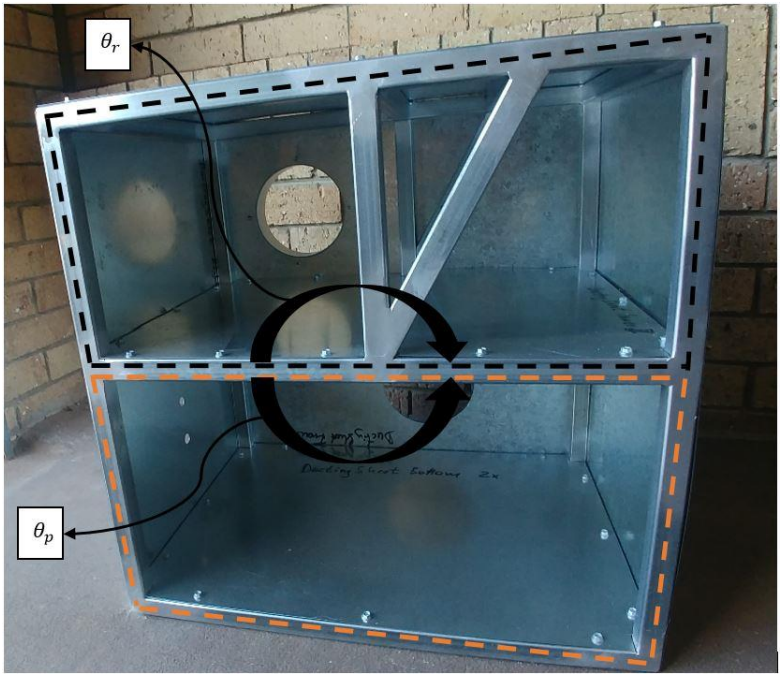

Figure 4.7: The duct with angular ratio (θ_p/θ_r) of 1.0.

Galvabond sheets were attached to the duct from all sides except the side that faces the DW cassette. Some small holes were made in the sheets for placing the measuring devices and other big holes (6”) to attach the air blowers and heaters. Silicon and duct tape were used to prevent the air from leaking. For thermal insulation, ceramic fibre mat insulation was used in the inner duct wall. Two layers of isolation were used for the wall between process and regeneration sections.

4.2.2.2 Air blowers

Two exhaust air blowers are used for the process and regeneration air streams. The blowers are manufactured by Cloudray Laser Technology Co. The blower specifications are presented in Table 4.1.

Table 4.2: Air blower specifications.

Voltage	Frequency	Power	Speed	Discharge	Full pressure	Inlet and outlet Diameter	Blower Dimensions
220V/380V	50 Hz	750 W	2800 rpm	20 m^3/min	1.9 kPa	145 mm	241×410×440 mm

4.2.2.3 Regeneration heater

For the purpose of reactivate the DW, heat from different sources could be used such as, renewable energy like solar or geothermal, electric heaters, or fuel powered heaters. In this setup, an industrial LPG heater is used. By varying the gap between the regeneration inlet and the heater, the inlet regeneration temperature is controlled.

4.2.2.4 Process air heater and humidifier

Some tests are conducted in the winter season. Therefore, due to the low air temperature, an electric ceramic 220V heater is used in the process air inlet to control its temperature to be around 30°C. In Addition, in order to imitate humid weather, an air humidifier is utilised when needed to raise the level of air humidity.

4.3 Measuring and control devices

The parameters measured during the experiments are as follows:

1. Inlet Process airspeed, temperature, and relative humidity
2. Outlet process air temperature and relative humidity
3. Inlet Regeneration airspeed, temperature, and relative humidity

4. Desiccant wheel rotational speed.

RHT-DM-485-LCD transmitter from Novus Automation is used to measure the temperature and the relative humidity with a resolution of 0.1°C and 0.1%, respectively. It is controlled by a microprocessor with high precision and stability sensors. Therefore, it was connected to a personal PC for configuration and data logging throughout an RS485 interface using Modbus RTU. ModScan32 is a Modbus master software that is used to configure the transmitter as well as to demonstrate real-time data logging.

The smart anemometer Testo 405i is used to measure the airspeed with 0.01 m/s resolution. It is connected to a smartphone. The measuring process, display the values and create reports take place by Bluetooth via the Testo Smart Tools App.

The DW rotational speed was measured by determining the required time for a full revolution manually due to its low rotational speed being unsuitable for a tachometer.

Three controllers are used to control the rotational speed of the DW and the air blowers. The rotational speed of the DW varies from 0 – 82.75 RPH, while the airspeed in the duct varies between 0 – 5 m/s.

4.4 System operation

4.4.1 Test Procedure

To start an experimental test, the following procedures are followed sequentially:

1) Configure the instruments and sensors,
2) Set up both ducts on the required angular ratio,
3) Adjust the DW rotational speed to the required rotational speed,
4) Turn on the air blowers and control their speed to the desired value,

5) Turn on the heater and adjust the regeneration air temperature by varying the gap between the heater and the regeneration section inlet,
6) Connect the sensors with the PC and start collecting the sensors readings.

Each test is carried out in steady-state conditions which occurs after 4-6 minutes from operating the system. In each session at least 300 samples for the air temperature and humidity are registered with 1 Hz frequency. The obtained data are processed by eliminating the outlier values. The demonstrative values for every measurement are obtained when reaching the steady state condition.

4.4.2 Test Conditions

The setup and the experiments were conducted in a facility near the University of Southern Queensland (USQ), Toowoomba campus. According to the Australian Bureau of Meteorology (BOM), Toowoomba lies at 641 m above sea level. Toowoomba's climate is categorized as warm and temperate. The hot season lasts from November to March. While, the cool season lasts from May to August. Toowoomba's temperature and humidity climate condition are as follows: the mean maximum temperature is 28.5°C in January and 16.8°C in July, the mean minimum temperature is 17.7°C in January and 6.6°C in July, and the mean relative humidity varies between 40-76% around the year.

Due to COVID-19 pandemic, the experiments were conducted at a car park near the university main campus. The chosen place is indoor, the air is not treated, and well ventilated. All safety measurements were taken into consideration during the system assembly and when carrying out the experiments.

4.5 Analysis of experimental data

In order to analyse and optimise the operation of the DW as a function of the operational parameters and the dimensionless parameters, a number of effectiveness parameters that deal

with both heat and mass transfer via the DW are considered as follows (refer to Figure 4.1 for process and regeneration streams points):

1- Dehumidification Effectiveness (η_{deh}): this mass transfer effectiveness parameter considers the dehumidification process across the DW (Mandegari & Pahlavanzadeh 2009):

$$\eta_{deh} = \frac{Y_1 - Y_2}{Y_1} \tag{4.10}$$

where Y_1, Y_2 are the process air specific humidity before and after the DW, respectively.

2- Dehumidification Coefficient of Performance (DCOP): it presents dehumidification capacity and energy utilisation performance. It is defined by the ratio of air dehumidification thermal power to regeneration thermal power (Ge, Ziegler & Wang 2010). The DCOP expressed as:

$$DCOP = \frac{\dot{m}_a \, \Delta h_{fg} \, (Y_1 - Y_2)}{\dot{m}_r \, (h_7 - h_1)} \tag{4.11}$$

where

$\dot{m}_a$: process air flow rate

$\dot{m}_r$: regeneration air flow rate

$(h_7 - h_1)$: enthalpy difference between the regeneration air and process air.

Δh_{fg}: latent heat of condensation, which evaluated by the empirical equation (Angrisani et al. 2013):

$$\Delta h_{fg} = -0.614342 \times 10^{-4} \, T_1^3 + 0.158927 \times 10^{-2} \, T_1^2 - 2.36418 \times T_1 + 2500.79 \tag{4.12}$$

In case if the regeneration air is an environmental air, the enthalpy difference $(h_7 - h_1)$ represents specific regeneration thermal power. Moreover, the equation expressed as:

$$DCOP = \frac{\dot{m}_a \, \Delta h_{fg} \, (\omega_1 - \omega_2)}{\dot{m}_r \, c_{pr} (T_7 - T_1)} \tag{4.13}$$

where c_{pr} is the regeneration air specific heat.

3- Sensible Energy Ratio (SER): it is defined by the ratio between process air heating thermal power and regeneration thermal power. This term is used to evaluate the increase of treated air sensible energy content upon removal of its latent energy content (Enteria et al. 2009):

$$SER = \frac{\dot{m}_a \, c_{pa} \, (T_2 - T_1)}{\dot{m}_r \, c_{pa} (T_7 - T_1)} \tag{4.14}$$

A maximum value for η_{deh} and DCOP is desirable, which represents superior dehumidification performances. On the other hand, a higher value for SER means a higher temperature value of the treated air and hence a higher cooling load which must be avoided. In studies conducted by Angrisani et al. (2013) and Bareschino et al. (2015), the value of DW rotational speed was optimized as a function of the effectiveness parameters. They found that the optimum value of DW rotational speed maximise both η_{deh} and DCOP, while the value of SER is in the range of the lowest values.

4.6 Experimental accuracy and uncertainty

The systematic uncertainties in the experimental results are affected by the accuracy of the measuring sensors. In this study, three parameters were measured by sensors; airspeed, temperature, and humidity. The manufacturers of the measuring instruments provided a calibration report for the sensors. Also, they indicated the measuring ranges and the uncertainty of each sensor as shown in the table below.

Table 4.3: Main characteristics of different measuring devices used during the experiments.

Measurement	Sensors	Operation range	Accuracy *
Air temperature	NOVUS RHT-DM-485-LCD transmitter	–40.0°C to 100.0°C	(± 2.0 % of m.v.) (-40 - 0°C & 50 - 100°C) (± 1.0 % of m.v.) (0 - 50°C)
Air relative humidity	NOVUS RHT-DM-485-LCD transmitter	0.0 to 100.0 % RH	(± 5.0 % of m.v.) (0 - 20% & 80 - 100% RH) (± 3.0 % of m.v.) (20 - 80% RH)
Air speed	Testo 405i (Bluetooth thermal anemometer)	0 to 20 m/s	± (0.05 m/s + 2.5 % of m.v.) (0 - 2 m/s) ± (0.15 m/s + 2.5 % of m.v.) (2 - 20 m/s)

* m.v. stands for the measured value.

Considering a general case in which an experimental result, *r*, is a function of *j* measured variables X_i (Koronaki et al. 2013):

$$r = f\ (X_1, X_2, \dots, X_j) \tag{4.15}$$

where equation 4.6 is the data reduction equation used for determining *r* from the measured values of the variables X_i. Then the uncertainty in the result is given by:

$$U_r^2 = \left(\frac{\partial r}{\partial X_1}\right)^2 U_{X_1}^2 + \left(\frac{\partial r}{\partial X_2}\right)^2 U_{X_2}^2 + \cdots + \left(\frac{\partial r}{\partial X_j}\right)^2 U_{X_j}^2 \tag{4.16}$$

where U_{Xi} are the uncertainties in the measured variables X_i.

Based on these relationships, a detailed error analysis indicated that an overall uncertainty was within ±3.47% for the dehumidification Effectiveness (η_{deh}), ±5.10% for the Dehumidification Coefficient of Performance (DCOP), and ±6.84% for the Sensible Energy Ratio (SER). The detailed uncertainty calculations are illustrated in APPENDIX A: UNCERTAINTY ANALYSIS.

4.7 Conclusion and summary

The experimental setup described in this chapter has been designed for the purpose of conducting experimental investigations on the DW. The system has been built especially for the present work. The DW's cassette and the ducts were built in the USQ workshop. However,

the system assembly and the tests were run in a home car garage near the university because of COVID-19. The test procedures and the operating conditions are also reported.

Three effectiveness parameters, which deals with heat and mass transfer through the DW, are presented. The measuring instruments were calibrated by the manufacturing companies. The uncertainties of the performance indices caused by the uncertainty of the measuring instruments are calculated.

CHAPTER 5: DIMENSIONAL ANALYSIS

5.1 Introduction

Dimensional Analysis is a method where the number of indispensable independent parameters is reduced to non-dimensional groups by combining the dimensional and non-dimensional variables and constants and neglecting the non-essential variables (Cengel & Cimbala 2018). Also, it is a technique for knowledge acquisition for the physical phenomenon before undertaking a theoretical or experimental analysis. The application of the dimensional analysis method is prevalent in nearly all engineering fields, mainly in thermo-fluid mechanics. The benefits of the dimensional analysis method are (Gibbings 2011):

- Reduce the number of required experiments by reducing the independent variables, and thus reduce the cost needed.
- The effect of some variables can be determined easily by changing the other variables in the same group.
- The dimensional analysis method shows through experiments that there are some variables that have no effect on the physical phenomena. Therefore, these variables can be excluded.
- Presenting the results is more straightforward.
- The dimensional analysis is used to make the experiments practicable by sizing down the system in case if the system is too large, or sizing up if the system is too small.

A dimensional analysis method will be used in this study to reduce the number of variables that affect DW performance into a set of non-dimensional groups. The focus will be on three-parameter groups. First, the process air and climate parameters, such as the ambient temperature, the process air humidity, and the process air velocity. Second, regeneration air parameters, such as the regeneration air temperature, humidity, and velocity. Lastly, the DW

design and operational parameters, such as DW rotational speed, thickness, the area ratio of process air section to regeneration air section, channel height, width, thickness, desiccant porosity, and volume ratio of desiccant material in the layer.

The application of dimensional analysis to any phenomenal is dependent on: a deep understanding of the natural phenomena that is being examined, listing all the dependent and independent variables of the problem, creating a relationship between these variables according to their units, and finally testing the created non-dimensional groups' validity. Thus, in this chapter, the DW dependant and independent parameters will be introduced. Then, the non-dimensional groups will be formed and examined experimentally and via the computational model.

5.2 DW parameters

From the mathematical model that has been introduced in section 3.2 the performance indices found to be affected by the following parameters as shown in Table 5.1 and Figure 5.1:

Table 5.1: DW dependant and independent parameters.

No.	Parameter symbol	Description	Unit
Process air after the DW (Dependent)			
1	T_2	Process air temperature after the DW	K
2	Y_2	Process air humidity after the DW	kg-water/kg-dry-air
Ambient air (Independent)			
3	T_1	Process air temperature before the DW	K
4	Y_1	Process air humidity before the DW	kg-water/kg-dry-air
5	u_p	Process air speed	m/s
6	ρ_a	Process air density	kg/m^3
Regeneration air (Independent)			
7	T_7	Regeneration air temperature before the DW	K
8	Y_7	Regeneration air humidity before the DW	kg-water/kg-dry-air
9	u_r	Regeneration air speed	m/s
DW design (Independent)			
10	L	DW thickness	m
11	θ_p	Process section angle	Degree [°]
12	θ_r	Regeneration section angle	Degree [°]
13	a	Channel half height	m
14	b	Channel half width	m
15	δ	Channel thickness	m
16	N	DW rotational speed	RPH
17	Φ	Volume ratio of the desiccant material in layer	---
18	ε	Desiccant porosity	---
Desiccant material and matrix (Independent)			
19	r	Average radius of desiccant material grain	m
20	ρ_d	Desiccant material density	kg/m^3
21	c_{pd}	Desiccant material specific heat capacity	J/kg.k
22	k_d	Desiccant material thermal conductivity	W/m.K
23	ρ_m	Matrix density	kg/m^3
24	c_{pm}	Matrix specific heat capacity	J/kg.k
25	W	The equilibrium isotherm of desiccant material	kg-adsorbate/kg-adsorbent
26	q_{st}	Heat of sorption	J/kg
27	K_y	Coefficient of mass convection	$kg/m^2.s$
28	α	Convective mass transfer coefficient	$kW/ m^2.K$

In this study, the focus will be on the DWs that are most popular and widespread in the market: those utilise silica gel as a desiccant material. The DW's used channels are made of a ceramic fibre substrate. The properties of the desiccant material and the matrix are shown in Table 4.1. The thermodynamic properties of the desiccant material and the matrix are assumed to be constant in order to ease the system

modelling. Therefore, both desiccant material and matrix parameters are excluded from constructing the non-dimensional groups.

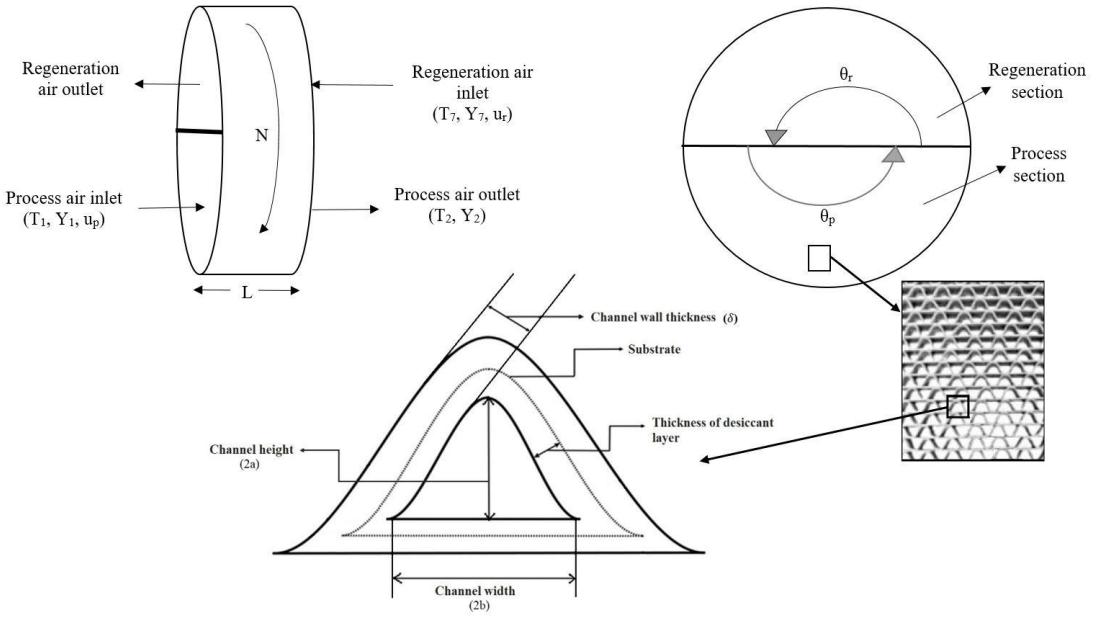

Figure 5.1: DW's parameters to form the non-dimensional groups.

5.3 Non-dimensional groups

The process of selecting the non-dimensional groups of this study, which depends on a trial and error approach, goes through several steps. First, investigating the DW dependant and independent parameters. Second, excluding the desiccant material parameters by assuming them as constants. Third, listing the parameters and state their units. Fourth, creating dimensionless relationships between the parameters depending on the physical understanding of the humidification and dehumidification process of the DW. And finally, testing the parameters combinations (which will be demonstrated in the next section).

Some of the independent parameters are interrelated like the process and regeneration sections angle, when increasing one variable the other one decreases by the same value. Therefore, the ratio of the process to regeneration section angle is considered as a non-dimensional group. Some parameters are already dimensionless, such as the process and regeneration air specific

humidity, the desiccant porosity, and the volume ratio of the desiccant in the layer. All the dimensionless parameters are considered as non-dimensional groups as well. The effects of these non-dimensional groups on the overall system performance will be demonstrated in the next chapter.

After running extensive experimental tests and simulation runs, the following non-dimensional groups are adopted for the independent parameters:

1) $\frac{K_y}{\rho_a \,.\, N \,.\, \delta}$
2) u_p/u_r
3) T_7/T_1
4) Y_1
5) Y_7
6) θ_p/θ_r
7) $\frac{C.L}{A_f}$
8) ε
9) Φ

Note that the channel height (a) and width (b) are used to calculate the channel perimeter (C) and the cross-sectional area of flow passage of one channel (A_f) as in equations 3.5 and 3.1, respectively. In addition, the DW diameter is not considered as an independent parameter because when increasing the DW diameter and keeping the airspeeds constant, the amount of supplied process and regeneration air will increase, and vice versa. A bigger DW diameter is used for a bigger cooling space, but it has no effect on the performance since both DWs have the same channel geometry and same airspeed. The number of independent parameters is reduced from 16 to 9 non-dimensional groups. In the next section, the testing methodology of the non-dimensional groups, and the testing results will be presented.

5.4 Testing the non-dimensional groups

The procedure to examine the non-dimensional groups is by varying different parameters values in the same group to attain the same non-dimensional group value and compare the results. The results are presented in terms of the non-dimensional performance indices which have been described in section 4.5. If the results are convergent and within the performance indices' uncertainty, the non-dimensional group can be adopted. When testing a non-dimensional group, the other non-dimensional groups' value remains constant. Some of the mentioned non-dimensional groups in the last section have been tested experimentally, and the others tested through the simulation model due to the difficulty of changing some parameters, such as the channel height, width and thickness, and the DW thickness. The parameters values to test the non-dimensional groups are chosen based on the literature and the common working condition for the DW.

5.4.1 Experimental examination of non-dimensional groups

In this sub-section, the experimentally tested non-dimensional groups will be presented, which are u_p/u_r and T_7/T_1. In the next sub-section, the computationally tested non-dimensional groups will be presented, which are $\frac{K_y}{\rho_a \,.\, N \,.\, \delta}$ and $\frac{C.L}{A_f}$.

The first non-dimensional group investigated experimentally was the process to regeneration airspeed ratio u_p/u_r. Two u_p/u_r values are examined; 0.5 and 1.0. For each value, two different airspeeds are chosen as shown in Table 5.2. The results of η_{deh}, DCOP, and SER for different (u_p/u_r) values show that changing the airspeeds, but keeping the speed ratio value constant does not affect the results as shown in Figure 5.2. Both results for 0.5 and 1.0 u_p/u_r are within the uncertainty of η_{deh}, DCOP, and SER, which presented in 4.6 Experimental accuracy and uncertainty. Therefore, the u_p/u_r ratio is considered to be the second non-dimensional group.

Table 5.2: Experimental test results for the non-dimensional group u_p/u_r.

Test No.	1	2	3	4
u_p/u_r (-)	0.5	0.5	1.0	1.0
System input parameters values				
u_p (m/s)	1.0	1.5	2.0	3.0
u_r (m/s)	2.0	3.0	2.0	3.0
T_1 (°C)	30.1	30.4	30.8	31.3
Y_1 (kg-water/kg-dry-air)	0.009431001	0.009410939	0.008746725	0.008640939
T_7 (°C)	70.4	70.1	67.5	68.3
Y_7 (kg-water/kg-dry-air)	0.005584640	0.005519119	0.005771152	0.005919119
θ_p/θ_r (-)	1.0	1.0	1.0	1.0
N (RPH)	15	15	15	15
P_{atm} (Pa)	94530	94530	94200	94200
System output parameters values				
T_2 (°C)	55.3	54.9	46.9	47.6
T_2 percentage difference (%)	0.73	0.73	1.48	1.48
Y_2 (kg-water/kg-dry-air)	0.004551959	0.004566174	0.004555381	0.004466174
Y_2 percentage difference (%)	0.31	0.31	1.98	1.98
Other non-dimensional groups values				
$\frac{K_y}{\rho_a \cdot N \cdot \delta}$ (-)	28631.87	28631.87	28631.87	28631.87
T_7/T_1 (-) ≈	1.13195	1.13195	1.13195	1.13195
$\frac{C.L}{A_f}$ (-)	226.458	226.458	226.458	226.458
ε (-)	0.4	0.4	0.4	0.4
Φ (-)	0.48	0.48	0.48	0.48

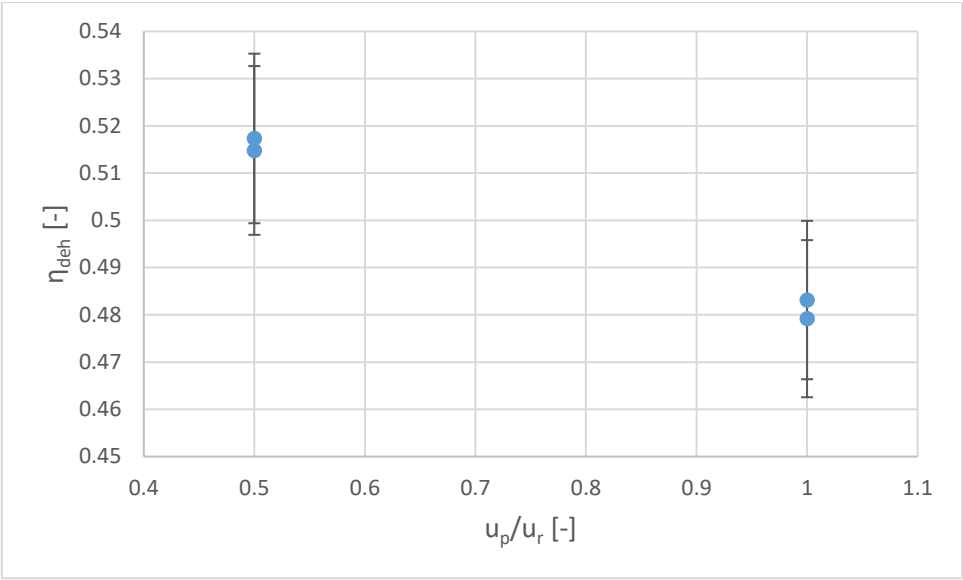

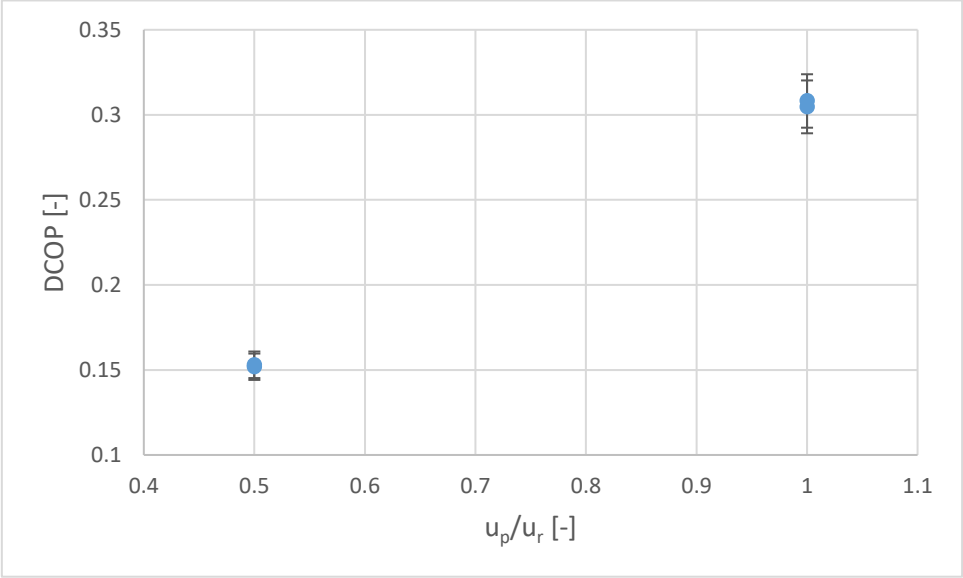

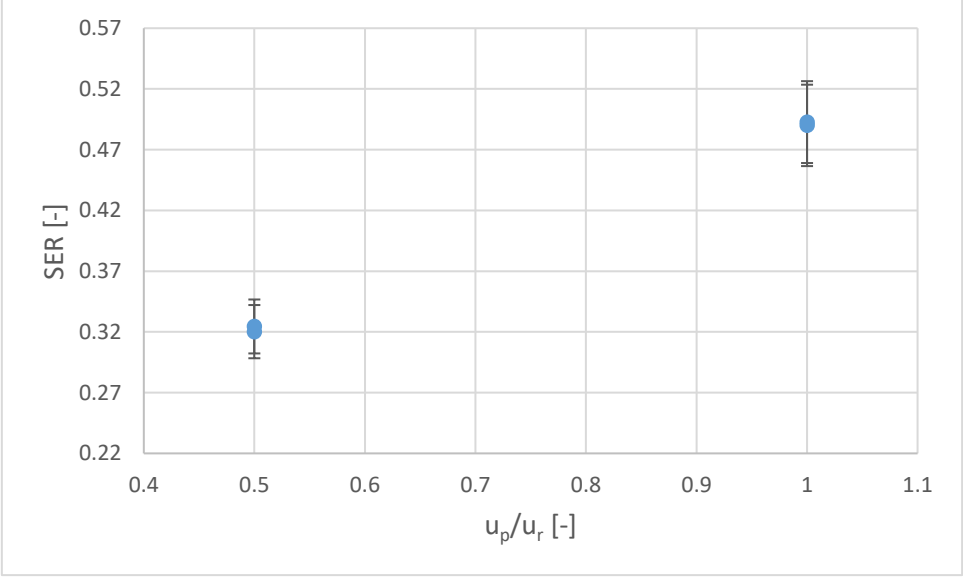

Figure 5.2: η_{deh}, DCOP, and SER as a function of u_p/u_r.

The second non-dimensional group investigated experimentally was the regeneration to process air temperature ratio T_7/T_1. Two T_7/T_1 values are examined; 1.111 and 1.144. For each value, three different air temperatures are chosen as shown in Table 5.3. The results of η_{deh}, DCOP, and SER for different T_7/T_1 values show that changing the air temperatures, but keeping the temperature ratio value constant does not affect the results as shown in Figure 5.3. Both results for 1.111 and 1.144 T_7/T_1 are within the uncertainty of η_{deh}, DCOP, and SER. Therefore, the T_7/T_1 ratio is considered to be the third non-dimensional group.

Table 5.3: Experimental test results of the non-dimensional group T_7/T_1.

Test No.	1	2	3	4	5	6
T_7/T_1 (-)	1.111	1.111	1.111	1.144	1.144	1.144
System input parameters' values						
T_7 (°C)	60.4 (333.55 K)	65.5 (338.65 K)	69.9 (343.05 K)	68.4 (341.55 K)	73.4 (346.55 K)	78.5 (351.65 K)
T_1 (°C)	27.1 (300.25 K)	31.7 (304.85 K)	35.6 (308.75 K)	25.3 (298.45 K)	29.7 (302.85 K)	34.1 (307.25 K)
Y_1 (kg-water/kg-dry-air)	0.008288708	0.00821154	0.00820903	0.008988708	0.00891154	0.00890903
Y_7 (kg-water/kg-dry-air)	0.005812113	0.005792571	0.005787788	0.005302113	0.005292571	0.005277788
u_p (m/s)	2.0	2.0	2.0	2.0	2.0	2.0
u_r (m/s)	2.0	2.0	2.0	2.0	2.0	2.0
θ_p/θ_r (-)	1	1	1	1	1	1
N (RPH)	15	15	15	15	15	15
P_{atm} (Pa)	94210	94210	94210	94510	94510	94510
System output parameters' values						
T_2 (°C)	40.9	45.7	49.8	44.4	49.1	53.8
Y_2 (kg-water/kg-dry-air)	0.004691342	0.004645454	0.004622455	0.004591342	0.004524545	0.004509246
Other non-dimensional groups' values						
$\frac{K_y}{\rho_a \,.\, N \,.\, \delta}$ (-)	28631.87	28631.87	28631.87	28631.87	28631.87	28631.87
u_p/u_r (-)	1.0	1.0	1.0	1.0	1.0	1.0
$\frac{C.L}{A_f}$ (-)	226.458	226.458	226.458	226.458	226.458	226.458
ε (-)	0.4	0.4	0.4	0.4	0.4	0.4
Φ (-)	0.48	0.48	0.48	0.48	0.48	0.48

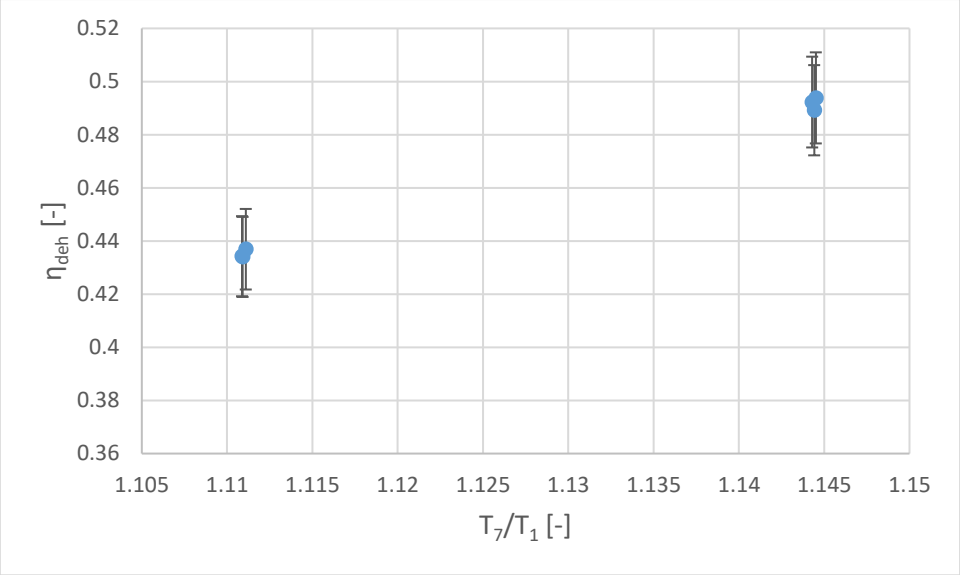

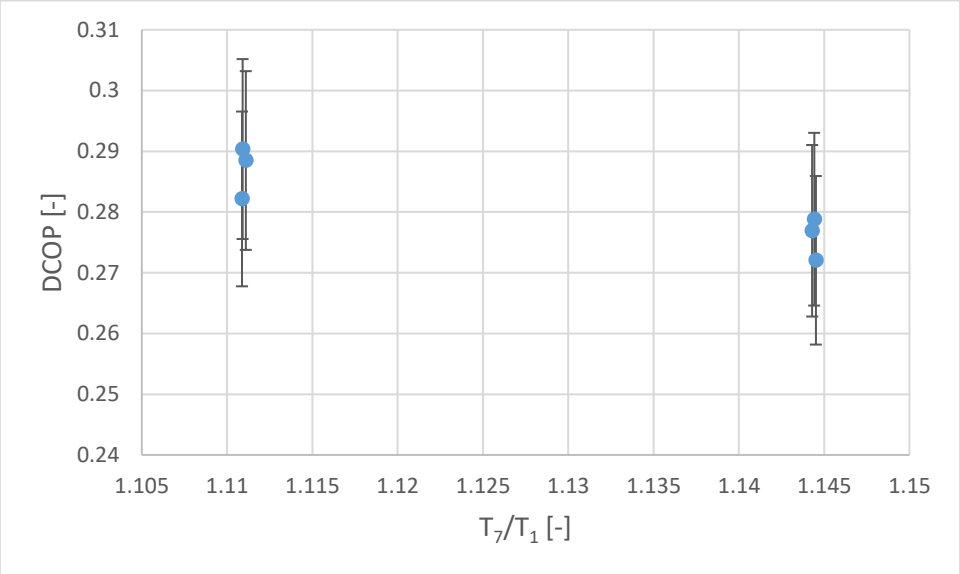

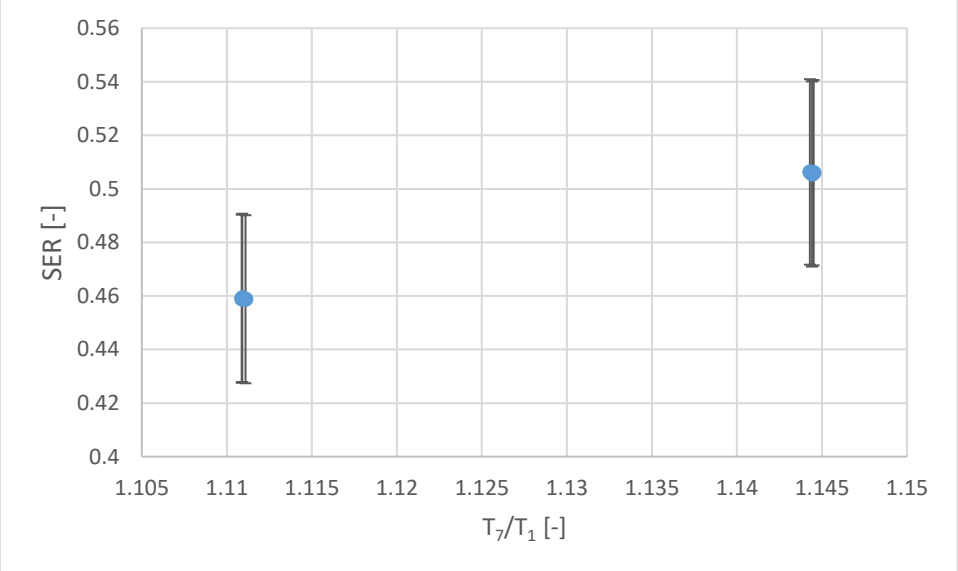

Figure 5.3: η_{deh}, DCOP, and SER as a function of T_7/T_1.

5.4.2 Simulation examination of non-dimensional groups

It was impractical or impossible to assess the effects of some non-dimensional groups experimentally because of the difficulty of changing some parameters values. Therefore, the mathematical model is used to test some of the non-dimensional groups by applying the same followed approach to test the non-dimensional groups experimentally. The remaining parameters are the DW rotational speed, the channel height, width and thickness, and the DW thickness. The simulation input parameters are identical in all cases as in Table 5.4 except as otherwise stated.

Table 5.4: Simulation input parameters' and non-dimensional groups' values for non-dimensional groups testing.

Input parameters' values					
N	15 RPH	u_r	2 m/s	δ	0.00034 m
T_1	30 °C	Y_1	0.012 kg-water/kg-dry-air	L	0.1 m
T_7	70 °C	Y_7	0.006 kg-water/kg-dry-air	ε	0.4
P_{atm}	95000 Pa	a	0.0012 m	Φ	0.48
u_p	2 m/s	b	0.0020 m	θ_p/θ_r	1.0
Non-dimensional groups' values					
T_7/T_1 (-)	1.13195	u_p/u_r (-)	1.0	$\frac{K_y}{\rho_a \,.\, N \,.\, \delta}$ (-)	28631.87
$\frac{C.L}{A_f}$ (-)	226.458				

Table 5.5 shows the results of testing $\frac{K_y}{\rho_a \,.\, N \,.\, \delta}$. Two $\frac{K_y}{\rho_a \,.\, N \,.\, \delta}$ values are examined; 28631.87 and 32000.0. For each value, two different DW rotational speed and channel thickness are chosen. The results of η_{deh}, DCOP, and SER for different $\frac{K_y}{\rho_a \,.\, N \,.\, \delta}$ values show that changing the DW rotational speed and channel thickness, but keeping the $\frac{K_y}{\rho_a \,.\, N \,.\, \delta}$ ratio value constant has only a slight effect on the results. Therefore, the $\frac{K_y}{\rho_a \,.\, N \,.\, \delta}$ ratio is considered to be the third non-dimensional group.

Table 5.5: output results for testing the non-dimensional group $\frac{K_y}{\rho_a \,.\, N \,.\, \delta}$, two values are examined by changing N and δ values.

	$\frac{K_y}{\rho_a \,.\, N \,.\, \delta}$	N (RPH)	δ (m) ||	T_2 (K)	Y_2 (kg-water/kg-dry-air)	η_{deh}	DCOP	SER
a)	28631.87	15.0	0.00034	319.26	0.007291498	0.392	0.321	0.455
b)	28631.87	11.25	0.00045333	319.17	0.007226523	0.398	0.326	0.452
c)	32000.0	18.367	0.00025	318.72	0.007575447	0.369	0.302	0.439
d)	32000.0	9.184	0.0005	318.54	0.007505849	0.375	0.307	0.434

Table 5.6 shows the results of testing $\frac{C.L}{A_f}$. Two different channel perimeter, DW thickness and three-channel air flow passage areas are chosen; in the first and second case, the channel perimeter remains constant, in the second and third case the DW thickness remains constant. The results of η_{deh}, DCOP, and SER for different $\frac{C.L}{A_f}$ values show that changing the DW thickness and channel height and width, but keeping the $\frac{C.L}{A_f}$ ratio value constant has only a slight effect on the results. Therefore, the $\frac{C.L}{A_f}$ ratio is considered to be the fourth non-dimensional group.

Table 5.6: Output results for testing the non-dimensional group $\frac{C.L}{A_f}$.

	$\frac{C.L}{A_f}$	C (m)	L (m)	A_f (m^2)	T_2 (K)	Y_2 (kg-water/kg-dry-air)	η_{deh}	DCOP	SER
a)	226.458	0.010870018	0.05	0.0000024	319.35	0.007249012	0.396	0.324	0.457
b)	226.458	0.010870018	0.1	0.0000048	319.26	0.007291498	0.392	0.321	0.455
c)	226.458	0.016305027	0.1	0.0000072	319.09	0.007338341	0.388	0.318	0.450

Varying the temperature between the process section and regeneration section causes a little change in the thermodynamic properties of the desiccant material and the matrix, like the density and the specific heat. But considering them as constant in the simulation model and excluding other parameters related to the desiccant material and matrix justify the small variation in the simulation performance indices results for the same non-dimensional group.

Other non-dimensional parameters combinations listed in the table below have been tested. But, when testing them by the same adopted methodology, the results of the performance

indices were extremely dissimilar. Thus, the non-dimensional parameters combinations listed in Table 5.7 cannot be considered as non-dimensional groups that can be used to characterise a system.

Table 5.7: Additional tested non-dimensional parameters combinations.

1)	a/b	4)	f	7)	$\frac{D_h . L}{A_t}$	10)	$\frac{N . L}{u_p}$
2)	L/δ	5)	$\frac{C . L}{A_t}$	8)	$\frac{N . D}{\sqrt{R . T_1}}$	11)	$\frac{N . L}{u_r}$
3)	C/D_h	6)	$\frac{D_h . L}{A_f}$	9)	$\frac{N . L}{\sqrt{R . T_1}}$	12)	$\frac{K_y \, . \, C}{\rho_a \, . \, A_t \, . \, N}$

All the conducted non-dimensional groups have a considerable effect on the system performance except the regeneration air humidity as will see in the next chapter. A change of Y_7 from 0.006 to 0.012 is relatively negligible because it causes a reduction in η_{deh}, DCOP, and SER by just 1.4%, 1.8%, and 0.5%, respectively.

5.5 Summary and conclusions

The dimensional analysis method is a technique to reduce the number of any phenomena variables by combining the related variables into non-dimensional groups. Some benefits of the dimensional analysis method are to reduce the number of required experiments and thus reduce the cost of conducted experiments as a conclusion of reducing the number of studied variables, study the effect of some parameters by changing other parameters values in the same group in case of extreme cases, and create a prototype by downsizing or enlarge the actual system to facilitate experimentation.

In this study, depending on the DW's mathematical model and the experimental setup, the DW's dependent and independent parameters are divided into three categories; the process air and climate parameters, regeneration air parameters, and the DW design and operational parameters. The desiccant material parameters are assumed to be constant.

In order to create the non-dimensional groups, the process went through the following steps; listing the independent and dependent parameters, identifying the units of the parameters, creating non-dimensional parameters combinations, and testing the created parameters combinations.

Varying different parameters values in the same non-dimensional parameters combinations and compare the output results is the method implemented to test the non-dimensional groups. If the results are convergent and within the performance indices' uncertainty, the non-dimensional group is adopted. Some non-dimensional groups have been tested experimentally and the others tested by the mathematical model due to the difficulty of changing some parameters experimentally. The number of independent parameters has been reduced from 16 to 9 non-dimensional groups.

CHAPTER 6: EXPERIMENTAL AND COMPUTATIONAL RESULTS AND DISCUSSION

6.1 Introduction

The experiments reported in this chapter are carried out in the system described in CHAPTER 4: EXPERIMENTAL SETUP OF THE DESICCANT WHEEL SYSTEM. The analysis of the non-dimensional groups is carried out referring to a base value. The results presented in CHAPTER 5: DIMENSIONAL ANALYSIS were solely to evaluate the non-dimensional groups and demonstrate their viability. In this chapter, first, the effect of each non-dimensional groups on the system performance will be investigated. Then, two of the non-dimensional groups are varied simultaneously in order to investigate their effects on the system performance and to study the relationship between each of the non-dimensional groups and another.

6.2 Investigating the effect of the non-dimensional groups on the system performance

The effect of the non-dimensional groups on the overall system performance will be studied. Only one non-dimensional group value will be varied, while all other non-dimensional groups' values will be set to the base value as in Table 6.1. This will help to determine the extent of their impacts on the outcome results. As regards the temperature and humidity values in table 6.1, the values are just approximate values, as the actual values are within ±0.7% and ±5.5%, respectively.

Table 6.1: The experimental and simulation non-dimensional groups tested, their range of tested values, and base value.

Non-dimensional groups	Values	Base value
$\frac{K_y}{\rho_a . N . \delta}$	17179.12 21473.90 28631.87 42947.80 85895.61	28631.87 (N = 15 RPH, δ = 0.00034 m)
u_p/u_r	0.333 0.5 1.0 2.0 3.0	1.0 ($u_p = u_r$ = 2 m/s)
T_7/T_1	1.066 1.099 1.132 1.165 1.198	1.132 (T_7 = 343.15K, T_1 = 303.15K)
Y_1	0.006 0.009 0.012	0.009
Y_7	0.006 0.009 0.012	0.006
θ_p/θ_r	1.0 2.0 3.0	1.0 ($\theta_p = \theta_r = 180^o$)
$\frac{C . L}{A_f}$	195.07 208.24 221.78 282.33	226.46
ε	0.2 0.3 0.4 0.5 0.6	0.4
Φ	0.3 0.4 0.5 0.6 0.7	0.48

Non-dimensional groups' values optimisation is a complicated process. For instance, a maximum value for η_{deh} and DCOP is desirable, which represents superior dehumidification performances and better energy utilisation. On the other hand, a higher value for SER means a higher temperature value of the treated air and hence a higher cooling load which must be avoided. The main advantage of using the DW integrated with the SDC system is to save energy

and utilise renewable energy sources for cooling purposes. Therefore, a proposed system to cover a specific cooling load will be introduced in CHAPTER 7: NON-DIMENSIONAL GROUPS' OPTIMISATION in order to compare the SDC system with the most conventional cooling technique, which is a VCC system. In addition, the non-dimensional groups' values will be optimised according to the highest achieved energy saving.

This section gives a general idea about how varying the non-dimensional groups' values will affect the system performance, while the explanation of the performance indices' curves will be illustrated in the next sections.

6.2.1 Experimental investigation of the non-dimensional groups on the system performance

The first six non-dimensional groups in Table 6.1 will be studied experimentally due to the possibility of changing their values. The three remaining non-dimensional groups will be studied through the mathematical simulation model.

Figure 6.1 shows the effect of the non-dimensional group $K_y/\rho_a.N.\delta$ on the system η_{deh}, DCOP, and SER. The experimental values listed in Table 6.1 were supplemented by the simulation model within the range 21473.90 to 48661.68 due to the difficulty to obtain a small variation in the DW rotational speed experimentally. It is clear that the maximum for both η_{deh} and DCOP occurs when $K_y/\rho_a.N.\delta$ is slightly smaller than 42947.80. Regarding the SER, it was found that the SER rapidly decreases to an asymptotic value of 0.45 with an increase in $K_y/\rho_a.N.\delta$ value. Therefore, it is found from the Figure 6.1 that the most effective tested value of $K_y/\rho_a.N.\delta$ was between 35789.84 and 48661.68, and most likely around 42947.80, which maximises the η_{deh} and DCOP, while the SER is found to be at one of the lowest values.

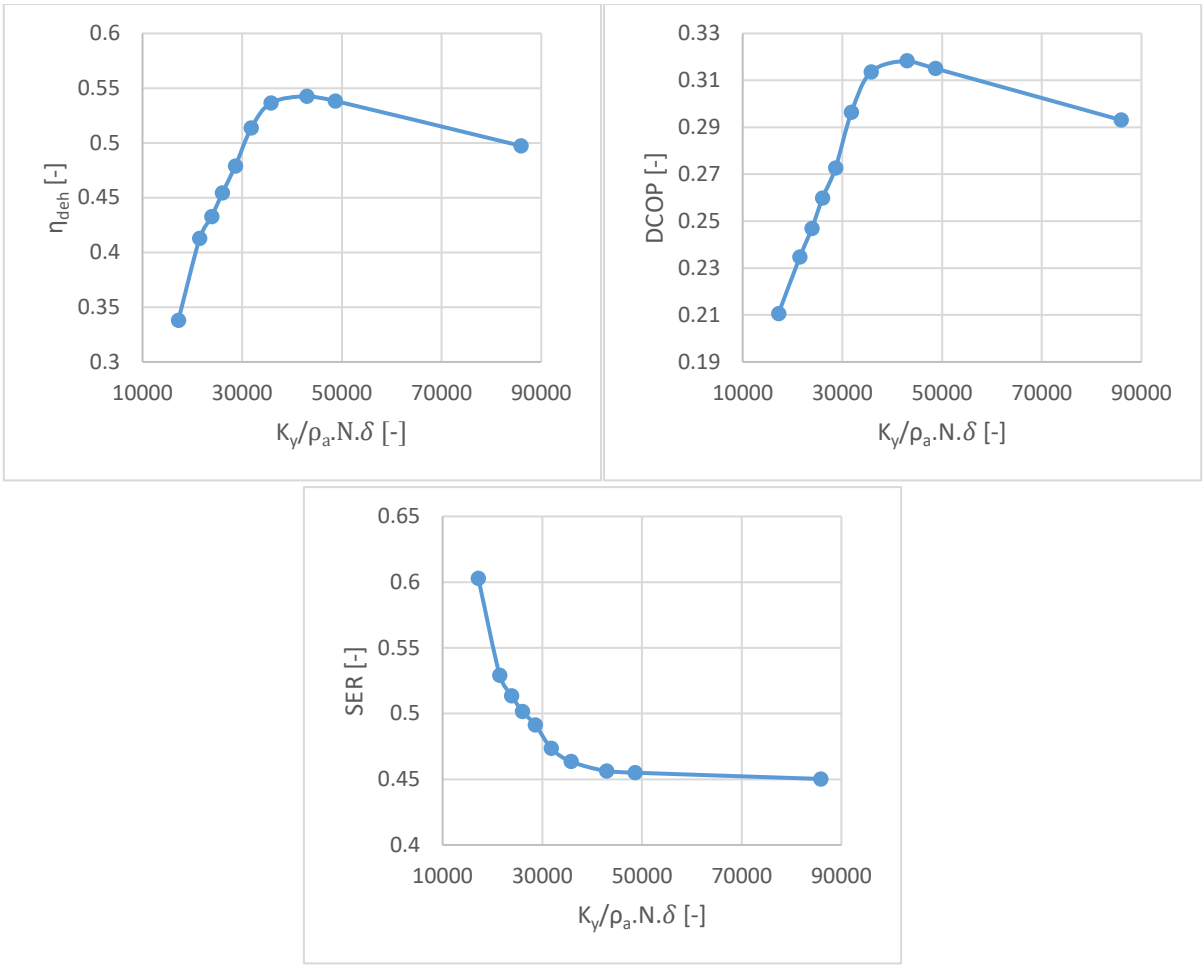

Figure 6.1: Effect of the non-dimensional group $K_y/\rho_a.N.\delta$ on the system η_{deh}, DCOP, and SER.

The effect of the non-dimensional group u_p/u_r on the system η_{deh}, DCOP, and SER is presented in Figure 6.2. It is observed that an increase in the u_p/u_r value decreases the η_{deh} and increases DCOP and SER. A slight decrease in the η_{deh} value between 0.333 and 0.5 of u_p/u_r is found then a considerable drop between 0.5 and 3.0.

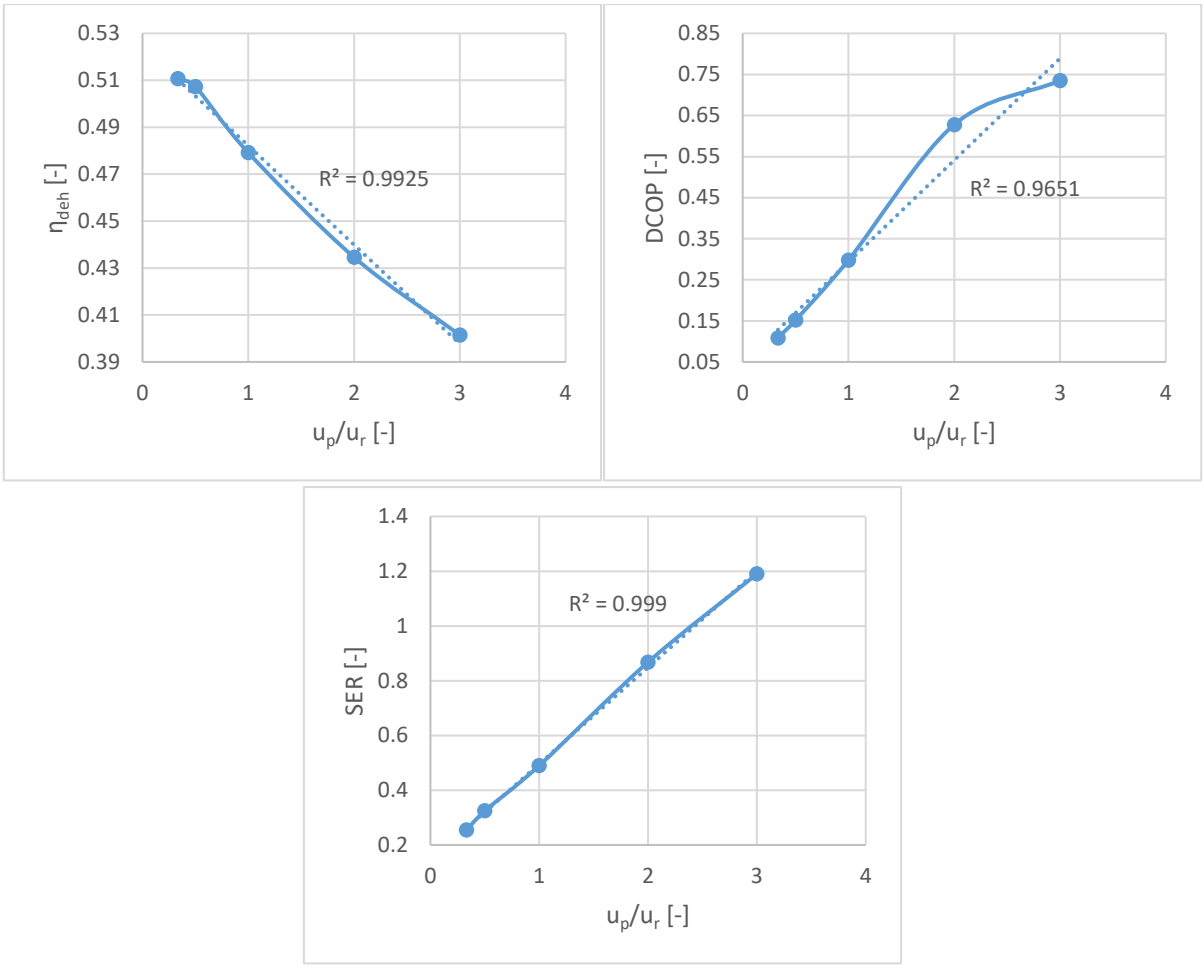

Figure 6.2: Effect of the non-dimensional group u_p/u_r on the system η_{deh}, DCOP, and SER.

Figure 6.3 illustrate the effect of the non-dimensional group T_7/T_1 on the system η_{deh}, DCOP, and SER. It is found that an increase in the T_7/T_1 value causes an increase in the η_{deh} and SER, while it decreases the DCOP. A sharp increase in the η_{deh} between 1.066 and 1.132 of T_7/T_1 was noticed, then asymptotically approaching the maximum value of 0.515.

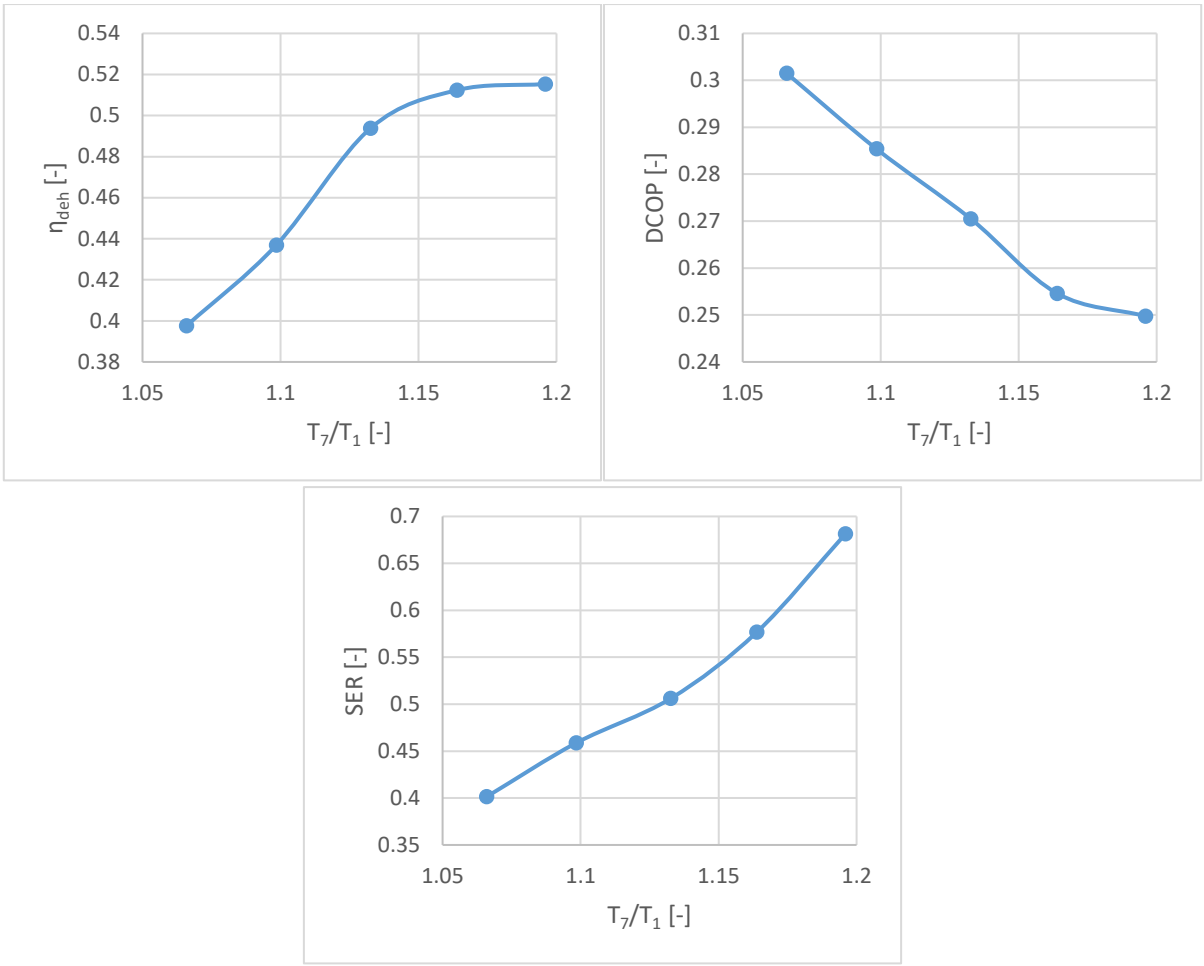

Figure 6.3: Effect of the non-dimensional group T_7/T_1 on the system η_{deh}, DCOP, and SER.

Figure 6.4 represents the effect of the non-dimensional group Y_1 on the system η_{deh}, DCOP, and SER. It is observed that η_{deh} is increasing with increase the process inlet humidity till it reaches the maximum at around 0.009, then it starts to drop. The behaviour of the DCOP and SER are similar, both are increasing with any increment in Y_1.

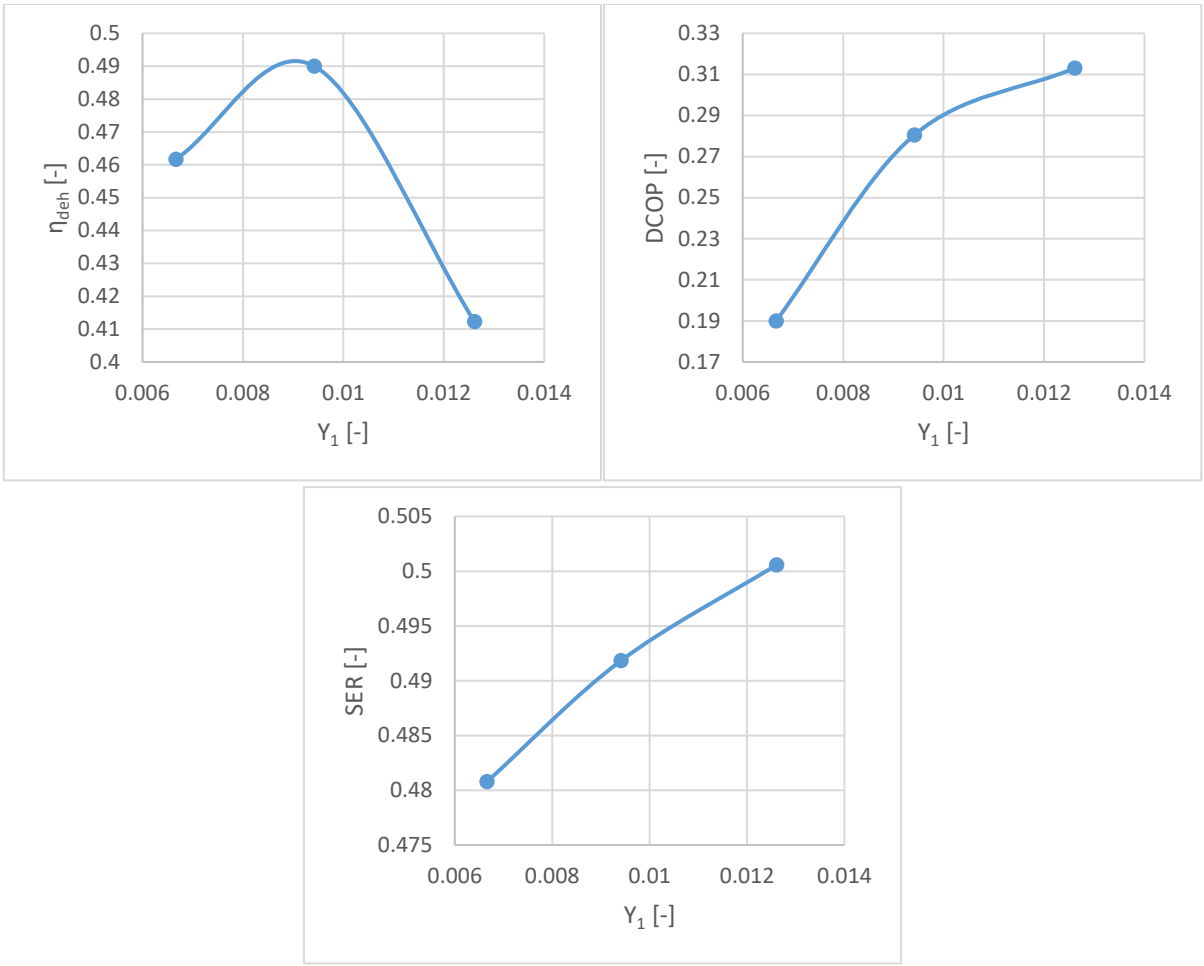

Figure 6.4: Effect of the non-dimensional group Y_1 on the system η_{deh}, DCOP, and SER.

The influence of varying the non-dimensional group Y_7 on the overall DW system performance is illustrated in Figure 6.5. The value of the performance indices' slightly decreases with an increase in the regeneration air inlet humidity. Considering the uncertainty for the performance indices η_{deh}, DCOP, and SER which equals to ±3.47%, ±5.1%, and ±6.84%, respectively as illustrated in section 4.6 Experimental accuracy and uncertainty, a lower Y_7 value leads to a little improvement in the system performance.

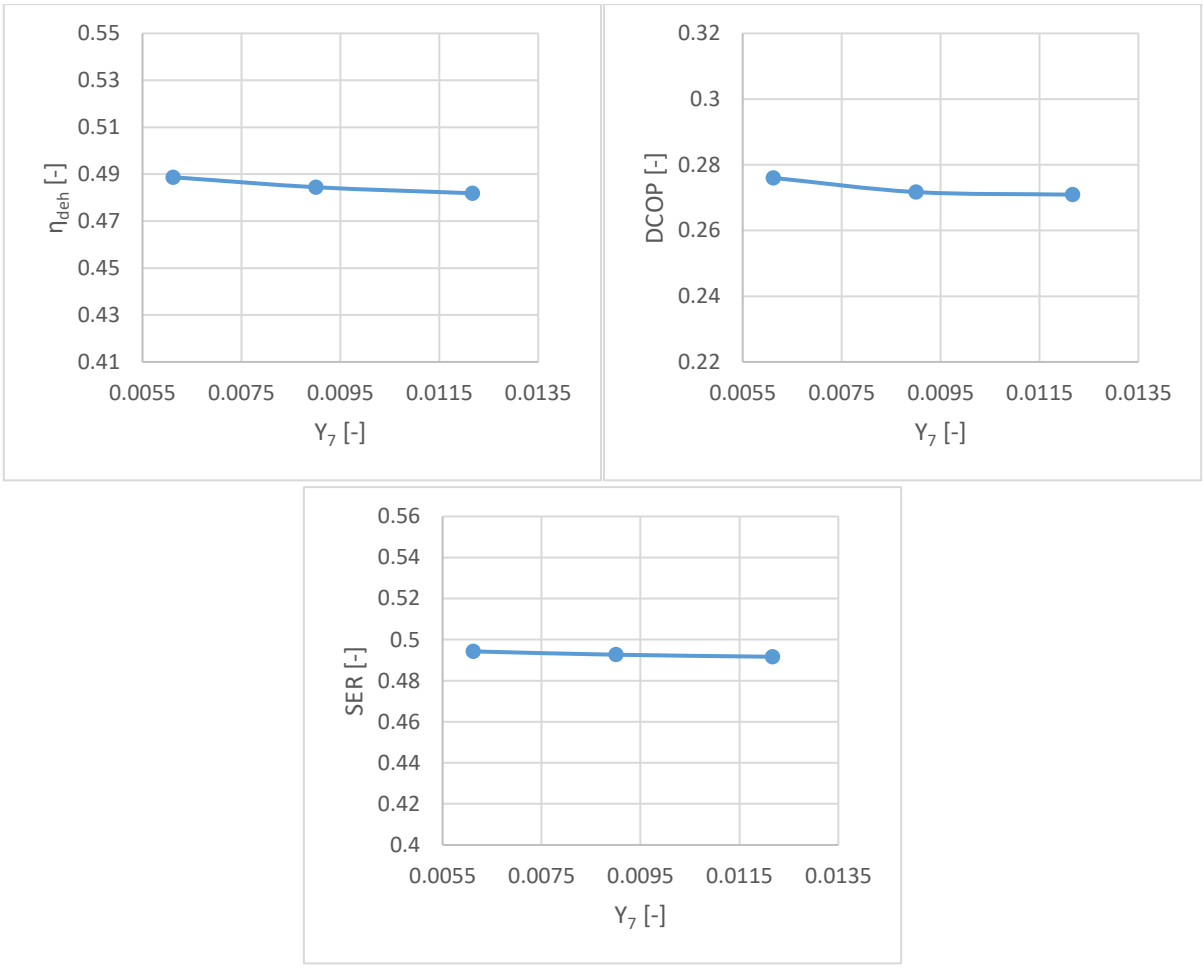

Figure 6.5: Effect of the non-dimensional group Y_7 on the system η_{deh}, DCOP, and SER.

Figure 6.6 shows the effect of the non-dimensional group θ_p/θ_r on the system η_{deh}, DCOP, and SER. The performance index curves are somewhat similar in terms of their behaviour in increasing or decreasing the performance indices curves to the non-dimensional group u_p/u_r. But the descent in the η_{deh} between the 1.0 and 2.0 of θ_p/θ_r is massive as well as the rise in SER.

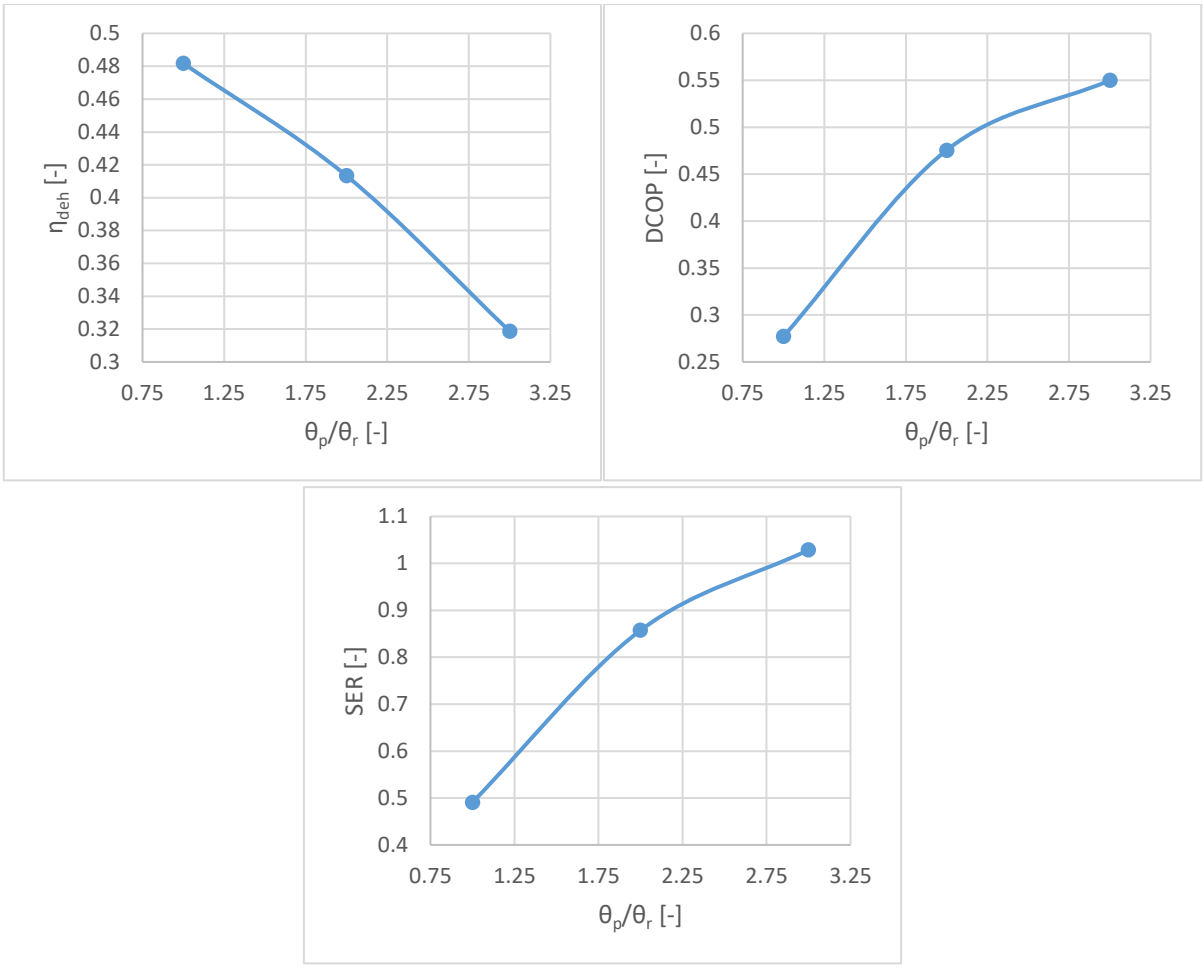

Figure 6.6: Effect of the non-dimensional group θ_p/θ_r on the system η_{deh}, DCOP, and SER.

6.2.2 Computational investigation of the non-dimensional groups on the system performance

The effect of varying the non-dimensional group $C.L/A_f$ on the DW system performance is elucidated in Figure 6.7. A positive linear relationship is obtained for the system η_{deh}, DCOP, and SER with increasing the value of $C.L/A_f$.

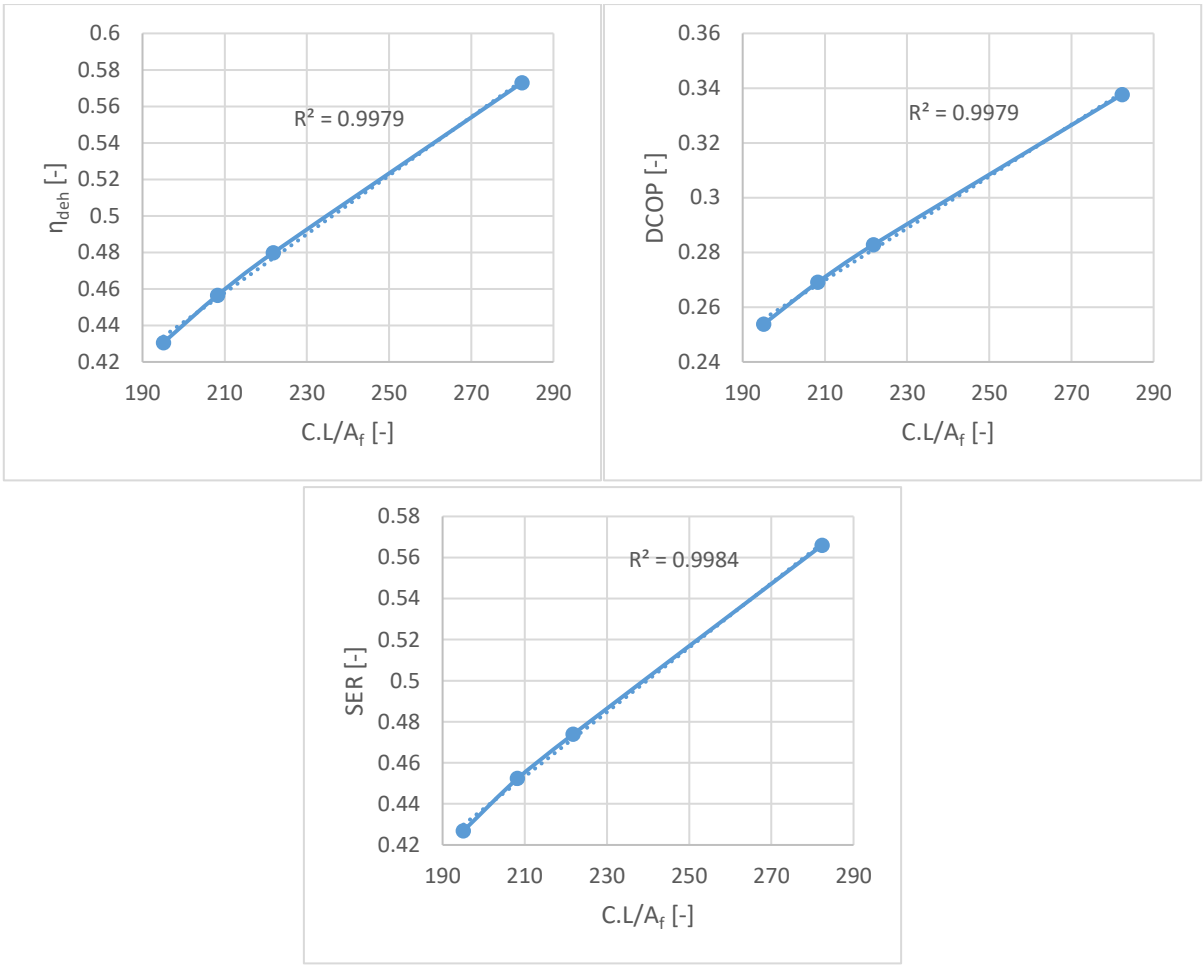

Figure 6.7: Effect of the non-dimensional group $C.L/A_f$ on the system η_{deh}, DCOP, and SER.

Figure 6.8 represents the effect of the non-dimensional group ε on the system η_{deh}, DCOP, and SER. The figure shows that any increment in the channel porosity causes a steady reduction in all of the performance indices' values. The electrical energy required to operate the process air fan increases with decreasing the channel porosity but as it is a small fraction of the total required energy, the overall energy does not change much. The power needed to operate the blowers in this study was around 0.8 kW in most cases compared with 20 kW total power added to the system. A reduction of porosity value causes an increase in the pressure drop in the passing air and thus increases the power needed to overcome the pressure drop. However, the increment in the power could be around 10% of the 0.8 kW which equals 0.08 kW and leads to a 0.4% decrease in the output result, and vice versa.

The output performance indices trend will not change, but it will be flattened downward by 0.4% at low porosity and flattened upward by 0.4% at high porosity. As a result, the effect of the added power to the air blower due to the pressure drop is negligible.

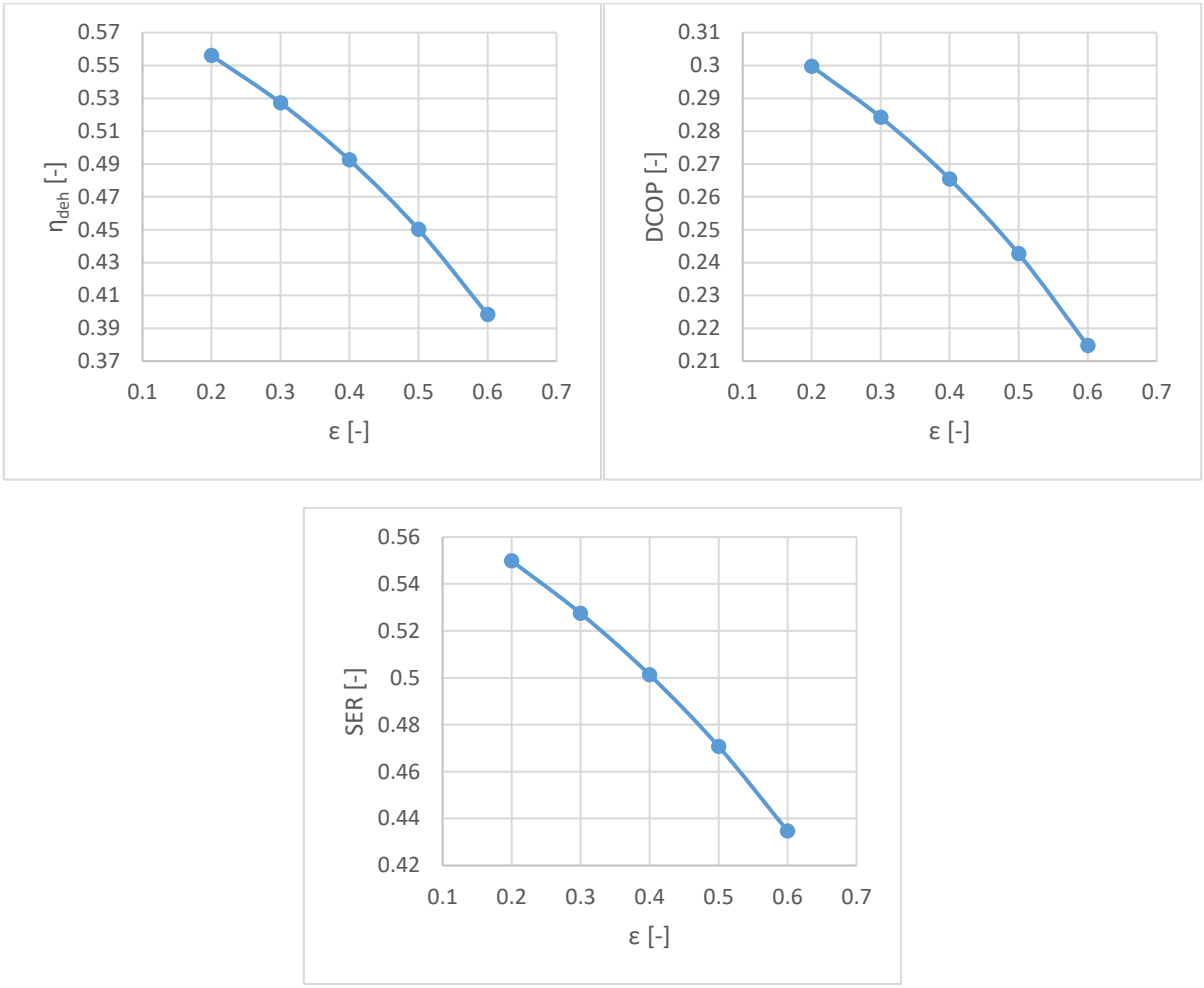

Figure 6.8: Effect of the non-dimensional group ε on the system η_{deh}, DCOP, and SER.

Figure 6.9 represents the effect of the non-dimensional group Φ on the system η_{deh}, DCOP, and SER. Unlike the non-dimensional group ε, the increase in the non-dimensional group Φ causes a steady increase in the DW η_{deh}, DCOP, and SER.

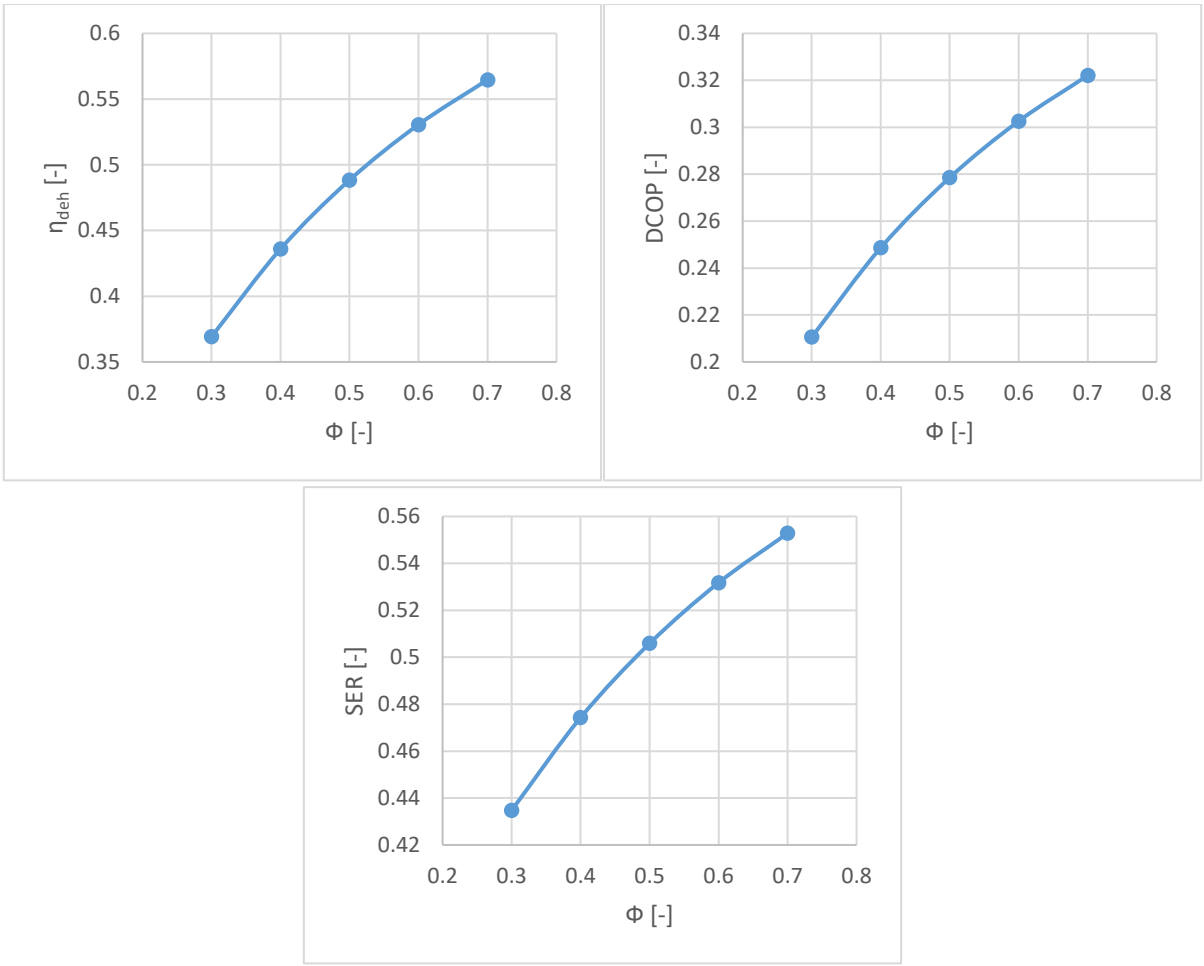

Figure 6.9: Effect of the non-dimensional group Φ on the system ηdeh, DCOP, and SER.

As have seen above, the effect on each non-dimensional groups on the performance indices is inconsistent. For all bar one of the non-dimensional groups, increasing the value of the non-dimensional group improves some system performance metrics, while making others worse. The amount and the manner of the effect on the system performance are divergent among the non-dimensional groups. All the non-dimensional groups have an undeniable impact on the overall system performance, except the humidity of the regeneration air. It was found that an increase in the regeneration air humidity has a minor effect on the η_{deh}, DCOP, and SER since the regeneration air at relatively high temperature is not saturated and can easily adsorb and reject the humidity in the desiccant material.

In order to validate the computational model for this study's operation conditions, the result of the experimental system is compared with the simulation outcomes. The chosen system input

parameters values are at the non-dimensional groups' base value to ensure all the parameters values are identical in both experimental and simulation model. For that reason, the experimental results of the non-dimensional group $K_y/\rho_a.N.\delta$ are compared with the computational outcome. It is found that the discrepancy for η_{deh}, DCOP, and SER are within ± 4.6%, ± 5.1%, and ± 4.9%, respectively.

6.3 Experimental investigating the effect of each non-dimensional groups on others in respect of the system performance

The system input and output data for this section which used to generate the graphs are presented in APPENDIX B: EXPERIMENTAL SYSTEM INPUT AND OUTPUT DATA.

6.3.1 The performance indices as a function of $K_y/\rho_a.N.\delta$

6.3.1.1 The performance indices as a function of $K_y/\rho_a.N.\delta$ for different u_p/u_r values

In Figure 6.10, η_{deh} as a function of $K_y/\rho_a.N.\delta$ for different u_p/u_r values is shown. The effect of $K_y/\rho_a.N.\delta$ is analogous in all u_p/u_r values. The experimental values listed in table 6.1 were supplemented by the simulation model within the range 21473.90 to 42947.80 due to the difficulty to obtain a small variation in the DW rotational speed experimentally. The figure shows that a decrease in the u_p/u_r value causes an increase in the η_{deh} at the same $K_y/\rho_a.N.\delta$ value. When increasing u_p with constant u_r, as in case of $u_p/u_r > 1.0$, the process air mass flow rate increases while the regeneration air flow rate remains fixed, introducing more humidity to be adsorbed while the regeneration process rate is the same in all situations. Therefore, when the regeneration airspeed is constant, the higher η_{deh} attained at lower process airspeed. In contrast, when increasing u_r with constant up, as in case of $(u_p/u_r) < 1.0$, the higher regeneration airspeed leads to more thermal energy provided to the DW in order to reactivate the desiccant material when the regeneration temperature is constant. Hence, disposal of the adsorbed humidity in the process section becomes more enhanced, easier, and faster. Under such

circumstances, the η_{deh} is improved. The optimum $K_y/\rho_a.N.\delta$ value decreases (i.e. the optimal DW rotational speed increases) with decreasing value of u_p/u_r to reduce the residence time in the regeneration section so it is matched with the reduced time required to dispose of the humidity due to the higher regeneration airspeed.

Figure 6.11 shows that DCOP behaves similarly to η_{deh}, except that an increase in u_p/u_r increases DCOP. The optimum $K_y/\rho_a.N.\delta$ value for all cases is in the vicinity of 42947.80.

SER as a function of $K_y/\rho_a.N.\delta$ for different u_p/u_r values is shown in Figure 6.12. The increase in the u_r value causes an increase in the dehumidification process, and thus, an increase in the released heat of adsorption and the treated process air temperature, as well as, the SER. However, the increase in the process air thermal energy due to the increase of u_p value has a much higher impact on the SER than the increase in the treated air temperature through the dehumidification process. Therefore, an increase in the u_p/u_r value causes an increase in the SER. As regards the effect of $K_y/\rho_a.N.\delta$ on the SER, at low DW rotational speed, the DW can smoothly get off the desorbed heat from the regeneration section. Accordingly, a lower $K_y/\rho_a.N.\delta$ value causes higher treated air temperature and higher SER as well.

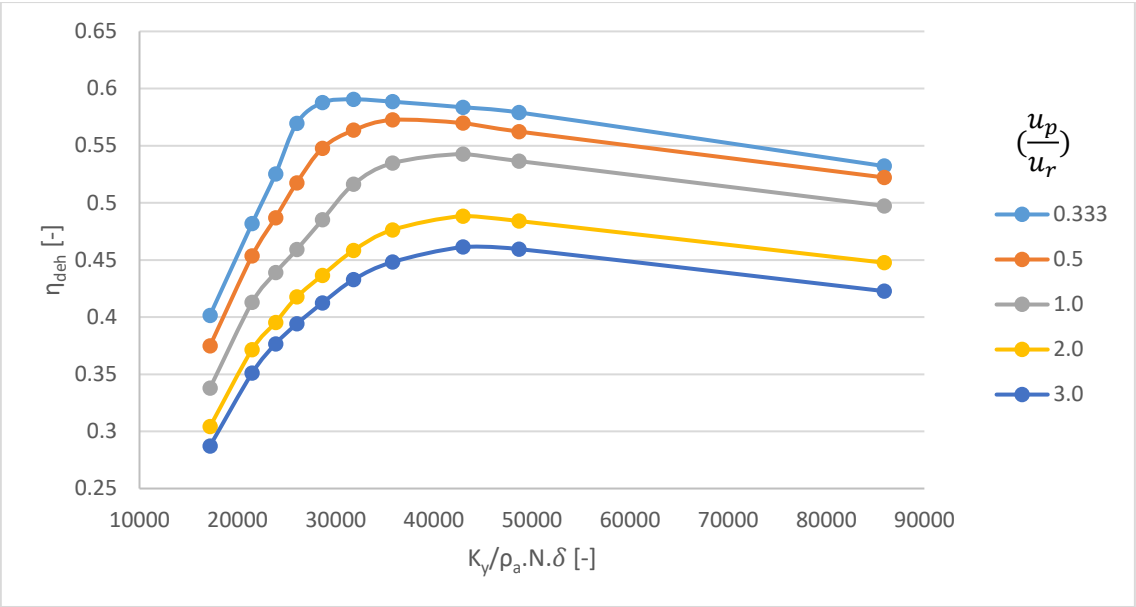

Figure 6.10: η_{deh} as a function of $K_y/\rho_a.N.\delta$ for different u_p/u_r values.

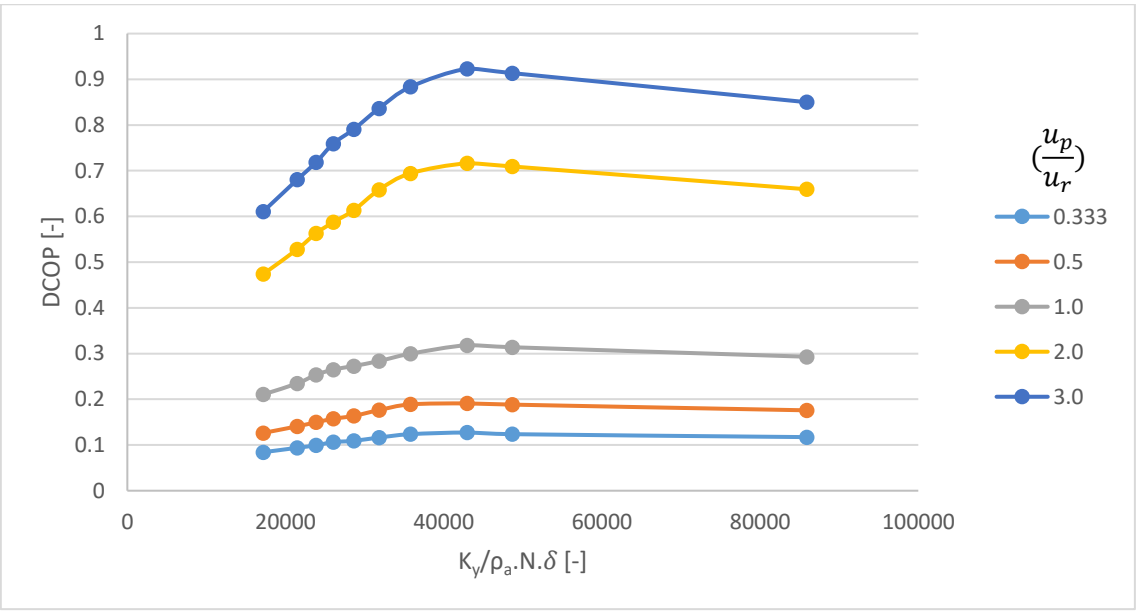

Figure 6.11: DCOP as a function of $K_y/\rho_a.N.\delta$ for different u_p/u_r values.

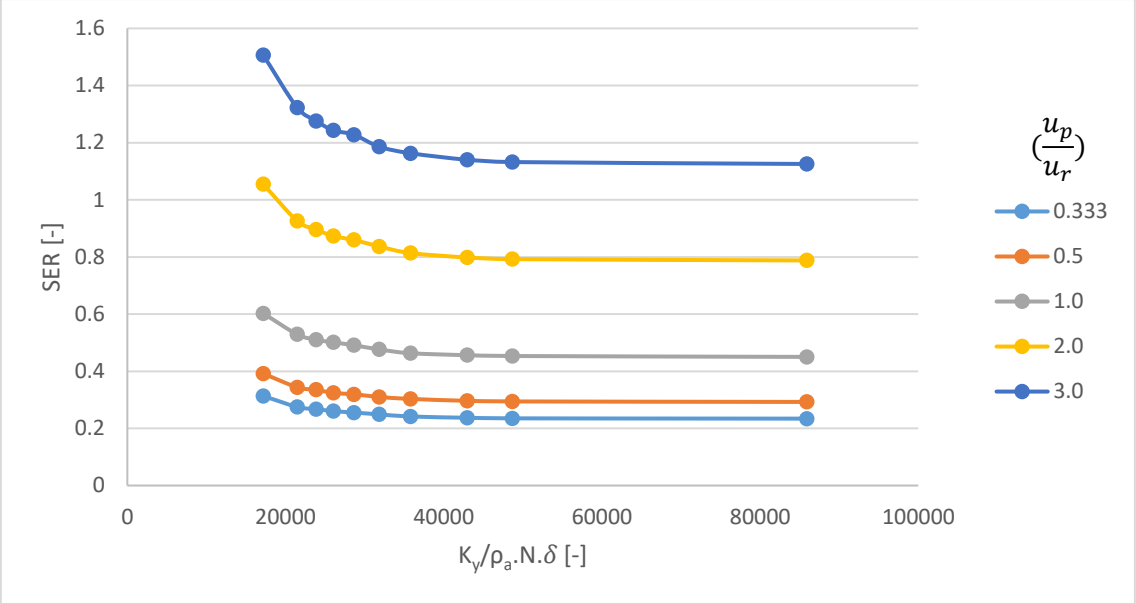

Figure 6.12: SER as a function of $K_y/\rho_a.N.\delta$ for different u_p/u_r values.

6.3.1.2 The performance indices as a function of $K_y/\rho_a.N.\delta$ for different T_7/T_1 values

In figure 6.13, η_{deh} as a function of $K_y/\rho_a.N.\delta$ for different T_7/T_1 values is shown. As in Figure 6.10, all values are examined experimentally except some values between 21473.90 and 42947.80 which are not stated in Table 6.1. A higher T_7/T_1 value means a higher regeneration temperature at constant process air temperature, which causes a higher value of dehumidification capability (De) (defined by the humidity difference of the process air after and before the DW) and as a result a higher η_{deh}. In fact, a higher regeneration temperature means a more effective reactivation process and then drier desiccant material after the regeneration section and more able to desorb and accordingly a higher De and η_{deh}. As in u_p/u_r case, the optimal $K_y/\rho_a.N.\delta$ value is decreased from the vicinity of 42947.80 to the vicinity of 31813.19 when the T_7/T_1 value is increased from 1.132 to 1.198.

As regards the DCOP, Figure 6.14 shows an increase in the T_7/T_1 causes an increase in the thermal power provided to the DW per mass flow rate, and hence increase the term ($h_7 - h_1$) with constant h_1. Therefore, an inverse relationship exists between the DCOP and the

temperature ratio. The highest DCOP in all cases was found to be at $K_y/\rho_a.N.\delta$ value in the vicinity of 42947.80.

For the treated process air thermal power, Figure 6.15 shows the SER as a function of $K_y/\rho_a.N.\delta$ for different T_7/T_1 values. An increase in the T_7/T_1 value causes a higher desiccant material temperature. Because the amount of heat transfer is proportional to the temperature difference, an increase of T_7/T_1 value causes an increase in the treated process air temperature. Also, as noted from the Figure 6.15, the SER value increases with $K_y/\rho_a.N.\delta$ reduction, because at high $K_y/\rho_a.N.\delta$ value, the DW's desiccant material eliminates the most absorbed heat through the process section at the constant process and regeneration airspeeds.

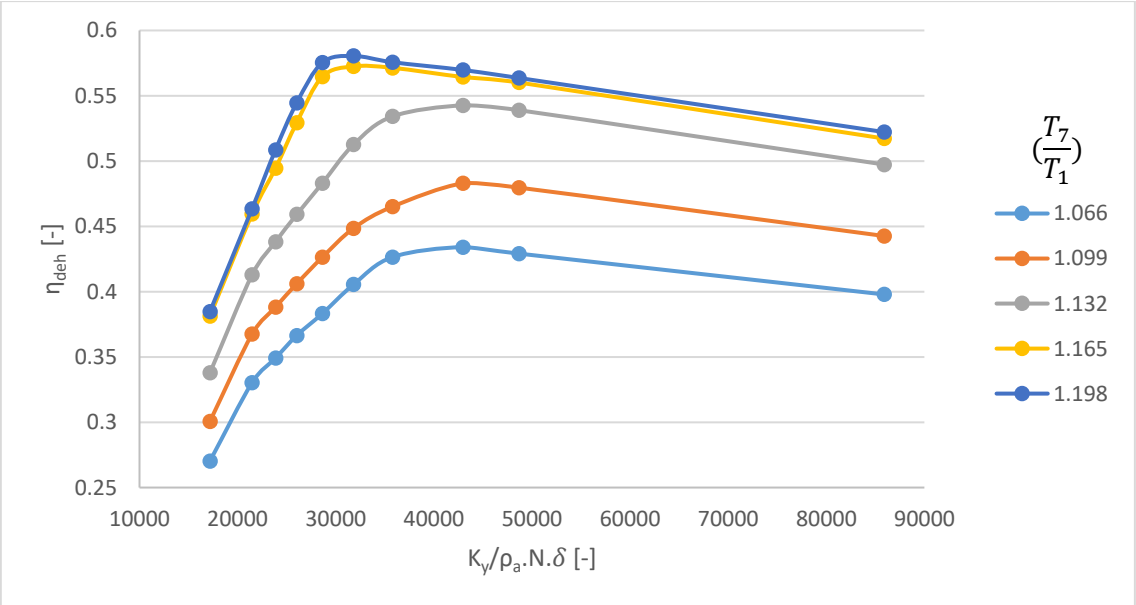

Figure 6.13: η_{deh} as a function of $K_y/\rho_a.N.\delta$ for different T_7/T_1 values.

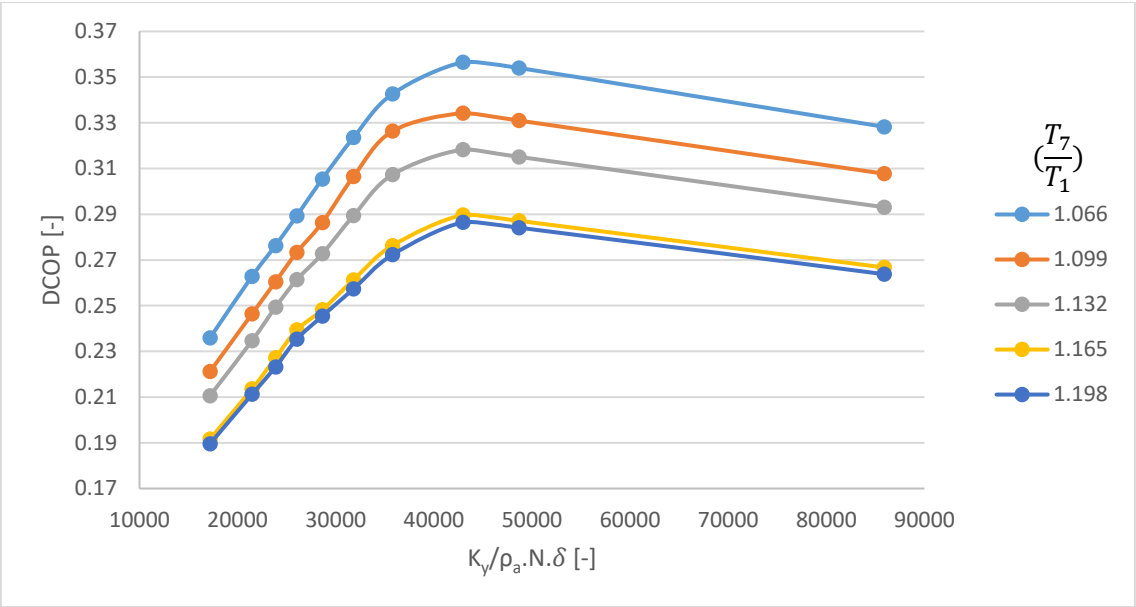

Figure 6.14: DCOP as a function of $K_y/\rho_a.N.\delta$ for different T_7/T_1 values.

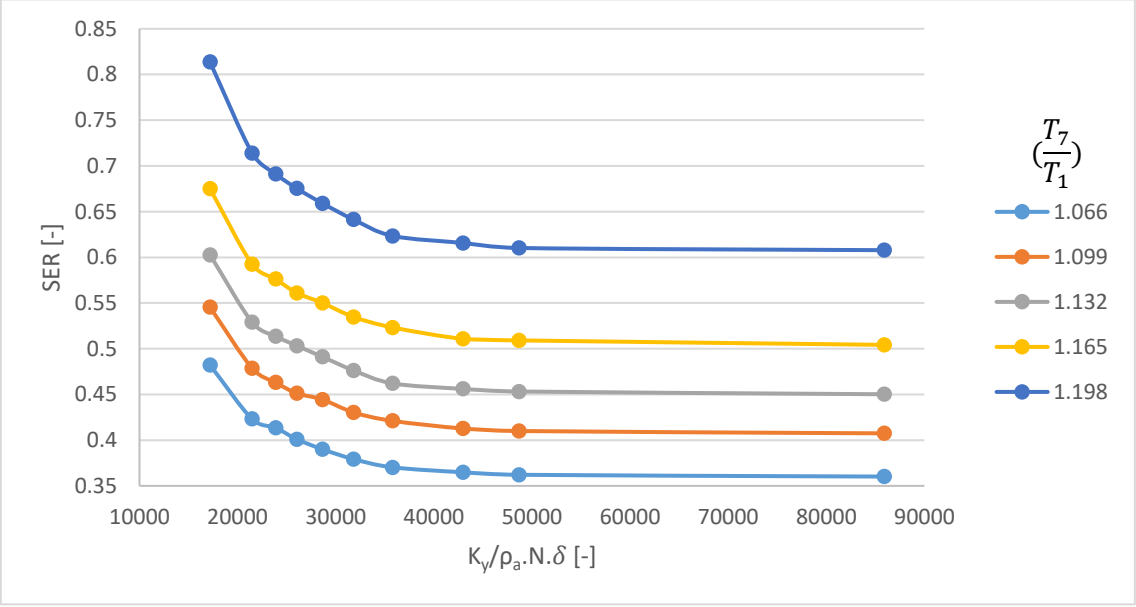

Figure 6.15: SER as a function of $K_y/\rho_a.N.\delta$ for different T_7/T_1 values.

6.3.1.3 The performance indices as a function of $K_y/\rho_a.N.\delta$ for different Y_1 values

In Figure 6.16, η_{deh} as a function of $K_y/\rho_a.N.\delta$ for different Y_1 values is shown. A higher value of Y_1 causes an increase in De. On the other hand, a high value of Y_1 produces a higher difference of vapour partial pressure between the desiccant material and the process air, which leads to a higher diffusion of water particles. In spite of that, η_{deh} increases with a little

increment of the Y_1 as illustrated in figure 6.16 for the value 0.009. But for a much higher Y_1 value as in the value 0.012, the value of η_{deh} is negatively affected. The optimal $K_y/\rho_a.N.\delta$ value for all cases is slightly less than 42947.80.

DCOP as a function of $K_y/\rho_a.N.\delta$ for different Y_1 values is shown in Figure 6.17. At a constant regeneration temperature in all cases, the regeneration thermal energy delivered to the DW is equal in all cases. As mentioned before, an increase in the Y_1 causes an increase in the De which forms a part of the DCOP numerator equation. As a result, a higher Y_1 value causes a higher DCOP value. The optimal $K_y/\rho_a.N.\delta$ value for all cases is in the vicinity of 42947.80.

Figure 6.18 shows the SER as a function of $K_y/\rho_a.N.\delta$ for different Y_1 values. An increase of Y_1 causes an increase in the dehumidification process, and it is accompanied by an increase in the released adsorption heat. Consequently, with constant regeneration and inlet process air temperatures, a higher treated process air temperature is caused by an increment of Y_1, and thus a slightly higher SER. A lower value of $K_y/\rho_a.N.\delta$ means a higher value of the DW rotational speed when the other variables are constants. With any increment in the rotational speed, the DW's desiccant material cannot remove the absorbed heat through the process section easily, as a result, a higher treated air temperature and higher SER.

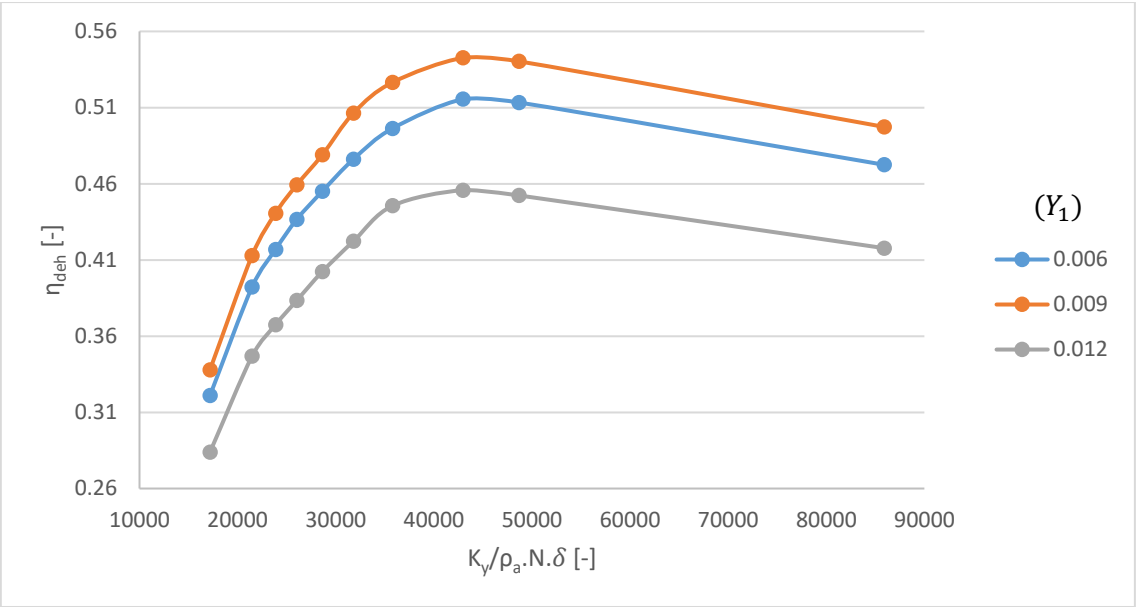

Figure 6.16: η_{deh} as a function of $K_y/\rho_a.N.\delta$ for different Y_1 values.

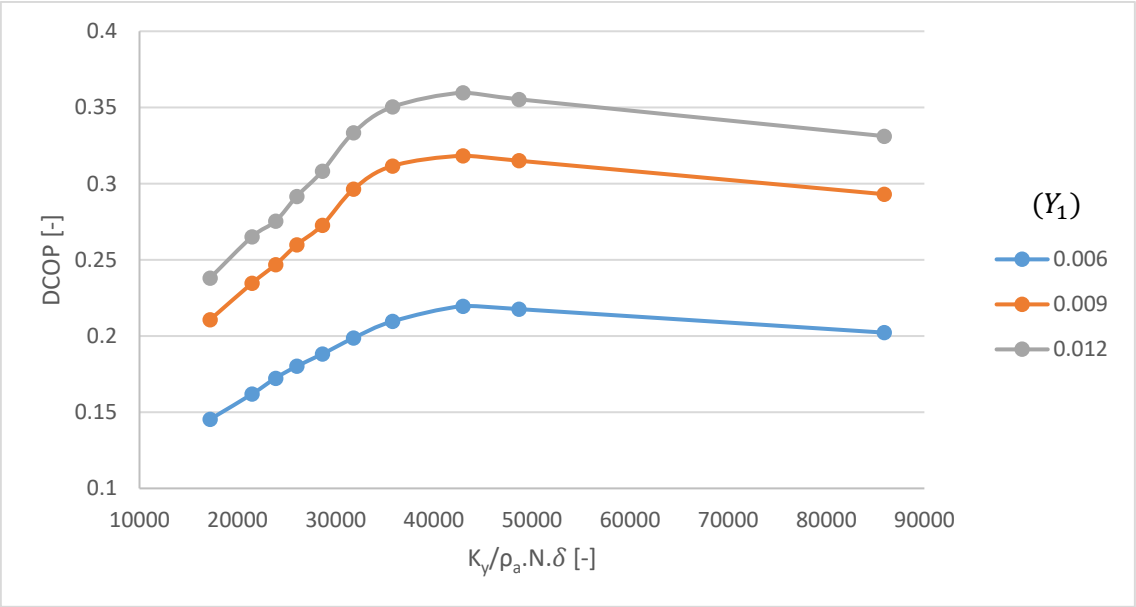

Figure 6.17: DCOP as a function of $K_y/\rho_a.N.\delta$ for different Y_1 values.

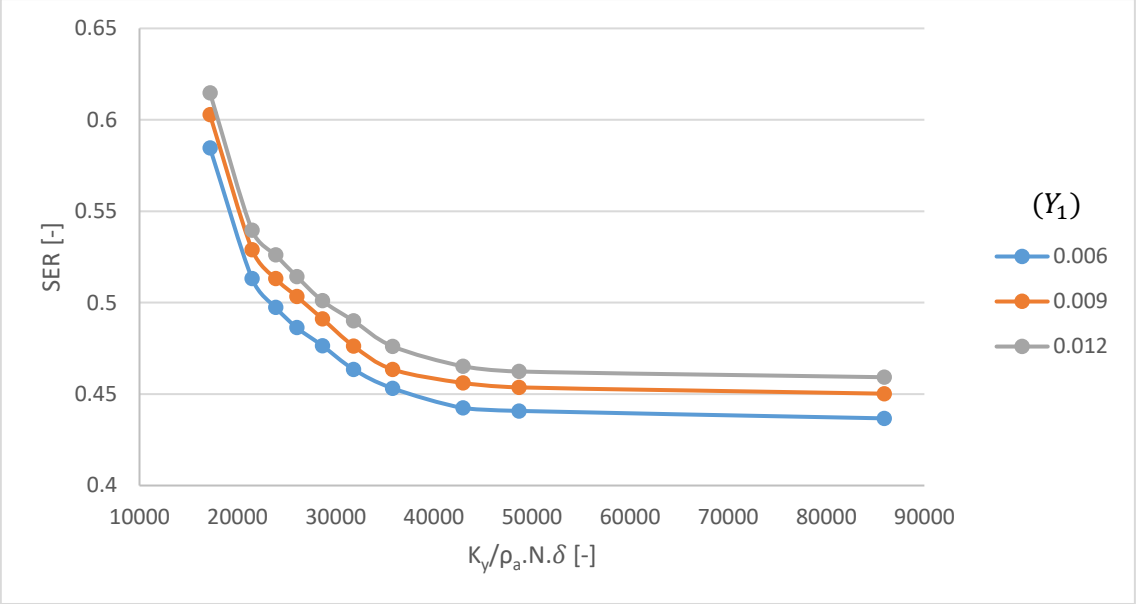

Figure 6.18: SER as a function of $K_y/\rho_a.N.\delta$ for different Y_1 values.

6.3.1.4 The performance indices as a function of $K_y/\rho_a.N.\delta$ for different θ_p/θ_r values

Unlike the previous non-dimensional groups, the terms of θ_p/θ_r are related. So, any increase in the θ_p causes a reduction of θ_r value. Figure 6.19 shows the η_{deh} as a function of $K_y/\rho_a.N.\delta$ for different θ_p/θ_r values. For lower θ_p/θ_r value, the regeneration section mass flow rate increase with the constant process and regeneration airspeed and the process mass flow rate decrease. In other words, more regeneration airflow rate to reactivate the DW while lower process air flow rate. In view of that, it was found that among the tested θ_p/θ_r ratios, the lower θ_p/θ_r value maximises the η_{deh}. Same as in Figure 6.16, the optimal $K_y/\rho_a.N.\delta$ value for all cases is in the vicinity of 42947.80. For lower $K_y/\rho_a.N.\delta$ the DW has an inadequate time to reactivate the desiccant material, especially for higher θ_p/θ_r values.

In Figure 6.20, DCOP as a function of $K_y/\rho_a.N.\delta$ for different θ_p/θ_r values is shown. At fixed process and regeneration airspeeds, the thermal energy provided to the DW increases when the θ_p/θ_r value decreases. Also, the mass flow rate ratio of the process to regeneration air decreases. Hence, an increase in the θ_p/θ_r value causes an increase in the DCOP and in SER as in Figure 6.21. The $K_y/\rho_a.N.\delta$ value that maximises the DCOP for all cases is close to 42947.80. Whereas

a lower $K_y/\rho_a.N.\delta$ value means a slower cooling process through the process air section, a higher treated air temperature, and higher SER.

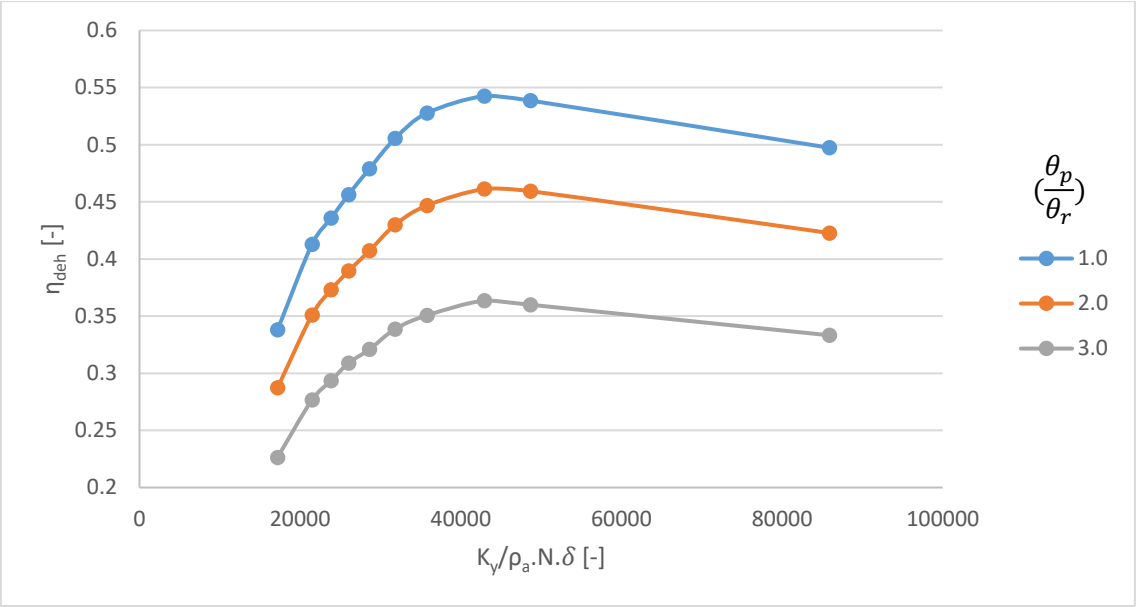

Figure 6.19: η_{deh} as a function of $K_y/\rho_a.N.\delta$ for different θ_p/θ_r values.

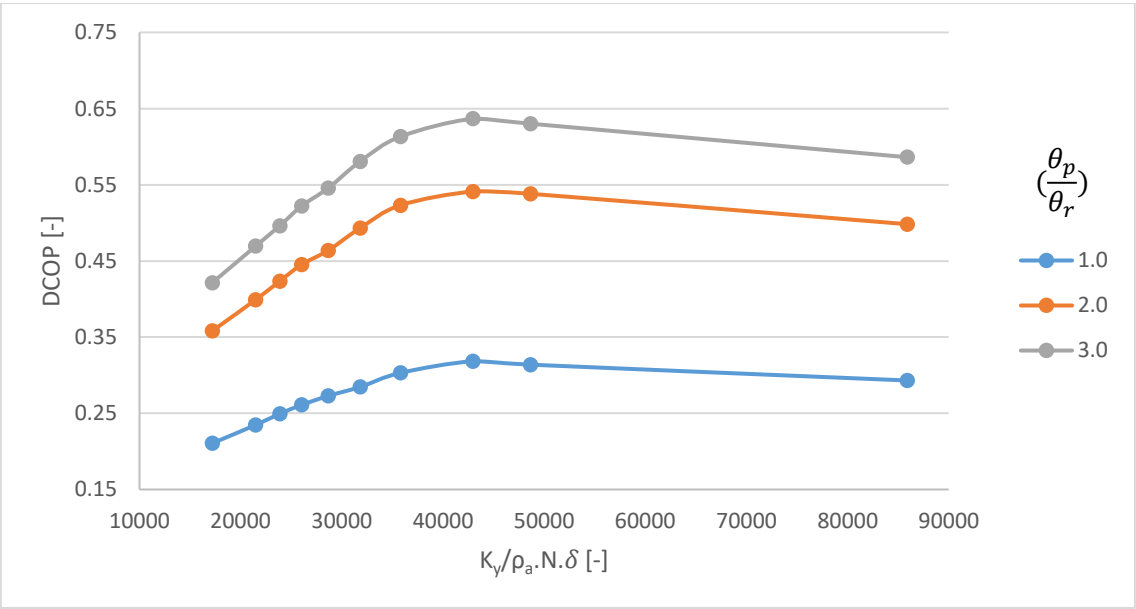

Figure 6.20: DCOP as a function of $K_y/\rho_a.N.\delta$ for different θ_p/θ_r values.

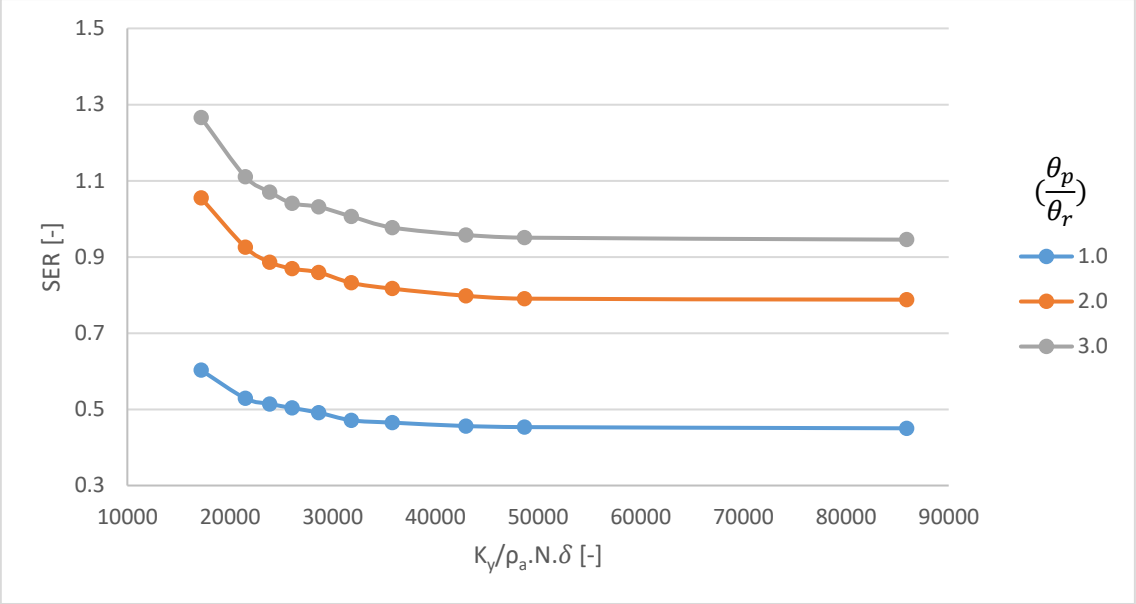

Figure 6.21: SER as a function of $K_y/\rho_a.N.\delta$ for different θ_p/θ_r values.

6.3.2 The performance indices as a function of u_p/u_r

6.3.2.1 The performance indices as a function of u_p/u_r for different T_7/T_1 values

In Figure 6.22, η_{deh} as a function of u_p/u_r for different T_7/T_1 values is shown. Generally, increasing the T_7/T_1 value leads to an increase in the η_{deh} value at the same u_p/u_r. The reason for this is due to increasing the regeneration temperature and keeping the process air temperature constant means more effective desiccant material reactivation process, more adsorbed humidity in the process section, and higher De as well as η_{deh}. The optimal u_p/u_r value in case of increasing T_7/T_1 value is also increased gradually due to less regeneration airspeed is required to reactivate the desiccant material in case of high regeneration temperature. Therefore, increasing the T_7/T_1 or decreasing the u_p/u_r values facilitates the regeneration process.

Figure 6.23 shows the DCOP as a function of u_p/u_r for different T_7/T_1 values. An increase in the T_7/T_1 causes an increase in the thermal power provided to the DW per mass flow rate and so a decrease in the DCOP. While an increase in the u_p/u_r value causes a rise in the air

dehumidification thermal power and a reduction in the regeneration thermal energy. Thus, a substantial increase in the system DCOP is experiential by increasing the u_p/u_r value.

As mentioned before, an increase in the T_7/T_1 values and keeping the process air temperature constant leads to the transfer of more thermal energy to the desiccant materials and higher treated process air temperature. Consequently, a higher SER is attained as in Figure 6.24. As regards the effect of u_p/u_r on the SER, two factors affect the result. First, increase the u_r value causes drier desiccant material, more dehumidification process and thus more released adsorption heat and higher treated process air temperature. Second, an increase in the u_p value causes a massive increase in the process air's thermal energy. Accordingly, the increase in the SER due to increasing the u_r is not as much as due to increasing the process airspeed. To conclude, increasing the u_p/u_r value leads to an increase in the SER.

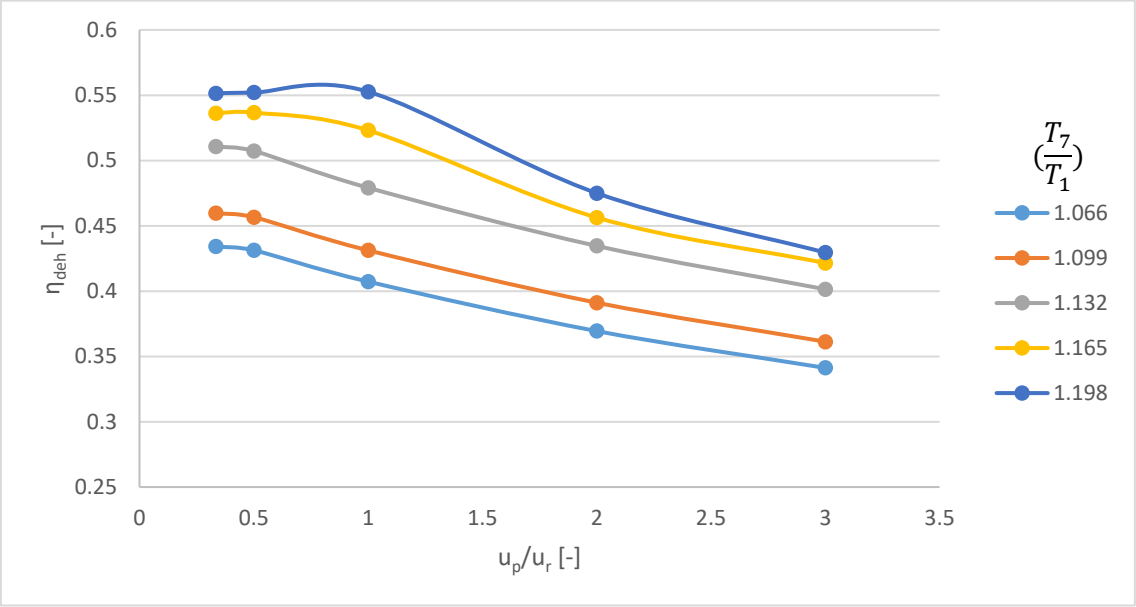

Figure 6.22: η_{deh} as a function of u_p/u_r for different T_7/T_1 values.

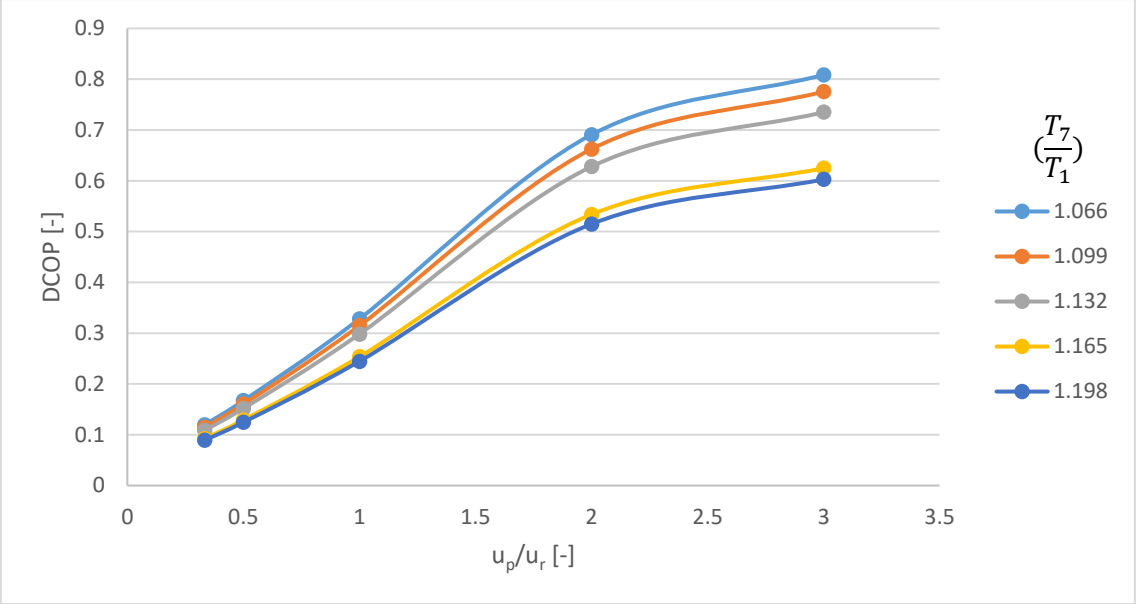

Figure 6.23: DCOP as a function of u_p/u_r for different T_7/T_1 values.

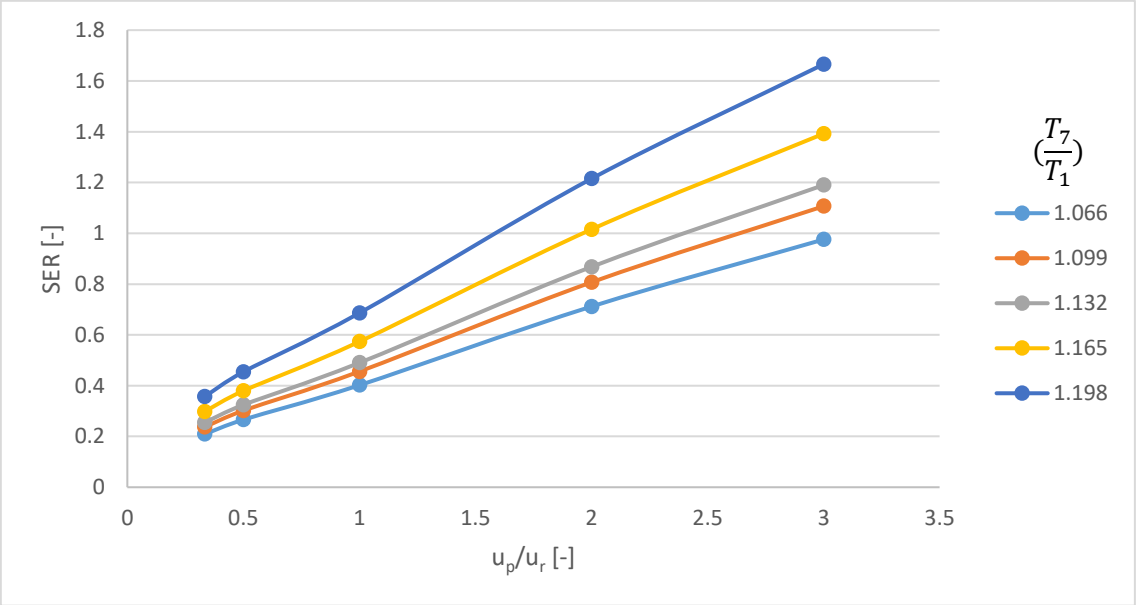

Figure 6.24: SER as a function of u_p/u_r for different T_7/T_1 values.

6.3.2.2 The performance indices as a function of u_p/u_r for different Y_1 values

Figure 6.25 shows the η_{deh} as a function of u_p/u_r for different Y_1 values. The effect of increasing Y_1 is illustrated in the description of Figure 6.16. The highest achieved η_{deh} is at Y_1 in the vicinity of 0.009. The slop of the η_{deh} drop with increasing the u_p/u_r value is varying due to humidity adsorbed amount, as follows:

- Less humidity is adsorbed in case the Y_1 equals 0.006. So, less amount of regeneration air is required to reactivate the desiccant material, which lifts the curve a little upward at higher u_p/u_r.
- For the case when Y_1 equals 0.012, more humidity is passing through the desiccant material especially at high process airspeed. So, increasing the ratio of process to regeneration air mass flow rate at high process air humidity will saturate the desiccant material and raise the humidity in the treated process air and diminish the η_{deh} at a higher rate.

For low $u_p/u_r < 1.0$, the high regeneration airspeed is capable to reactivate the total adsorbed humidity in all Y_1 cases.

The effect of varying u_p/u_r on the system DCOP for different Y_1 values is shown in Figure 6.26. As demonstrated in Figure 6.17, the more input process air humidity, the higher De and DCOP. Also, the effect of increasing the u_p/u_r is an increase in the air dehumidification thermal power and a proportional drop in the regeneration thermal energy, which risen the DCOP value as illustrated in Figure 6.11.

The increase in Y_1 value has a slight effect on the SER as shown in Figure 6.27. Higher De subsists when higher input process air humidity, which means higher adsorption thermal energy released and higher SER. On the other hand, the increase in the u_p/u_r causes an increase in the process air thermal energy, which leads to a major increase in the SER.

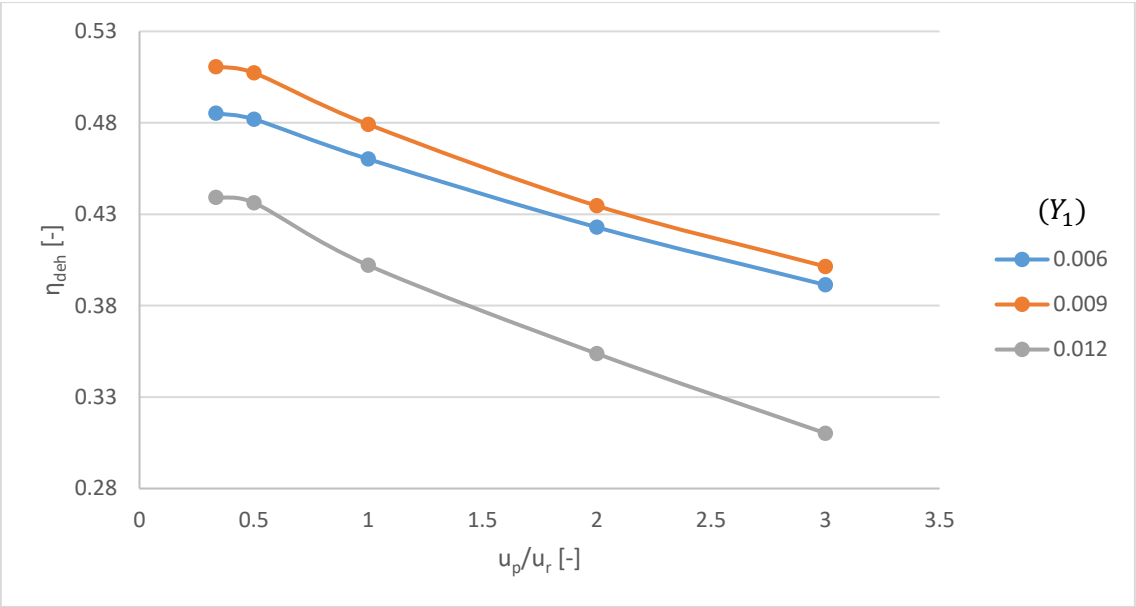

Figure 6.25: η_{deh} as a function of u_p/u_r for different Y_1 values.

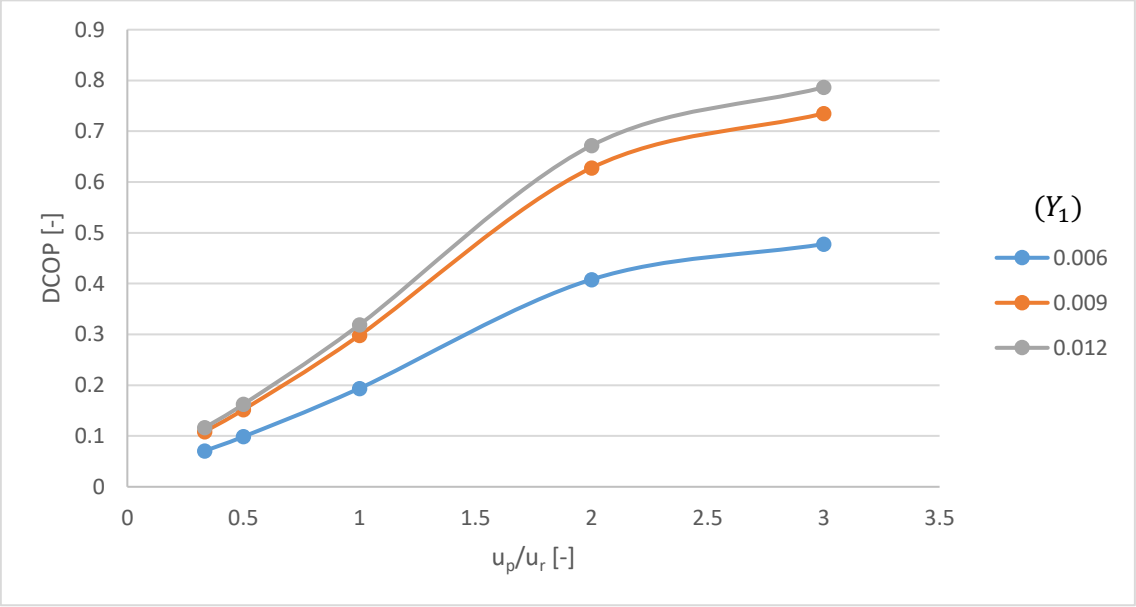

Figure 6.26: DCOP as a function of u_p/u_r for different Y_1 values.

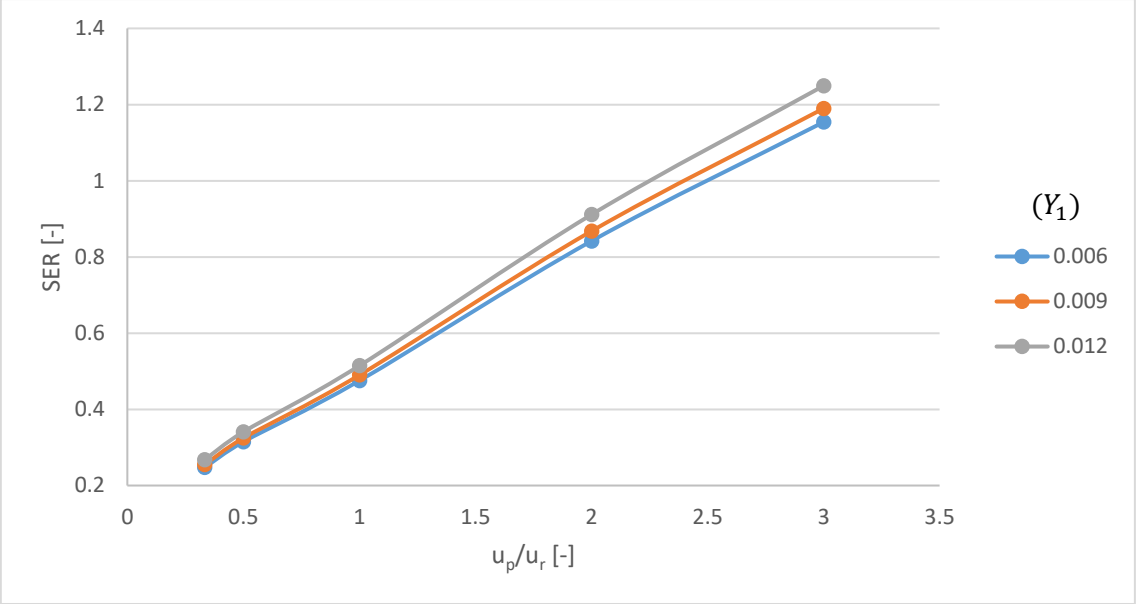

Figure 6.27: SER as a function of u_p/u_r for different Y_1 values.

6.3.2.3 The performance indices as a function of u_p/u_r for different θ_p/θ_r values

Figure 6.28 shows the η_{deh} as a function of u_p/u_r for different θ_p/θ_r values. Any rise in the θ_p/θ_r value and keeping the process and regeneration airspeed constant will increase the process mass flow rate and decrease the regeneration mass flow rate, which means a higher dehumidification process and lower regeneration process. Therefore, the increase in the θ_p/θ_r has a negative effect on the system η_{deh}.

In Figure 6.29, DCOP as a function of u_p/u_r for different θ_p/θ_r values is shown. Two factors affect the proportional increase in the DCOP. First, the increase in the θ_p/θ_r value causes a decrease in the thermal energy provided to the DW for the regeneration process in which rise the DCOP. Second, increasing the u_p/u_r value leads to an increase in the air dehumidification thermal power and a decrease in the regeneration thermal energy, which also raises the DCOP.

As shown in Figure 6.30, the SER increases with increasing the θ_p/θ_r value as illustrated in Figure 6.21 and increasing the u_p/u_r as illustrated in Figure 6.12. Both values increasing leads to an extraordinarily high value of about 2.5 of SER at the highest tested θ_p/θ_r and u_p/u_r.

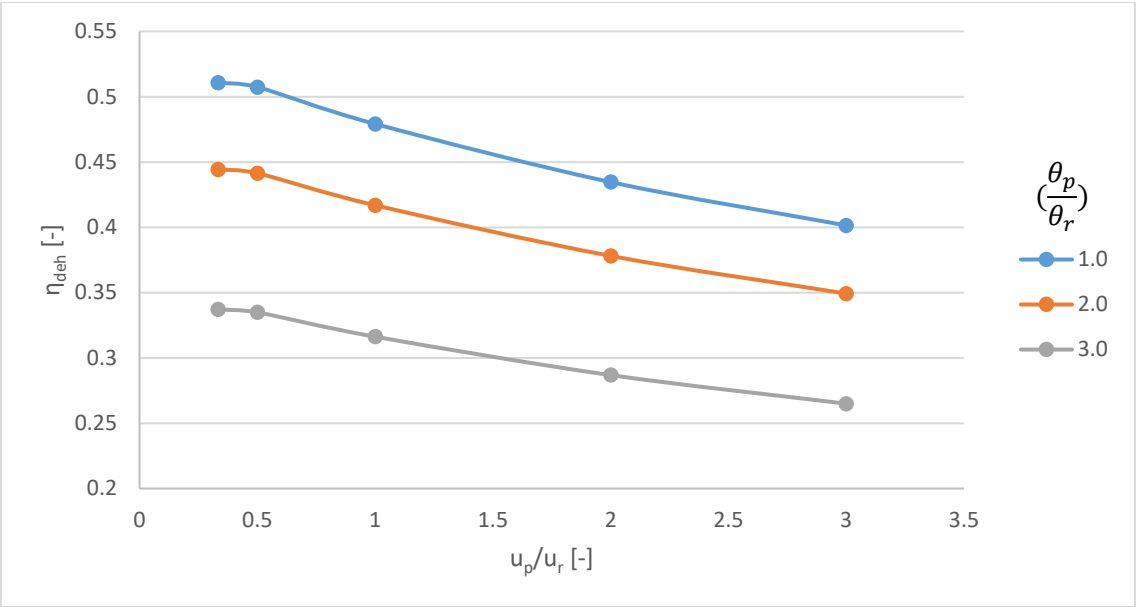

Figure 6.28: η_{deh} as a function of u_p/u_r for different θ_p/θ_r values.

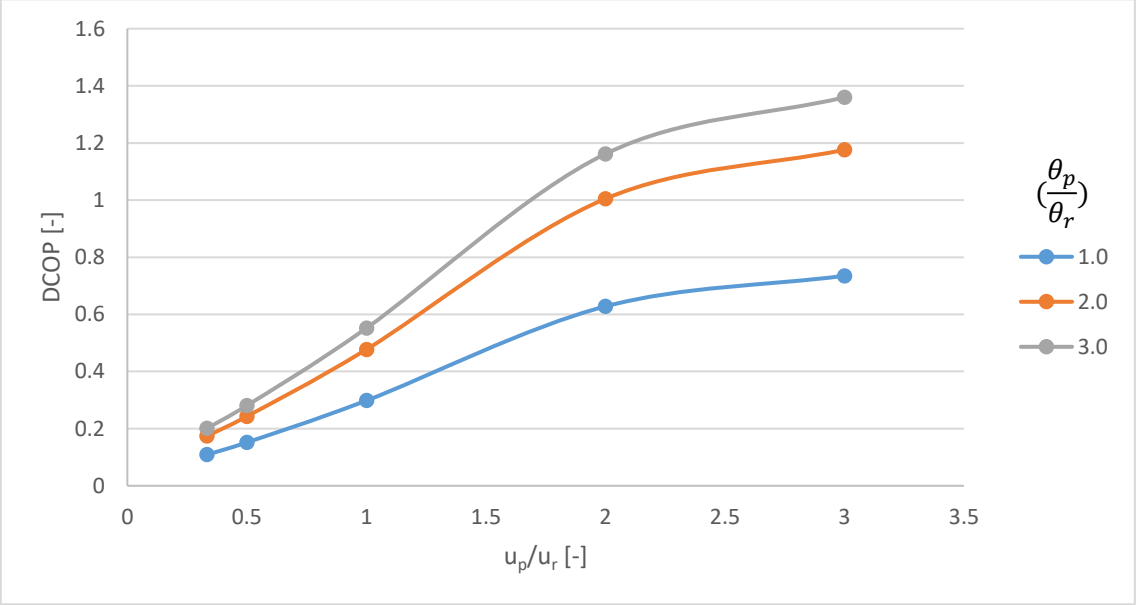

Figure 6.29: DCOP as a function of u_p/u_r for different θ_p/θ_r values.

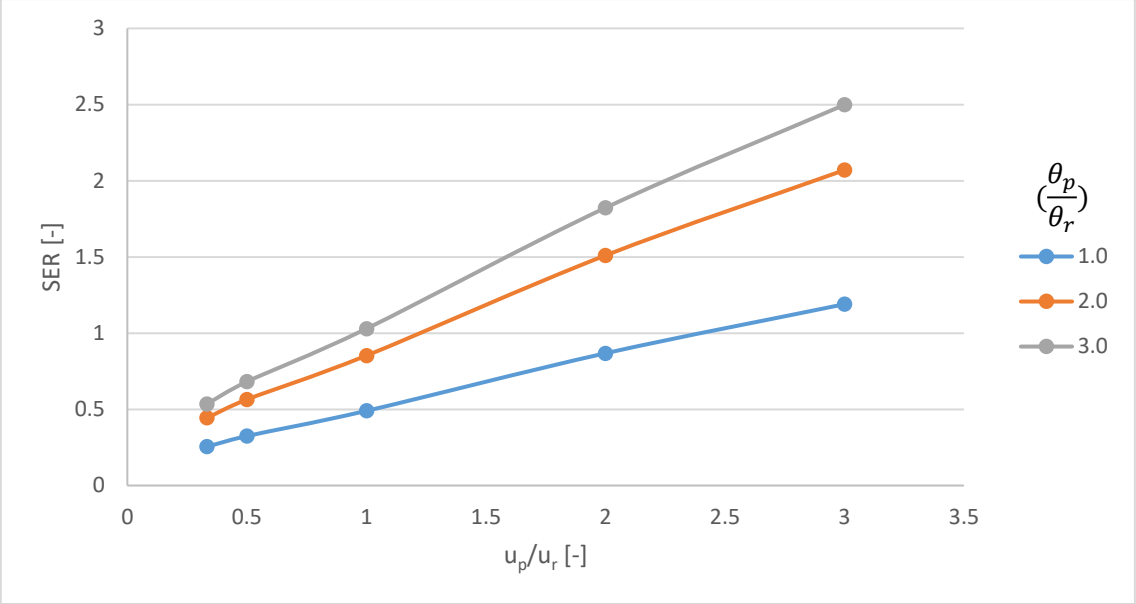

Figure 6.30: SER as a function of u_p/u_r for different θ_p/θ_r values.

6.3.3 The performance indices as a function of T_7/T_1

6.3.3.1 The performance indices as a function of T_7/T_1 for different Y_1 values

Figure 6.31 shows the η_{deh} as a function of T_7/T_1 for different Y_1 values. The results are matching the outcomes in Figure 6.13 and Figure 6.16. As mentioned before, the value of Y_1 in the vicinity of 0.009 achieved the highest η_{deh}. Due to that, a high value for process air humidity rises the De, but also it causes higher diffusion of water particles by increasing the difference of vapour partial pressure between the desiccant material and the process air, which reduces the capability of humidity dehumidification. Therefore, a very high Y_1 value has an inverse effect on the η_{deh}. With respect to the effect of changing the T_7/T_1 value, a higher regeneration temperature at a constant regeneration air speed reactivates the desiccant material easily and make it dryer. Thus, the desiccant material will be able to desorb more humidity in the next cycle wherein increases the η_{deh}.

In Figure 6.32, DCOP as a function of T_7/T_1 for different Y_1 values is shown. At a specific value of T_7/T_1, the regeneration thermal energy delivered to the DW is constant for different Y_1 values. The best utilisation of the energy provided ensues at the highest dehumidification

process. Accordingly, for different Y_1 values, the higher De leads to higher DCOP. An increase in the regeneration temperature leads to an increase in the enthalpy difference of regeneration and process air with constant inlet process air temperature. So, any increase in the T_7/T_1 value will lessen the DCOP.

High dehumidification process rate leads to the release of more adsorption heat to the process air, an increase in the treated air temperature, and thus an increase in SER. Regarding the effect of T_7/T_1, at constant regeneration airspeed, an increase in the regeneration air temperature causes an increase in the heat transfer rate with the desiccant material and a rise in its temperature. That absorbed heat by the desiccant material will be released to process air in the process section causing high treated air temperature and higher SER as shown in Figure 6.33.

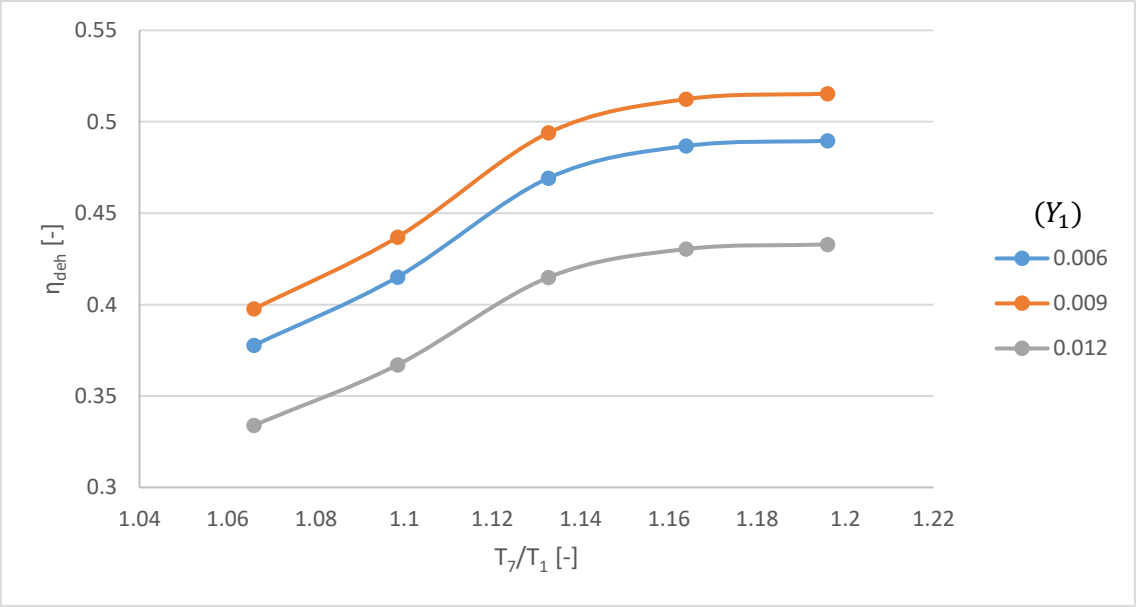

Figure 6.31: η_{deh} as a function of T_7/T_1 for different Y_1 values.

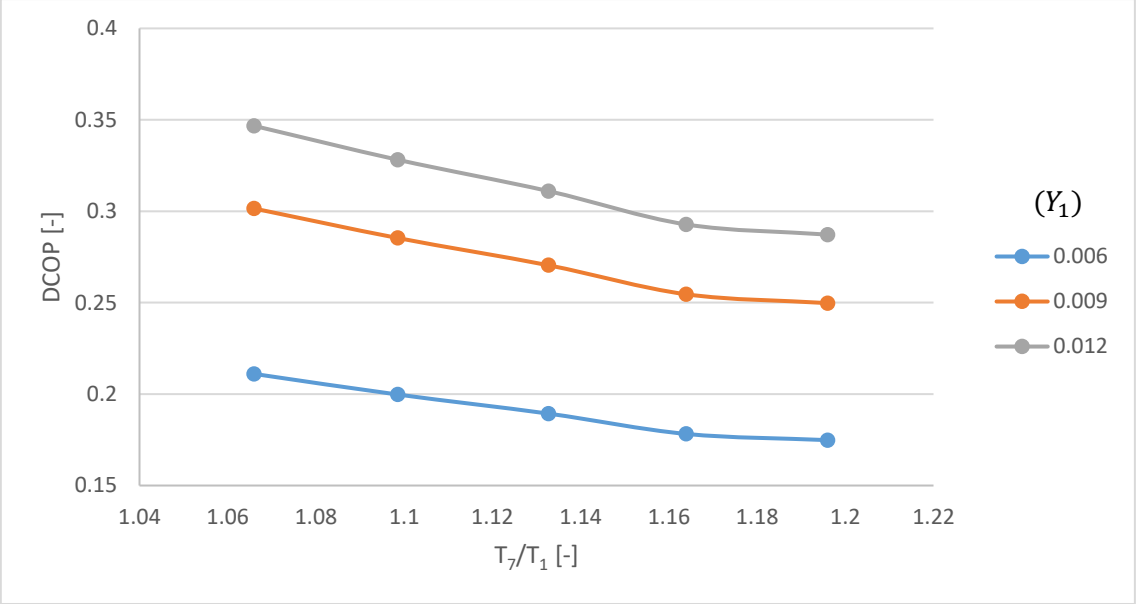

Figure 6.32: DCOP as a function of T_7/T_1 for different Y_1 values.

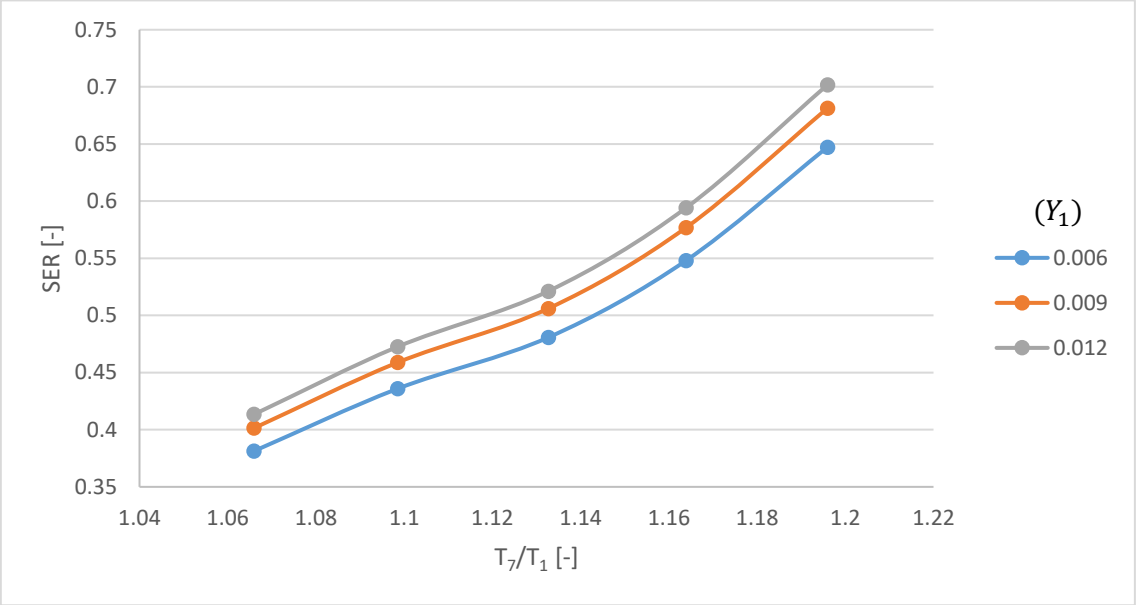

Figure 6.33: SER as a function of T_7/T_1 for different Y_1 values.

6.3.3.2 The performance indices as a function of T_7/T_1 for different θ_p/θ_r values

In Figure 6.34, η_{deh} as a function of T_7/T_1 for different θ_p/θ_r values is shown. At constant process and regeneration airspeeds, enlarging the θ_p/θ_r value causes an increase in the process to regeneration air mass flow rate, and thus, less regeneration air passes through the DW to reactivate the desiccant material for higher input humidity continent. So, increasing the θ_p/θ_r

value causes an inefficient reactivation process and lower η_{deh}. In contrast, increasing the T_7/T_1 enhances the desiccant material reactivation process and enhance the η_{deh}. It is noticed that at higher θ_p/θ_r values, the regeneration air is not capable to reactivate the desiccant material easily as at θ_p/θ_r equals 1.0, for that reason, it is required higher T_7/T_1 value.

In Figure 6.35, DCOP as a function of T_7/T_1 for different θ_p/θ_r values is shown. Increasing the θ_p/θ_r enhances the DCOP as better thermal energy utilising as lower regeneration thermal energy is provided at same airspeeds. While an increase in the T_7/T_1 value leads to an increase in the enthalpy difference between regeneration and process air. So, any increase in the T_7/T_1 value will reduce the DCOP.

At constant process and regeneration airspeeds, increasing the θ_p/θ_r value causes an increase in the process air heating thermal power while decreasing the regeneration thermal power, which ensures a high SER value. Also, increase the T_7/T_1 value causes an increase in the absorbed heat by the desiccant material in the regeneration section at fixed airspeed. That absorbed heat will transfer to the process air in the process section which results in a higher SER value. The increase in both θ_p/θ_r and T_7/T_1 values leads to a substantially higher SER at 1.43, as shown in Figure 6.36.

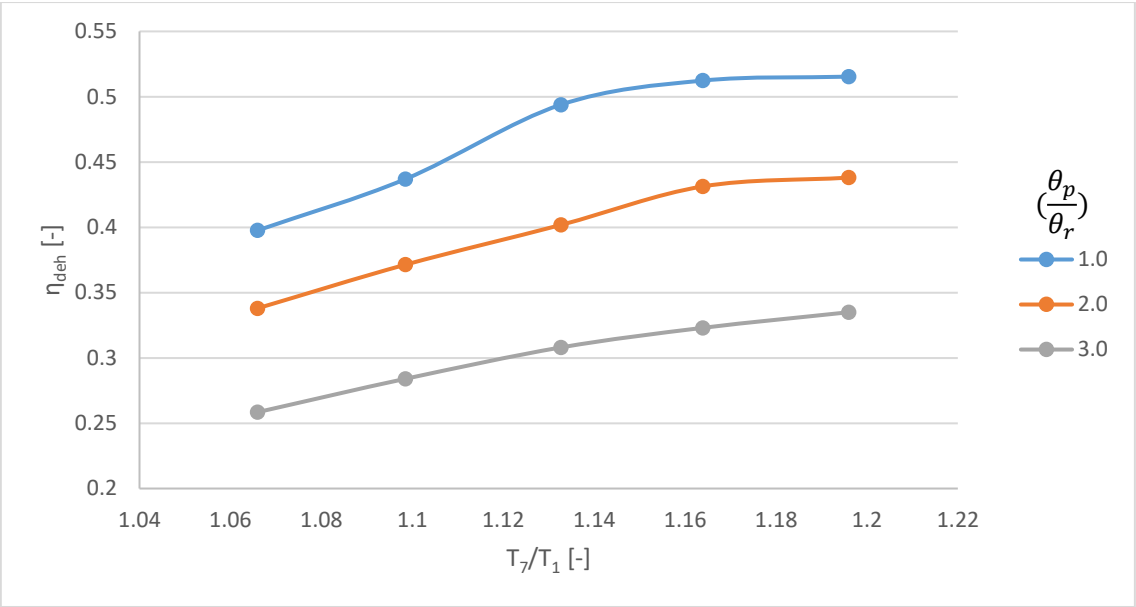

Figure 6.34: η_{deh} as a function of T_7/T_1 for different θ_p/θ_r values.

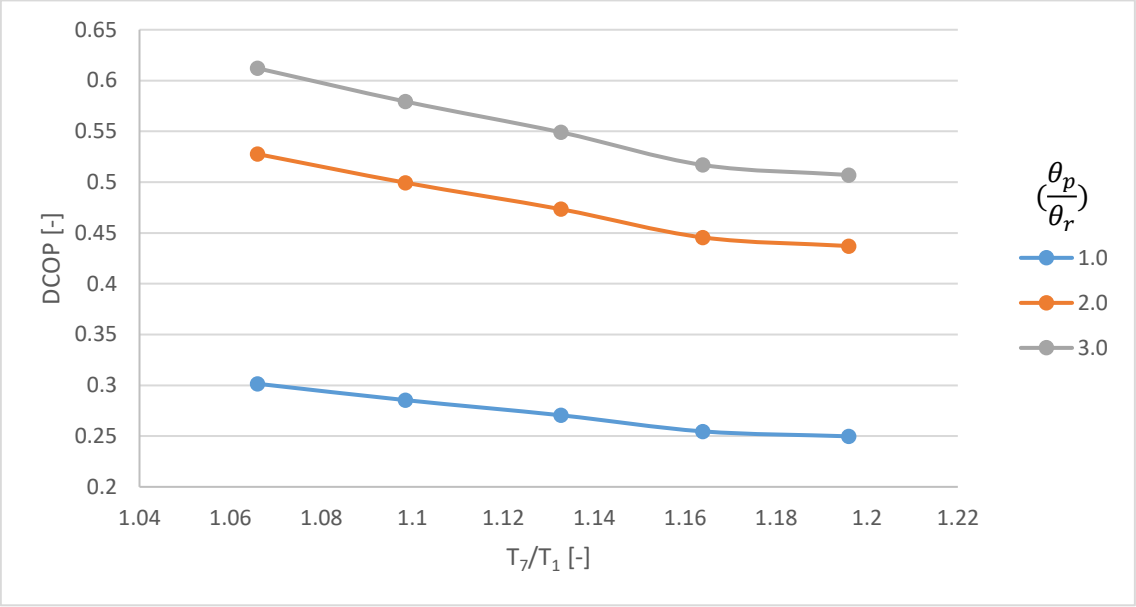

Figure 6.35: DCOP as a function of T_7/T_1 for different θ_p/θ_r values.

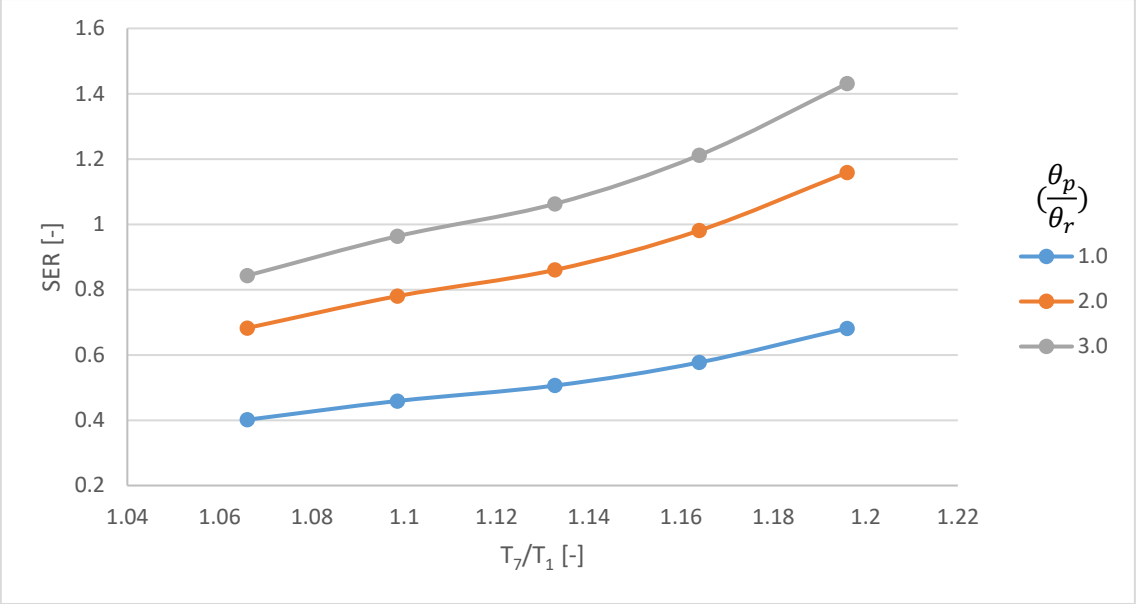

Figure 6.36: SER as a function of T_7/T_1 for different θ_p/θ_r values.

6.3.4 The performance indices as a function of Y_1

6.3.4.1 The performance indices as a function of Y_1 for different θ_p/θ_r values

The effect of varying Y_1 on the system η_{deh} for different θ_p/θ_r values is shown in Figure 6.37. The results match the outcomes in Figure 6.16, Figure 6.19, Figure 6.25, Figure 6.28, Figure 6.31, and Figure 6.34. Increasing the θ_p/θ_r leads to a rise in the η_{deh}. Also, the achieved highest η_{deh} is at Y_1 in the vicinity of 0.009 for all cases.

Figure 6.38 shows the η_{deh} as a function of Y_1 for different θ_p/θ_r values. Increasing the θ_p/θ_r value and keeping the airspeeds constant, means a higher process air mass flow rate passes through the DW, higher dehumidification rate, lower regeneration thermal energy delivered, and accordingly higher DCOP. An increment in the Y_1 causes an increase in De, as explained before and an increase in the DCOP as a result.

Due to the increase in the process air thermal power, decrease the regeneration thermal power or both together by increasing the θ_p/θ_r value, the SER value gets higher as elucidated before.

Moreover, a slight increase in the SER was detected due to increasing Y_1 as shown in Figure 6.39.

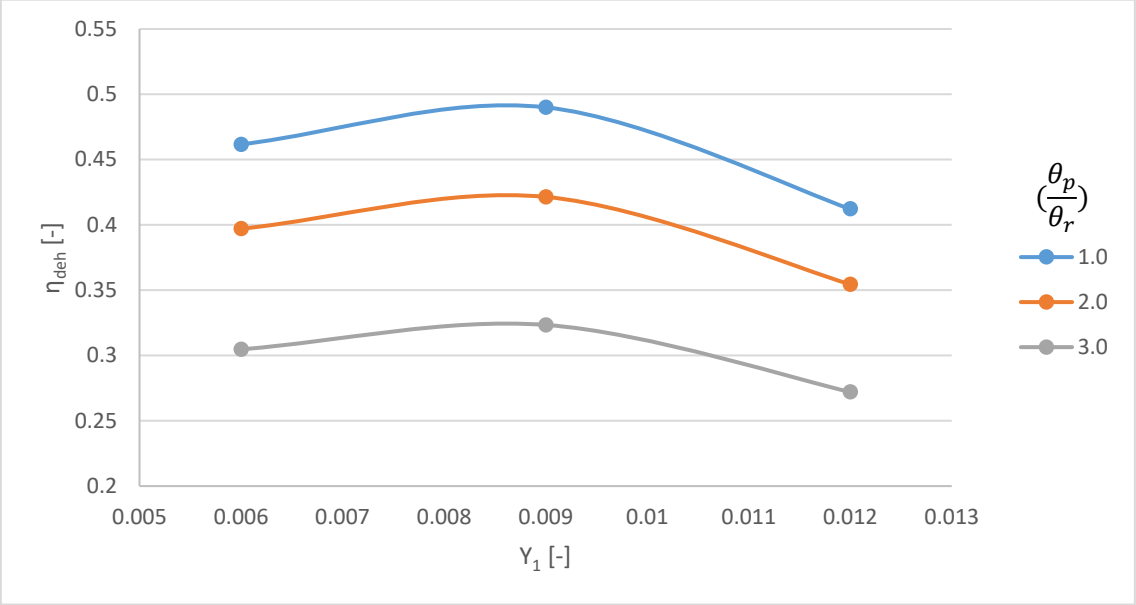

Figure 6.37: η_{deh} as a function of Y_1 for different θ_p/θ_r values.

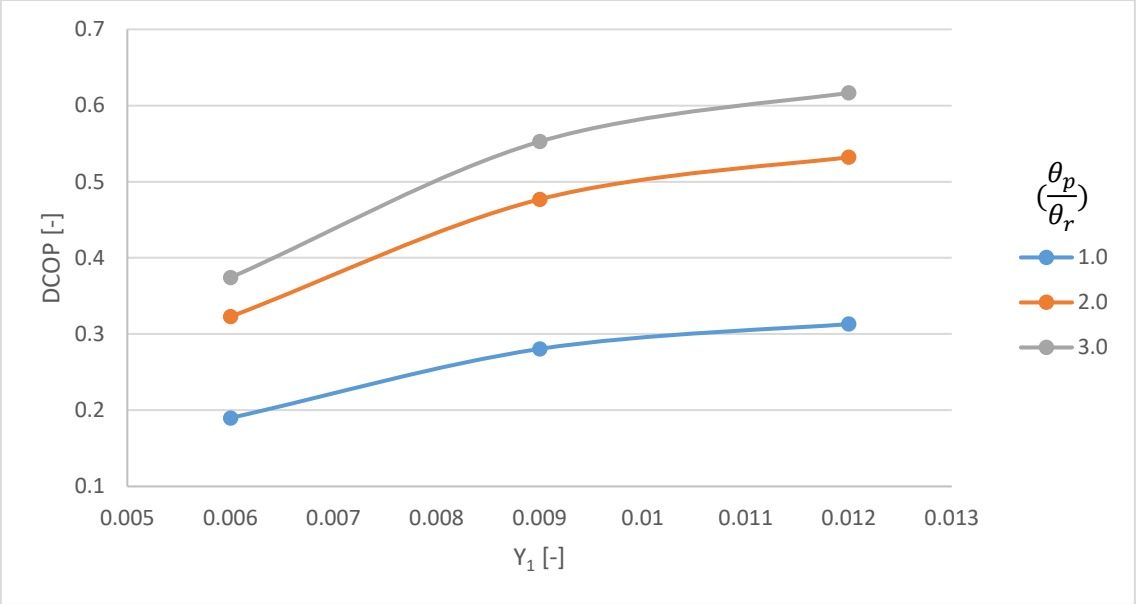

Figure 6.38: DCOP as a function of Y_1 for different θ_p/θ_r values.

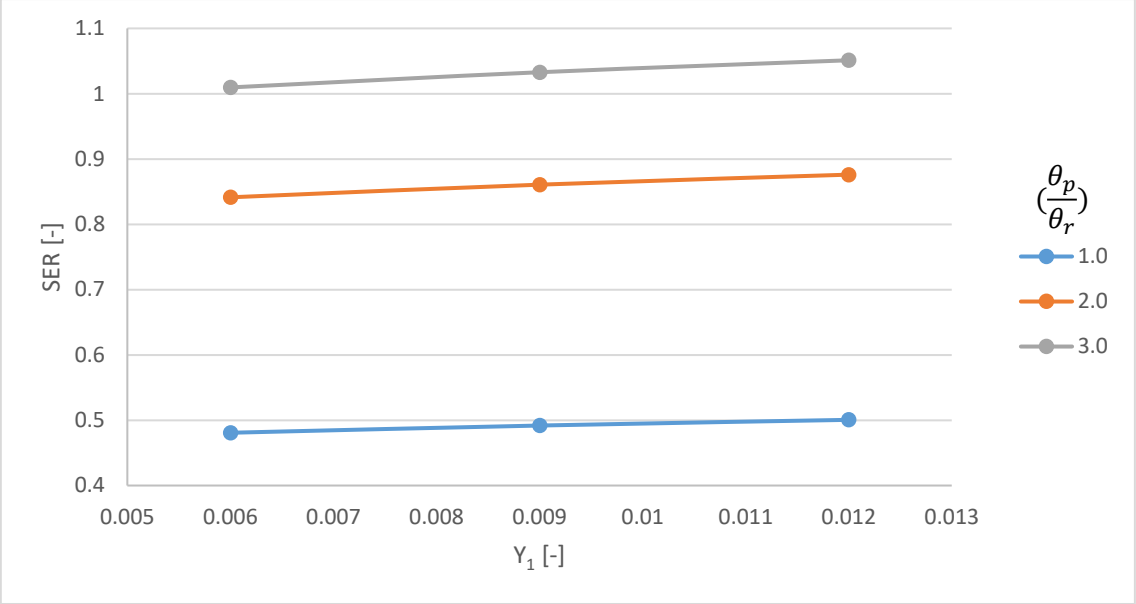

Figure 6.39: SER as a function of Y_1 for different θ_p/θ_r values.

6.4 Computational investigating the effect of each non-dimensional groups on others in respect of the system performance

The three remaining non-dimensional groups are mainly related to the DW's channel geometry and design parameters. These non-dimensional groups, which are: $C.L/A_f$, ε, and Φ, will be tested by the computational simulation model. In this section, the effect of the five experimentally tested non-dimensional groups on the system performance for varying these three non-dimensional groups will be studied.

6.4.1 The effect of varying $C.L/A_f$ on other non-dimensional groups in respect of the system performance

For the non-dimensional group $C.L/A_f$, the main factor that affects the system performance is the contact surface of process air and the DW channel wall. Increasing the contact surface leads to an increase in the dehumidification process, and thus the η_{deh} and the DCOP. Contrariwise, it increases the released adsorption heat and thus the SER.

The amount of contacting surface of process air and the channel walls are determined by the friction force. Increasing the friction force means more process air contacts the DW channel walls. Cengel and Cimbala (2018) stated that the friction force amount in the channel is directly proportional to the channel perimeter and inverse proportional to the channel hydraulic diameter. The channel hydraulic diameter is proportional to the channel airflow passage area as in equation 3.6. So, there is an inverse relationship between the friction force of process air with the channel wall and the channel airflow passage area. As a result, increasing the contact surface of process air and the channel walls by increasing the non-dimensional group $C.L/A_f$ nominator's variables C or L, or decreasing the denominator A_f, leads to heighten the η_{deh} and the DCOP values, but increase the SER value as well.

It was found that increase the $C.L/A_f$ value from 195.07 to 282.33 has the same impact on all the five experimentally tested non-dimensional groups and the two other simulations tested non-dimensional groups. The effect of increasing $C.L/A_f$ value as follow:

- For the four $C.L/A_f$ tested values; which are: 195.07, 208.24, 221.78, and 282.33; the percentage of the increment in the η_{deh} and the DCOP for all values over 195.07 value are identical and equal to 5.9%, 11.5%, and 33.1%, respectively. Figure 6.40 and Figure 6.41 show an example of the effect of varying $K_y/\rho_a.N.\delta$ on the system η_{deh} and DCOP for different $C.L/A_f$ values.
- The increment percentage in the SER over the SER at $C.L/A_f$ equals 195.07 is 6.0%, 11.1%, and 32.7%. Figure 6.42 shows an example of the effect of varying $K_y/\rho_a.N.\delta$ on the system SER for different $C.L/A_f$ values.

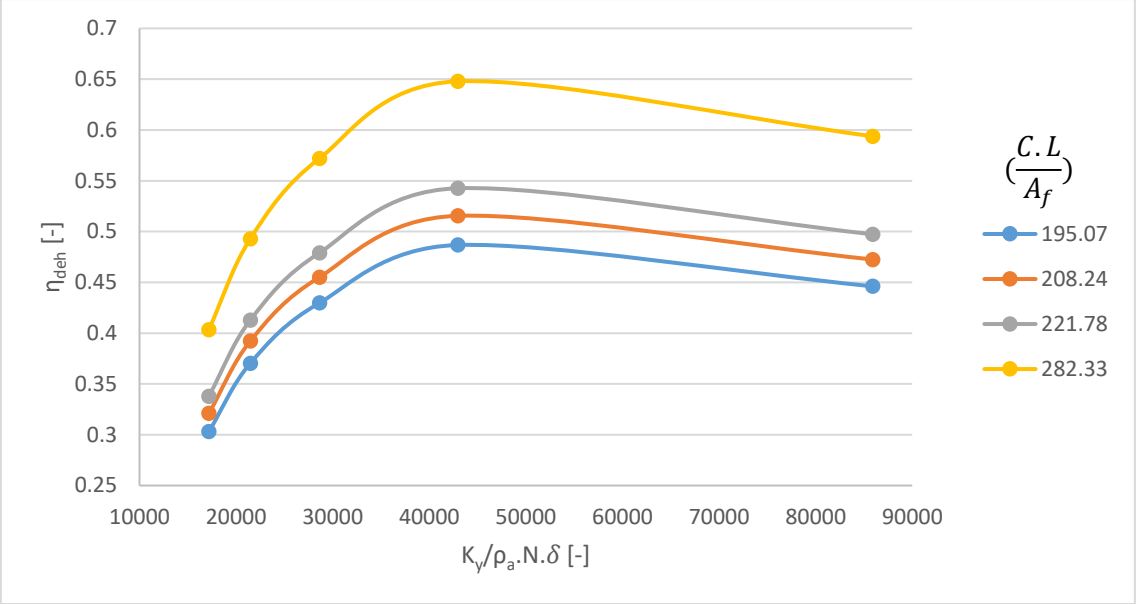

Figure 6.40: η_{deh} as a function of $K_y/\rho_a.N.\delta$ for different $C.L/A_f$ values.

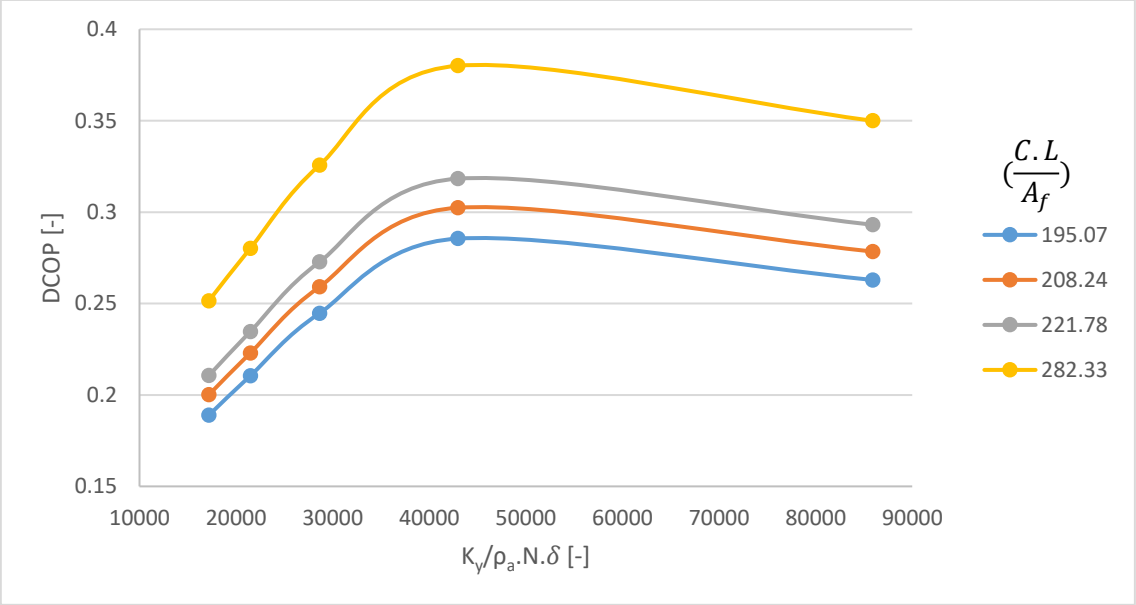

Figure 6.41: DCOP as a function of $K_y/\rho_a.N.\delta$ for different $C.L/A_f$ values.

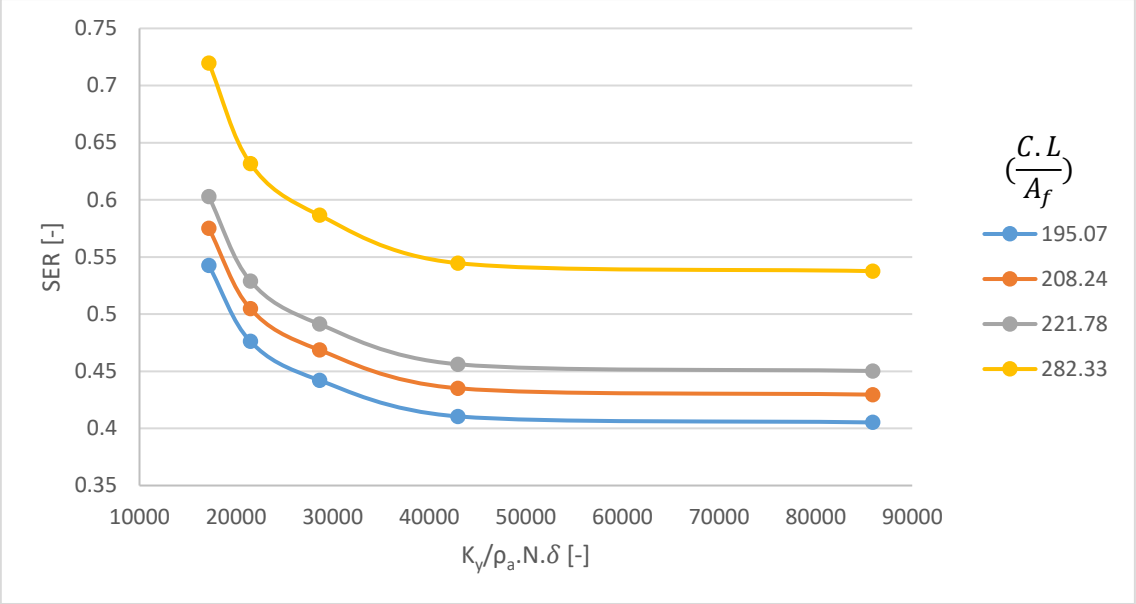

Figure 6.42: SER as a function of $K_y/\rho_a.N.\delta$ for different $C.L/A_f$ values.

6.4.2 The effect of varying ε on other non-dimensional groups in respect of the system performance

The influence of increasing the porosity in desiccant on the system performance is the opposite effect of increasing the non-dimensional group $C.L/A_f$. An increase in the ε causes a reduction in the contact surface between the process air and the channel walls. So, an increase in the ε has a negative effect on the dehumidification process and thus η_{deh} and the DCOP. A reduction in the dehumidification process leads to reduce the released adsorption heat to process air and thus reduce the SER value.

It was found that the effect of increasing the ε value is similar for all the non-dimensional groups. An ε range between 0.2 and 0.6 is tested with 0.1 increments. The percentage of the decrement in the η_{deh} and the DCOP for all values over 0.2 value are identical and equal to -5.2%, -11.5%, -19.1%, and -28.3%, respectively. Figure 6.43 and Figure 6.44 show an example in the reduction in the η_{deh} and the DCOP for the non-dimensional group $K_y/\rho_a.N.\delta$ by increasing ε.

The decrement percentage in the SER comparing with the SER at ε equals to 0.2 is -4.4%, -9.1%, -14.6%, and -21.2%. Figure 6.45 shows an example of the effect of varying $K_y/\rho_a.N.\delta$ on the system SER for different ε values.

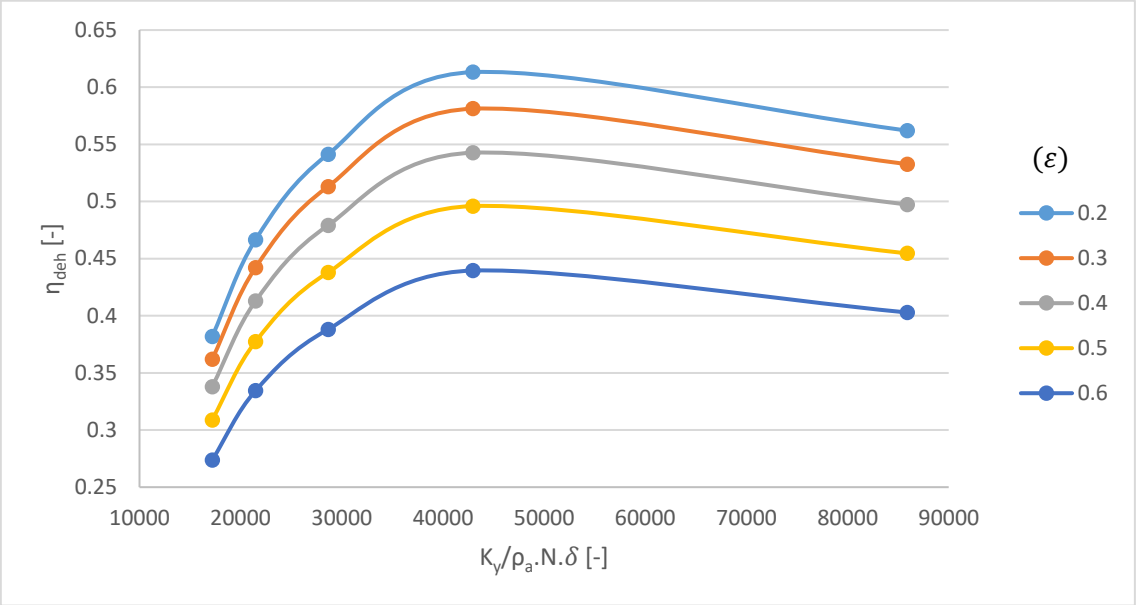

Figure 6.43: η_{deh} as a function of $K_y/\rho_a.N.\delta$ for different ε values.

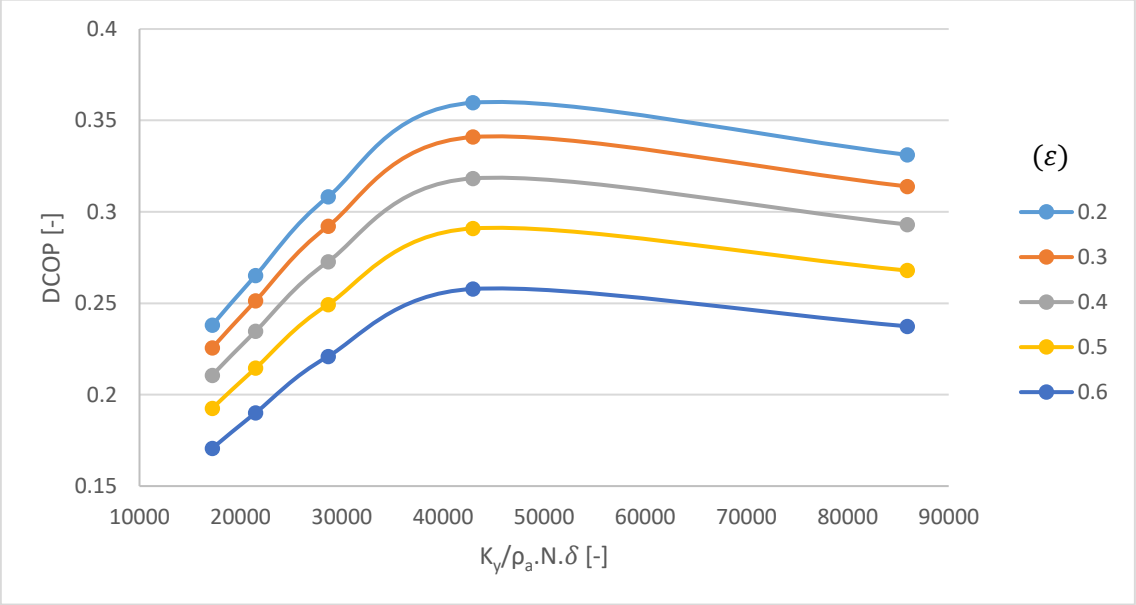

Figure 6.44: DCOP as a function of $K_y/\rho_a.N.\delta$ for different ε values.

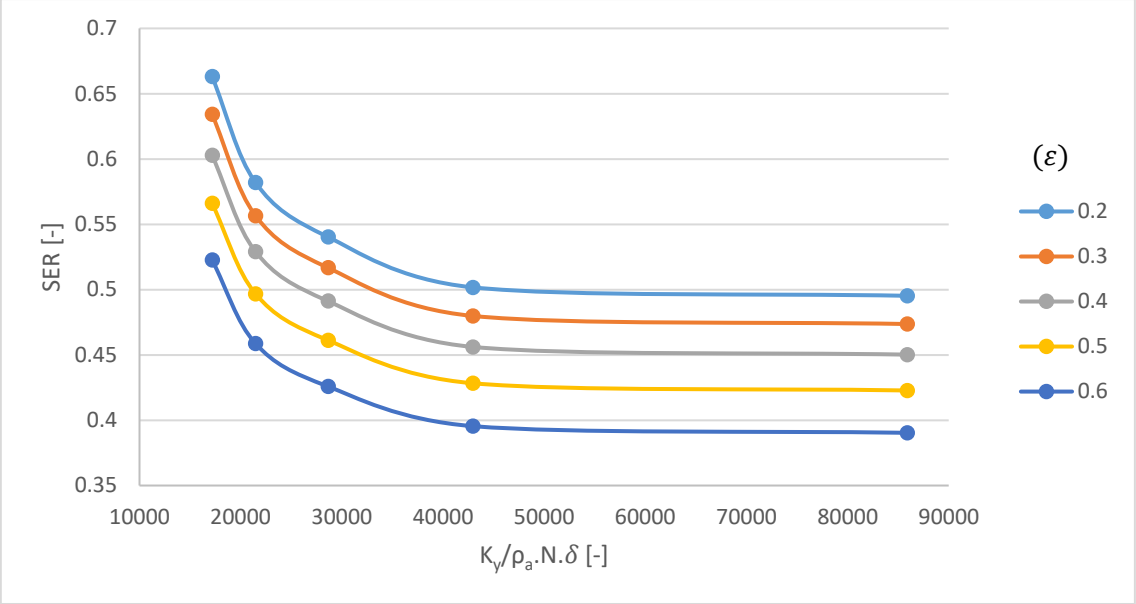

Figure 6.45: SER as a function of $K_y/\rho_a.N.\delta$ for different ε values.

6.4.3 The effect of varying Φ on other non-dimensional groups in respect of the system performance

Increasing the desiccant volume ratio in the layer means increasing the quantity of the desiccant material grains in the layer, which leads to more ability to adsorb and detain the humidity. Consequently, increasing the non-dimensional group Φ causes an increase in the dehumidification process and thus η_{deh} and the DCOP. Also, an increment in the dehumidification process leads to an increase in the released adsorption heat to process air and thus the SER value.

It was found that the effect of increasing the Φ value is similar for all the non-dimensional groups. An Φ range between 0.3 and 0.7 is tested with 0.1 increments. The percentage of the increment in the η_{deh} and the DCOP for all values over 0.3 value are identical and equal to 18.1%, 32.3%, 43.7%, and 52.9%, respectively. Figure 6.46 and Figure 6.47 show an example in the increment in the η_{deh} and the DCOP for the non-dimensional group $K_y/\rho_a.N.\delta$ by increasing Φ.

The increment percentage in the SER comparing with the SER at Φ equals 0.3 is 9.0%, 16.3%, 22.2%, and 27.1%. Figure 6.48 shows an example of the effect of varying $K_y/\rho_a.N.\delta$ on the system SER for different Φ values.

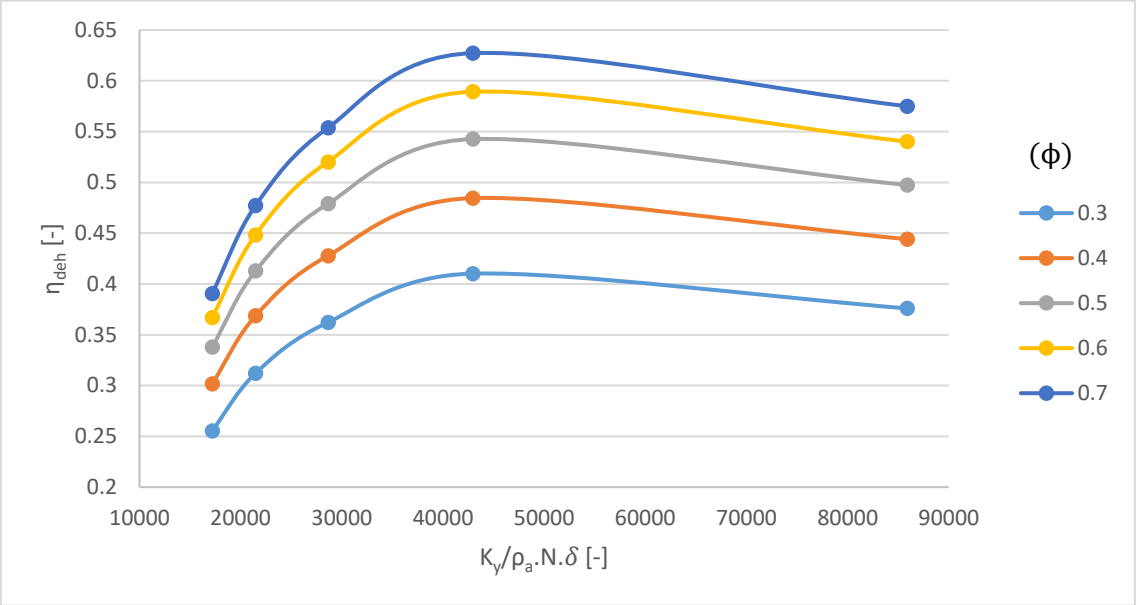

Figure 6.46: η_{deh} as a function of $K_y/\rho_a.N.\delta$ for different Φ values.

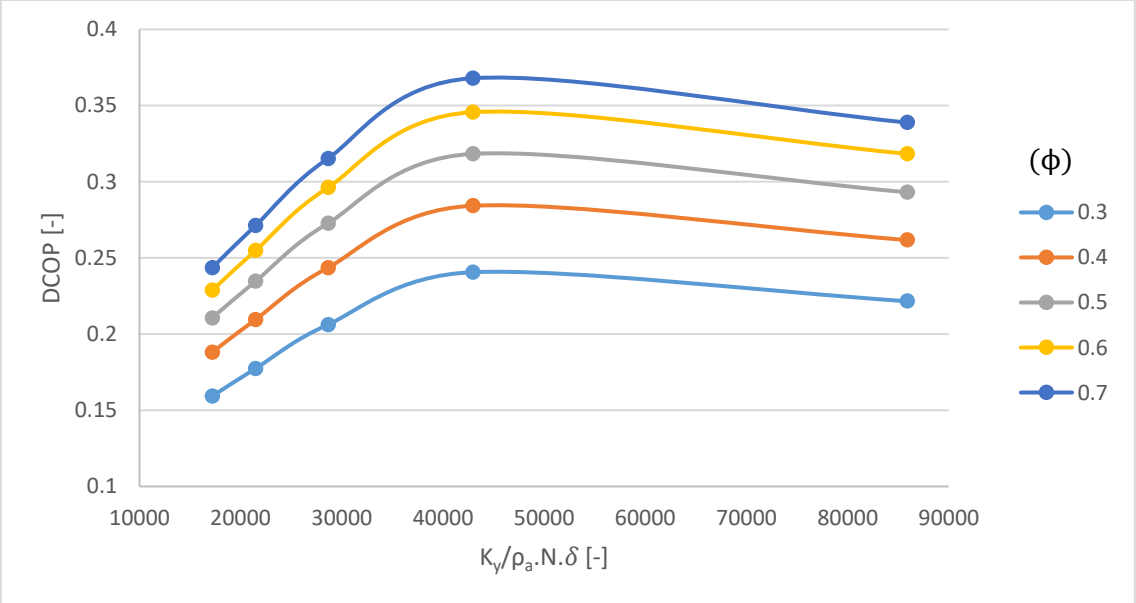

Figure 6.47: DCOP as a function of $K_y/\rho_a.N.\delta$ for different Φ values.

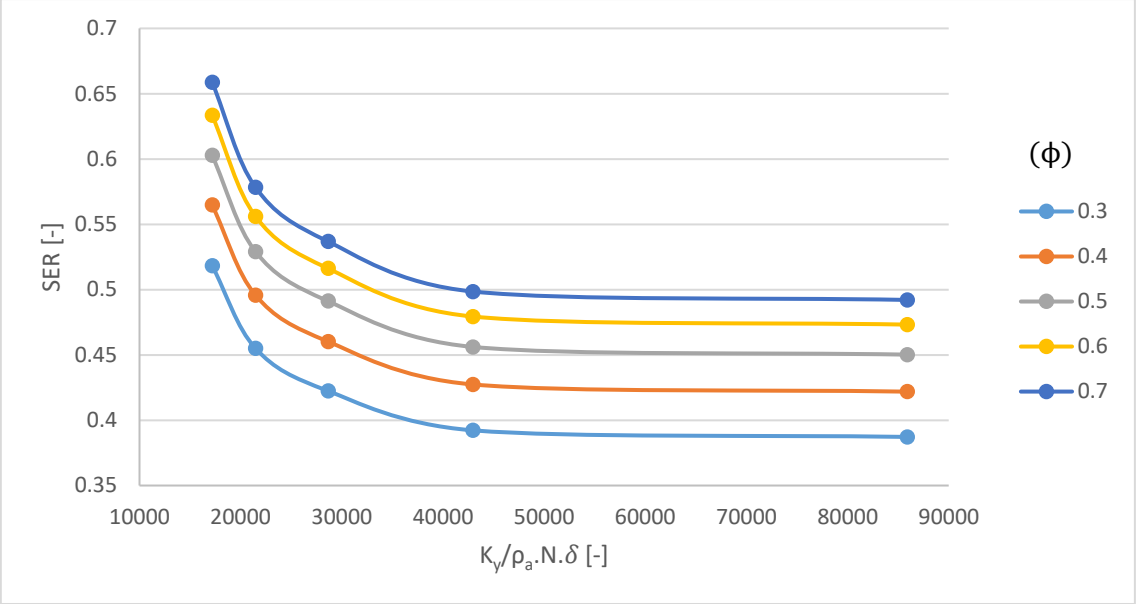

Figure 6.48: SER as a function of $K_y/\rho_a.N.\delta$ for different Φ values.

6.5 Summary and conclusions

In this chapter, the behaviour and the performance of the DW system were studied. The same DW system was used in all experiments, which was presented in chapter four. Also, the simulation model, which was presented in chapter three, was used to study the effect of some non-dimensional groups which cannot easily experimentally change their parameters. The simulation model was validated experimentally under this study's operating condition. It was found that the discrepancy for the performance indices was within ±5.1%. The non-dimensional groups operating range and the effect on the performance indices were identified in the first part of this chapter. Then, two of the non-dimensional groups were varied at the same time to investigate how each non-dimensional group affects others as regards the system performance.

The outcomes in this chapter can be summarised as follow:

- Increasing the non-dimensional group $K_y/\rho_a.N.\delta$ causes an increase in the η_{deh} and the DCOP till reach a maximum value in the vicinity of 42947.80 then start to decrease. While the SER decreases with increasing $K_y/\rho_a.N.\delta$ value. The optimal value was found

to be in the vicinity of 42947.80 in most cases. But for the system η_{deh}, it is decreased to a close of 31813.19 in case of low u_p/u_r or high T_7/T_1 due to the enhancement in the regeneration process and to avoid the desiccant material overheating.

- Decreasing the non-dimensional group u_p/u_r value leads to enhance the dehumidification process by providing more regeneration thermal energy to reactivate the desiccant material and thus increase the η_{deh}. But, it also causes a decrease in the air dehumidification thermal power, increases the provided regeneration thermal energy, and decreases the DCOP and SER as a result. For the system η_{deh}, the optimal u_p/u_r value in case of increasing T_7/T_1 value is also increased gradually from 0.333 to 1.0 due to less regeneration airspeed is required to reactivate the desiccant material in case of high regeneration temperature.
- A better regeneration process is attained by increasing the non-dimensional group T_7/T_1. So, increasing the T_7/T_1 value causes an increase in the η_{deh}, but also increases the SER due to the high provided regeneration thermal energy. On the other hand, it decreases the DCOP because of the increase in the delivered thermal power to the DW per mass flow rate.
- Increasing the non-dimensional group Y_1 causes an increase in the De. But a very high Y_1 value leads to an increase in the diffusion of water particles which negatively affect the η_{deh}. So, η_{deh} increases with increasing Y_1 till reach around 0.009 then start to drop. The increase in the De which accompanied by increasing Y_1 causes an increase in the DCOP as well as the SER duo to the rise in the adsorption heat.
- It was found that the non-dimensional group Y_7 has an inconsiderable effect on the system performance. This is because at a relatively high air temperature, the regeneration air is unsaturated and can easily adsorb and reject the humidity hold by the desiccant material. So, investigating the effect of varying Y_7 on other non-

dimensional groups and optimizing Y_7 as regards the energy consumption in CHAPTER 7: NON-DIMENSIONAL GROUPS' OPTIMISATION are both excluded.

- At fixed process and regeneration airspeeds, increasing the non-dimensional group θ_p/θ_r value leads to an increase in the process air mass flow rate and thus increases the dehumidification process. But, it reduces the regeneration mass flow rate, reduces the regeneration thermal power, and becomes unable to reactivate the desiccant material due to excessive humidity. As a result, increasing θ_p/θ_r value causes a reduction in the η_{deh} value and an increase in the system DCOP and SER.
- Increasing the contact surface between the process air and the desiccant material causes an enhancement in the dehumidification process and an increment in the η_{deh} and the DCOP, which can be achieved by increasing $C.L/A_f$ value. But it increases the SER as well due to the increase in the adsorption heat released. The effect of increasing $C.L/A_f$ is identical to all the non-dimensional groups. Increase $C.L/A_f$ value from 195.07 to 282.33 cause a 33.1% increment in the η_{deh} and the DCOP and a 32.7% increment in the SER.
- Increasing ε has a negative impact on the η_{deh} and the DCOP as it reduces the contact surface between the process air and the desiccant material in the layer. A lessening in the dehumidification process because of increasing ε value causes a reduction in the released adsorption heat and thus a reduction in the SER value. The effect of increasing ε value is identical to all the non-dimensional groups. Increase ε value from 0.2 to 0.6 cause a -28.3% decrement in the η_{deh} and the DCOP and a -21.2% decrement in the SER.
- Increasing Φ value means a higher amount of desiccant material particles in the layer and more capability to adsorb the humidity, which increases the η_{deh} and the DCOP. Also, it increases the SER since more adsorption heat is released to the process air. The

effect of increasing Φ value is identical to all the non-dimensional groups. Increase Φ value from 0.3 to 0.7 cause a 52.9% increment in the η_{deh} and the DCOP and a 27.1% increment in the SER.

In some of the non-dimensional groups, the optimal value is clear. But, in most of them, the optimum value is not clear due to the desired high value of η_{deh} and DCOP, an undesired high value of SER. Therefore, this chapter is to demonstrate the importance of presenting a new optimization method which followed in the next chapter.

CHAPTER 7: NON-DIMENSIONAL GROUPS' OPTIMISATION

7.1 Introduction

The main advantage of using thermally driven cooling systems as a standalone system or combined with conventional systems is to reduce the amount of consumed energy. Therefore, energy performance analysis is a key factor when designing, operating, and optimising thermally based air conditioning systems. In order to evaluate the preference of utilising the thermally driven air conditioning systems in terms of energy saving, it is essential to compare the system performance with a common and widespread reference system, which is the conventional VCC system in this study.

7.2 Optimisation procedure and calculations

A Pennington cycle SDC system introduced by La et al. (2010) will be used in this study to compare both systems, but the direct evaporative cooler in the process side is replaced with a VCC system to ensure that the air is supplied with the required condition. The Pennington cycle is considered as one of the most common SDC cycles. Figure 7.1 shows the Pennington mode SDC system. The process numbers are matching the numbers in Figure 1.2. The process air is ambient air, while the regeneration air is a return air from the cooling space. The sensible heat exchanger is used to cool down the process air after the DW and to heat the return air a little before further heat to be added by the heat source to regenerate the DW. Additional air cooling is taking place by the VCC system in order to reduce the temperature to the desired condition and remove extra humidity.

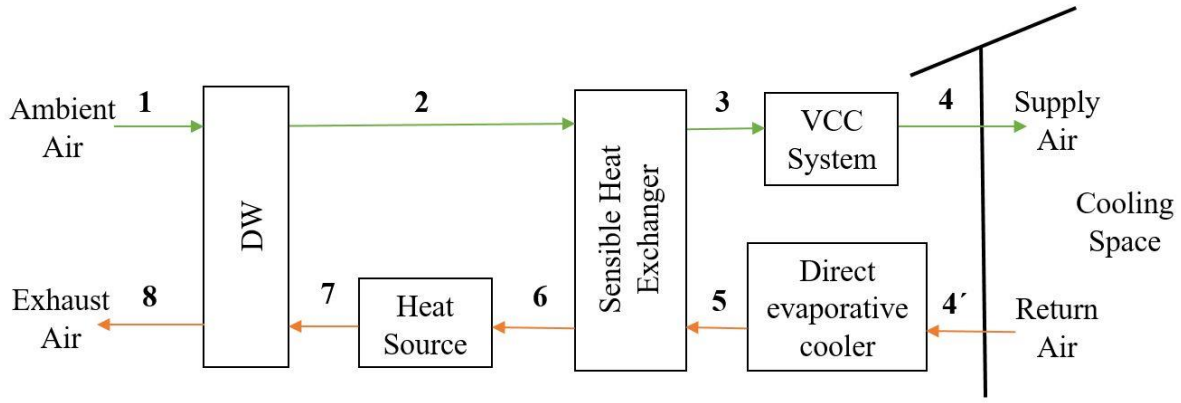

Figure 7.1: Pennington cycle SDC system consists of DW, heat source for regeneration, sensible heat exchanger, direct evaporative cooler, and VCC system for cooling the air to the desire condition.

The conventional VCC system is an electric chiller that is based on vapour compression technology. The efficiency index used to demonstrate its performance is the Energy Efficiency Ratio (EER) (defined by the ratio of the total cooling load to the effective power input) (Henning et al. 2013). EER is given by the following equation:

$$EER = \frac{\dot{Q}_c}{\dot{W}} \tag{7.1}$$

where $\dot{W}$ is the power input, and $\dot{Q}_c$ is the cooling load, which consists of sensible and latent cooling loads and are given by:

$$\dot{Q}_{sen} = \dot{m}\, c_{pa}\, dT \tag{7.2}$$

$$\dot{Q}_{lat} = \dot{m}\, \Delta h_{vap}\, dY \tag{7.3}$$

where Δh_{vap} is the latent heat of vaporization, dT and dY are the temperature and specific humidity difference before and after the VCC system. The EER value depends on the VCC compressor type and the manufacturer's choice of material and working fluid. The average EER value is 3.0 (Henning et al. 2013).

The cooling load depends on the supplied air to the VCC unit condition and the required output air condition. Cengel and Boles (2015) stated that the human comfort air conditions are when

the environment temperature between 22-27°C and the relative humidity 40-60%. They also reported that the supplied air to the cooling space should be at a lower temperature and the right humidity. Therefore, a target cooling load of 10 kW and a supply air of temperature 18°C and relative humidity 50-55% will be set for the comparison. The return air condition depends on the contents of the cooling space. In this study, the temperature of the return air will be set to 24°C and the relative humidity to 55% at 1.0 atmospheric pressure.

The direct evaporative cooler is used to cool down the return air from the cooling space before entering the sensible heat exchanger. The performance index used to determine the characteristics of the evaporative cooler is saturation effectiveness (determine how close the conditioned air to the saturation condition) and given by (Saman et al. 2010):

$$\eta_{evap} = \frac{T_{1,db} - T_{2,db}}{T_{1,db} - T_{1,wb}} \tag{7.4}$$

where $T_{1,db}$ is the entering air dry-bulb temperature, $T_{2,db}$ is the leaving air dry-bulb temperature, and $T_{1,wb}$ is the entering air wet-bulb temperature. The leaving air from the evaporative cooler has a lower dry-bulb temperature, while the same wet-bulb temperature of the entering air. According to ASHRAE Handbook (2007), the effectiveness value is between 85-95%. So, an effectiveness value of 90% will be set for the comparison. Similar to the VCC system, the power needed to operate the evaporative cooler is calculated by equation 7.5. The average EER for an evaporative cooler is around 15.0 (Torkaman & Ghassembaglou 2015). The cooling load is calculated by:

$$\dot{Q}_{c,evap} = \dot{m}\, c_{pa}\, \Delta T \tag{7.5}$$

A plate heat exchanger with an average effectiveness of $\eta_{exch} = 70\%$ is proposed to be used for the comparison. Neglecting the pressure drop and the heat loss from the heat exchanger, the output temperature is calculated from (Wetter 1999):

$$\eta_{exch} = \frac{\dot{C}_i\,(T_i - T_e)}{\dot{C}_{min}\,(T_i - T_o)} \tag{7.6}$$

where T_i is the inlet temperature of the first air stream, T_e is the outlet temperature of the first air stream, T_o is the inlet temperature of the second air stream, $\dot{C}_i$ is the capacity flow for the first air stream and calculated by:

$$\dot{C}_i = \dot{m}_i c_{pi} \tag{7.7}$$

and $\dot{C}_{min}$ is the minimum capacity flow between the two air streams.

For the aim of comparing a combined SDC system with a VCC system and a standalone VCC system, the following new performance index (η_{comp}) is introduced referring to the same cooling load. The higher η_{comp} value, the higher energy saving by the additional SDC system. η_{comp} is calculated by:

$$\eta_{comp} = \frac{\dot{W}_{VCC\ 1-4}}{\dot{W}_{VCC\ 3-4} + \dot{W}_{ad}} \tag{7.8}$$

where $\dot{W}_{VCC\ 1-4}$ is the power needed to overcome the cooling load for the standalone VCC system (1: stands for the ambient air, 4: stands for the supplied air to the cooling space); $\dot{W}_{VCC\ 3-4}$ is the power needed to overcome the cooling load for the VCC system in the combined SDC system (3: stands for the air after the sensible heat exchanger, 4: stands for the supplied air to the cooling space); and $\dot{W}_{ad}$ is the power needed to run the additional devices related to the SDC system. If the η_{comp} value is between 0.0 and 1.0, the standalone VCC system is more efficient than the combined SDC system with the VCC system. If it is exactly 1.0, which mean that both systems consume the same amount of energy; therefore the standalone VCC system is superior due to the additional cost of the SDC system. If the η_{comp} value is more than 1.0, here the energy required to operate the combined SDC system with the VCC system is less than the standalone VCC system.

The additional equipment in the SDC system that are required power to operate are the process air blower, the regeneration air blower, the DW rotating drive motor, the evaporative cooler, and the heat source. Therefore, $\dot{W}_{ad}$ can be expressed as:

$$\dot{W}_{ad} = \dot{W}_{blower,p} + \dot{W}_{blower,r} + \dot{W}_{rotational} + \dot{W}_{evap} + \dot{W}_{heat} \quad (7.9)$$

In this study, the power needed to operate the air blowers and to rotate the DW is measured using a clamp multimeter by measuring the flowing current and multiplying it with the supplied voltage. The amount of supplied heat to the air from the heat source is calculated by:

$$\dot{W}_{heat} = \dot{m}_r(h_7 - h_6) \quad (7.10)$$

Total dependence on electricity or fossil fuel for the required heat to regenerate the DW is inefficient way from economic and energy consumption points of view (Henning et al. 2013). Consequently, electrical or fossil fuel heaters should be used just as a backup for renewable energy sources. Solar thermal is the most common technology in thermally-based cooling techniques. Therefore, in the case of the added heat to the regeneration air from solar thermal energy, the added heat is assumed to be zero and the comparison performance index becomes $\eta_{comp,solar}$.

In this study, the comparison between the two systems will transpire according to the source of regeneration thermal energy; fossil fuel or solar thermal. In addition, the percentage of solar thermal energy required for the comparison performance index to be unity ($\eta_{comp} = 1$) will be presented. This percentage represents the minimum amount of solar thermal energy or any other renewable source energy that should be applied to ensure just equality between both systems in respect of energy consumption. The percentage can be calculated by:

$$\%\ solar = 1 - \frac{\dot{W}_{heat,\,\eta_{comp}=1}}{\dot{W}_{heat}} \quad (7.11)$$

where $\dot{W}_{heat,\,\eta_{comp}=1}$ is the needed heat to regenerate the DW to achieve $\eta_{comp} = 1.0$, which can be calculated by:

$$\dot{W}_{heat,\,\eta_{comp}=1} = \dot{W}_{VCC\ 1-4} - (\dot{W}_{VCC\ 3-4} + \dot{W}_{ad,solar}) \tag{7.12}$$

the $\dot{W}_{ad,solar}$ represents the additional power needed to operate the SDC system without the heat source. Therefore, the solar percentage can be represented by:

$$\%\ solar = 1 - \frac{\dot{W}_{VCC\ 1-4}(\eta_{comp,solar} - 1)}{\eta_{comp,solar} \times \dot{W}_{heat}} \tag{7.13}$$

Finally, the non-dimensional groups will be optimised according to the highest attained comparison performance index when the solar thermal energy is used to regenerate the DW. Taking into account that the calculations refer to the solar heat added are approximate and only representative of a special case.

7.3 Optimisation results

In this section, only one non-dimensional group value will be varied, while all other non-dimensional groups' values will be set to the base value as in Table 6.1 except for the Y_1, which set to be around 0.015. In order to fill the gaps and state optimal values with more certainty, the experimental values listed in Table 6.1 for the first six non-dimensional groups (except Y_7) were supplemented by the simulation model. Each point of the output results represents a standalone case. The air conditions (temperature and humidity) of each point 1-7 of figure 7.1 are calculated, then the required heat added, power input, or heat loss are calculated. The VCC power could be a different set of data but the same non-dimensional values are adopted as the base value in table 6.1 except for the Y1, which is set to be around 0.015. Therefore, the VCC calculations are approximate and only representative of a special case.

Figure 7.2 shows the comparison performance index (η_{comp}) and the comparison performance index using solar thermal energy to reactivate the DW ($\eta_{comp,solar}$) for different $K_y/\rho_a.N.\delta$ values. It is clear that an increase in $K_y/\rho_a.N.\delta$ between 17179.12 and 28631.87 causes an increase in the $\eta_{comp,solar}$ value from 1.47 to 1.98 then the $\eta_{comp,solar}$ value becomes steady around 2.0. Then, a drop in $\eta_{comp,solar}$ value was found. Varying $K_y/\rho_a.N.\delta$ value has a slight impact on the η_{comp} value, as the η_{comp} value decreased from 0.223 to 0.211 for the full tested range of $K_y/\rho_a.N.\delta$. The percentage of solar thermal energy should be applied to achieve $\eta_{comp} = 1.0$ is vary between 87.9 - 91.7%, while the minimum is at the $K_y/\rho_a.N.\delta$ value 42947.80.

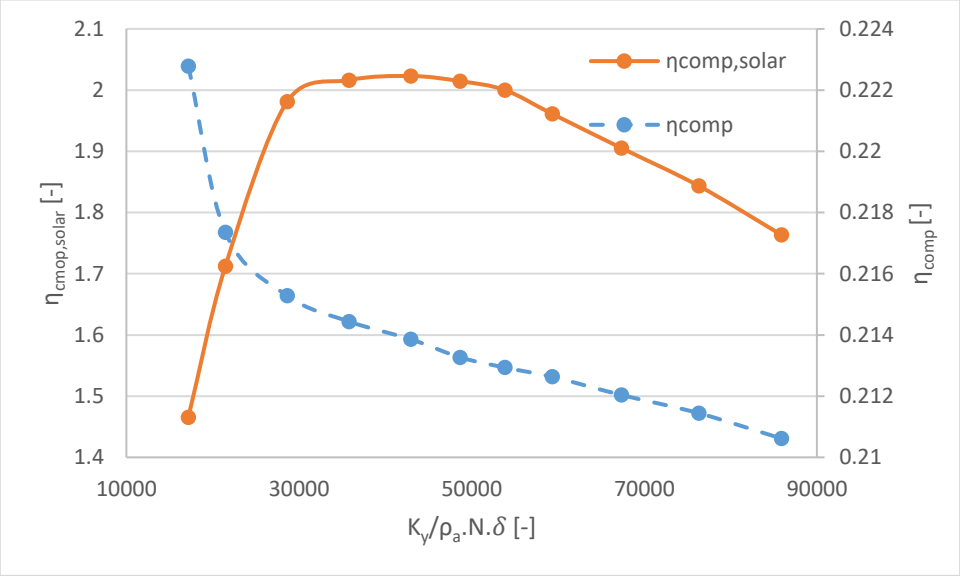

Figure 7.2: Effect of the non-dimensional group $K_y/\rho_a.N.\delta$ on the η_{comp} and $\eta_{comp,solar}$.

The effect of the non-dimensional group u_p/u_r on the η_{comp} and $\eta_{comp,solar}$ is shown in Figure 7.3. It is observed that an increase in u_p/u_r causes a significant increase in the η_{comp} value. The $\eta_{comp,solar}$ value increases from 1.13 to the maximum value of 1.96 with increase u_p/u_r from 0.33 to 1.125, then decreases to 1.0 for further increase in the u_p/u_r value till 3.0. Therefore, the optimal u_p/u_r values is between 1.0 and 1.25 and it is in the vicinity of 1.125. The percentage of solar thermal energy applied to achieve $\eta_{comp} = 1.0$ is vary between 99.4% at (u_p/u_r) equals 0.33, then starts to decrease to 88.0% at the u_p/u_r value at 1.125, after that it increases again to 99.3% at u_p/u_r equals 3.0.

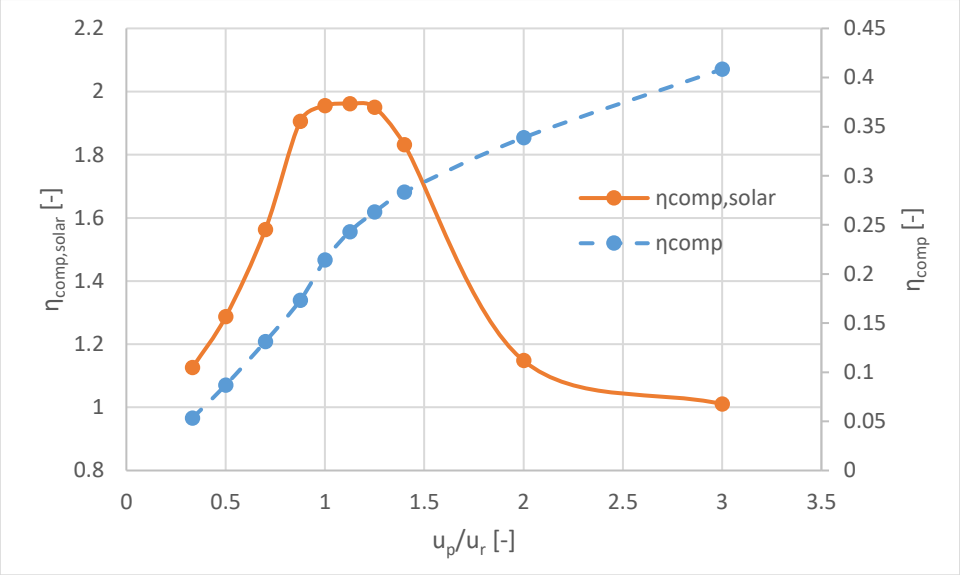

Figure 7.3: Effect of the non-dimensional group u_p/u_r on the η_{comp} and $\eta_{comp,solar}$.

Figure 7.4 illustrate the effect of the non-dimensional group T_7/T_1 on the η_{comp} and $\eta_{comp,solar}$. A substantial decrease in η_{comp} value from 0.33 to 0.18 is observed by increasing the T_7/T_1 value. The $\eta_{comp,solar}$ value increases from 1.92 to the maximum value of 2.00 with an increase in T_7/T_1 from 1.066 to 1.098, $\eta_{comp,solar}$ value still at one of the highest values of 1.98 at T_7/T_1 equals 1.133 then decreases to 1.46 for an additional increase in the T_7/T_1. The optimal T_7/T_1 value is found to be between 1.098 and 1.133. The percentage of solar thermal energy applied to achieve η_{comp} = 1.0 is almost linear increased from 80.9 – 93.6%, while the percentage is 85.1% at T_7/T_1 equals 1.098.

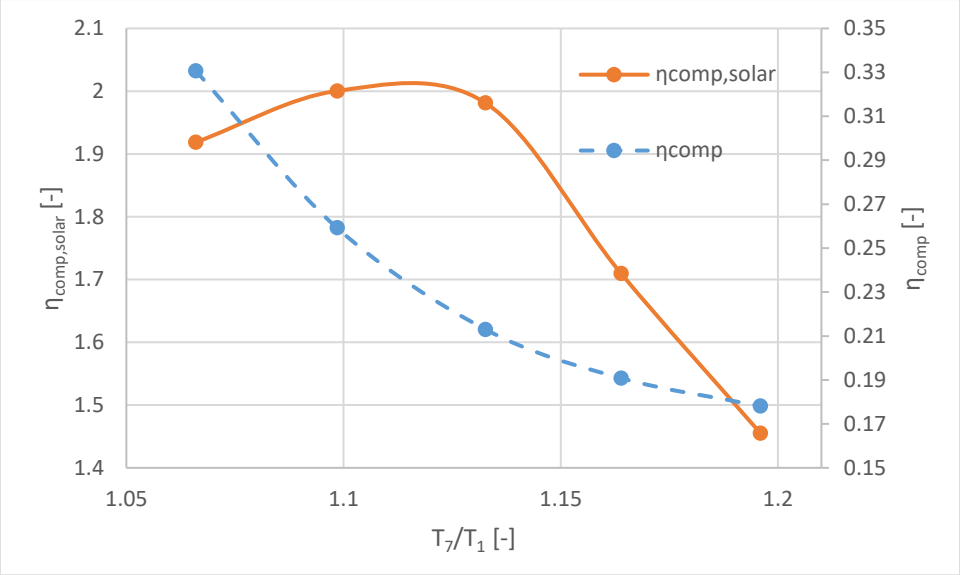

Figure 7.4: Effect of the non-dimensional group T_7/T_1 on the η_{comp} and $\eta_{comp,solar}$.

Figure 7.5 represents the effect of the non-dimensional group Y_1 on the η_{comp} and $\eta_{comp,solar}$. Increase the Y_1 value to about 0.021 leads to a nearly linear increment of the η_{comp} from 0.09 to 0.36, then reach a steady state after that value at about 0.37. Also, it leads to an increase in the $\eta_{comp,solar}$ till reach the maximum point of 1.97 at Y_1 equals between 0.0156 and 0.0184 then the $\eta_{comp,solar}$ value becomes almost steady at the same value. Therefore, the optimal Y_1 value is greater than 0.015. The percentage of solar thermal energy applied to achieve $\eta_{comp} = 1.0$ is practically linear decreased from 101.0% to 78.7%. The percentage of 101.0% at Y_1 equals 0.0067 means that if the total heat is supplied even from a solar thermal source, the SDC system is not feasible from an energy consumption perspective due to the low air humidity content and thus low latent load.

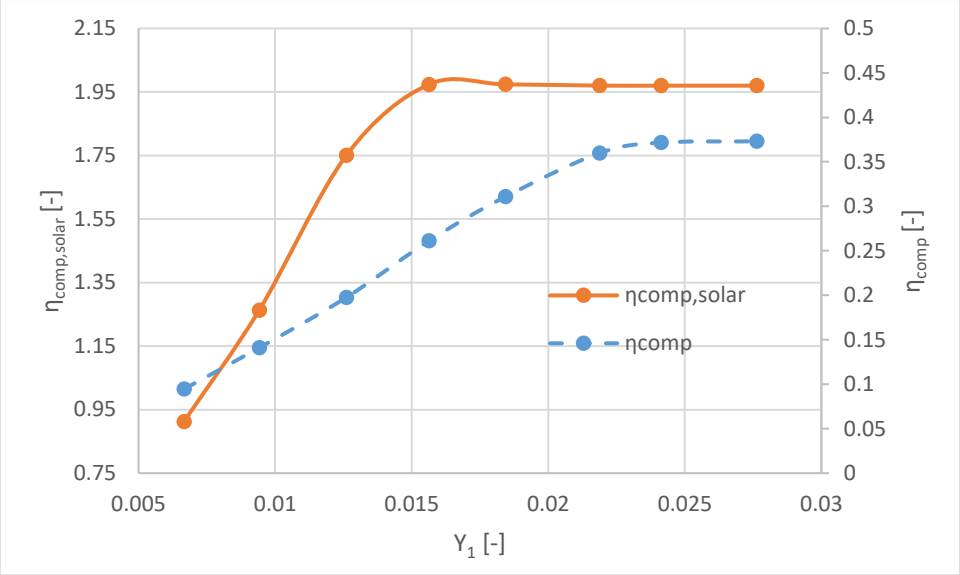

Figure 7.5: Effect of the non-dimensional group Y_1 on the η_{comp} and $\eta_{comp,solar}$.

The influence of varying the non-dimensional group θ_p/θ_r on the η_{comp} and $\eta_{comp,solar}$ is illustrated in Figure 7.6. An increase in the θ_p/θ_r value leads to a nearly linear increment of the η_{comp} from 0.20 to 0.40. However, it leads to increase the $\eta_{comp,solar}$ to a maximum point of 2.05 at θ_p/θ_r in the vicinity of 0.875 then start to drop to the minimum value of 1.0 at θ_p/θ_r equals 3.0. Therefore, the optimal θ_p/θ_r value among the tested values is between 0.75 and 1.0 and it is at the vicinity of 0.875. The minimum solar thermal percentage to achieve η_{comp} = 1.0 of 87.7% is attained at the θ_p/θ_r value 0.875, then it starts to increase till 100% at θ_p/θ_r equals 3.0.

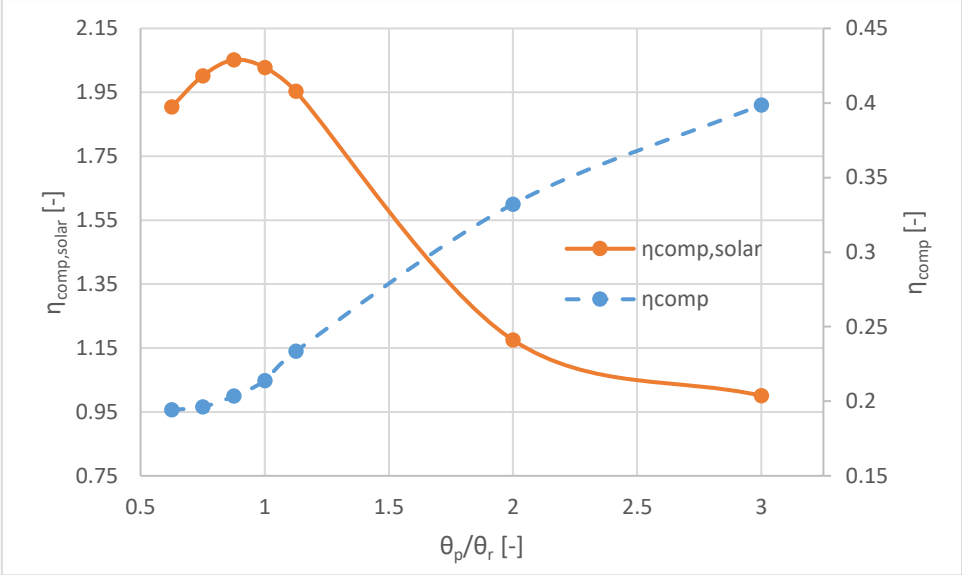

Figure 7.6: Effect of the non-dimensional group θ_p/θ_r on the η_{comp} and $\eta_{comp,solar}$.

The effect of varying the non-dimensional group $C.L/A_f$ on the η_{comp} and $\eta_{comp,solar}$ is elucidated in Figure 7.7. An increase in the $C.L/A_f$ value results in a slight increase in the η_{comp} from 0.21 to 0.23. Unlike all previous non-dimensional parameters, varying the $C.L/A_f$ value causes a small variation in $\eta_{comp,solar}$ between 1.83 and 1.97. The maximum achieved $\eta_{comp,solar}$ was at $C.L/A_f$ between 221.8 and 237.7 and it is close to 230.3. In addition, the percentage of solar thermal energy applied to achieve $\eta_{comp} = 1.0$ is slightly decreased from 89.4 – 87.6% for the whole tested range, while the percentage is 88.1% at $C.L/A_f$ equals 230.3.

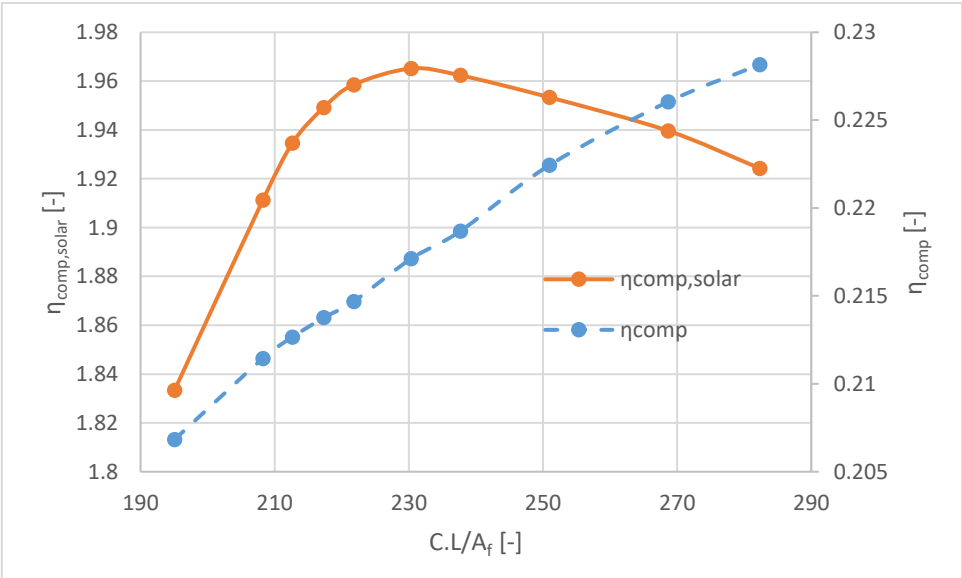

Figure 7.7: Effect of the non-dimensional group $C.L/A_f$ on the η_{comp} and $\eta_{comp,solar}$.

Figure 7.8 represents the effect of the non-dimensional group ε on the η_{comp} and $\eta_{comp,solar}$. Increasing ε value causes a slight decrease in the η_{comp} value from 0.227 to 0.206. As regards the $\eta_{comp,solar}$, an increase in the ε causes an increase in the $\eta_{comp,solar}$ to a maximum value of 2.01 at ε just before 0.4, then starts to drop to reach 1.67 value at ε equals 0.6. The optimal ε value among the tested values is close to 0.4. The percentage of solar thermal energy applied to achieve η_{comp} = 1.0 stays constant at 87.6% for the ε value between 0.2-0.4, then linearly increased to 90.6%. Figure 7.8 was provided without including the required electrical energy of process and regeneration blowers as explained earlier in section 6.2.2, so the sharp decrease is more likely due to the decrease of contact surface.

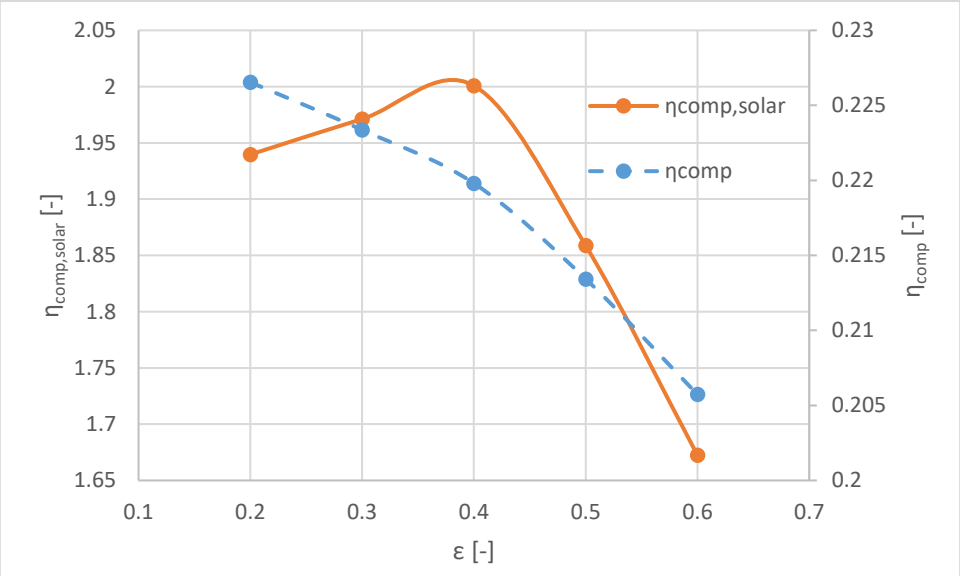

Figure 7.8: Effect of the non-dimensional group ε on the η_{comp} and $\eta_{comp,solar}$.

The effect of varying the non-dimensional group Φ on the η_{comp} and $\eta_{comp,solar}$ is presented in Figure 7.9. A slight increase in the η_{comp} from 0.204 to 0.227 is noticed by increasing Φ. An increase in the Φ causes an increase in the $\eta_{comp,solar}$ to a maximum value of 1.96 at Φ equals 0.6, then starts to decrease to 1.94 at Φ equals 0.7. The optimal Φ value is in the vicinity of 0.6. The percentage of solar thermal energy applied to achieve η_{comp} = 1.0 is decreased from 91.3% to 87.6% at Φ equals 0.6, then remains steady till Φ equals 0.7.

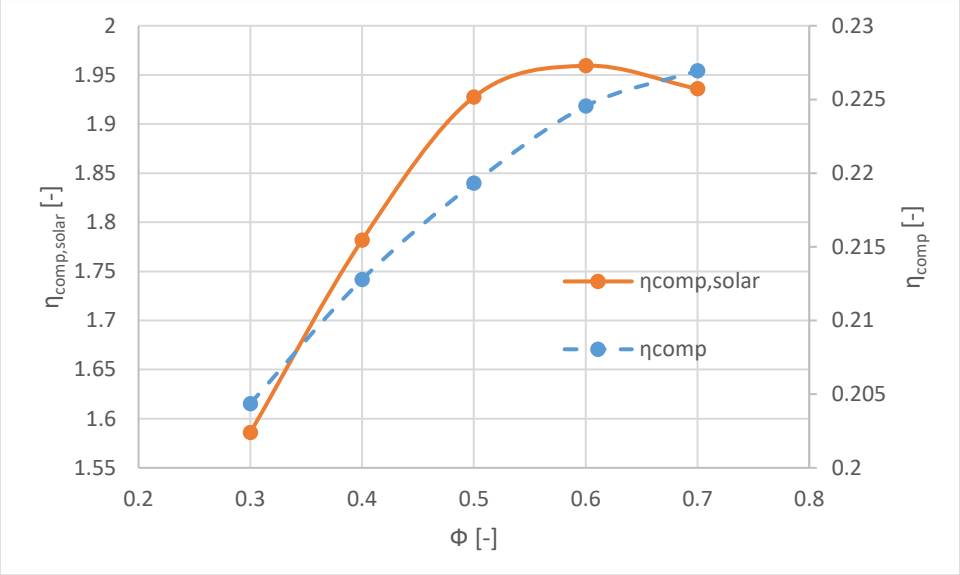

Figure 7.9: Effect of the non-dimensional group Φ on the η_{comp} and $\eta_{comp,solar}$.

7.4 Summary and conclusion

In this chapter, optimising the non-dimensional groups presented in CHAPTER 5: DIMENSIONAL ANALYSIS is carried out. The optimisation is based on comparing the combined SDC system and VCC system with a standalone VCC system. The Pennington cycle SDC system is chosen for comparison with replacing the direct evaporative cooler in the process side with the VCC system to ensure covering the cooling load and provide the same air condition to the cooling space. The calculations related to the sensible heat exchanger, direct evaporative cooler, VCC system and the heat add to the regeneration air are presented. In addition, a new performance index (η_{comp}) is presented for comparison. In the case of the added heat to the regeneration air from renewable energy sources (in this case it is assumed to be solar thermal energy), the added heat is assumed to be zero and the comparison performance index becomes $\eta_{comp,solar}$. The optimisation is carried out referring to $\eta_{comp,solar}$.

The maximum achieved $\eta_{comp,solar}$ in all cases is around 2.0, which means that the standalone VCC system needs two times more power than the combined SDC system with the VCC system

for the same cooling load and operation conditions. The optimal non-dimensional groups' values are as follow:

- the optimal ($K_y/\rho_a.N.\delta$) range is between 28631.87 and 48661.68,
- the optimal (u_p/u_r) value is between 1.0 and 1.25 and it is in the vicinity of 1.125,
- the optimal (T_7/T_1) range is between 1.098 and 1.133,
- the optimal (Y_1) is when it is greater than 0.015,
- the optimal (θ_p/θ_r) value is in the vicinity of 0.875,
- the optimal ($C.L/A_f$) value is between 221.8 and 237.7 and it is close to 230.3,
- the optimal (ε) value is just before 0.4,
- the optimal (Φ) value is in the vicinity of 0.6.

Based on the comparison, using the combined SDC by VCC system without solar energy is not recommended as the comparison ratio (η_{comp}) was always less than 1, but recommended with a solar energy source. As solar energy is available during days, the combined system particularly recommended for use in offices and workshops that are open during the days. Moreover, it is recommended for use day and night where continues renewable heat source is available such as geothermal or waste heat sources.

The percentage of solar thermal energy to achieve $\eta_{comp} = 1.0$ is presented. This percentage represents the minimum amount of solar thermal energy that should be applied to ensure equality between both systems in respect of energy consumption. It was found that the percentage values vary between 78.7 - 101%. The average percentage at the optimal non-dimensional groups' values is around 88%.

CHAPTER 8: CONCLUSIONS, SUMMARY, AND FUTURE RESEARCH

8.1 Introduction

The research presented in this thesis has mainly concerned the performance optimisation of the DW system. This chapter first describes the work and the importance of this research. Then summarizes the main conclusions from this research and discusses the possible improvement in the DW operational and design parameters as related to the system performance. Finally, proposed future researches related to the current research are presented.

8.2 Description of work

SDC system is considered one of the thermal-based air cooling systems. SDC systems have several significant advantages over other systems such as, the relatively low desiccant activation temperature which can be from renewable resources, inexpensive and environmentally friendly desiccant material, and safe to use a refrigerant as SDC system uses air and water. The main part of the SDC system is the DW, which is responsible for the dehumidification process. The DW rotates continuously through two air streams, which separates the DW into process and regeneration sections. Considering the DW as an open system, both mass (moisture) and energy are conserved in the air streams and the desiccant material.

Many studies have been reported in the literature about studying the effect of some operational and climate parameters on the overall system performance. It is concluded that the most influential operational parameters on DW performance are DW rotation speed, regeneration temperature, and airflow rates through the DW. According to previous studies, ranges of the best values or a specific value are given that maximises the system COP regardless of the effect

of other parameters. At the time of writing, there has been no study that combined the parameters into non-dimensional form. The benefits of creating the non-dimensional groups are to reduce the required experiments and to study the effect of some parameters that cannot be changed through experiments by changing other parameters values in the same group. Also, there are very few studies that considered the channel geometry and design parameters. And there has been no study that optimises the most influential operational parameters on DW performance related to design parameters. Therefore, in this research, non-dimensional groups have been formed and tested experimentally and through simulation. Then, how these non-dimensional groups are related in terms of performance indices are presented.

8.3 Summary and conclusions

The outcomes of this research can be summarised into three groups, general outcomes related to the simulation model, non-dimensional groups' elicitation, and the effect of different values of the non-dimensional groups on the system performance.

8.3.1 GSR and GSSR simulation models

Among GSR and GSSR DW mathematical models, the following conclusions have been drawn:

- Both GSR and GSSR models are used effectively to simulate the DW.
- Because of the inclusion of the heat conduction and mass diffusion within the solid desiccant layer in the GSSR model, it is more accurate than the GSR model.
- And by comparing 1-D and 2-D GSSR models, it was found that the results of both models are very convergent. Previous studies show good results for the 1-D GSSR model which can be achieved with a maximum error of 15% from experimental results. Therefore, the 1-D GSSR model is used in this study to simulate the DW.

- By validation the simulation outcomes in this study with different published experimental results, the 1-D GSSR model has proven to be effective and well agree with the experimental results under different operation conditions.

8.3.2 Non-dimensional groups' elicitation

The dimensional analysis technique is a method to lessen the variables number of any physical phenomena into a set of dimensionless variables combination by creating a relationship between them according to their dimensions. Conducting the dimensional analysis method has some advantages such as experiment cost reduction due to the reduction in the number of required experiments by reducing the number of studied variables, to facilitate studying the effect of some parameters by changing other parameter's values in the same group in extreme cases, and to create a prototype by downsizing or enlarge the actual system to simplify experimentation.

Considering the desiccant material parameters to be constant during the operation, the DW's dependent and independent parameters are divided into three categories; the process air and climate parameters, regeneration air parameters, and the DW design and operational parameters.

The following steps are the process of creating the non-dimensional groups; listing the independent and dependent parameters, identifying the units of the parameters, creating non-dimensional parameters combinations, and testing the created parameters combinations.

The applied method to test the created non-dimensional parameters combinations is by keeping the combination value constant and varying the values of its parameters. If the output results are similar, then the parameter combination is considered as a non-dimensional group. Some non-dimensional groups have been tested experimentally and the others tested by the

mathematical model due to the difficulty of changing some parameters experimentally. The number of independent parameters has been reduced from 16 to 9 non-dimensional groups.

8.3.3 The effect of the non-dimensional groups on the system performance

The experimental aperture has been designed and built for the purpose of conducting investigations related to testing the non-dimensional groups, identify the operating range, the effect on the performance indices, and their optimal values. The simulation model is used as a complement to the experimental setup where some parameters values cannot be varied experimentally. The simulation model is validated experimentally under this study's operating condition. It was found that the deviation for the performance indices is within ±5.1%.

Some of the non-dimensional groups are tested and studied as regards the performance indices experimentally such as u_p/u_r, T_7/T_1, Y_1, Y_7 and θ_p/θ_r. While others are tested and studied as regards the performance indices through the simulation model such as $C.L/A_f$, ε, and Φ. In the case of the non-dimensional group $K_y/\rho_a.N.\delta$, it has been tested by the simulation model due to the inability of change the channel thickness experimentally for the same DW and studied as regards the performance indices experimentally by changing the DW rotational speed value.

The effect of the non-dimensional groups on the performance indices are as follow:

- The optimal $K_y/\rho_a.N.\delta$ value is in the vicinity of 42947.80 in most cases which maximise the η_{deh} and the DCOP while the SER in the lowest values.
- The optimal $K_y/\rho_a.N.\delta$ value is decreased to about 28631.87 in case of low u_p/u_r or high T_7/T_1.
- A positive effect of decreasing u_p/u_r value on η_{deh} leads to enhance the dehumidification process by providing more regeneration thermal energy to reactivate the desiccant material.

- Decreasing u_p/u_r value causes a decrease in the air dehumidification thermal power, increases the provided regeneration thermal energy, and decreases the DCOP and SER.
- The optimal u_p/u_r value in case of increasing T_7/T_1 value is also increased gradually from 0.333 to 1.0.
- Increasing the T_7/T_1 value causes an increase in the η_{deh} because of the enhancement in the regeneration process, but also increases the SER due to the high provided regeneration thermal energy.
- Increasing the T_7/T_1 value decreases the DCOP because of the increase in the delivered thermal power to the DW per mass flow rate.
- The effect of increasing Y_1 value is an increase in the De and thus η_{deh} and DCOP. Also, it causes an increase in the SER due to the rise in the released adsorption heat.
- High Y_1 values lead to an increase in the diffusion of water particles which negatively affect the η_{deh}.
- It was found that the non-dimensional group Y_7 has an inconsiderable effect on the system performance.
- Increasing θ_p/θ_r value leads to an increase in the process air mass flow rate and thus increases the dehumidification process. But, it reduces the regeneration mass flow rate, reduces the regeneration thermal power, and becomes unable to reactivate the desiccant material because of the immoderate delivered humidity.
- Increasing θ_p/θ_r value causes a reduction in the η_{deh} value and an increase in the system DCOP and SER.
- Increasing $C.L/A_f$ value causes an increase in the contact surface between the process air and the desiccant material which enhances the dehumidification process and an increment in the η_{deh} and the DCOP.

- Increasing C.L/A_f value increases the SER as well due to the increase in the released adsorption heat.
- The effect of increasing C.L/A_f is identical to all the non-dimensional groups.
- Increase C.L/A_f value from 195.07 to 282.33 cause a 33.1% increment in the η_{deh} and the DCOP and a 32.7% increment in the SER.
- Increasing ε reduces the contact surface between the process air and the desiccant material and thus negatively affect the η_{deh} and the DCOP.
- A lessening in the dehumidification process because of increasing ε value causes a reduction in the released adsorption heat and thus a reduction in the SER value.
- The effect of increasing ε is identical to all the non-dimensional groups.
- Increase ε value from 0.2 to 0.6 cause a -28.3% decrement in the η_{deh} and the DCOP and a -21.2% decrement in the SER.
- Increasing the amount of desiccant material particles in the layer by increasing Φ value causes a higher adsorbing amount of humidity which increases the η_{deh} and the DCOP.
- Increasing Φ value increases the SER since more adsorption heat is released to the process air.
- The effect of increasing Φ is identical to all the non-dimensional groups.
- Increase Φ value from 0.3 to 0.7 cause a 52.9% increment in the η_{deh} and the DCOP and a 27.1% increment in the SER.

8.3.4 Non-dimensional groups' optimisation

The non-dimensional groups' optimisation was conducted based on comparing the combined SDC system and VCC system with a standalone VCC system. The Pennington cycle SDC system was chosen for the comparison. A new performance index (η_{comp}) was presented for comparison. In the case of the added heat to the regeneration air from renewable energy sources

(in this case it is assumed to be solar thermal energy), the added heat was assumed to be zero and the comparison performance index becomes $\eta_{comp,solar}$, which was used for the optimisation. The maximum achieved $\eta_{comp,solar}$ in all cases was around 2.0, which means that the standalone VCC system needs two times more power than the combined SDC system with the VCC system for the same cooling load and operation conditions.

Some of the non-dimensional groups' optimal value was in the vicinity of a specific point such as u_p/u_r at 1.125, θ_p/θ_r at 0.875, $C.L/A_f$ at 230.3, ε at 0.4, and Φ at 0.6. While for other non-dimensional groups, the optimal values were a range such as, $K_y/\rho_a.N.\delta$ between 28631.87 and 48661.68 and T_7/T_1 between 1.098 and 1.133. The only non-dimensional group that the optimal value was an open interval is Y_1 at any value greater than 0.015.

The percentage of solar thermal energy to unity the comparison performance index was presented which represents the minimum amount of solar thermal energy that should be applied to ensure just equality between both systems in respect of energy consumption. It was found that the percentage values vary between 78.7 - 101%, while the average percentage at the optimal non-dimensional groups' values was around 88%.

8.4 Future research

While the proposed objectives of this research have been achieved, further research would be beneficial to extend the research outcomes. The following areas are recommended for further research:

- Test different desiccant materials to investigate if the same non-dimensional groups are applicable. In addition, in the case of testing new desiccant materials, consider the desiccant material variables in conducting the dimensional analysis method.
- The most common DW's channel shape is the sinusoidal shape. Some DW's have different channel geometry, such as triangular, circular, and rectangular. It would be

useful to investigate the process air output condition for different channel shapes. Also, to investigate for different channel shapes if the same channel perimeter and airflow passage area will affect the results of the non-dimensional groups especially $C.L/A_f$.

- It is essential to conduct a study about the economic feasibility of utilising the SDC system for air conditioning considering the effect of the non-dimensional groups' optimum operating condition of the system payback period.
- The DW configuration used in this research for testing the non-dimensional groups and to study their effect on the system performance is based on providing fresh air for both process and regeneration because the DW system is not connected to a cooling space. But for the optimisation, one system configuration which is the Pennington cycle and a proposed air cooling space were presented and the calculations are carried out based on the conditions of the supply and return air to the cooling space. Therefore, it would be essential to study the effect of other different configurations on the overall system performance and their effect on the non-dimensional groups. Some configurations mix by the identified percentage of the ambient air with the return air from the cooling space and provide that mixture to either process or regeneration sections or both.

REFERENCES

Ahmed, MH, Kattab, NM & Fouad, M 2005, 'Evaluation and optimization of solar desiccant wheel performance', *Renewable Energy*, vol. 30, no. 3, pp. 305-25.

Angrisani, G, Roselli, C & Sasso, M 2013, 'Effect of rotational speed on the performances of a desiccant wheel', *Applied Energy*, vol. 104, pp. 268-75.

Angrisani, G, Minichiello, F, Roselli, C & Sasso, M 2012, 'Experimental analysis on the dehumidification and thermal performance of a desiccant wheel', *Applied Energy*, vol. 92, pp. 563-72.

Angrisani, G, Capozzoli, A, Minichiello, F, Roselli, C & Sasso, M 2011, 'Desiccant wheel regenerated by thermal energy from a microcogenerator: Experimental assessment of the performances', *Applied Energy*, vol. 88, no. 4, pp. 1354-65.

ASHRAE Handbook 2007, *HVAC applications*, American Society of Heating, Refrigerating and Air-Conditioning Engineers, Inc.

Bareschino, P, Diglio, G, Pepe, F, Angrisani, G, Roselli, C & Sasso, M 2015, 'Modelling of a rotary desiccant wheel: Numerical validation of a Variable Properties Model', *Applied Thermal Engineering*, vol. 78, pp. 640-8.

Camargo, JR, Godoy Jr, E & Ebinuma, CD 2005, 'An evaporative and desiccant cooling system for air conditioning in humid climates', *Journal of the Brazilian Society of Mechanical Sciences and Engineering*, vol. 27, no. 3, pp. 243-7.

Çarpinlioglu, MÖ & Yildirim, M 2005, 'A methodology for the performance evaluation of an experimental desiccant cooling system', *International Communications in Heat and Mass Transfer*, vol. 32, no. 10, pp. 1400-10.

Cengel, Y & Boles, M 2015, *Thermodynamics: An Engineering Approach*, 8th edn, McGraw-Hill Education.

Cengel, YA & Cimbala, JM 2018, *Fluid Mechanics: Fundamentals and Applications, Forth Edition*, New York: McGraw-Hill Education.

Charoensupaya, D & Worek, WM 1988, 'Parametric study of an open-cycle adiabatic, solid, desiccant cooling system', *Energy*, vol. 13, no. 9, pp. 739-47.

Charoensupaya, D & Worek, WM 1989, 'Dynamic sorption of porous adsorbents—Comparison of experimental results with numerical predictions', *International Communications in Heat and Mass Transfer*, vol. 16, no. 5, pp. 681-91.

Cheng, D, Peters, EAJF & Kuipers, JAM 2017, 'Performance study of heat and mass transfer in an adsorption process by numerical simulation', *Chemical Engineering Science*, vol. 160, pp. 335-45.

Choudhury, B, Chatterjee, PK & Sarkar, JP 2010, 'Review paper on solar-powered air-conditioning through adsorption route', *Renewable and Sustainable Energy Reviews*, vol. 14, no. 8, pp. 2189-95.

Chung, JD & Lee, D-Y 2009, 'Effect of desiccant isotherm on the performance of desiccant wheel', *International Journal of Refrigeration*, vol. 32, no. 4, pp. 720-6.

Chung, JD & Lee, D-Y 2011, 'Contributions of system components and operating conditions to the performance of desiccant cooling systems', *International Journal of Refrigeration*, vol. 34, no. 4, pp. 922-7.

Chung, JD, Lee, D-Y & Yoon, SM 2009, 'Optimization of desiccant wheel speed and area ratio of regeneration to dehumidification as a function of regeneration temperature', *Solar Energy*, vol. 83, no. 5, pp. 625-35.

Comino, F & Ruiz de Adana, M 2016, 'Experimental and numerical analysis of desiccant wheels activated at low temperatures', *Energy and Buildings*, vol. 133, pp. 529-40.

De Antonellis, S, Joppolo, CM & Molinaroli, L 2010, 'Simulation, performance analysis and optimization of desiccant wheels', *Energy and Buildings*, vol. 42, no. 9, pp. 1386-93.

De Antonellis, S, Intini, M, Joppolo, CM, Molinaroli, L & Romano, F 2015, 'Desiccant wheels for air humidification: An experimental and numerical analysis', *Energy Conversion and Management*, vol. 106, pp. 355-64.

Department of Environment and Energy 2013, *HVAC Energy Breakdown, factsheet*, Australian Government, viewed 22 Augast 2017, <http://ee.ret.gov.au/>.

Department of the Environment and Energy 2020, *Australian Energy Statistics, Table O*.

Dunkle, R 1965, 'Method of solar air conditioning', *Mechanical and Chemical Engineering Transactions of the Institute of Engineers*, vol. 73, pp. 73–8.

Eicker, U, Schürger, U, Köhler, M, Ge, T, Dai, Y, Li, H & Wang, R 2012, 'Experimental investigations on desiccant wheels', *Applied Thermal Engineering*, vol. 42, pp. 71-80.

El-Agouz, SA & Kabeel, AE 2015, 'Thermal Analysis of a Novel Integrated Air Conditioning System with Geothermal Energy', *Journal of Energy Engineering*, vol. 141, no. 3, p. 04014030.

El-Agouz, SA, Sathyamurthy, R & A, MM 2018, 'Improvement of humidification–dehumidification desalination unit using a desiccant wheel', *Chemical Engineering Research and Design*, vol. 131, pp. 104-16.

Enteria, N, Yoshino, H, Mochida, A, Takaki, R, Satake, A, Yoshie, R, Mitamura, T & Baba, S 2009, 'Construction and initial operation of the combined solar thermal and electric desiccant cooling system', *Solar Energy*, vol. 83, no. 8, pp. 1300-11.

Fasfous, A, Asfar, J, Al-Salaymeh, A, Sakhrieh, A, Al_hamamre, Z, Al-bawwab, A & Hamdan, M 2013, 'Potential of utilizing solar cooling in The University of Jordan', *Energy Conversion and Management*, vol. 65, pp. 729-35.

Fong, KF, Chow, TT, Lee, CK, Lin, Z & Chan, LS 2010, 'Comparative study of different solar cooling systems for buildings in subtropical city', *Solar Energy*, vol. 84, no. 2, pp. 227-44.

Gao, Z, Mei, VC & Tomlinson, JJ 2005, 'Theoretical analysis of dehumidification process in a desiccant wheel', *Heat and Mass Transfer*, vol. 41, no. 11, pp. 1033-42.

Ge, TS, Ziegler, F & Wang, RZ 2010a, 'A mathematical model for predicting the performance of a compound desiccant wheel (A model of compound desiccant wheel)', *Applied Thermal Engineering*, vol. 30, no. 8-9, pp. 1005-15.

Ge, TS, Li, Y, Wang, RZ & Dai, YJ 2008b, 'A review of the mathematical models for predicting rotary desiccant wheel', *Renewable and Sustainable Energy Reviews*, vol. 12, no. 6, pp. 1485-528.

Ge, TS, Dai, YJ, Wang, RZ & Li, Y 2008a, 'Experimental investigation on a one-rotor two-stage rotary desiccant cooling system', *Energy*, vol. 33, no. 12, pp. 1807-15.

Ge, TS, Ziegler, F, Wang, RZ & Wang, H 2010b, 'Performance comparison between a solar driven rotary desiccant cooling system and conventional vapor compression system (performance study of desiccant cooling)', *Applied Thermal Engineering*, vol. 30, no. 6-7, pp. 724-31.

Ge, TS, Dai, YJ, Li, Y & Wang, RZ 2012, 'Simulation investigation on solar powered desiccant coated heat exchanger cooling system', *Applied Energy*, vol. 93, pp. 532-40.

Geankoplis, CJ 2003, *Transport processes and separation process principles:(includes unit operations)*, 4 edn, Prentice Hall Professional Technical Reference.

Gibbings, JC 2011, *Dimensional analysis*, Springer Science & Business Media.

Golubovic, MN & Worek, WM 2004, 'Influence of Elevated Pressure on Sorption in Desiccant Wheels', *Numerical Heat Transfer, Part A: Applications*, vol. 45, no. 9, pp. 869-86.

Golubovic, MN, Hettiarachchi, HDM & Worek, WM 2007, 'Evaluation of rotary dehumidifier performance with and without heated purge', *International Communications in Heat and Mass Transfer*, vol. 34, no. 7, pp. 785-95.

Halliday, S.P., Beggs, C.B. and Sleigh, P.A., 2002. The use of solar desiccant cooling in the UK: a feasibility study. Applied Thermal Engineering, 22(12), pp.1327-1338.

Heidarinejad, G & Pasdarshahri, H 2010, 'The effects of operational conditions of the desiccant wheel on the performance of desiccant cooling cycles', *Energy and Buildings*, vol. 42, no. 12, pp. 2416-23.

Henning, H-M, Motta, M & Mugnier, D 2013, *Solar cooling handbook: a guide to solar assisted cooling and dehumidification processes*, Birkhäuser.

IEA 2005, *World Energy Outlook 2004*, International Energy Agency, Paris, France.

Intini, M, Goldsworthy, M, White, S & Joppolo, CM 2015, 'Experimental analysis and numerical modelling of an AQSOA zeolite desiccant wheel', *Applied Thermal Engineering*, vol. 80, pp. 20-30.

Jani, DB, Mishra, M & Sahoo, PK 2016, 'Solid desiccant air conditioning – A state of the art review', *Renewable and Sustainable Energy Reviews*, vol. 60, pp. 1451-69.

Joudi, KA & Madhi, SM 1987, 'An experimental investigation into a solar assisted desiccant-evaporative air-conditioning system', *Solar Energy*, vol. 39, no. 2, pp. 97-107.

Kabeel, A.E. and Bassuoni, M.M., 2013. Feasibility study and life cycle assessment of two air dehumidification systems. Global Adv Res Phy App Sci, 2, pp.8-16.

Kanoğlu, M, Bolattürk, A & Altuntop, N 2007, 'Effect of ambient conditions on the first and second law performance of an open desiccant cooling process', *Renewable Energy*, vol. 32, no. 6, pp. 931-46.

Koronaki, I, Papoutsis, E, Papaefthimiou, V & Rogdakis, E 2016, 'Numerical and experimental analysis of a solid desiccant wheel', *Thermal Science*, vol. 20, no. 2, pp. 613-21.

Koronaki, IP, Rogdakis, E & Kakatsiou, T 2013, 'Experimental assessment and thermodynamic analysis of a solar desiccant cooling system', *International Journal of Sustainable Energy*, vol. 32, no. 2, pp. 121-36.

Kousar, R., Ali, M., Sheikh, N.A. and Khushnood, S., 2021. Holistic integration of multi-stage dew point counter flow indirect evaporative cooler with the solar-assisted desiccant cooling system: A techno-economic evaluation. Energy for Sustainable Development, 62, pp.163-174.

La, D, Dai, YJ, Li, Y, Wang, RZ & Ge, TS 2010, 'Technical development of rotary desiccant dehumidification and air conditioning: A review', *Renewable and Sustainable Energy Reviews*, vol. 14, no. 1, pp. 130-47.

La, D., Dai, Y., Li, Y., Ge, T. and Wang, R., 2011. Case study and theoretical analysis of a solar driven two-stage rotary desiccant cooling system assisted by vapor compression air-conditioning. Solar energy, 85(11), pp.2997-3009.

Lunde, P 1976, 'Preliminary Design of a Solar-Powered Desiccant Air Conditioning System Using Silica Gel', *Final progress report for USERDA, Hartford, Connecticut: The centre for the enviornment and man, Inc*.

Ma, Y, Saha, SC, Miller, W & Guan, L 2017, 'Parametric Analysis of Design Parameter Effects on the Performance of a Solar Desiccant Evaporative Cooling System in Brisbane, Australia', *Energies*, vol. 10, no. 7, p. 849.

Mandegari, MA & Pahlavanzadeh, H 2009, 'Introduction of a new definition for effectiveness of desiccant wheels', *Energy*, vol. 34, no. 6, pp. 797-803.

Mandegari, MA & Pahlavanzadeh, H 2013, 'A Study on the Optimization of an Air Dehumidification Desiccant System', *Journal of Thermal Science and Engineering Applications*, vol. 5, no. 4.

Mandegari, MA, Pahlavanzadeh, H & Farzad, S 2014, 'Energy approach analysis of desiccant wheel operation', *Energy Systems*, vol. 5, no. 3, pp. 551-69.

Manzer, LE 1990, 'The CFC-Ozone Issue: Progress on the Development of Alternatives to CFCs', *Science*, vol. 249, no. 4964, pp. 31-5.

Misha, S, Mat, S, Ruslan, MH, Salleh, E & Sopian, K 2015, 'Performance of a solar assisted solid desiccant dryer for kenaf core fiber drying under low solar radiation', *Solar Energy*, vol. 112, pp. 194-204.

Muthu, S, Talukdar, P & Jain, S 2016, 'Effect of Regeneration Section Angle on the Performance of a Rotary Desiccant Wheel', *Journal of Thermal Science and Engineering Applications*, vol. 8, no. 1.

Narayanan, R, Saman, WY, White, SD & Goldsworthy, M 2011, 'Comparative study of different desiccant wheel designs', *Applied Thermal Engineering*, vol. 31, no. 10, pp. 1613-20.

Nellis, G & Klein, S 2009, *Heat transfer*, Cambridge University Press, New York.

Nelson, JS, Beckman, WA, Mitchell, JW & Close, DJ 1978, 'Simulations of the performance of open cycle desiccant systems using solar energy', *Solar Energy*, vol. 21, no. 4, pp. 273-8.

Nia, FE, van Paassen, D & Saidi, MH 2006, 'Modeling and simulation of desiccant wheel for air conditioning', *Energy and Buildings*, vol. 38, no. 10, pp. 1230-9.

Niemann, P, Richter, F, Speerforck, A & Schmitz, G 2019, 'Desiccant-Assisted Air Conditioning System Relying on Solar and Geothermal Energy during Summer and Winter', *Energies*, vol. 12, no. 16.

Niu, J & Zhang, L 2002, 'Effects of wall thickness on the heat and moisture transfers in desiccant wheels for air dehumidification and enthalpy recovery', *International Communications in Heat and Mass Transfer*, vol. 29, no. 2, pp. 255-68.

Panaras, G, Mathioulakis, E, Belessiotis, V & Kyriakis, N 2010, 'Theoretical and experimental investigation of the performance of a desiccant air-conditioning system', *Renewable Energy*, vol. 35, no. 7, pp. 1368-75.

Pennington, NA 1955, *Humidity changer for air-conditioning*, United States Patents, United States.

Pesaran, AA & Mills, AF 1987, 'Moisture transport in silica gel packed beds—I. Theoretical study', *International Journal of Heat and Mass Transfer*, vol. 30, no. 6, pp. 1037-49.

Rafique, MM 2016, 'Heat and Mass Transfer between Humid Air and Desiccant Channels—A Theoretical Investigation', *Modern Environmental Science and Engineering*, vol. 2, no. 1, pp. 44-50.

Rafique, MM, Rehman, S, Lashin, A & Al Arifi, N 2016a, 'Analysis of a Solar Cooling System for Climatic Conditions of Five Different Cities of Saudi Arabia', *Energies*, vol. 9, no. 2, p. 75.

Rafique, MM, Gandhidasan, P, Rehman, S & Alhems, LM 2016b, 'Performance analysis of a desiccant evaporative cooling system under hot and humid conditions', *Environmental Progress & Sustainable Energy*, vol. 35, no. 5, pp. 1476-84.

Ruivo, CR, Costa, JJ & Figueiredo, AR 2006, 'Analysis of Simplifying Assumptions for the Numerical Modeling of the Heat and Mass Transfer in a Porous Desiccant Medium', *Numerical Heat Transfer, Part A: Applications*, vol. 49, no. 9, pp. 851-72.

Ruivo, CR, Costa, JJ & Figueiredo, AR 2007a, 'On the behaviour of hygroscopic wheels: Part I – channel modelling', *International Journal of Heat and Mass Transfer*, vol. 50, no. 23-24, pp. 4812-22.

Ruivo, CR, Costa, JJ & Figueiredo, AR 2007b, 'On the behaviour of hygroscopic wheels: Part II – rotor performance', *International Journal of Heat and Mass Transfer*, vol. 50, no. 23-24, pp. 4823-32.

Ruivo, CR, Angrisani, G & Minichiello, F 2015, 'Influence of the rotation speed on the effectiveness parameters of a desiccant wheel: An assessment using experimental data and manufacturer software', *Renewable Energy*, vol. 76, pp. 484-93.

Sahlot, M & Riffat, SB 2016, 'Desiccant cooling systems: a review', *International Journal of Low-Carbon Technologies*.

Saman, W, Bruno, F & Tay, S 2010, 'Technical Research on Evaporative Air Conditioners and Feasibility of Rating and their Energy Performance', *University of South Australia: Adelaide, Australia*.

San, J & Hsiau, S 1993, 'Effect of axial solid heat conduction and mass diffusion in a rotary heat and mass regenerator', *International Journal of Heat and Mass Transfer*, vol. 36, no. 8, pp. 2051-9.

Sherony, D & Solbrig, C 1970, 'Analytical investigation of heat or mass transfer and friction factors in a corrugated duct heat or mass exchanger', *International Journal of Heat and Mass Transfer*, vol. 13, no. 1, pp. 145-59.

Simonson, C & Besant, R 1997, 'Heat and Moisture Transfer in Desiccant Coated Rotary Energy Exchangers: Part I. Numerical Model', *HVAC&R Research*, vol. 3, no. 4, pp. 325-50.

Sphaier, LA & Worek, WM 2004, 'Analysis of heat and mass transfer in porous sorbents used in rotary regenerators', *International Journal of Heat and Mass Transfer*, vol. 47, no. 14-16, pp. 3415-30.

Sphaier, LA & Worek, WM 2006, 'Comparisons between 2-D and 1-D Formulations of Heat and Mass Transfer in Rotary Regenerators', *Numerical Heat Transfer, Part B: Fundamentals*, vol. 49, no. 3, pp. 223-37.

Subramanyam, N, Maiya, MP & Murthy, SS 2004, 'Application of desiccant wheel to control humidity in air-conditioning systems', *Applied Thermal Engineering*, vol. 24, no. 17-18, pp. 2777-88.

Torkaman, L & Ghassembaglou, N 2015, 'Evaporative Air Coolers Optimization for Energy Consumption Reduction and Energy Efficiency Ratio Increment', *International Journal of Mechanical and Mechatronics Engineering*, vol. 9, no. 4, pp. 622-7.

Wetter, M 1999, 'Air-to-Air Plate Heat Exchanger', *Simulation Research Group Building technologies Department Environmental Energy technologies Division Lawrence Berkeley National Laboratory Berkeley, CA*, vol. 94720.

Xuan, S & Radermacher, R 2005, 'Transient simulation for desiccant and enthalpy wheels', *International sorption heat pump conference*, pp. 22-4.

Yadav, A & Bajpai, VK 2013, 'Numerical and experimental investigation of operating parameters of solar-powered desiccant wheel in India', *Heat Transfer-Asian Research*, vol. 42, no. 1, pp. 1-30.

Yong, L, Sumathy, K, Dai, YJ, Zhong, JH & Wang, RZ 2006, 'Experimental study on a hybrid desiccant dehumidification and air conditioning system', *Journal of Solar Energy Engineering, Transactions of the ASME*, vol. 128, no. 1, pp. 77-82.

Zdravkov, B, Čermák, J, Šefara, M & Janků, J 2007, 'Pore classification in the characterization of porous materials: A perspective', *Open Chemistry*, vol. 5, no. 2, pp. 385-95.

Zendehboudi, A & Esmaeili, H 2015, 'Effect of supply/regeneration section area ratio on the performance of desiccant wheels in hot and humid climates: an experimental investigation', *Heat and Mass Transfer*, vol. 52, no. 6, pp. 1175-81.

Zhang, L & Niu, J 2002, 'Performance comparisons of desiccant wheels for air dehumidification and enthalpy recovery', *Applied Thermal Engineering*, vol. 22, no. 12, pp. 1347-67.

Zhang, X, Dai, Y & Wang, R 2003, 'A simulation study of heat and mass transfer in a honeycombed rotary desiccant dehumidifier', *Applied Thermal Engineering*, vol. 23, no. 8, pp. 989-1003.

Zhang, XJ, Dai, YJ & Wang, RZ 2003, 'A simulation study of heat and mass transfer in a honeycombed rotary desiccant dehumidifier', *Applied Thermal Engineering*, vol. 23, no. 8, pp. 989-1003.

Zheng, W & Worek, WM 1993, 'Numerical simulation of combined heat and mass transfer processes in a rotary dehumidifier', *Numerical Heat Transfer, Part A: Applications*, vol. 23, no. 2, pp. 211-32.

Zheng, W, Worek, WM & Novosel, D 1995, 'Effect of Operating Conditions on Optimal Performance of Rotary Dehumidifiers', *Journal of Energy Resources Technology*, vol. 117, no. 1, pp. 62-6.

Zouaoui, A, Zili-Ghedira, L & Ben Nasrallah, S 2017, 'Solid desiccant solar air conditioning unit in Tunisia: Numerical study', *International Journal of Refrigeration*, vol. 74, pp. 662-81.

APPENDIX A: UNCERTAINTY ANALYSIS

The system performance indices are given by the equations (4.1), (4.4), and (4.5). The experimentally measured variables in these equations are: $Y_1, Y_2\ \dot{m}_a, \dot{m}_r, T_1, T_2$, and T_7. So, the equation (4.6) can be expressed as:

$$\eta_{deh} = f\ (\ Y_1, Y_2) \tag{A.17}$$

$$DCOP = f\ (\ Y_1, Y_2\ \dot{m}_a, \dot{m}_r, T_1, T_7) \tag{A.18}$$

$$SER = f\ (\ \dot{m}_a, \dot{m}_r, T_1, T_2, T_7) \tag{A.19}$$

The uncertainty of the equations (4.1), (4.4), and (4.5) are determined by the equation (4.7) and can be expressed as:

1) The uncertainty of the Dehumidification Effectiveness (η_{deh}):

$$U_{\eta_{deh}}^2 = \left(\frac{\partial \eta_{deh}}{\partial Y_1}\right)^2 U_{\omega_1}^2 + \left(\frac{\partial \eta_{deh}}{\partial Y_2}\right)^2 U_{\omega_2}^2 \tag{A.20}$$

$$U_{\eta_{deh}}^2 = \left(\frac{-Y_2}{Y_1^2}\right)^2 U_{\omega_1}^2 + \left(\frac{1}{Y_1}\right)^2 U_{\omega_2}^2 \tag{A.21}$$

2) The uncertainty of the Dehumidification Coefficient of Performance (DCOP):

$$\begin{aligned} U_{DCOP}^2 = {} & \left(\frac{\partial DCOP}{\partial \dot{m}_a}\right)^2 U_{\dot{m}_a}^2 + \left(\frac{\partial DCOP}{\partial \dot{m}_r}\right)^2 U_{\dot{m}_r}^2 + \left(\frac{\partial DCOP}{\partial Y_1}\right)^2 U_{\omega_1}^2 \\ & + \left(\frac{\partial DCOP}{\partial Y_2}\right)^2 U_{\omega_2}^2 + \left(\frac{\partial DCOP}{\partial T_7}\right)^2 U_{T_7}^2 + \left(\frac{\partial DCOP}{\partial T_1}\right)^2 U_{T_1}^2 \end{aligned} \tag{A.22}$$

$$U_{DCOP}^2 = \left(\frac{\Delta h_{fg}\,(Y_1 - Y_2)}{\dot{m}_r\, c_{pa}(T_7 - T_1)}\right)^2 U_{\dot{m}_a}^2 + \left(-\frac{\dot{m}_a\, \Delta h_{fg}\,(Y_1 - Y_2)}{\dot{m}_r^2\, c_{pa}(T_7 - T_1)}\right)^2 U_{\dot{m}_r}^2$$
$$+ \left(\frac{\dot{m}_a\, \Delta h_{fg}}{\dot{m}_r\, c_{pa}(T_7 - T_1)}\right)^2 U_{\omega_1}^2$$
$$+ \left(-\frac{\dot{m}_a\, \Delta h_{fg}}{\dot{m}_r\, c_{pa}(T_7 - T_1)}\right)^2 U_{\omega_2}^2 \qquad \text{(A.23)}$$
$$+ \left(-\frac{\dot{m}_a\, \Delta h_{fg}\,(Y_1 - Y_2)}{\dot{m}_r\, c_{pa}(T_7 - T_1)^2}\right)^2 U_{T_7}^2$$
$$+ \left(\frac{\dot{m}_a\, \Delta h_{fg}\,(Y_1 - Y_2)}{\dot{m}_r\, c_{pa}(T_7 - T_1)^2}\right)^2 U_{T_1}^2$$

3) The uncertainty of the Sensible Energy Ratio (SER):

$$U_{SER}^2 = \left(\frac{\partial SER}{\partial \dot{m}_a}\right)^2 U_{\dot{m}_a}^2 + \left(\frac{\partial SER}{\partial \dot{m}_r}\right)^2 U_{\dot{m}_r}^2 + \left(\frac{\partial SER}{\partial T_2}\right)^2 U_{T_2}^2 + \left(\frac{\partial SER}{\partial T_1}\right)^2 U_{T_1}^2$$
$$+ \left(\frac{\partial SER}{\partial T_7}\right)^2 U_{T_7}^2 \qquad \text{(A.24)}$$

$$U_{SER}^2 = \left(\frac{c_{pa}\,(T_2 - T_1)}{\dot{m}_r\, c_{pa}(T_7 - T_1)}\right)^2 U_{\dot{m}_a}^2 + \left(-\frac{\dot{m}_a\, c_{pa}\,(T_2 - T_1)}{\dot{m}_r^2\, c_{pa}(T_7 - T_1)}\right)^2 U_{\dot{m}_r}^2$$
$$+ \left(\frac{\dot{m}_a\, c_{pa}}{\dot{m}_r\, c_{pa}(T_7 - T_1)}\right)^2 U_{T_2}^2$$
$$+ \left(\frac{\dot{m}_a\, c_{pa}\,(T_2 - T_7)}{\dot{m}_r\, c_{pa}(T_1 - T_7)^2}\right)^2 U_{T_1}^2 \qquad \text{(A.25)}$$
$$+ \left(-\frac{\dot{m}_a\, c_{pa}\,(T_2 - T_1)}{\dot{m}_r\, c_{pa}(T_7 - T_1)^2}\right)^2 U_{T_7}^2$$

The highest possible values of the experimental measured values and their uncertainty are shown in the table below.

Table A.1: The maximum values of the measured values and their uncertainty.

Measured value	Maximum value	Uncertainty
Y_1 [kg-water/kg-dry-air]	0.017853534	±0.000868977
Y_2 [kg-water/kg-dry-air]	0.011789534	±0.00023149
$\dot{m}_a$[kg/s]	0.975	±0.0609375
$\dot{m}_r$[kg/s]	0.975	±0.0609375
T_1 [°C]	40.0	±0.4
T_2 [°C]	80.0	±1.6
T_7 [°C]	100.0	±2.0

The value of $Y_1$and Y_2 are based on 90% RH and 60% RH, respectively at standard state conditions (25°C and 101.325 kPa), while the value of $\dot{m}_a$ and $\dot{m}_r$ are based on 4 m/s air velocity.

Therefore, after applying the maximum values on equations (A.5), (A.7), and (A.9), the uncertainty of the performance indices will be within ± 3.47% for the dehumidification Effectiveness (η_{deh}), ± 5.1% for the Dehumidification Coefficient of Performance (DCOP), and ± 6.84% for the sensible Energy Ratio (SER).

APPENDIX B: EXPERIMENTAL SYSTEM INPUT AND OUTPUT DATA

Table B.1: System input and output parameters' values at (u_p/u_r = 0.333) for figures 6.10, 6.11, and 6.12.

Test No.	1	2	3	4	5
System input values					
T_1 (℃)	28.7 ± 0.3	28.3 ± 0.3	28.6 ± 0.3	27.7 ± 0.3	27.9 ± 0.3
RH_1 (%)	38.9 ± 1.2	39 ± 1.2	38.3 ± 1.2	41.1 ± 1.2	38.3 ± 1.2
Y_1 (kg-water/kg-dry-air)	0.010199208 ± 0.000301185	0.009985743 ± 0.000294978	0.009979973 ± 0.000294810	0.010162195 ± 0.000300109	0.009572921 ± 0.000282963
T_7 (℃)	70.2 ± 1.4	70.5 ± 1.4	69.5 ± 1.4	73.3 ± 1.5	69.3 ± 1.4
RH_7 (%)	3.1 ± 0.2	2.8 ± 0.1	3.0 ± 0.2	2.2 ± 0.1	3.1 ± 0.2
Y_7 (kg-water/kg-dry-air)	0.006492671 ± 0.000321445	0.005935503 ± 0.000294108	0.006091737 ± 0.000301779	0.005250344 ± 0.000260428	0.006241840 ± 0.000309144
u_p (m/s)	1.0 ± 0.1	1.0 ± 0.1	1.0 ± 0.1	1.0 ± 0.1	1.0 ± 0.1
u_r (m/s)	3.0 ± 0.2	3.0 ± 0.2	3.0 ± 0.2	3.0 ± 0.2	3.0 ± 0.2
θ_p/θ_r (-)	1	1	1	1	1
N (RPH)	5	10	15	20	25
P_{atm} (Pa)	94300	94300	94300	94300	94300
System output values					
T_2 (℃)	45 ± 0.5	48.4 ± 0.5	50.4 ± 1.0	54.2 ± 1.1	56.1 ± 1.1
RH_2 (%)	9.1 ± 0.5	7.1 ± 0.4	7.1 ± 0.4	6.4 ± 0.3	6.1 ± 0.3
Y_2 (kg-water/kg-dry-air)	0.005767792 ± 0.000287178	0.005345884 ± 0.000266423	0.00595801 ± 0.000294426	0.006455638 ± 0.000319630	0.006719410 ± 0.000333703

Table B.2: System input and output parameters' values at (u_p/u_r = 0.5) for figures 6.10, 6.11, and 6.12.

Test No.	1	2	3	4	5
System input values					
T_1 (℃)	30.9 ± 0.3	31.1 ± 0.3	31.6 ± 0.3	32.1 ± 0.3	32.3 ± 0.3
RH_1 (%)	33.2 ± 1.0	31.7 ± 1.0	31.2 ± 0.9	29.5 ± 0.9	29.4 ± 0.9
Y_1 (kg-water/kg-dry-air)	0.009870861 ± 0.000291636	0.009528401 ± 0.000281666	0.009651944 ± 0.000285264	0.009385679 ± 0.000277508	0.009461864 ± 0.000279728
T_7 (℃)	70.1 ± 1.4	71 ± 1.4	72.7 ± 1.5	71.1 ± 1.4	72.9 ± 1.5
RH_7 (%)	3.4 ± 0.2	2.8 ± 0.1	2.7 ± 0.1	2.6 ± 0.1	2.4 ± 0.1
Y_7 (kg-water/kg-dry-air)	0.007089502 ± 0.000350677	0.006059397 ± 0.000300191	0.006285452 ± 0.000311284	0.005647094 ± 0.000287235	0.005628821 ± 0.000279042
u_p (m/s)	1.0 ± 0.1	1.0 ± 0.1	1.0 ± 0.1	1.0 ± 0.1	1.0 ± 0.1
u_r (m/s)	2.0 ± 0.2	2.0 ± 0.2	2.0 ± 0.2	2.0 ± 0.2	2.0 ± 0.2
θ_p/θ_r (-)	1	1	1	1	1
N (RPH)	5	10	15	20	25
P_{atm} (Pa)	94400	94400	94400	94400	94400
System output values					
T_2 (℃)	40.5 ± 0.4	45.3 ± 0.5	50.9 ± 1.0	52.6 ± 1.1	54.7 ± 1.1
RH_2 (%)	13.3 ± 0.7	9.1 ± 0.5	7.3 ± 0.4	7.0 ± 0.4	7.0 ± 0.4
Y_2 (kg-water/kg-dry-air)	0.006676948 ± 0.00033116	0.005909675 ± 0.000291344	0.006232383 ± 0.000309985	0.006544577 ± 0.000323134	0.007234278 ± 0.00035776

Table B.3: System input and output parameters' values at (u_p/u_r = 1.0) for figures 6.10, 6.11, and 6.12.

Test No.	1	2	3	4	5
System input values					
T_1 (℃)	27.8 ± 0.3	28.0 ± 0.3	27.8 ± 0.3	27.8 ± 0.3	28.1 ± 0.3
RH_1 (%)	36.8 ± 1.1	35.7 ± 1.1	36.1 ± 1.1	37.3 ± 1.1	37.3 ± 1.1
Y_1 (kg-water/kg-dry-air)	0.009140771 ± 0.000270368	0.008969882 ± 0.000265383	0.008964392 ± 0.000265223	0.009266817 ± 0.000274043	0.009433965 ± 0.000278915
T_7 (℃)	70.6 ± 1.4	70.1 ± 1.4	69.8 ± 1.4	73.1 ± 1.5	69.7 ± 1.4
RH_7 (%)	2.5 ± 0.1	2.6 ± 0.1	2.9 ± 0.1	1.9 ± 0.1	2.8 ± 0.1
Y_7 (kg-water/kg-dry-air)	0.005318911 ± 0.000263802	0.005414402 ± 0.000268499	0.005966491 ± 0.00029563	0.004492143 ± 0.000223076	0.005733715 ± 0.000284196
u_p (m/s)	2.0 ± 0.2	2.0 ± 0.2	2.0 ± 0.2	2.0 ± 0.2	2.0 ± 0.2
u_r (m/s)	2.0 ± 0.2	2.0 ± 0.2	2.0 ± 0.2	2.0 ± 0.2	2.0 ± 0.2
θ_p/θ_r (-)	1	1	1	1	1
N (RPH)	5	10	15	20	25
P_{atm} (Pa)	94270	94270	94270	94270	94270
System output values					
T_2 (℃)	45.1 ± 0.5	44.9 ± 0.5	46.7 ± 0.5	48.7 ± 0.5	50.2 ± 1.0
RH_2 (%)	7.2 ± 0.4	6.5 ± 0.3	7.0 ± 0.4	7.1 ± 0.4	7.5 ± 0.4
Y_2 (kg-water/kg-dry-air)	0.004594681 ± 0.000228443	0.004102507 ± 0.000156995	0.004849665 ± 0.000241077	0.005440767 ± 0.000270558	0.006246450 ± 0.000308047

Table B.4: System input and output parameters' values at (u_p/u_r = 2.0) for figures 6.10, 6.11, and 6.12.

Test No.	1	2	3	4	5
System input values					
T_1 (℃)	31.6 ± 0.3	33.4 ± 0.3	31.0 ± 0.3	29.4 ± 0.3	28.6 ± 0.3
RH_1 (%)	30.9 ± 0.9	28.0 ± 0.8	31.3 ± 0.9	33.3 ± 1.0	34.3 ± 1.0
Y_1 (kg-water/kg-dry-air)	0.009585549 ± 0.00028333	0.009619159 ± 0.000284309	0.009379023 ± 0.000277314	0.009094503 ± 0.000269019	0.00893907 ± 0.000264484
T_7 (℃)	71.5 ± 1.4	71.6 ± 1.4	71.3 ± 1.4	70.9 ± 1.4	71.5 ± 1.4
RH_7 (%)	2.3 ± 0.1	2.6 ± 0.1	2.1 ± 0.1	2.0 ± 0.1	2.1 ± 0.1
Y_7 (kg-water/kg-dry-air)	0.005092005 ± 0.000252635	0.005787287 ± 0.000286829	0.00460597 ± 0.000228689	0.004309897 ± 0.000214085	0.004645914 ± 0.000230659
u_p (m/s)	2.0 ± 0.2	2.0 ± 0.2	2.0 ± 0.2	2.0 ± 0.2	2.0 ± 0.2
u_r (m/s)	1.0 ± 0.1	1.0 ± 0.1	1.0 ± 0.1	1.0 ± 0.1	1.0 ± 0.1
θ_p/θ_r (-)	1	1	1	1	1
N (RPH)	5	10	15	20	25
P_{atm} (Pa)	94130	94130	94130	94130	94130
System output values					
T_2 (℃)	40.6 ± 0.4	43.4 ± 0.4	44.1 ± 0.4	46.1 ± 0.5	47.8 ± 0.5
RH_2 (%)	10.3 ± 0.5	8.3 ± 0.4	8.9 ± 0.4	8.2 ± 0.4	8.4 ± 0.4
Y_2 (kg-water/kg-dry-air)	0.005230377 ± 0.000258542	0.004881980 ± 0.000241484	0.005441711 ± 0.000268561	0.005557874 ± 0.000274308	0.006201316 ± 0.000306384

Table B.5: System input and output parameters' values at (u_p/u_r = 3.0) for figures 6.10, 6.11, and 6.12.

Test No.	1	2	3	4	5
System input values					
T_1 (℃)	31.1 ± 0.3	32.7 ± 0.3	32.9 ± 0.3	33.3 ± 0.3	33.5 ± 0.3
RH_1 (%)	29.4 ± 0.9	27.3 ± 0.8	26.8 ± 0.8	26.5 ± 0.8	25.6 ± 0.8
Y_1 (kg-water/kg-dry-air)	0.008852933 ± 0.000261971	0.009006717 ± 0.000266458	0.008941372 ± 0.000264552	0.009044502 ± 0.00026756	0.008833265 ± 0.000261396
T_7 (℃)	69.8 ± 1.4	70.9 ± 1.4	69.6 ± 1.4	73.3 ± 1.5	73.8 ± 1.5
RH_7 (%)	2.6 ± 0.1	2.5 ± 0.1	2.8 ± 0.1	1.8 ± 0.1	1.9 ± 0.1
Y_7 (kg-water/kg-dry-air)	0.005351981 ± 0.000265429	0.005396721 ± 0.00026763	0.005717247 ± 0.000283387	0.004296952 ± 0.000213446	0.004634994 ± 0.00023012
u_p (m/s)	3.0 ± 0.2	3.0 ± 0.2	3.0 ± 0.2	3.0 ± 0.2	3.0 ± 0.2
u_r (m/s)	1.0 ± 0.1	1.0 ± 0.1	1.0 ± 0.1	1.0 ± 0.1	1.0 ± 0.1
θ_p/θ_r (-)	1	1	1	1	1
N (RPH)	5	10	15	20	25
P_{atm} (Pa)	94130	94130	94130	94130	94130
System output values					
T_2 (℃)	40.4 ± 0.4	42.8 ± 0.4	43.4 ± 0.4	45.8 ± 0.5	47.3 ± 0.5
RH_2 (%)	10.6 ± 0.5	9.1 ± 0.5	9.5 ± 0.5	9.2 ± 0.5	8.8 ± 0.4
Y_2 (kg-water/kg-dry-air)	0.005338570 ± 0.000263252	0.005148864 ± 0.000256586	0.005576378 ± 0.000276413	0.006143289 ± 0.000303081	0.006335321 ± 0.000312954

Table B.6: System input and output parameters' values at (T_7/T_1 = 1.066) for figures 6.13, 6.14, and 6.15.

Test No.	1	2	3	4	5
System input values					
T_1 (℃)	29.5 ± 0.3	30.5 ± 0.3	31.2 ± 0.3	31.7 ± 0.3	32.0 ± 0.3
RH_1 (%)	38.9 ± 1.2	35.9 ± 1.1	34.5 ± 1.0	33.3 ± 1.0	32.7 ± 1.0
Y_1 (kg-water/kg-dry-air)	0.010691189 ± 0.000315475	0.010449499 ± 0.000308457	0.010453718 ± 0.000308580	0.010381284 ± 0.000306476	0.010369709 ± 0.000306140
T_7 (℃)	50.7 ± 1.0	52.6 ± 1.1	51.2 ± 1.0	49.9 ± 0.5	50.9 ± 1.0
RH_7 (%)	10.3 ± 0.5	9.6 ± 0.5	10.2 ± 0.5	10.6 ± 0.5	10.3 ± 0.5
Y_7 (kg-water/kg-dry-air)	0.008786888 ± 0.000433525	0.008994245 ± 0.000443617	0.008921049 ± 0.000440055	0.008689511 ± 0.000428784	0.008875461 ± 0.000437837
u_p (m/s)	2.0 ± 0.2	2.0 ± 0.2	2.0 ± 0.2	2.0 ± 0.2	2.0 ± 0.2
u_r (m/s)	2.0 ± 0.2	2.0 ± 0.2	2.0 ± 0.2	2.0 ± 0.2	2.0 ± 0.2
θ_p/θ_r (-)	1	1	1	1	1
N (RPH)	5	10	15	20	25
P_{atm} (Pa)	94320	94320	94320	94320	94320
System output values					
T_2 (℃)	35.0 ± 0.4	36.5 ± 0.4	38.1 ± 0.4	38.9 ± 0.4	39.6 ± 0.4
RH_2 (%)	20.1 ± 1.0	17.1 ± 0.9	17.6 ± 0.9	17.7 ± 0.9	17.4 ± 0.9
Y_2 (kg-water/kg-dry-air)	0.007508824 ± 0.000371302	0.006923441 ± 0.000343174	0.007785827 ± 0.000385495	0.008181607 ± 0.000404856	0.008368883 ± 0.000413282

Table B.7: System input and output parameters' values at (T_7/T_1 = 1.099) for figures 6.13, 6.14, and 6.15.

Test No.	1	2	3	4	5
System input values					
T_1 (℃)	31.8 ± 0.3	31.3 ± 0.3	31.6 ± 0.3	31.9 ± 0.3	31.8 ± 0.3
RH_1 (%)	34.9 ± 1.0	35.4 ± 1.1	34.3 ± 1.0	33.2 ± 1.0	34.1 ± 1.0
Y_1 (kg-water/kg-dry-air)	0.01095097 ± 0.000323012	0.010792609 ± 0.000318418	0.010635361 ± 0.000313854	0.01046906 ± 0.000309026	0.010695627 ± 0.000315604
T_7 (℃)	61.1 ± 1.2	60.8 ± 1.2	62.0 ± 1.2	61.6 ± 1.2	60.6 ± 1.2
RH_7 (%)	5.6 ± 0.3	5.9 ± 0.3	5.4 ± 0.3	5.3 ± 0.3	5.3 ± 0.3
Y_7 (kg-water/kg-dry-air)	0.007832618 ± 0.000387000	0.008143083 ± 0.000402152	0.007871420 ± 0.000388895	0.007582070 ± 0.000374763	0.007237418 ± 0.000357914
u_p (m/s)	2.0 ± 0.2	2.0 ± 0.2	2.0 ± 0.2	2.0 ± 0.2	2.0 ± 0.2
u_r (m/s)	2.0 ± 0.2	2.0 ± 0.2	2.0 ± 0.2	2.0 ± 0.2	2.0 ± 0.2
θ_p/θ_r (-)	1	1	1	1	1
N (RPH)	5	10	15	20	25
P_{atm} (Pa)	94330	94330	94330	94330	94330
System output values					
T_2 (℃)	40.7 ± 0.4	41.3 ± 0.4	43.9 ± 0.4	45.1 ± 0.5	45.8 ± 0.5
RH_2 (%)	13.5 ± 0.7	11.9 ± 0.6	11.7 ± 0.6	11.4 ± 0.6	11.8 ± 0.6
Y_2 (kg-water/kg-dry-air)	0.006857150 ± 0.000339998	0.006273600 ± 0.000309394	0.007020217 ± 0.000348707	0.007326324 ± 0.000361549	0.007859456 ± 0.000387964

Table B.8: System input and output parameters' values at (T_7/T_1 = 1.132) for figures 6.13, 6.14, and 6.15.

Test No.	1	2	3	4	5
System input values					
T_1 (℃)	31.5 ± 0.3	32.0 ± 0.3	31.9 ± 0.3	31.9 ± 0.3	32.0 ± 0.3
RH_1 (%)	35.8 ± 1.1	32.7 ± 1.0	31.8 ± 1.0	32.0 ± 1.0	32.2 ± 1.0
Y_1 (kg-water/kg-dry-air)	0.011045611 ± 0.000325756	0.010369709 ± 0.000306140	0.010021560 ± 0.000296020	0.010085611 ± 0.000297882	0.010208548 ± 0.000301456
T_7 (℃)	73.1 ± 1.5	70.4 ± 1.4	70.3 ± 1.4	71.4 ± 1.4	71.4 ± 1.4
RH_7 (%)	2.5 ± 0.1	2.3 ± 0.1	3.1 ± 0.2	2.3 ± 0.1	2.5 ± 0.1
Y_7 (kg-water/kg-dry-air)	0.005921058 ± 0.000293399	0.00484515 ± 0.000240478	0.006519669 ± 0.000322769	0.005059763 ± 0.000251048	0.005503637 ± 0.000272888
u_p (m/s)	2.0 ± 0.2	2.0 ± 0.2	2.0 ± 0.2	2.0 ± 0.2	2.0 ± 0.2
u_r (m/s)	2.0 ± 0.2	2.0 ± 0.2	2.0 ± 0.2	2.0 ± 0.2	2.0 ± 0.2
θ_p/θ_r (-)	1	1	1	1	1
N (RPH)	5	10	15	20	25
P_{atm} (Pa)	94320	94320	94320	94320	94320
System output values					
T_2 (℃)	47.0 ± 0.5	48.6 ± 0.5	49.2 ± 0.5	51.9 ± 1.0	52.8 ± 1.1
RH_2 (%)	8.2 ± 0.4	6.6 ± 0.3	7.4 ± 0.4	7.0 ± 0.4	7.1 ± 0.4
Y_2 (kg-water/kg-dry-air)	0.005800992 ± 0.000286618	0.005048719 ± 0.000250104	0.005829832 ± 0.000289000	0.00630205 ± 0.000312512	0.006732673 ± 0.000331248

Table B.9: System input and output parameters' values at (T_7/T_1 = 1.165) for figures 6.13, 6.14, and 6.15.

Test No.	1	2	3	4	5
System input values					
T_1 (℃)	30.6 ± 0.3	30.1 ± 0.3	30.8 ± 0.3	31.1 ± 0.3	31.3 ± 0.3
RH_1 (%)	33.1 ± 1.0	35.0 ± 1.1	33.4 ± 1.0	33.4 ± 1.0	33.5 ± 1.0
Y_1 (kg-water/kg-dry-air)	0.009693918 ± 0.000286486	0.009963538 ± 0.000294332	0.009898036 ± 0.000292426	0.010072581 ± 0.000297503	0.010221461 ± 0.000301832
T_7 (℃)	81.1 ± 1.6	82.1 ± 1.6	82.2 ± 1.6	80.5 ± 1.6	80.3 ± 1.6
RH_7 (%)	1.5 ± 0.1	1.4 ± 0.1	1.3 ± 0.1	1.4 ± 0.1	1.5 ± 0.1
Y_7 (kg-water/kg-dry-air)	0.004942584 ± 0.000245277	0.004800587 ± 0.000238282	0.004473183 ± 0.000222141	0.004499751 ± 0.000223452	0.004784555 ± 0.000237492
u_p (m/s)	2.0 ± 0.2	2.0 ± 0.2	2.0 ± 0.2	2.0 ± 0.2	2.0 ± 0.2
u_r (m/s)	2.0 ± 0.2	2.0 ± 0.2	2.0 ± 0.2	2.0 ± 0.2	2.0 ± 0.2
θ_p/θ_r (-)	1	1	1	1	1
N (RPH)	5	10	15	20	25
P_{atm} (Pa)	94170	94170	94170	94170	94170
System output values					
T_2 (℃)	51.1 ± 1.0	53.8 ± 1.1	58.3 ± 1.2	60.5 ± 1.2	61.3 ± 1.2
RH_2 (%)	5.2 ± 0.3	4.3 ± 0.2	3.9 ± 0.2	4.2 ± 0.2	4.5 ± 0.2
Y_2 (kg-water/kg-dry-air)	0.004476481 ± 0.000223516	0.004251736 ± 0.000210894	0.004769059 ± 0.000237010	0.005689630 ± 0.000282769	0.006373841 ± 0.000314350

Table B.10: System input and output parameters' values at (T_7/T_1 = 1.198) for figures 6.13, 6.14, and 6.15.

Test No.	1	2	3	4	5
System input values					
T_1 (℃)	29.9 ± 0.3	31.1 ± 0.3	32.3 ± 0.3	32.2 ± 0.3	31.9 ± 0.3
RH_1 (%)	36.1 ± 1.1	33.2 ± 1.0	31.2 ± 0.9	31.2 ± 0.9	31.5 ± 0.9
Y_1 (kg-water/kg-dry-air)	0.010161806 ± 0.000300098	0.010011296 ± 0.000295721	0.010075469 ± 0.000297587	0.010017509 ± 0.000295902	0.009941571 ± 0.000293693
T_7 (℃)	91.3 ± 1.8	92.1 ± 1.8	91.4 ± 1.8	90.9 ± 1.8	92.1 ± 1.8
RH_7 (%)	1.0 ± 0.1	0.9 ± 0.1	1.1 ± 0.1	1.2 ± 0.1	1.1 ± 0.1
Y_7 (kg-water/kg-dry-air)	0.004900071 ± 0.000243183	0.004542028 ± 0.000225537	0.005414855 ± 0.000268522	0.005800371 ± 0.000287471	0.005560393 ± 0.000275678
u_p (m/s)	2.0 ± 0.2	2.0 ± 0.2	2.0 ± 0.2	2.0 ± 0.2	2.0 ± 0.2
u_r (m/s)	2.0 ± 0.2	2.0 ± 0.2	2.0 ± 0.2	2.0 ± 0.2	2.0 ± 0.2
θ_p/θ_r (-)	1	1	1	1	1
N (RPH)	5	10	15	20	25
P_{atm} (Pa)	94170	94170	94170	94170	94170
System output values					
T_2 (℃)	59.6 ± 1.2	61.8 ± 1.2	66.1 ± 1.3	68.4 ± 1.4	70.8 ± 1.4
RH_2 (%)	3.2 ± 0.2	2.5 ± 0.1	2.6 ± 0.1	2.7 ± 0.1	2.5 ± 0.1
Y_2 (kg-water/kg-dry-air)	0.004177431 ± 0.000206623	0.003618533 ± 0.000178648	0.004476373 ± 0.000225553	0.005145720 ± 0.000259231	0.005417792 ± 0.000266367

Table B.11: System input and output parameters' values at (Y_1 = 0.006) for figures 6.16, 6.17, and 6.18.

Test No.	1	2	3	4	5
System input values					
T_1 (℃)	31.1 ± 0.3	30.6 ± 0.3	30.4 ± 0.3	30.9 ± 0.3	31.6 ± 0.3
RH_1 (%)	22.5 ± 0.7	22.9 ± 0.7	23.0 ± 0.7	22.4 ± 0.7	22.1 ± 0.7
Y_1 (kg-water/kg-dry-air)	0.006732399 ± 0.000199873	0.006657457 ± 0.000197671	0.006609505 ± 0.000196262	0.006624994 ± 0.000196715	0.006805256 ± 0.000202013
T_7 (℃)	71.4 ± 1.4	71.6 ± 1.4	70.9 ± 1.4	69.9 ± 1.4	71.0 ± 1.4
RH_7 (%)	3.0 ± 0.2	2.9 ± 0.1	30.1 ± 0.2	3.3 ± 0.2	3.0 ± 0.2
Y_7 (kg-water/kg-dry-air)	0.006609700 ± 0.000327181	0.006442626 ± 0.000318992	0.006685799 ± 0.000330910	0.006818044 ± 0.000337388	0.006496038 ± 0.000321610
u_p (m/s)	2.0 ± 0.2	2.0 ± 0.2	2.0 ± 0.2	2.0 ± 0.2	2.0 ± 0.2
u_r (m/s)	2.0 ± 0.2	2.0 ± 0.2	2.0 ± 0.2	2.0 ± 0.2	2.0 ± 0.2
θ_p/θ_r (-)	1	1	1	1	1
N (RPH)	5	10	15	20	25
P_{atm} (Pa)	94410	94410	94410	94410	94410
System output values					
T_2 (℃)	39.6 ± 0.4	43.4 ± 0.4	45.6 ± 0.5	48.1 ± 0.5	48.8 ± 0.5
RH_2 (%)	6.8 ± 0.3	5.1 ± 0.3	5.0 ± 0.3	4.8 ± 0.2	5.4 ± 0.3
Y_2 (kg-water/kg-dry-air)	0.003230377 ± 0.000161293	0.002981980 ± 0.000147919	0.003241711 ± 0.000162516	0.003587874 ± 0.000177184	0.004131316 ± 0.000206484

Table B.12: System input and output parameters' values at (Y_1 = 0.009) for figures 6.16, 6.17, and 6.18.

Test No.	1	2	3	4	5
System input values					
T_1 (℃)	29.9 ± 0.3	30.3 ± 0.3	30.9 ± 0.3	31.6 ± 0.3	30.3 ± 0.3
RH_1 (%)	34.2 ± 1.0	34.3 ± 1.0	33.1 ± 1.0	31.9 ± 1.0	33.9 ± 1.0
Y_1 (kg-water/kg-dry-air)	0.009594905 ± 0.000283603	0.009851757 ± 0.00029108	0.009840659 ± 0.000290757	0.009871932 ± 0.000291667	0.009735069 ± 0.000287684
T_7 (℃)	70.5 ± 1.4	70.7 ± 1.4	71.0 ± 1.4	69.8 ± 1.4	69.9 ± 1.4
RH_7 (%)	2.8 ± 0.1	2.7 ± 0.1	2.7 ± 0.1	2.9 ± 0.1	2.9 ± 0.1
Y_7 (kg-water/kg-dry-air)	0.005929155 ± 0.000293797	0.005765376 ± 0.000285752	0.005840958 ± 0.000289465	0.005958196 ± 0.000295223	0.005984302 ± 0.000296505
u_p (m/s)	2.0 ± 0.2	2.0 ± 0.2	2.0 ± 0.2	2.0 ± 0.2	2.0 ± 0.2
u_r (m/s)	2.0 ± 0.2	2.0 ± 0.2	2.0 ± 0.2	2.0 ± 0.2	2.0 ± 0.2
θ_p/θ_r (-)	1	1	1	1	1
N (RPH)	5	10	15	20	25
P_{atm} (Pa)	94400	94400	94400	94400	94400
System output values					
T_2 (℃)	40.1 ± 0.4	43.9 ± 0.4	47.2 ± 0.5	49.7 ± 0.5	50.2 ± 1.0
RH_2 (%)	8.8 ± 0.4	6.8 ± 0.3	6.4 ± 0.3	6.4 ± 0.3	6.9 ± 0.3
Y_2 (kg-water/kg-dry-air)	0.004334681 ± 0.000214442	0.004102507 ± 0.000202469	0.004519665 ± 0.000225772	0.005140767 ± 0.000256034	0.005746450 ± 0.000283002

Table B.13: System input and output parameters' values at (Y_1 = 0.012) for figures 6.16, 6.17, and 6.18.

Test No.	1	2	3	4	5
System input values					
T_1 (℃)	32.1 ± 0.3	31.7 ± 0.3	31.6 ± 0.3	30.3 ± 0.3	30.7 ± 0.3
RH_1 (%)	38.8 ± 1.2	39.2 ± 1.2	39.5 ± 1.2	41.9 ± 1.3	41.2 ± 1.2
Y_1 (kg-water/kg-dry-air)	0.012403569 ± 0.000365045	0.012246271 ± 0.000360502	0.012270272 ± 0.000361195	0.012077046 ± 0.000355612	0.012153277 ± 0.000357815
T_7 (℃)	72.3 ± 1.4	71.8 ± 1.4	71.3 ± 1.4	71.1 ± 1.4	72.0 ± 1.4
RH_7 (%)	2.6 ± 0.1	2.8 ± 0.1	2.8 ± 0.1	2.9 ± 0.1	2.7 ± 0.1
Y_7 (kg-water/kg-dry-air)	0.005947331 ± 0.000294689	0.006272873 ± 0.000310667	0.006138711 ± 0.000304084	0.006305289 ± 0.000312257	0.006099046 ± 0.000302137
u_p (m/s)	2.0 ± 0.2	2.0 ± 0.2	2.0 ± 0.2	2.0 ± 0.2	2.0 ± 0.2
u_r (m/s)	2.0 ± 0.2	2.0 ± 0.2	2.0 ± 0.2	2.0 ± 0.2	2.0 ± 0.2
θ_p/θ_r (-)	1	1	1	1	1
N (RPH)	5	10	15	20	25
P_{atm} (Pa)	94400	94400	94400	94400	94400
System output values					
T_2 (℃)	43.5 ± 0.4	47.3 ± 0.5	49.9 ± 0.5	52.6 ± 1.1	54.7 ± 1.1
RH_2 (%)	10.5 ± 0.5	8.3 ± 0.4	7.8 ± 0.4	7.2 ± 0.4	7.4 ± 0.4
Y_2 (kg-water/kg-dry-air)	0.006216948 ± 0.000306243	0.005909675 ± 0.00029432	0.006332383 ± 0.000315195	0.006744577 ± 0.000332371	0.007634278 ± 0.000378216

Table B.14: System input and output parameters' values at (θ_p/θ_r = 1.0) for figures 6.19, 6.20, and 6.21.

Test No.	1	2	3	4	5
System input values					
T_1 (℃)	28.7 ± 0.3	29.1 ± 0.3	29.2 ± 0.3	29.1 ± 0.3	29.4 ± 0.3
RH_1 (%)	37.4 ± 1.1	37.3 ± 1.1	37.4 ± 1.1	37.7 ± 1.1	37.6 ± 1.1
Y_1 (kg-water/kg-dry-air)	0.009792342 ± 0.000289351	0.009999747 ± 0.000295385	0.010086421 ± 0.000297906	0.010108726 ± 0.000298554	0.010261700 ± 0.000303001
T_7 (℃)	69.1 ± 1.4	69.6 ± 1.4	69.4 ± 1.4	70.3 ± 1.4	70.1 ± 1.4
RH_7 (%)	2.7 ± 0.1	2.5 ± 0.1	2.8 ± 0.1	2.5 ± 0.1	2.6 ± 0.1
Y_7 (kg-water/kg-dry-air)	0.005377951 ± 0.000266706	0.005086586 ± 0.000252368	0.005652834 ± 0.000280222	0.005244347 ± 0.002611163	0.005408615 ± 0.002692598
u_p (m/s)	2.0 ± 0.2	2.0 ± 0.2	2.0 ± 0.2	2.0 ± 0.2	2.0 ± 0.2
u_r (m/s)	2.0 ± 0.2	2.0 ± 0.2	2.0 ± 0.2	2.0 ± 0.2	2.0 ± 0.2
θ_p/θ_r (-)	1	1	1	1	1
N (RPH)	5	10	15	20	25
P_{atm} (Pa)	94370	94370	94370	94370	94370
System output values					
T_2 (℃)	40.7 ± 0.4	42.7 ± 0.4	43.9 ± 0.4	44.6 ± 0.4	45.8 ± 0.5
RH_2 (%)	8.5 ± 0.4	7.5 ± 0.4	8.1 ± 0.4	8.3 ± 0.4	8.3 ± 0.4
Y_2 (kg-water/kg-dry-air)	0.004308824 ± 0.000213939	0.004223441 ± 0.000209815	0.004885827 ± 0.000241269	0.005151607 ± 0.000256372	0.005468883 ± 0.000272723

Table B.15: System input and output parameters' values at (θ_p/θ_r = 2.0) for figures 6.19, 6.20, and 6.21.

Test No.	1	2	3	4	5
System input values					
T_1 (℃)	30.6 ± 0.3	30.4 ± 0.3	30.7 ± 0.3	31.5 ± 0.3	30.9 ± 0.3
RH_1 (%)	36.8 ± 1.1	36.9 ± 1.1	37.0 ± 1.1	34.9 ± 1.0	35.7 ± 1.1
Y_1 (kg-water/kg-dry-air)	0.010775386 ± 0.000317918	0.010679400 ± 0.000315133	0.010898524 ± 0.000321491	0.010759640 ± 0.000317461	0.010632579 ± 0.000313774
T_7 (℃)	71.2 ± 1.4	71.0 ± 1.4	70.8 ± 1.4	72.1 ± 1.4	72.2 ± 1.4
RH_7 (%)	2.4 ± 0.1	2.6 ± 0.1	2.7 ± 0.1	2.3 ± 0.1	2.4 ± 0.1
Y_7 (kg-water/kg-dry-air)	0.005234457 ± 0.000259647	0.005625677 ± 0.000278887	0.005793574 ± 0.000287137	0.005213100 ± 0.002595670	0.005465197 ± 0.000270997
u_p (m/s)	2.0 ± 0.2	2.0 ± 0.2	2.0 ± 0.2	2.0 ± 0.2	2.0 ± 0.2
u_r (m/s)	2.0 ± 0.2	2.0 ± 0.2	2.0 ± 0.2	2.0 ± 0.2	2.0 ± 0.2
θ_p/θ_r (-)	2	2	2	2	2
N (RPH)	5	10	15	20	25
P_{atm} (Pa)	94350	94350	94350	94350	94350
System output values					
T_2 (℃)	37.1 ± 0.4	38.5 ± 0.4	39.4 ± 0.4	40.9 ± 0.4	41.6 ± 0.4
RH_2 (%)	12.8 ± 0.6	11.5 ± 0.6	13.1 ± 0.7	12.8 ± 0.6	12.5 ± 0.6
Y_2 (kg-water/kg-dry-air)	0.005357150 ± 0.000265353	0.005173600 ± 0.000257273	0.006220217 ± 0.000307674	0.006566324 ± 0.000325741	0.006679456 ± 0.000330139

Table B.16: System input and output parameters' values at (θ_p/θ_r = 3.0) for figures 6.19, 6.20, and 6.21.

Test No.	1	2	3	4	5
System input values					
T_1 (℃)	31.4 ± 0.3	31.9 ± 0.3	32.1 ± 0.3	32.1 ± 0.3	32.4 ± 0.3
RH_1 (%)	36.6 ± 1.1	36.2 ± 1.1	35.9 ± 1.1	36.1 ± 1.1	36.0 ± 1.1
Y_1 (kg-water/kg-dry-air)	0.011227775 ± 0.000331036	0.011429983 ± 0.000336893	0.011465600 ± 0.000337925	0.011530659 ± 0.000339808	0.011699362 ± 0.000344691
T_7 (℃)	70.9 ± 1.4	71.6 ± 1.4	72.4 ± 1.4	72.1 ± 1.4	71.8 ± 1.4
RH_7 (%)	2.7 ± 0.1	2.8 ± 0.1	2.6 ± 0.1	2.7 ± 0.1	2.8 ± 0.1
Y_7 (kg-water/kg-dry-air)	0.005818781 ± 0.000288376	0.006222239 ± 0.000308183	0.005976151 ± 0.000296104	0.006128661 ± 0.000303591	0.006276231 ± 0.000310831
u_p (m/s)	2.0 ± 0.2	2.0 ± 0.2	2.0 ± 0.2	2.0 ± 0.2	2.0 ± 0.2
u_r (m/s)	2.0 ± 0.2	2.0 ± 0.2	2.0 ± 0.2	2.0 ± 0.2	2.0 ± 0.2
θ_p/θ_r (-)	3	3	3	3	3
N (RPH)	5	10	15	20	25
P_{atm} (Pa)	94350	94350	94350	94350	94350
System output values					
T_2 (℃)	36.6 ± 0.4	37.9 ± 0.4	38.6 ± 0.4	39.1 ± 0.4	39.9 ± 0.4
RH_2 (%)	15.2 ± 0.8	14.0 ± 0.7	15.1 ± 0.8	15.9 ± 0.8	15.8 ± 0.8
Y_2 (kg-water/kg-dry-air)	0.006207431 ± 0.000306608	0.006098533 ± 0.000303193	0.006856373 ± 0.000339689	0.007425720 ± 0.000367489	0.007697792 ± 0.000381225

Table B.17: System input and output parameters' values at (T_7/T_1 = 1.066) for figures 6.22, 6.23, and 6.24.

Test No.	1	2	3	4	5
System input values					
T_1 (℃)	30.4 ± 0.3	29.9 ± 0.3	30.7 ± 0.3	31.2 ± 0.3	31.1 ± 0.3
RH_1 (%)	35.4 ± 1.1	33.6 ± 1.0	31.8 ± 1.0	31.4 ± 0.9	30.4 ± 0.9
Y_1 (kg-water/kg-dry-air)	0.010235926 ± 0.000302252	0.009427064 ± 0.000278714	0.009341816 ± 0.000276229	0.009494939 ± 0.000280691	0.009134854 ± 0.000270196
T_7 (℃)	51.6 ± 1.0	51.3 ± 1.0	52.3 ± 1.0	52.1 ± 1.0	49.2 ± 0.5
RH_7 (%)	9.0 ± 0.5	8.6 ± 0.4	8.2 ± 0.4	9.3 ± 0.5	9.7 ± 0.5
Y_7 (kg-water/kg-dry-air)	0.008012253 ± 0.000395769	0.007538266 ± 0.000372622	0.007549445 ± 0.000373169	0.008491447 ± 0.000419135	0.007662224 ± 0.000378679
u_p (m/s)	1.0 ± 0.1	2.0 ± 0.2	2.0 ± 0.2	2.0 ± 0.2	3.0 ± 0.2
u_r (m/s)	3.0 ± 0.2	3.0 ± 0.2	2.0 ± 0.2	1.0 ± 0.1	1.0 ± 0.1
θ_p/θ_r (-)	1	1	1	1	1
N (RPH)	15	15	15	15	15
P_{atm} (Pa)	94370	94370	94370	94370	94370
System output values					
T_2 (℃)	37.4 ± 0.4	38.6 ± 0.4	39.5 ± 0.4	40.5 ± 0.4	40.3 ± 0.4
RH_2 (%)	18.2 ± 0.9	14.9 ± 0.7	14.3 ± 0.7	14.3 ± 0.7	14.4 ± 0.7
Y_2 (kg-water/kg-dry-air)	0.007759383 ± 0.000383527	0.006763551 ± 0.000335116	0.006822619 ± 0.000337612	0.007202108 ± 0.000356187	0.007170920 ± 0.000354869

Table B.18: System input and output parameters' values at (T_7/T_1 = 1.099) for figures 6.22, 6.23, and 6.24.

Test No.	1	2	3	4	5
System input values					
T_1 (℃)	32.5 ± 0.3	32.6 ± 0.3	32.3 ± 0.3	32.4 ± 0.3	32.2 ± 0.3
RH_1 (%)	29.4 ± 0.9	28.5 ± 0.9	29.2 ± 0.9	29.4 ± 0.9	28.6 ± 0.9
Y_1 (kg-water/kg-dry-air)	0.009576600 ± 0.000283070	0.009332565 ± 0.00027596	0.009401579 ± 0.000277971	0.009521638 ± 0.000281469	0.009152654 ± 0.000270715
T_7 (℃)	62.0 ± 1.2	61.6 ± 1.2	61.6 ± 1.2	62.8 ± 1.3	60.5 ± 1.2
RH_7 (%)	5.4 ± 0.3	5.1 ± 0.3	4.9 ± 0.2	4.8 ± 0.2	4.9 ± 0.2
Y_7 (kg-water/kg-dry-air)	0.007869730 ± 0.000388812	0.007291035 ± 0.000360536	0.007001893 ± 0.000346390	0.007247831 ± 0.000358423	0.006652789 ± 0.000329293
u_p (m/s)	1.0 ± 0.1	2.0 ± 0.2	2.0 ± 0.2	2.0 ± 0.2	3.0 ± 0.2
u_r (m/s)	3.0 ± 0.2	3.0 ± 0.2	2.0 ± 0.2	1.0 ± 0.1	1.0 ± 0.1
θ_p/θ_r (-)	1	1	1	1	1
N (RPH)	15	15	15	15	15
P_{atm} (Pa)	94350	94350	94350	94350	94350
System output values					
T_2 (℃)	43.2 ± 0.4	44.8 ± 0.4	45.3 ± 0.5	46.0 ± 0.5	46.1 ± 0.5
RH_2 (%)	11.6 ± 0.6	9.1 ± 0.5	8.9 ± 0.4	9.3 ± 0.5	9.1 ± 0.5
Y_2 (kg-water/kg-dry-air)	0.006732850 ± 0.000333259	0.005731274 ± 0.000284077	0.005774118 ± 0.000285089	0.006235080 ± 0.000308813	0.006127228 ± 0.000303720

Table B.19: System input and output parameters' values at (T_7/T_1 = 1.132) for figures 6.22, 6.23, and 6.24.

Test No.	1	2	3	4	5
System input values					
T_1 (℃)	32.3 ± 0.3	32.5 ± 0.3	32.2 ± 0.3	32.3 ± 0.3	31.7 ± 0.3
RH_1 (%)	30.4 ± 0.9	29.6 ± 0.9	29.3 ± 0.9	30.5 ± 0.9	31.4 ± 0.9
Y_1 (kg-water/kg-dry-air)	0.009797195 ± 0.000289492	0.009645872 ± 0.000285087	0.009383077 ± 0.000277432	0.009829932 ± 0.000290445	0.009779643 ± 0.000288981
T_7 (℃)	72.7 ± 1.5	73.5 ± 1.5	70.5 ± 1.4	72.1 ± 1.4	69.8 ± 1.4
RH_7 (%)	2.1 ± 0.1	2.0 ± 0.1	2.5 ± 0.1	2.4 ± 0.1	2.4 ± 0.1
Y_7 (kg-water/kg-dry-air)	0.004881899 ± 0.000242288	0.004809172 ± 0.000238705	0.005293010 ± 0.000262528	0.005443486 ± 0.000269930	0.004926998 ± 0.000244510
u_p (m/s)	1.0 ± 0.1	2.0 ± 0.2	2.0 ± 0.2	2.0 ± 0.2	3.0 ± 0.2
u_r (m/s)	3.0 ± 0.2	3.0 ± 0.2	2.0 ± 0.2	1.0 ± 0.1	1.0 ± 0.1
θ_p/θ_r (-)	1	1	1	1	1
N (RPH)	15	15	15	15	15
P_{atm} (Pa)	94320	94320	94320	94320	94320
System output values					
T_2 (℃)	50.3 ± 1.0	51.7 ± 1.0	51.7 ± 1.0	51.8 ± 1.0	51.6 ± 1.0
RH_2 (%)	7.5 ± 0.4	5.3 ± 0.3	5.0 ± 0.3	5.3 ± 0.3	5.5 ± 0.3
Y_2 (kg-water/kg-dry-air)	0.006247390 ± 0.000309417	0.004719284 ± 0.000234275	0.004437858 ± 0.000221010	0.004742694 ± 0.000235429	0.004874569 ± 0.000241927

Table B.20: System input and output parameters' values at (T_7/T_1 = 1.165) for figures 6.22, 6.23, and 6.24.

Test No.	1	2	3	4	5
System input values					
T_1 (℃)	32.3 ± 0.3	32.5 ± 0.3	32.1 ± 0.3	32.1 ± 0.3	32.3 ± 0.3
RH_1 (%)	32.2 ± 1.0	29.1 ± 0.9	30.0 ± 0.9	30.5 ± 0.9	29.2 ± 0.9
Y_1 (kg-water/kg-dry-air)	0.010386981 ± 0.000304905	0.009480451 ± 0.000280269	0.009555422 ± 0.000282453	0.009717168 ± 0.000287163	0.009404615 ± 0.000276485
T_7 (℃)	80.2 ± 1.6	81.2 ± 1.6	81.3 ± 1.6	82.3 ± 1.6	82.3 ± 1.6
RH_7 (%)	1.5 ± 0.1	1.4 ± 0.1	1.5 ± 0.1	1.4 ± 0.1	1.4 ± 0.1
Y_7 (kg-water/kg-dry-air)	0.004757470 ± 0.002369671	0.004621923 ± 0.002302405	0.004974788 ± 0.002477485	0.004831606 ± 0.002406455	0.004831606 ± 0.002406455
u_p (m/s)	1.0 ± 0.1	2.0 ± 0.2	2.0 ± 0.2	2.0 ± 0.2	3.0 ± 0.2
u_r (m/s)	3.0 ± 0.2	3.0 ± 0.2	2.0 ± 0.2	1.0 ± 0.1	1.0 ± 0.1
θ_p/θ_r (-)	1	1	1	1	1
N (RPH)	15	15	15	15	15
P_{atm} (Pa)	94320	94320	94320	94320	94320
System output values					
T_2 (℃)	52.5 ± 1.1	54.5 ± 1.1	55.0 ± 1.1	55.9 ± 1.1	56.4 ± 1.1
RH_2 (%)	6.0 ± 0.3	3.7 ± 0.2	3.3 ± 0.2	3.5 ± 0.2	3.4 ± 0.2
Y_2 (kg-water/kg-dry-air)	0.005531731 ± 0.000275836	0.003769545 ± 0.000187398	0.003466851 ± 0.000171200	0.003813464 ± 0.000189569	0.003832820 ± 0.000188587

Table B.21: System input and output parameters' values at ($T_7/T_1 = 1.198$) for figures 6.22, 6.23, and 6.24.

Test No.	1	2	3	4	5
System input values					
T_1 (℃)	32.2 ± 0.3	31.7 ± 0.3	31.3 ± 0.3	31.2 ± 0.3	31.1 ± 0.3
RH_1 (%)	31.3 ± 0.9	28.4 ± 0.9	29.6 ± 0.9	30.4 ± 0.9	29.9 ± 0.9
Y_1 (kg-water/kg-dry-air)	0.010037138 ± 0.000296473	0.008834863 ± 0.000261443	0.009002613 ± 0.000266338	0.009195996 ± 0.000271979	0.008990171 ± 0.000265975
T_7 (℃)	90.9 ± 1.8	88.3 ± 1.8	90.7 ± 1.8	93.7 ± 1.9	92.6 ± 1.9
RH_7 (%)	1.1 ± 0.1	1.2 ± 0.1	1.2 ± 0.1	1.0 ± 0.1	1.1 ± 0.1
Y_7 (kg-water/kg-dry-air)	0.005306058 ± 0.000263170	0.005242380 ± 0.000260037	0.005748907 ± 0.000284943	0.005357102 ± 0.000265681	0.005659079 ± 0.000280529
u_p (m/s)	1.0 ± 0.1	2.0 ± 0.2	2.0 ± 0.2	2.0 ± 0.2	3.0 ± 0.2
u_r (m/s)	3.0 ± 0.2	3.0 ± 0.2	2.0 ± 0.2	1.0 ± 0.1	1.0 ± 0.1
θ_p/θ_r (-)	1	1	1	1	1
N (RPH)	15	15	15	15	15
P_{atm} (Pa)	94290	94290	94290	94290	94290
System output values					
T_2 (℃)	63.0 ± 1.3	63.0 ± 1.3	62.1 ± 1.2	62.5 ± 1.3	62.4 ± 1.2
RH_2 (%)	2.7 ± 0.1	1.8 ± 0.1	1.7 ± 0.1	2.0 ± 0.1	2.1 ± 0.1
Y_2 (kg-water/kg-dry-air)	0.004076820 ± 0.000203531	0.002710805 ± 0.000135673	0.002540844 ± 0.000122990	0.002976777 ± 0.000147363	0.003112422 ± 0.000154029

Table B.22: System input and output parameters' values at ($Y_1 = 0.006$) for figures 6.25, 6.26, and 6.27.

Test No.	1	2	3	4	5
System input values					
T_1 (℃)	30.4 ± 0.3	29.9 ± 0.3	30.7 ± 0.3	31.2 ± 0.3	31.1 ± 0.3
RH_1 (%)	20.3 ± 0.6	19.9 ± 1.0	20.2 ± 0.6	19.6 ± 1.0	19.7 ± 1.0
Y_1 (kg-water/kg-dry-air)	0.005828830 ± 0.000173289	0.005548993 ± 0.000275118	0.005901769 ± 0.000175438	0.005892965 ± 0.000292019	0.005889178 ± 0.000291833
T_7 (℃)	70.6 ± 1.4	70.1 ± 1.4	69.8 ± 1.4	71.3 ± 1.4	69.7 ± 1.4
RH_7 (%)	2.5 ± 0.1	2.6 ± 0.1	2.9 ± 0.1	2.5 ± 0.1	2.8 ± 0.1
Y_7 (kg-water/kg-dry-air)	0.005318911 ± 0.000263802	0.005414402 ± 0.000268499	0.005966491 ± 0.000295630	0.005482818 ± 0.000271864	0.005733715 ± 0.000284196
u_p (m/s)	1.0 ± 0.1	2.0 ± 0.2	2.0 ± 0.2	2.0 ± 0.2	3.0 ± 0.2
u_r (m/s)	3.0 ± 0.2	3.0 ± 0.2	2.0 ± 0.2	1.0 ± 0.1	1.0 ± 0.1
θ_p/θ_r (-)	1	1	1	1	1
N (RPH)	15	15	15	15	15
P_{atm} (Pa)	94370	94370	94370	94370	94370
System output values					
T_2 (℃)	40.5 ± 0.4	40.3 ± 0.4	39.5 ± 0.4	38.6 ± 0.4	37.4 ± 0.4
RH_2 (%)	5.7 ± 0.3	4.6 ± 0.2	4.7 ± 0.2	5.8 ± 0.3	7.0 ± 0.4
Y_2 (kg-water/kg-dry-air)	0.002859383 ± 0.000141928	0.002263551 ± 0.000113317	0.002222619 ± 0.000110923	0.002602108 ± 0.000130405	0.002970920 ± 0.000147454

Table B.23: System input and output parameters' values at (Y_1 = 0.009) for figures 6.25, 6.26, and 6.27.

Test No.	1	2	3	4	5
System input values					
T_1 (℃)	32.3 ± 0.3	32.5 ± 0.3	32.1 ± 0.3	32.1 ± 0.3	32.3 ± 0.3
RH_1 (%)	30.7 ± 1.0	29.1 ± 0.9	30.0 ± 0.9	30.5 ± 0.9	29.8 ± 0.9
Y_1 (kg-water/kg-dry-air)	0.009895416 ± 0.000306641	0.009480451 ± 0.000280269	0.009555422 ± 0.000282453	0.009717168 ± 0.000287163	0.009600844 ± 0.00027806
T_7 (℃)	70.2 ± 1.4	70.5 ± 1.4	71.2 ± 1.4	71.8 ± 1.4	69.7 ± 1.4
RH_7 (%)	2.8 ± 0.1	2.8 ± 0.1	2.6 ± 0.1	2.5 ± 0.1	2.9 ± 0.1
Y_7 (kg-water/kg-dry-air)	0.005857175 ± 0.000290262	0.005935503 ± 0.000294108	0.005676464 ± 0.000281383	0.005599521 ± 0.000277601	0.005937267 ± 0.000294195
u_p (m/s)	1.0 ± 0.1	2.0 ± 0.2	2.0 ± 0.2	2.0 ± 0.2	3.0 ± 0.2
u_r (m/s)	3.0 ± 0.2	3.0 ± 0.2	2.0 ± 0.2	1.0 ± 0.1	1.0 ± 0.1
θ_p/θ_r (-)	1	1	1	1	1
N (RPH)	15	15	15	15	15
P_{atm} (Pa)	94320	94320	94320	94320	94320
System output values					
T_2 (℃)	43.5 ± 0.4	42.5 ± 0.4	42.1 ± 0.4	41.7 ± 0.4	41.4 ± 0.4
RH_2 (%)	7.7 ± 0.4	5.9 ± 0.3	5.6 ± 0.3	6.4 ± 0.3	6.9 ± 0.3
Y_2 (kg-water/kg-dry-air)	0.004531731 ± 0.000224739	0.003289545 ± 0.000163405	0.003066851 ± 0.000151863	0.003413464 ± 0.000169937	0.003632820 ± 0.000180332

Table B.24: System input and output parameters' values at (Y_1 = 0.012) for figures 6.25, 6.26, and 6.27.

Test No.	1	2	3	4	5
System input values					
T_1 (℃)	32.1 ± 0.3	32.3 ± 0.3	31.6 ± 0.3	30.9 ± 0.3	31.1 ± 0.3
RH_1 (%)	36.4 ± 1.1	36.8 ± 1.1	37.2 ± 1.1	37.3 ± 1.1	37.6 ± 1.1
Y_1 (kg-water/kg-dry-air)	0.011622000 ± 0.000342452	0.011888951 ± 0.000350175	0.011542539 ± 0.000340152	0.011111634 ± 0.000327670	0.011334147 ± 0.000334118
T_7 (℃)	72.9 ± 1.5	72.7 ± 1.5	71.0 ± 1.4	71.1 ± 1.4	70.1 ± 1.4
RH_7 (%)	2.4 ± 0.1	2.7 ± 0.1	2.8 ± 0.1	2.6 ± 0.1	2.8 ± 0.1
Y_7 (kg-water/kg-dry-air)	0.005628821 ± 0.000279042	0.006285452 ± 0.000311284	0.006059397 ± 0.000300191	0.005647094 ± 0.000287235	0.005826692 ± 0.000288764
u_p (m/s)	1.0 ± 0.1	2.0 ± 0.2	2.0 ± 0.2	2.0 ± 0.2	3.0 ± 0.2
u_r (m/s)	3.0 ± 0.2	3.0 ± 0.2	2.0 ± 0.2	1.0 ± 0.1	1.0 ± 0.1
θ_p/θ_r (-)	1	1	1	1	1
N (RPH)	15	15	15	15	15
P_{atm} (Pa)	94400	94400	94400	94400	94400
System output values					
T_2 (℃)	41.7 ± 0.4	41.5 ± 0.4	41.4 ± 0.4	41.1 ± 0.4	40.8 ± 0.4
RH_2 (%)	12.8 ± 0.6	11.2 ± 0.6	10.3 ± 0.5	11.1 ± 0.6	12.0 ± 0.6
Y_2 (kg-water/kg-dry-air)	0.006847390 ± 0.000339679	0.005919284 ± 0.000294071	0.005437858 ± 0.000269001	0.005742694 ± 0.000285326	0.006124569 ± 0.000303590

Table B.25: System input and output parameters' values at ($\theta_p/\theta_r = 1.0$) for figures 6.28, 6.29, and 6.30.

Test No.	1	2	3	4	5
System input values					
T_1 (℃)	29.2 ± 0.3	29.4 ± 0.3	31.6 ± 0.3	31.7 ± 0.3	31.0 ± 0.3
RH_1 (%)	34.3 ± 1.0	34.1 ± 1.0	30.9 ± 0.9	31.9 ± 1.0	31.7 ± 1.0
Y_1 (kg-water/kg-dry-air)	0.009261866 ± 0.000273899	0.009316263 ± 0.000275485	0.009585549 ± 0.000283330	0.009617376 ± 0.000284257	0.009500714 ± 0.000280859
T_7 (℃)	70.9 ± 1.4	71.3 ± 1.4	71.5 ± 1.4	71.6 ± 1.4	71.5 ± 1.4
RH_7 (%)	2.5 ± 0.1	2.5 ± 0.1	2.3 ± 0.1	2.4 ± 0.1	2.3 ± 0.1
Y_7 (kg-water/kg-dry-air)	0.005396721 ± 0.000267630	0.005491045 ± 0.000272268	0.005092005 ± 0.000252635	0.005338289 ± 0.000264755	0.005092005 ± 0.000252635
u_p (m/s)	1.0 ± 0.1	2.0 ± 0.2	2.0 ± 0.2	2.0 ± 0.2	3.0 ± 0.2
u_r (m/s)	3.0 ± 0.2	3.0 ± 0.2	2.0 ± 0.2	1.0 ± 0.1	1.0 ± 0.1
θ_p/θ_r (-)	1	1	1	1	1
N (RPH)	15	15	15	15	15
P_{atm} (Pa)	94130	94130	94130	94130	94130
System output values					
T_2 (℃)	50.3 ± 1.0	51.7 ± 1.0	51.7 ± 1.0	51.8 ± 1.0	51.6 ± 1.0
RH_2 (%)	5.9 ± 0.3	4.3 ± 0.2	4.1 ± 0.2	4.2 ± 0.2	4.7 ± 0.2
Y_2 (kg-water/kg-dry-air)	0.004876820 ± 0.000243873	0.003810805 ± 0.000190443	0.003640844 ± 0.000181582	0.003776777 ± 0.000186928	0.004212422 ± 0.000207143

Table B.26: System input and output parameters' values at ($\theta_p/\theta_r = 2.0$) for figures 6.28, 6.29, and 6.30.

Test No.	1	2	3	4	5
System input values					
T_1 (℃)	31.1 ± 0.3	32.7 ± 0.3	32.9 ± 0.3	31.4 ± 0.3	31.1 ± 0.3
RH_1 (%)	29.9 ± 0.9	27.3 ± 0.8	26.8 ± 0.8	29.5 ± 0.9	30.4 ± 0.9
Y_1 (kg-water/kg-dry-air)	0.009005673 ± 0.000266428	0.009006717 ± 0.000266458	0.008941372 ± 0.000264552	0.009039508 ± 0.000267415	0.009158488 ± 0.000270885
T_7 (℃)	70.9 ± 1.4	69.8 ± 1.4	69.6 ± 1.4	70.7 ± 1.4	71.1 ± 1.4
RH_7 (%)	2.5 ± 0.1	2.6 ± 0.1	2.6 ± 0.1	2.4 ± 0.1	2.4 ± 0.1
Y_7 (kg-water/kg-dry-air)	0.005396721 ± 0.000267630	0.005351981 ± 0.000265429	0.005305388 ± 0.000263137	0.005134311 ± 0.000254718	0.005224131 ± 0.000259138
u_p (m/s)	1.0 ± 0.1	2.0 ± 0.2	2.0 ± 0.2	2.0 ± 0.2	3.0 ± 0.2
u_r (m/s)	3.0 ± 0.2	3.0 ± 0.2	2.0 ± 0.2	1.0 ± 0.1	1.0 ± 0.1
θ_p/θ_r (-)	2	2	2	2	2
N (RPH)	15	15	15	15	15
P_{atm} (Pa)	94130	94130	94130	94130	94130
System output values					
T_2 (℃)	49.1 ± 0.5	49.7 ± 0.5	50.1 ± 1.0	50.4 ± 1.0	50.7 ± 1.0
RH_2 (%)	6.9 ± 0.3	5.5 ± 0.3	4.9 ± 0.2	5.3 ± 0.3	5.6 ± 0.3
Y_2 (kg-water/kg-dry-air)	0.005447390 ± 0.000268661	0.004419284 ± 0.000220648	0.004037858 ± 0.000200523	0.004442694 ± 0.000220154	0.004774569 ± 0.000236104

Table B.27: System input and output parameters' values at ($\theta_p/\theta_r = 3.0$) for figures 6.28, 6.29, and 6.30.

Test No.	1	2	3	4	5
System input values					
T_1 (℃)	29.4 ± 0.3	30.1 ± 0.3	30.0 ± 0.3	30.8 ± 0.3	31.2 ± 0.3
RH_1 (%)	35.1 ± 1.1	34.3 ± 1.0	34.2 ± 1.0	32.6 ± 1.0	31.8 ± 1.0
Y_1 (kg-water/kg-dry-air)	0.009587476 ± 0.000283386	0.009759034 ± 0.002895899	0.009673236 ± 0.000285884	0.009655193 ± 0.000285358	0.009636429 ± 0.000284812
T_7 (℃)	71.4 ± 1.4	71.1 ± 1.4	70.8 ± 1.4	71.3 ± 1.4	70.5 ± 1.4
RH_7 (%)	2.6 ± 0.1	2.7 ± 0.1	2.5 ± 0.1	2.6 ± 0.1	2.7 ± 0.1
Y_7 (kg-water/kg-dry-air)	0.005733785 ± 0.000284200	0.005879542 ± 0.000291360	0.005369905 ± 0.000266311	0.005709032 ± 0.000282984	0.005728314 ± 0.000283931
u_p (m/s)	1.0 ± 0.1	2.0 ± 0.2	2.0 ± 0.2	2.0 ± 0.2	3.0 ± 0.2
u_r (m/s)	3.0 ± 0.2	3.0 ± 0.2	2.0 ± 0.2	1.0 ± 0.1	1.0 ± 0.1
θ_p/θ_r (-)	3	3	3	3	3
N (RPH)	15	15	15	15	15
P_{atm} (Pa)	94190	94190	94190	94190	94190
System output values					
T_2 (℃)	47.0 ± 0.5	48.6 ± 0.5	49.2 ± 0.5	51.3 ± 1.0	51.8 ± 1.0
RH_2 (%)	8.9 ± 0.4	6.9 ± 0.3	6.1 ± 0.3	6.6 ± 0.3	6.9 ± 0.3
Y_2 (kg-water/kg-dry-air)	0.006300992 ± 0.000311527	0.005248719 ± 0.000261838	0.004829832 ± 0.000238540	0.005802050 ± 0.000286473	0.006232673 ± 0.000306960

Table B.28: System input and output parameters' values at ($Y_1 = 0.006$) for figures 6.31, 6.32, and 6.33.

Test No.	1	2	3	4	5
System input values					
T_1 (℃)	31.4 ± 0.3	31.5 ± 0.3	30.7 ± 0.3	29.8 ± 0.3	30.7 ± 0.3
RH_1 (%)	20.1 ± 0.6	19.7 ± 1.0	20.6 ± 0.6	21.9 ± 0.7	20.7 ± 0.6
Y_1 (kg-water/kg-dry-air)	0.006109098 ± 0.000181543	0.006020981 ± 0.000298305	0.006013976 ± 0.000178743	0.00607072 ± 0.000180413	0.006043454 ± 0.000179611
T_7 (℃)	51.9 ± 1.0	62.1 ± 1.2	71.4 ± 1.4	80.3 ± 1.6	91.2 ± 1.8
RH_7 (%)	6.7 ± 0.3	4.2 ± 0.2	2.7 ± 0.1	1.9 ± 0.1	1.2 ± 0.1
Y_7 (kg-water/kg-dry-air)	0.006028390 ± 0.000298669	0.006124742 ± 0.000303398	0.005939239 ± 0.000294292	0.006054070 ± 0.000299930	0.005848828 ± 0.000289852
u_p (m/s)	2.0 ± 0.2	2.0 ± 0.2	2.0 ± 0.2	2.0 ± 0.2	2.0 ± 0.2
u_r (m/s)	2.0 ± 0.2	2.0 ± 0.2	2.0 ± 0.2	2.0 ± 0.2	2.0 ± 0.2
θ_p/θ_r (-)	1	1	1	1	1
N (RPH)	15	15	15	15	15
P_{atm} (Pa)	94460	94460	94460	94460	94460
System output values					
T_2 (℃)	36.5 ± 0.4	41.6 ± 0.4	45.6 ± 0.5	51.3 ± 1.0	59.8 ± 1.2
RH_2 (%)	11.2 ± 0.6	7.4 ± 0.4	5.3 ± 0.3	3.5 ± 0.2	2.1 ± 0.1
Y_2 (kg-water/kg-dry-air)	0.004500992 ± 0.000224393	0.003948719 ± 0.000195172	0.003429832 ± 0.000172179	0.003042050 ± 0.000151450	0.002752673 ± 0.000136426

Table B.29: System input and output parameters' values at (Y_1 = 0.009) for figures 6.31, 6.32, and 6.33.

Test No.	1	2	3	4	5
System input values					
T_1 (℃)	30.2 ± 0.3	30.8 ± 0.3	31.1 ± 0.3	30.5 ± 0.3	30.3 ± 0.3
RH_1 (%)	33.2 ± 1.0	33.0 ± 1.0	32.9 ± 1.0	33.1 ± 1.0	33.4 ± 1.0
Y_1 (kg-water/kg-dry-air)	0.009469226 ± 0.000279942	0.009747144 ± 0.000288035	0.009888452 ± 0.000292148	0.009607405 ± 0.000283967	0.009583085 ± 0.000283259
T_7 (℃)	50.6 ± 1.0	60.1 ± 1.2	71.2 ± 1.4	80.4 ± 1.6	90.7 ± 1.8
RH_7 (%)	7.4 ± 0.4	4.8 ± 0.2	3.0 ± 0.2	2.0 ± 0.1	1.3 ± 0.1
Y_7 (kg-water/kg-dry-air)	0.006247169 ± 0.000309406	0.006387464 ± 0.000316287	0.006549153 ± 0.000324214	0.006402046 ± 0.000317002	0.006221455 ± 0.000308144
u_p (m/s)	2.0 ± 0.2	2.0 ± 0.2	2.0 ± 0.2	2.0 ± 0.2	2.0 ± 0.2
u_r (m/s)	2.0 ± 0.2	2.0 ± 0.2	2.0 ± 0.2	2.0 ± 0.2	2.0 ± 0.2
θ_p/θ_r (-)	1	1	1	1	1
N (RPH)	15	15	15	15	15
P_{atm} (Pa)	94460	94460	94460	94460	94460
System output values					
T_2 (℃)	37.4 ± 0.4	42.6 ± 0.4	49.7 ± 0.5	56.9 ± 1.1	64.8 ± 1.3
RH_2 (%)	15.5 ± 0.8	10.5 ± 0.5	6.4 ± 0.3	3.7 ± 0.2	2.3 ± 0.1
Y_2 (kg-water/kg-dry-air)	0.006600992 ± 0.000326289	0.005917194 ± 0.000291963	0.005129832 ± 0.000255871	0.004202050 ± 0.000209848	0.003832673 ± 0.000187695

Table B.30: System input and output parameters' values at (Y_1 = 0.012) for figures 6.31, 6.32, and 6.33.

Test No.	1	2	3	4	5
System input values					
T_1 (℃)	31.8 ± 0.3	31.1 ± 0.3	31.5 ± 0.3	30.4 ± 0.3	29.9 ± 0.3
RH_1 (%)	36.7 ± 1.0	36.4 ± 1.0	36.3 ± 1.0	37.9 ± 1.0	39.1 ± 1.1
Y_1 (kg-water/kg-dry-air)	0.012238241 ± 0.000302319	0.012044400 ± 0.000296684	0.001209958 ± 0.000302643	0.012082491 ± 0.000297791	0.012133371 ± 0.000299271
T_7 (℃)	52.1 ± 1.0	60.9 ± 1.2	71.9 ± 1.4	80.7 ± 1.6	90.2 ± 1.8
RH_7 (%)	5.3 ± 0.3	3.8 ± 0.2	2.1 ± 0.1	1.5 ± 0.1	1.0 ± 0.1
Y_7 (kg-water/kg-dry-air)	0.004807877 ± 0.000238641	0.004822249 ± 0.000259873	0.004711558 ± 0.000233894	0.004849532 ± 0.000240693	0.004685986 ± 0.000232634
u_p (m/s)	2.0 ± 0.2	2.0 ± 0.2	2.0 ± 0.2	2.0 ± 0.2	2.0 ± 0.2
u_r (m/s)	2.0 ± 0.2	2.0 ± 0.2	2.0 ± 0.2	2.0 ± 0.2	2.0 ± 0.2
θ_p/θ_r (-)	1	1	1	1	1
N (RPH)	15	15	15	15	15
P_{atm} (Pa)	94430	94430	94430	94430	94430
System output values					
T_2 (℃)	35.3 ± 0.4	39.6 ± 0.4	44.2 ± 0.4	49.3 ± 0.5	55.8 ± 1.1
RH_2 (%)	20.8 ± 0.6	14.6 ± 0.7	10.1 ± 0.5	6.8 ± 0.3	4.5 ± 0.2
Y_2 (kg-water/kg-dry-air)	0.007900992 ± 0.000234087	0.007008719 ± 0.000346336	0.006129832 ± 0.000305403	0.005402050 ± 0.000266579	0.004862673 ± 0.000242310

Table B.31: System input and output parameters' values at (θ_p/θ_r = 1.0) for figures 6.34, 6.35, and 6.36.

Test No.	1	2	3	4	5
System input values					
T_1 (℃)	29.1 ± 0.3	29.4 ± 0.3	29.4 ± 0.3	29.7 ± 0.3	29.9 ± 0.3
RH_1 (%)	35.1 ± 1.1	34.9 ± 1.0	34.8 ± 1.0	34.5 ± 1.0	34.4 ± 1.0
Y_1 (kg-water/kg-dry-air)	0.009406093 ± 0.000278103	0.009518670 ± 0.000281382	0.009490980 ± 0.000280576	0.009575526 ± 0.000283038	0.009660200 ± 0.000285504
T_7 (℃)	50.2 ± 1.0	59.8 ± 1.2	70.4 ± 1.4	80.1 ± 1.6	91.3 ± 1.8
RH_7 (%)	7.1 ± 0.4	4.5 ± 0.2	2.8 ± 0.1	1.9 ± 0.1	1.2 ± 0.1
Y_7 (kg-water/kg-dry-air)	0.005881481 ± 0.000291455	0.005909839 ± 0.000292848	0.005908451 ± 0.000292780	0.006013836 ± 0.000297955	0.005879911 ± 0.000291378
u_p (m/s)	2.0 ± 0.2	2.0 ± 0.2	2.0 ± 0.2	2.0 ± 0.2	2.0 ± 0.2
u_r (m/s)	2.0 ± 0.2	2.0 ± 0.2	2.0 ± 0.2	2.0 ± 0.2	2.0 ± 0.2
θ_p/θ_r (-)	1	1	1	1	1
N (RPH)	15	15	15	15	15
P_{atm} (Pa)	94320	94320	94320	94320	94320
System output values					
T_2 (℃)	36.7 ± 0.4	42.4 ± 0.4	48.6 ± 0.5	54.3 ± 1.1	61.1 ± 1.2
RH_2 (%)	17.0 ± 0.9	11.4 ± 0.6	7.2 ± 0.4	4.6 ± 0.2	3.1 ± 0.2
Y_2 (kg-water/kg-dry-air)	0.006985827 ± 0.000344936	0.006320217 ± 0.000314152	0.005539832 ± 0.000272851	0.004669059 ± 0.000230763	0.004356373 ± 0.000214196

Table B.32: System input and output parameters' values at (θ_p/θ_r = 2.0) for figures 6.34, 6.35, and 6.36.

Test No.	1	2	3	4	5
System input values					
T_1 (℃)	31.1 ± 0.3	31.2 ± 0.3	31.1 ± 0.3	31.5 ± 0.3	31.7 ± 0.3
RH_1 (%)	37.6 ± 1.1	37.6 ± 1.1	37.8 ± 1.1	36.9 ± 1.1	36.5 ± 1.1
Y_1 (kg-water/kg-dry-air)	0.011343936 ± 0.000334401	0.011410272 ± 0.000336322	0.011405383 ± 0.000336181	0.011391218 ± 0.000335771	0.011397168 ± 0.000335943
T_7 (℃)	51.4 ± 1.0	60.8 ± 1.2	70.7 ± 1.4	81.3 ± 1.6	90.0 ± 1.8
RH_7 (%)	6.7 ± 0.3	4.6 ± 0.2	2.9 ± 0.1	1.9 ± 0.1	1.4 ± 0.1
Y_7 (kg-water/kg-dry-air)	0.064382498 ± 0.000291849	0.006331258 ± 0.000313530	0.006202004 ± 0.000307190	0.006314869 ± 0.000312727	0.006537633 ± 0.000323649
u_p (m/s)	2.0 ± 0.2	2.0 ± 0.2	2.0 ± 0.2	2.0 ± 0.2	2.0 ± 0.2
u_r (m/s)	2.0 ± 0.2	2.0 ± 0.2	2.0 ± 0.2	2.0 ± 0.2	2.0 ± 0.2
θ_p/θ_r (-)	2	2	2	2	2
N (RPH)	15	15	15	15	15
P_{atm} (Pa)	94320	94320	94320	94320	94320
System output values					
T_2 (℃)	37.6 ± 0.4	42.4 ± 0.4	47.7 ± 0.5	53.8 ± 1.1	60.2 ± 1.2
RH_2 (%)	20.1 ± 0.6	14.1 ± 0.7	9.5 ± 0.5	5.8 ± 0.3	4.0 ± 0.2
Y_2 (kg-water/kg-dry-air)	0.008685827 ± 0.000257011	0.007850217 ± 0.000388603	0.006929832 ± 0.000344085	0.005769059 ± 0.000284042	0.005356373 ± 0.000265166

Table B.33: System input and output parameters' values at (θ_p/θ_r = 3.0) for figures 6.34, 6.35, and 6.36.

Test No.	1	2	3	4	5
System input values					
T_1 (℃)	30.5 ± 0.3	30.1 ± 0.3	31.1 ± 0.3	31.4 ± 0.3	30.9 ± 0.3
RH_1 (%)	31.5 ± 0.9	32.7 ± 1.0	03.8 ± 0.9	30.1 ± 0.9	31.2 ± 0.9
Y_1 (kg-water/kg-dry-air)	0.009232413 ± 0.000270463	0.009278001 ± 0.000274369	0.009255843 ± 0.000273724	0.009201289 ± 0.000272133	0.009269363 ± 0.000274118
T_7 (℃)	51.1 ± 1.0	60.9 ± 1.2	70.1 ± 1.4	79.8 ± 1.6	91.6 ± 1.8
RH_7 (%)	5.6 ± 0.3	3.6 ± 0.2	2.4 ± 0.1	1.6 ± 0.1	1.0 ± 0.1
Y_7 (kg-water/kg-dry-air)	0.004839117 ± 0.000240180	0.004963776 ± 0.000246321	0.004988697 ± 0.000247548	0.004991804 ± 0.000247701	0.004945028 ± 0.000245398
u_p (m/s)	2.0 ± 0.2	2.0 ± 0.2	2.0 ± 0.2	2.0 ± 0.2	2.0 ± 0.2
u_r (m/s)	2.0 ± 0.2	2.0 ± 0.2	2.0 ± 0.2	2.0 ± 0.2	2.0 ± 0.2
θ_p/θ_r (-)	3	3	3	3	3
N (RPH)	15	15	15	15	15
P_{atm} (Pa)	94380	94380	94380	94380	94380
System output values					
T_2 (℃)	36.1 ± 0.4	40.4 ± 0.4	45.2 ± 0.5	51.3 ± 1.0	56.1 ± 1.1
RH_2 (%)	18.9 ± 0.9	13.6 ± 0.7	9.2 ± 0.5	5.7 ± 0.3	4.2 ± 0.2
Y_2 (kg-water/kg-dry-air)	0.007485827 ± 0.000370819	0.006820217 ± 0.000336902	0.005929832 ± 0.000293096	0.004969059 ± 0.000246895	0.004656373 ± 0.000229529

Table B.34: System input and output parameters' values at (θ_p/θ_r = 1.0) for figures 6.37, 6.38, and 6.39.

Test No.	1	2	3
System input values			
T_1 (℃)	29.7 ± 0.3	29.9 ± 0.3	30.2 ± 0.3
RH_1 (%)	24.2 ± 0.7	34.3 ± 1.0	42.9 ± 1.3
Y_1 (kg-water/kg-dry-air)	0.006675280 ± 0.000198195	0.009616153 ± 0.000284222	0.012074012 ± 0.000355525
T_7 (℃)	70.4 ± 1.4	70.9 ± 1.4	71.5 ± 1.4
RH_7 (%)	3.1 ± 0.2	3.0 ± 0.2	2.9 ± 0.1
Y_7 (kg-water/kg-dry-air)	0.006537658 ± 0.000323651	0.006463734 ± 0.000320027	0.006410703 ± 0.000317427
u_p (m/s)	2.0 ± 0.2	2.0 ± 0.2	2.0 ± 0.2
u_r (m/s)	2.0 ± 0.2	2.0 ± 0.2	2.0 ± 0.2
θ_p/θ_r (-)	1	1	1
N (RPH)	15	15	15
P_{atm} (Pa)	94470	94470	94470
System output values			
T_2 (℃)	47.0 ± 0.5	47.8 ± 0.5	49.2 ± 0.5
RH_2 (%)	4.9 ± 0.2	6.4 ± 0.3	9.3 ± 0.5
Y_2 (kg-water/kg-dry-air)	0.003420992 ± 0.000170968	0.004648719 ± 0.000232568	0.007299832 ± 0.000362669

Table B.35: System input and output parameters' values at ($\theta_p/\theta_r = 2.0$) for figures 6.37, 6.38, and 6.39.

Test No.	1	2	3
System input values			
T_1 (℃)	31.6 ± 0.3	31.2 ± 0.3	31.0 ± 0.3
RH_1 (%)	18.1 ± 0.9	30.8 ± 0.9	39.9 ± 1.2
Y_1 (kg-water/kg-dry-air)	0.005560141 ± 0.000275666	0.009302786 ± 0.000275092	0.011964299 ± 0.000352353
T_7 (℃)	71.9 ± 1.4	70.2 ± 1.4	71.1 ± 1.4
RH_7 (%)	2.4 ± 0.1	2.8 ± 0.1	2.7 ± 0.1
Y_7 (kg-water/kg-dry-air)	0.005845222 ± 0.000267266	0.005849037 ± 0.000289862	0.005863204 ± 0.000290558
u_p (m/s)	2.0 ± 0.2	2.0 ± 0.2	2.0 ± 0.2
u_r (m/s)	2.0 ± 0.2	2.0 ± 0.2	2.0 ± 0.2
θ_p/θ_r (-)	2	2	2
N (RPH)	15	15	15
P_{atm} (Pa)	94450	94450	94450
System output values			
T_2 (℃)	49.2 ± 0.5	48.9 ± 0.5	50.1 ± 1.0
RH_2 (%)	4.1 ± 0.2	6.6 ± 0.3	9.5 ± 0.5
Y_2 (kg-water/kg-dry-air)	0.003198719 ± 0.000159868	0.005129832 ± 0.000253550	0.007852050 ± 0.000387569

Table B.36: System input and output parameters' values at ($\theta_p/\theta_r = 3.0$) for figures 6.37, 6.38, and 6.39.

Test No.	1	2	3
System input values			
T_1 (℃)	29.7 ± 0.3	29.9 ± 0.3	30.6 ± 0.3
RH_1 (%)	21.7 ± 0.7	34.1 ± 1.0	40.6 ± 1.2
Y_1 (kg-water/kg-dry-air)	0.005980333 ± 0.000177752	0.009561276 ± 0.000282623	0.01189652 ± 0.000350394
T_7 (℃)	69.4 ± 1.4	70.8 ± 1.4	71.1 ± 1.4
RH_7 (%)	2.9 ± 0.1	2.8 ± 0.1	2.7 ± 0.1
Y_7 (kg-water/kg-dry-air)	0.005851615 ± 0.000289989	0.006003799 ± 0.000297462	0.005863204 ± 0.000290558
u_p (m/s)	2.0 ± 0.2	2.0 ± 0.2	2.0 ± 0.2
u_r (m/s)	2.0 ± 0.2	2.0 ± 0.2	2.0 ± 0.2
θ_p/θ_r (-)	3	3	3
N (RPH)	15	15	15
P_{atm} (Pa)	94450	94450	94450
System output values			
T_2 (℃)	47.8 ± 0.5	48.9 ± 0.5	50.4 ± 1.0
RH_2 (%)	5.2 ± 0.3	7.2 ± 0.4	10.2 ± 0.5
Y_2 (kg-water/kg-dry-air)	0.003779832 ± 0.000188988	0.005552050 ± 0.000276610	0.008552673 ± 0.000422394